

Joana Maria Lopes Delgado

Mestre em Conservação e Restauro



**Restoring Medieval
Stained-Glass Transparency:
Use of New Task Specific Luminescent
Ionic Liquids for Corrosion Crusts Removal**

Dissertação para obtenção do Grau de Doutor em Conservação e
Restauro do Património

Especialidade em Ciências da Conservação

Orientador: Márcia Vilarigues, Professor Auxiliar, DRC, FCT/UNL

Co-orientadores: César A.T. Laia, Investigador Auxiliar, DQ, FCT/UNL

Luís C. Branco, Investigador Principal, DQ, FCT/UNL

Júri:

Presidente: Prof. Doutor José Paulo Barbosa Mota

Arguentes: Prof. Doutor Joost Caen

Prof. Doutor António Jorge Dias Parola

Vogais: Prof. Doutora Maria Helena Figueira Vaz Fernandes

Prof. Doutora Isabel Maria Delgado Jana Marrucho Ferreira



FACULDADE DE
CIÊNCIAS E TECNOLOGIA
UNIVERSIDADE NOVA DE LISBOA

Março 2016

Restoring Medieval Stained-Glass Transparency: Use of New Task Specific Luminescent Ionic Liquids for Corrosion Crusts Removal

Copyright © Joana Delgado, Faculdade de Ciências e Tecnologia, Universidade Nova de Lisboa.

A Faculdade de Ciências e Tecnologia da Universidade Nova de Lisboa têm o direito, perpétuo e sem limites geográficos, de arquivar e publicar esta dissertação através de exemplares impressos reproduzidos em papel ou de forma digital, ou por qualquer outro meio conhecido ou que venha a ser inventado, e de a divulgar através de repositórios científicos e de admitir a sua cópia e distribuição com objectivos educacionais ou de investigação, não comerciais, desde que seja dado crédito ao autor e editor.

“First God made heaven and earth. The earth was without form and void, and darkness was upon the face of the deep; and the Spirit of God was moving over the face of the waters. And God said, "Let there be light"; and there was light.

And God saw that the light was good; and God separated the light from the darkness. God called the light Day, and the darkness he called Night. And there was evening and there was morning, one day.”

Genesis

“I am too late for the birth of birds
but have come just in time for the
opening of a red chocolate bar”

Matilde Campilho, *O Acrobata*, in *Jóquei*

Acknowledgements

This project was held between April 2011 and March 2015, mostly in the campus Faculdade de Ciência e Tecnologia in Caparica, and for some time in Artesis Hogeschool in Antwerp, now University of Antwerp, Belgium, in autumn 2012, and it was financially supported by the Fundação para a Ciência e Tecnologia (SFRH/BD/72808/2010).

I wish to thank first of all, my supervisors, Márcia Vilarigues, César Laia and Luís Branco, who introduced me the idea for this project and were absolutely essential for its materialization and completion, not only for their knowledge and expertise but also for their friendship and constant support. Also a very special thank you to my colleagues; Inês Coutinho and Susana Coentro, who started this journey with me, and were there during all the stages of this project, both of joy and of despair; to Alexandra Rodrigues, Andreia Machado, Hélia Marçal, and later on Amanda Pinto, Fernanda Barroso and Francisca Pulido Valente, who joined a bit later, but for that were not less important. To everybody in Vicarte – in special to the late Solange Muralha, who is deeply missed – and in REQUIMTE, who made it a pleasure to go to work every day. To Ana Maria Martins and Cremilde Cascalheira, who were (and are) always there for us.

I would also like to leave my expression of gratitude for my colleagues in the stained glass conservation studio in the University of Antwerp, who were very welcoming during my stay. And of course a very special word of appreciation to Prof. Dr. Joost Caen, who received me in Antwerp and made me feel as part of the family, but also for his weariless support and advice during and after my stay in Belgium. I also wish to thank Ms. L. Seliger (The Cathedral Studios, Canterbury), Mr. C. Larkum (Sidney Sussex College, Cambridge), and again Prof. Dr. Joost Caen and Dr. Kristel de Vis from the University of Antwerp, for the archaeological samples provided for this study, which without any doubt enriched the discussion tremendously.

For all the time spent helping me analyze the samples in the Scanning Electron Microscope, I must present my sincere acknowledgement to Dr. Daniela Nunes and Dr. Elvira Fortunato, from CENIMAT/I3N; to Maria João Furtado, Filipe Martinho and Dr. Rui Silva, for the help given analyzing the samples in the Optical Microscope available in CENIMAT/I3N. Also a special thank you to Dr. Anabela Raymundo (Instituto Superior de Agronomia), Dr. Luís Cerqueira Alves (Centro de Ciências e Tecnologias Nucleares (C²TN)), Pedro Redol (Monastery of Batalha), and to the members of my Thesis Advisory Committee, Dr. Isabel Marrucho (Instituto de Tecnologia Química e Biológica) and Lisa Piloni (The Metropolitan Museum of Art). And of course to Mani Hosseinzadeh, for his precious help and support with the synthesis and characterization of an important part of the ionic liquids used during this project.

And finally, but far from being the least, I wish to thank to my family and friends, to Ana, António, Francisco, Joana and Matěj, and all my new colleagues and friends in Prague, for the love and friendship, who inspire me every day and without whom this would not be. And for always believing in me, especially in those moments when I did not.

Resumo

A transparência é uma característica cuja preservação é fundamental num painel de vitral. A passagem da luz é a essência desta forma de arte, sendo, portanto, uma peça crucial da sua intenção original, tanto através do vidro colorido como das pinturas. O vitral medieval é caracterizado por um conteúdo relativamente elevado de óxidos alcalinos e alcalino-terrosos, sobretudo potássio, cálcio e sódio, bem como um reduzido conteúdo de sílica comparativamente ao vidro contemporâneo. Os iões sódicos e potássicos são lixiviados e, uma vez em contacto com a atmosfera, é formada uma camada de sílica-gel (superfície hidratada rica em sílica), seguindo-se conseqüentemente a formação de uma crosta de corrosão. Esta é composta sobretudo por sais insolúveis, como carbonato (CaCO_3), sulfato (CaSO_4) e oxalato (CaC_2O_4) de cálcio, que são bastante difíceis de remover da superfície do vidro. Os métodos que apresentam maior eficiência na remoção destas crostas – como agentes quelantes (ex.: soluções de EDTA), ácidos fracos e resinas iónicas – são os mesmos que podem induzir danos ou riscos a longo prazo na superfície do vidro.

Esta investigação teve como objetivo desenvolver um novo produto – um líquido iónico (LI) – para a remoção da corrosão em vitral medieval, que fosse eficaz e não-nocivo tanto para o vitral como para o utilizador. Para facilitar a remoção completa da corrosão e do material de limpeza (o líquido iónico) após o procedimento, o LI foi composto usando um fluoróforo – líquido iónico intrinsecamente luminescente. O objetivo foi dotar o LI de uma função dupla: ter um ponto de interação com iões metálicos (neste caso, Ca^{2+}), exibindo ao mesmo tempo fluorescência.

Os efeitos na superfície do vidro modelo de três LIs diferentes, uma solução de EDTA e um ambiente de humidade relativa elevada são descritos e comparados. Foi ainda feita uma comparação entre a eficiência de dois LIs e uma solução de EDTA na remoção de crostas de corrosão, usando fragmentos de vitral arqueológico corroído. Os testes realizados confirmaram a eficácia do líquido iónico na remoção das crostas de corrosão e demonstraram igualmente que não ocorreram quaisquer alterações na superfície do vidro nem na crosta de corrosão remanescente, mesmo quando em contacto direto com os líquidos iónicos durante um longo período de tempo.

Palavras-chave: vitral / vidro medieval / líquidos iónicos / corrosão do vidro / composição química / métodos de limpeza

Abstract

Transparency is a fundamental feature to preserve on a stained-glass panel. The passage of light is the essence of this art form and, as so, a crucial piece of its original intention, both through the colored glass as through the paintings. Medieval stained-glass is characterized by a relatively high content of alkali and alkali-earth ion oxides, mainly potassium, calcium and sodium, and low contents of silica compared to contemporary glass. These ions are leached, and when in contact with the atmosphere a gel-layer (hydrated silica-rich surface) is formed, and consequently there is the formation of a corrosion crust. This is mainly composed by insoluble salts such as calcium carbonate (CaCO_3), sulfate (CaSO_4) and oxalate (CaC_2O_4), which are very difficult to remove from the glass surface. The methods that present higher efficiency for the removal of those crusts – like chelate agents (e.g. EDTA solutions), weak acids and ionic resins – are the same that may induce damage or long-term risks to the glass surface.

The aim of this research was to develop a new product – an ionic liquid (IL) – for the removal of medieval stained-glass corrosion that is effective and harmless both for the stained-glass and for the user. To assure the complete removal of both corrosion and cleaning material (the ionic liquid) after the procedure, the IL was functionalized using a light emitting marker – intrinsically luminescent ionic liquid. It was our objective to have an IL with a dual function: having a binding site for metal cations (in this case, Ca^{2+}), while exhibiting bright fluorescence.

The effects on the surface of model glass of three different ILs, an EDTA solution and the effect of a high relative humidity (RH) environment are described and compared. A comparison between the efficiency of two ILs and an EDTA solution for the corrosion crusts removal was made using corroded archaeological stained glass samples. The tests performed confirmed the effectiveness of the cleaning material in removing the corrosion crusts, and also demonstrated that there were no detected alterations to the glass surface even when in direct contact with the ionic liquids for a long period of time.

Key words: stained-glass / medieval glass / ionic liquids / glass corrosion / chemical composition / cleaning methods

Published paper: J.M. Delgado, A. Raymundo, M. Vilarigues, L.C. Branco, C.A.T. Laia, *Characterization of a Novel Intrinsic Luminescent Room-Temperature Ionic Liquid Based on $[\text{P}_{6,6,6,14}][\text{ANS}]$* , Chemistry - A European Journal 21 (2015), 726-732.

Submitted paper: J.M. Delgado, D. Nunes, E. Fortunato, C.A.T. Laia, L.C. Branco, M. Vilarigues, *The effect of three luminescent ionic liquids on the glass surface – first step to stained glass cleaning*, International Journal of Applied Glass Science. Submitted in March 2016.

Symbols and notations

μ -PIXE – micro-Particle Induced X-Ray Emission

[ANS] – 8-Anilino-1-naphthalenesulfonic acid

[C₂O₅MIM] – 1-[2-(2-Methoxyethoxy)ethyl]-3-methylimidazolium

EDTA – ethylenediaminetetraacetic acid

FTIR – Fourier Transform Infrared

HLLA – High Lime Low Alkali

¹H-NMR – Nuclear Magnetic Resonance

IL – Ionic Liquid

NIR – Near Infrared

LEDs – Light-Emitting Diode

OM – Optical Microscopy

[P_{6,6,6,14}] – Trihexyl(tetradecyl)phosphonium

RH – Relative Humidity

[PyrCOO] - 1-Pyrenecarboxylic

RT – Room Temperature

SEM – Scanning Electron Microscopy

SEM-EDS – Scanning Electron Microscopy with Energy Dispersive Scattering

T – Temperature

UV– Ultra violet

Vis – Visible

wt% - weight percent

Contents

	Introduction	1
Chapter 1	Medieval Stained-Glass	3
1.1	Medieval stained glass windows: paintings in light	3
1.2	Glass production in the Middle-Ages: a short historical introduction	4
1.3	Nature and structure of medieval stained-glass	6
1.4	But what is glass?	9
1.5	Glass corrosion: mechanism of formation	11
1.6	Glass cleaning: State of the art in cleaning technology	15
1.7	Ionic liquids: Introducing a new alternative	16
Chapter 2	Ionic Liquids	17
2.1	What is an ionic liquid? Ionic liquids properties and advantages	17
2.2	Ionic liquids synthesis	19
2.2.1	Synthesis method	19
2.2.2	Equipment and methods	19
2.2.3	Ionic liquids synthesized	20
2.2.4	Why these molecules?	21
2.3	[P _{6,6,6,14}][ANS] – characterization	23
2.3.1	Synthesis of [P _{6,6,6,14}][ANS]	24
2.3.2	Characterization of the IL [P _{6,6,6,14}][ANS]	25
2.3.3	DSC and rheology studies	25
2.3.4	Contact angle	26
2.3.5	NMR studies	27
2.3.6	UV/vis. Absorption Spectroscopy and Emission Spectroscopy Studies	28
2.4	Characterization of other intrinsically luminescent room temperature ionic liquids	30
2.4.1	[C ₅ O ₂ MIM][ANS]	30
2.4.2	[P _{6,6,6,14}][PyrCOO]	30
2.5	Potential applications	32

Chapter 3	Experimental procedure and techniques	33
3.1	Production of model glass	34
3.2	Corrosion essays: artificial corrosion	35
3.3	Archaeological stained glass samples	35
3.4	Experimental design for the comparison of the ionic liquids effect on model glass	37
3.5	Experimental design for the mid-term effects of the [P _{6,6,6,14}][ANS] IL	38
3.6	Morphologic analysis	39
3.7	Chemical analysis	40
Chapter 4	Corrosion crusts removal: model glass	41
4.1	Samples characterization	41
4.2	Comparison of the effect of ILs and EDTA with high RH on the model glass surface	42
4.3	Mid-term effect of the [P _{6,6,6,14}][ANS] IL on the glass surface	50
4.4	<i>Grisaille</i> : Application of the IL [P _{6,6,6,14}][ANS] on <i>grisaille</i> painted glass	51
4.4.1	Effect of the IL on the <i>grisaille</i> layer	53
4.5	Conclusions	54
Chapter 5	Corrosion crusts removal: archaeological stained-glass	55
5.1	Archaeological stained-glass samples	55
5.2	Comparison of the effect of ILs and EDTA on the glass surface	56
5.3	Effect of the [P _{6,6,6,14}][ANS] IL on the glass surface	60
5.4	Before and after [P _{6,6,6,14}][ANS]	64
5.5	Possible mechanisms and effects: a general comparison between the IL and EDTA	66
5.6	Conclusions	66
	Conclusions	67
	What comes next? Further suggestions to be developed in the future	67
	References	69

Appendix I	Complementary data related to Chapter 2	81
i)	Nuclear Magnetic Resonance (NMR) of the [P _{6,6,6,14}][ANS], [C ₅ O ₂ MIM][ANS] and [P _{6,6,6,14}][PyrCOO] ionic liquids	82
ii)	[C ₅ O ₂ MIM][ANS] IL complementary data	88
iii)	[P _{6,6,6,14}][PyrCOO] IL complementary data	89
Appendix II	Complementary data related to Chapter 4	91
i)	Optical Microscope images of model glass samples	92
ii)	SEM images of model glass samples' surface	101
Appendix III	Complementary data related to Chapter 5	105
i)	Archaeological stained-glass fragments: images of the interior and exterior surfaces of the samples.	107
ii)	SEM-EDS elementary mapping of archaeological stained glass samples Cant 001, 002, 003, 004, 005, 006, 028, 033 and 034.	113
iii)	Cant 042 before and after the application of [P _{6,6,6,14}][ANS] IL	119

List of figures

- Figure 1.1** Medieval stained-glass windows at Cathedral of Our Lady of Chartres, France. **3**
- Figure 1.2** Stained glass Windows in the abside (left) and colors reflected on the wall and on the stained glass windows (right) at Monastery of Santa Maria da Vitória in Batalha, Portugal. **4**
- Figure 1.3** *The Pit of Memnon, depicting glassblowing, from The Travels of Sir John Mandeville (p. 21-22, plate 27). Manuscript dated from 14-15th century (British Library).* **5**
- Figure 1.4** Different phases of the production of a crown glass plate. **(a)** Plate XI: Wood Glass Making, Operation of Shaping the Tip of the Ball and Blowing it over the Trough, **(b)** Plate XV: Wood Glass Making, Operation of Heating the Ball to Open it and Make the Pane and Carry it to the Embers Pit, **(c)** Plate XVI: Wood Glass Making, Operation of Placing the Pane in the Pit and of Refiring it in the Furnace. From *Planches d'Encyclopedie or Dictionnaire raisonnée des Arts et Metiers* by Diderot and D'Alembert. **6**
- Figure 1.5** **(a)** Simplified scheme of the grisaille layer before and after the firing of the glass fragment. **(b)** *Saint Joseph*, 16th c., Monastery of Batalha, Portugal and **(c)** *Face detail*, 16th c., Convento de Cristo, Tomar, Portugal. **7**
- Figure 1.6** Methodology for making a stained glass panel. **(a)** In the first place, a full size cartoon is made, showing the lead lines around each glass fragment, as well as the colors and details to be painted on the glass; **(b)** then, the glass – colored or transparent – is cut to size, following the cut-lines from the cartoon; **(c)** also according to the cartoon, the *grisaille* painting is made, **(d)** using different tools and brushes, some of the details being made after the paint is dry. The fragments are fired in a kiln, for the paint – *grisaille*, yellow silver staining or, later on, enamels – to adhere to the glass surface. **(e)** By the time all the glass pieces are prepared, they are gathered on the cartoon, over a usually wooden base, and set together by lead came cut to size. **(f)** After completing this process, each junction is soldered, **(g)** and cemented on both sides in order to make the panel more resistant and waterproof, being left for a few days to harden. **(h)** Finally, the panel is complete. These images are stills from the video “Making a stained glass panel”, that can be seen on the Victoria and Albert Museum website. **8**

Figure 1.7	Example of a two dimensional structure of a soda-lime glass with a low content of Al_2O_3 .	9
Figure 1.8	Classification of glass used in the production of window glass panes, based on their major composition.	10
Figure 1.9	Types of glass more commonly used in the production of stained glass windows in Europe, from the 13 th to the 20 th century.	11
Figure 1.10	Glass corrosion mechanism (weathering) starts with a clean and un-corroded surface (a) . The formation of a water film occurs, due to the atmospheric conditions, allowing ionic exchange between the ions H^+ and H_3O^+ of water and the alkaline ions present in glass, which may be reinforced by the presence of acid gases (b) . This lixiviation reaction starts slowly, but accelerates overtime; after the formation of a hydrated layer (light blue in the figure), rich in silica and alkaline oxides (c) , the glass surface becomes more resistant to the attack of water and the surface pH increases. The crystalline corrosion products (salts) stay in the glass surface after the water evaporates (d) .	12
Figure 1.11	SEM-EDS elementary maps of a cross-sectioned archeological sample, presenting Si, O, Ca and Fe elementary maps. 150x magnification.	13
Figure 1.12	<i>Figura aureolada</i> , 15th century stained-glass panel from the Monastery of Batalha, Portugal. Reflected and transmitted light (left) and reflected light (right).	14
Figure 2.1	Functional groups from [ANS] and [PyrCOO] anions molecules where the calcium ions will likely bind.	22
Figure 2.2	Functional groups in the $[\text{C}_5\text{O}_2\text{MIM}]$ cation molecule more probable to form a link with calcium ions.	22
Figure 2.3	EDTA molecule with the indication of the areas likely to bind with calcium ions.	22
Figure 2.4	Molecular structures of [ANS] anion and $[\text{P}_{6,6,6,14}]$ cation.	23
Figure 2.5	$[\text{P}_{6,6,6,14}][\text{ANS}]$ in daylight and under UV light, 365 nm.	24

Figure 2.6	(a) DSC measurements of [P _{6,6,6,14}][ANS] and (b) viscosity of [P _{6,6,6,14}][ANS] in heating (circles) and cooling (triangles) cycle. Viscosity values of the heating cycle were fitted with the VTF equation (see text) giving the parameters inserted in the figure.	26
Figure 2.7	Contact angle variation with time of a [P _{6,6,6,14}][ANS] IL drop on a clean glass surface, and images of this drop at a given time (0, 10, 20, 76 and 118 seconds).	27
Figure 2.8	¹ H-NMR spectra of pure [P _{6,6,6,14}][ANS] for heating (black lines) and cooling (grey lines) cycle containing (a) aromatic and (b) aliphatic resonances.	28
Figure 2.9	[P _{6,6,6,14}][ANS] UV/vis absorption and fluorescence spectra ($\lambda_{\text{ex}}=370$ nm).	29
Figure 2.10	[P _{6,6,6,14}][ANS] temperature dependence of the fluorescence spectra ($\lambda_{\text{ex}}=370$ nm).	29
Figure 2.11	Molecular structures of [C ₅ O ₂ MIM] cation and [ANS] anion.	30
Figure 2.12	Molecular structures of [P _{6,6,6,14}] cation and [PyrCOO] anion.	31
Figure 2.13	[P _{6,6,6,14}][PyrCOO] IL under natural light (transparent yellowish IL) and under UV light (blue photoluminescence, not as intense as the IL containing [ANS]).	31
Figure 3.1	Stages of production of the glass roundel and final result.	34
Figure 3.2	Experimental design for the experiments comparing the effects of different environment and compounds on model glass samples. Each parameter was tested in 2 samples.	37
Figure 3.3	Scheme of division of an archaeological sample: Section A (control group), section B ([P _{6,6,6,14}][ANS]), section C ([C ₅ O ₂ MIM][ANS]) and section D (EDTA solution).	38
Figure 3.4	Experimental procedure for testing the long term effect of the ionic liquid [P _{6,6,6,14}][ANS] on the glass. (a) One sample was left without any IL, being the control sample. A drop of IL was deposited on 3 samples of each group. (b) An emission spectra was measured for each sample. (c) The samples were put in a desiccator under vacuum. (d) The emission spectra was measured, (e) and the IL was removed using a swab impregnated with a solution of water:ethanol (1:1/v:v). Its complete removal was always controlled using an UV-light lamp and by the emission spectra.	39

- Figure 4.1** Comparison between the [P_{6,6,6,14}][ANS] and the [P_{6,6,6,14}][PyrCOO] ILs applied on a transparent model glass sample after 1 hour and after 1 week, under natural day light and under UV-light. The visual behavior of the other IL, [C₅O₂MIM][ANS] is similar to [P_{6,6,6,14}][ANS]. **42**
- Figure 4.2** Optical microscope images of the surface of the model glass samples, with a 5x magnification **(a)** of a control sample, from group A, **(b)** a sample from group B, left for 4 weeks in an 88% RH atmosphere, **(c)** a sample from group C, that was in contact with [P_{6,6,6,14}][ANS] IL for 4 weeks, **(d)** a sample from group D, that was in contact with [C₅O₂MIM][ANS] IL for 4 weeks, **(e)** a sample from group E, that was in contact with [P_{6,6,6,14}][PyrCOO] IL for 4 weeks and **(f)** a sample from group F, that was in a solution of 3% EDTA + 3% NH₄HCO₃ in distilled water, pH 8.26, for 1 week. Optical microscope image with 10 x magnification **(g)** of the surface of a sample from group B, left for 4 weeks in an 88% RH atmosphere and **(h)** of a sample from group F, left for 1 day in a solution of 3% EDTA + 3% NH₄HCO₃ in distilled water, pH 8.26. **43**
- Figure 4.3** SEM image of the surface of a model glass sample from group B after being for 7 days in a high RH environment **(a)** 500x magnification and **(b)** 1000x magnification. SEM image of the surface of a model glass sample from group F after being for **(c)** 7 days in an EDTA solution, 500x magnification, **(d)** and for 28 days in an EDTA solution, 1000x magnification. **45**
- Figure 4.4** Raman spectra, range 200 to 1200 cm⁻¹, of the model glass samples of all groups. **46**
- Figure 4.5** Linescan profile (intensities of Ca, Si and K) measured on a cross-sectioned **(a)** model glass sample from the control group (group A), **(b)** model glass sample left for 1 week in a high RH atmosphere (group B) and **(c)** model glass sample immersed in an EDTA solution for 1 week (group F). The red line in the linescan indicates where the glass bulk starts. On the right of each linescan profile, there is the correspondent image of the line where the measure was made, marked as a yellow line with 50 μm. **48**
- Figure 4.6** Linescan profile (intensities of Ca, Si and K) measured on a cross-sectioned **(a)** model glass sample after the application of the [P_{6,6,6,14}][ANS] IL for 1 week (group C), **(b)** model glass sample after the application of the [C₅O₂MIM][ANS] IL for 1 week (group D) and **(c)** model glass sample after the application of the [P_{6,6,6,14}][PyrCOO] IL for 1 week (group E). The red line in the linescan indicates where the glass bulk starts. On the right of each linescan profile, there is the correspondent image of the line where the measure was made, marked as a yellow line with 50 μm. **49**

- Figure 4.7** Emission spectra of the IL **(a)** 4 weeks after the application of the IL on a model glass sample and **(b)** after the removal of the IL. **50**
- Figure 4.8** SEM image of the surface of an un-corroded sample – Group A – **(a)** before and **(b)** after the application of [P_{6,6,6,14}][ANS] IL for 12 weeks, 200x magnification. SEM image of the surface of an artificially corroded sample from Group B **(c)** before and **(d)** after the application of [P_{6,6,6,14}][ANS] IL for 12 weeks, 100x magnification. **51**
- Figure 4.9** Optical microscope images of the surface of the model glass samples, with a 5x magnification **(a)** of a *grisaille* painted sample, after the removal of the [P_{6,6,6,14}][ANS] IL using a dry swab, bright field filter, **(b)** and the same sample under UV-light filter **(c)** after the removal of the IL using a swab impregnated with a water:ethanol (1:1) solution once, and **(d)** after another passage with a swab impregnated in the same solution. **52**
- Figure 4.10** Optical microscope images of the surface of the model glass samples, with a 5x magnification of *grisaille* painted model glass samples that were in contact with [P_{6,6,6,14}][ANS] IL for: **(a)** 15 minutes, **(b)** 1 day, **(c)** 1 week and **(d)** 28 days, all after the removal of the IL using a swab impregnated with a water:ethanol (1:1). **53**
- Figure 5.1** Scheme of division of an archaeological sample: Section A (control group), section B ([P_{6,6,6,14}][ANS]), section C ([C₅O₂MIM][ANS]) and section D (EDTA solution). **56**
- Figure 5.2** SEM images and EDS maps of a cross-sectioned archaeological sample **(a)** before and **(b)** after the application of the [P_{6,6,6,14}][ANS] IL, **(c)** after the application of the [C₅O₂MIM][ANS] IL and **(d)** after the application of the and EDTA solution. The corresponding EDS maps for Si, O, Ca and Fe are presented. In these images it is possible to see a layer very rich in Si (hydrated layer), and another above very rich in Ca (corrosion layer), as well as the Fe (corresponding to the *grisaille* layer). **57**
- Figure 5.3** FTIR spectra of archeological samples, before and after the application of the IL and EDTA, with the indication of the most representative peaks. **58**
- Figure 5.4** pH of the surface of samples Cant 028, Cant 033 and Cant 034, before and after the application of [P_{6,6,6,14}][ANS] IL, [C₅O₂MIM][ANS] IL and an EDTA solution. For every sample, three measurements were made, and the average is presented in the chart above, with the respective value indicated. The standard deviation is <0.07 for all samples except Cant 028 (a) (0.19) and Cant 033 (c) (0.14). **59**

- Figure 5.5** Archaeological sample **(a)** before and **(b)** after cleaning tests using [P_{6,6,6,14}][ANS] IL, under natural light, **(c)** and after the cleaning tests, under 365 nm UV-light. **60**
- Figure 5.6** **(a)** Emission spectra of the IL **(i)** 4 weeks after the application of the IL on a model glass sample and **(ii)** after the removal of the IL. **(b)** Emission spectra of the IL **(i)** when it is applied on an archaeological sample, **(ii)** after 4 weeks, **(iii)** after the removal of the IL **(iv)** and after being photodegraded using a Solar lamp for 1 minute and **(v)** 10 minutes. **61**
- Figure 5.7** Optical microscope image of the surface of an archaeological sample **(a)** before and **(b)** after cleaning tests using [P_{6,6,6,14}][ANS] IL. 5x magnification, dark field filter. SEM image of the surface of an archaeological sample **(c)** before **(d)** and after the application of [P_{6,6,6,14}][ANS] IL for 12 weeks, 200x magnification. **61**
- Figure 5.8** FTIR spectra of the corrosion present in the surface of an archaeological sample **(a)** before and **(b)** after the application of the [P_{6,6,6,14}][ANS] IL. **62**
- Figure 5.9** SEM-EDS elementary maps of a cross-sectioned archeological sample **(a)** before and **(b)** after the application of the IL [P_{6,6,6,14}][ANS]. 100x magnification. **63**
- Figure 5.10** Archaeological stained glass fragment before and after the application of [P_{6,6,6,14}][ANS] IL, with reflected light (a,b) and transmitted light (c,d). **64**
- Figure 5.11** Archaeological stained glass fragment before and after the application of [P_{6,6,6,14}][ANS] IL, with reflected light (a,b) and transmitted light (c,d). **65**

List of tables

Table 2.1	Detailed information about the cations used.	20
Table 2.2	Detailed information about the anions used.	21
Table 2.3	UV/vis spectroscopy measurements of $[P_{6,6,6,14}][ANS]$.	28
Table 3.1	Composition of the glass produced.	34
Table 3.2	Composition of the archaeological stained-glass samples (% mol and % weight).	36
Table 4.1	Identification of the Raman bands associated with the components of the Si–O stretching and bending modes.	46

Introduction

The idea for the use of ionic liquids to remove glass corrosion emerged and was developed in a previous project at the Conservation and Restoration Department, Vicarte and REQUIMTE, all at FCT-UNL, starting from 2009. The project had very promising results, but one of the problems that came upon was the difficulty in detecting the presence of the ionic liquid on the glass surface after the cleaning procedure. Having this problem in mind, a new alternative was suggested: the use of a luminescent marker to allow an easy detection of the presence of the ionic liquid. This idea was developed and the results of the synthesis and application of novel intrinsically luminescent ionic liquids for corrosion crusts removal are here presented.

One of the most important, but also delicate, phases in the conservation practice is the cleaning process, no matter what is the material. It is also a controversial topic, which makes it important to understand and debate. Corrosion crusts are a result of the deterioration of original material, being a part of the history of the object. However, these crusts can also block the passage of light, one of the most important elements in a stained glass panel. In such cases the corrosion crusts become an obstacle to the visualization of the object in its entire splendor. As corrosion has a protective role, it is very important to have into consideration that any cleaning procedure should remove the corrosion deposits only as far as necessary to improve the transparency, without damaging the hydrated glass surface underneath as the gel-layer protects the glass beneath. There is a balance that needs to be obtained between the preservation of the original material and the preservation of the original essence of the stained-glass panel.

From these considerations, the first chapter of this document is devoted to understand and give a general idea about the importance of stained-glass as an artistic and religious expression in the middle-ages, being this understanding fundamental to comprehend the work of art as a whole. To this follows a description of what is glass as a material, how it was produced in the middle-ages, as well as a succinct introduction of the glass corrosion mechanisms. Finally, an approach on the state of the art of glass corrosion removal from stained-glass and an introduction to the new solution proposed: luminescent ionic liquids.

In the second chapter, a short introduction to what is an ionic liquid is made, followed by the description of the synthesis method of the luminescent ionic liquids that will be tested as well as its characterization. A more in depth study and characterization was carried in the case of the trihexyl(tetradecyl)phosphonium 8-Anilino-1-naphthalenesulfonic acid ionic liquid ($[P_{6,6,6,14}][ANS]$ IL), with results published in 2015 in Chemistry - A European Journal (DOI: 10.1002/chem. 201402534, ref. **[Delgado 2015]**).

The third chapter describes the experimental design and analytical techniques used in the development of the study of the effects of the ionic liquids on the model and archaeological stained glass fragments, which is developed in chapters four and five. The composition of both model glass samples and archaeological stained glass fragments is also presented.

On the fourth and fifth chapters, the application of the ionic liquids is described. The cleaning tests and consequent effects of the ILs tested on the surface of model glass samples will be developed in the fourth chapter, being these results compared to the effect of an aqueous solution of ethylenediaminetetraacetic acid (EDTA) and ammonium bicarbonate (NH_4HCO_3) and a high relative humidity (RH) environment. Preliminary tests were also carried out in model glass samples painted with *grisaille* (which consists in a mixture of ground glass, iron or copper oxide and a binder, that was applied to the glass surface and then fired; a more detailed introduction to *grisaille* can be found in Chapter 1), being the results presented in the end of this fourth chapter.

Finally a description of the tests performed on stained glass archaeological fragments is presented, using two selected ILs and the EDTA solution. In this chapter the aim is to understand the effect these substances have on the corrosion crusts chemical and morphological characteristics, as well as to determine the effectiveness in the corrosion crusts removal.

Chapter 1

Medieval Stained-Glass

In this chapter, the material aspect of the medieval stained-glass will be developed, starting by understanding what is glass and how was the stained-glass produced in the middle-ages. Then, an insight on the glass corrosion process, as it is important to understand the nature of glass corrosion before discussing new solutions for its removal. Finally, an approach on the state of the art of glass corrosion removal from stained-glass is made, as well as an introduction to the new solution proposed and developed during this project: luminescent ionic liquids.

1.1 – Medieval stained glass windows: paintings in light

In most cultures, the concept of light and clarity holds a positive connotation, associated to the birth of each new day. There are several references on the Bible relating God to light, categorizing it as something mystical and divine, which enlightens the believers. As Saint John refers in the New Testament, Christ said “I am the light that came into the world, that whosoever believeth on me should not abide in darkness” (John, 12:46).

“One cannot conceive the sense and grandiosity of a great gothic cathedral without the light and color atmosphere that its stained-glass windows create”. [Alcaide 1969] No other artistic support incorporates, like glass, this fundamental element of the artistic work – light –, neither works with it in such an intimate way. In figures 1.1 and 1.2, the mystical atmosphere of the different buildings, provided by the stained glass windows, is evident.

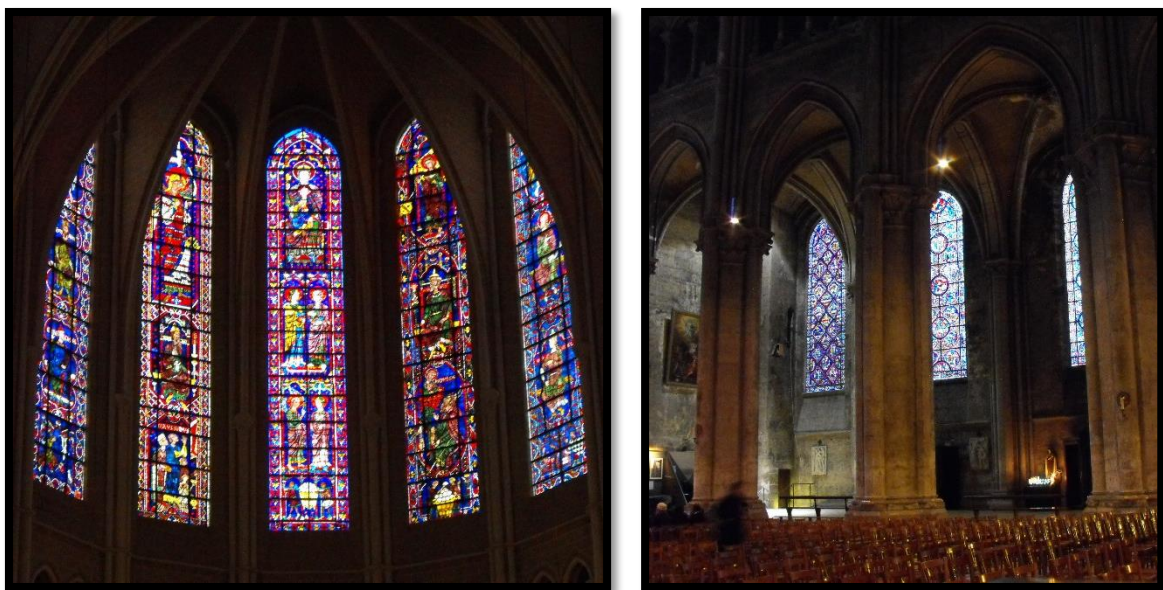


Figure 1.1: Medieval stained-glass windows at Cathedral of Our Lady of Chartres, France (Joana Delgado ©).

Glass technology itself is very fond of fire, and like this full of symbolism. The creation of stained-glass windows consisted, in the Middle Ages, as a way to express Faith, being its primal objective to ornate the house of God. Through the glass and the colorful lights that resulted from the application of the stained-glass panels, that filtered the entrance of light by projecting colors on the inside of the church – similar to precious stones –, there was created an atmosphere propitious to a mystical adoration, suggesting a semblance to the divine (figure 1.2). [Aubert 1983; Caviness 1985, pp. 548-554; Worringer 1992, Raguin 2003] Pierre de Roissy, chancellor of the chapter of Chartres, said that the windows that are in church and through which it transmits light from the Sun means the Holy Scriptures, which protect us from evil and illuminate us all (c.1200). The poetics and aesthetics of light can be extended to the precious stones, translucent material that reflected colored lights, bringing a theological reflection that can be associated with the heavenly Jerusalem. [Duby 1993] However, the high prices and the difficulties inherent to its execution made it particularly rare in Portugal, when compared to the expression it had in the rest of Europe, from the Middle-Ages until nowadays. [Custódio 2000, Redol 2000]



Figure 1.2: Stained glass Windows in the abside (left) and colors reflected on the wall and on the stained glass windows (right) at Monastery of Santa Maria da Vitória in Batalha, Portugal (Joana Delgado ©).

1.2 – Glass production in the Middle-Ages: a short historical introduction

According to Jorge Custódio, the diffusion of the use of glass in houses and buildings is a medieval urban phenomenon, as it occurred in the context of the development of the cities during the Late Middle Ages and it was associated to the construction of the great medieval cathedrals and other edifications in the metropolises, being an innovation in the sense that allowed the isolation of the buildings maintaining a natural illumination. [Eco 1989, pp. 56-65; Custódio 2000]

On the first half of the 12th century Theophilus Presbyter, a Benedictin monk, wrote *De diversis artibus*, one of the most famous manuscripts describing the manufacturing and artistic techniques used to produce a stained-glass panel (amongst other techniques used in various applied arts). [Barroca 2002, pp. 288-289] The raw materials used in the production of glass were sand, ashes of plants (wood from trees such as beech – potash glass –, or from marine plants – soda glass) and colored by adding specific metallic oxides. It is important to mention that many times the color in the glass was granted involuntarily by impurities present in the raw materials. [Redol 2003] In figure 1.3, an illustration from a manuscript dated from the 15th century, the several phases of the production of glass objects are portrayed, from collecting the raw materials, the glass blowing and manufacture, to the inspection of the final pieces. [Raguin 2003]

Should you intend to make glass, first cut a quantity of beech-wood logs and dry them. Then burn them together in a clean spot, and, carefully collecting the ashes, take care that you mix no earth with them. (...)

Then take two parts of the ashes (...) and a third part of sand, carefully purged of earth and from the stones which you may have brought from the water, mix them in a clean place.

Theophilus, *De diversis artibus*
The second book, Chapter I and Chapter IV
[Presbyter 1979]

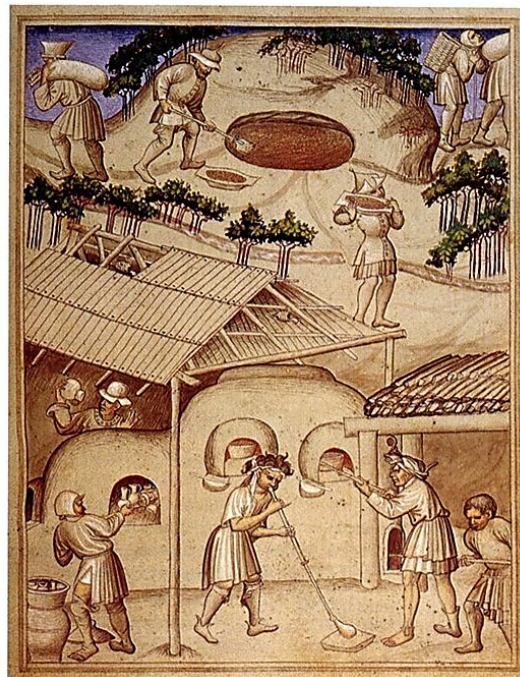


Figure 1.3: *The Pit of Memnon*, depicting glassblowing, from *The Travels of Sir John Mandeville* (p. 21-22, plate 27). Manuscript dated from the 15th century (British Library, Add. 24189, f.16). [Raguin 2003, p. 37]

There were two main methods to produce glass sheets, crown and cylinder, both glass blowing methods. With the blowpipe, a portion of fused glass is collected from the furnace, being immediately blown to form a hollow globe (figure 1.4 a). [Redol 2003] For the crown glass, this globe is transferred from the blowpipe to a punty and then reheated and flattened by spinning out the glass globe into a flat disk (figure 1.4 b and c). [Redol 2003] With this method, the resulting glass sheet has a round shape, with a variable thickness from the irregularly shaped center – called bullseye – to the edge, allowing a lower variety of dimensions and shapes when cutting the glass pieces, when compared to cylinder glass. [Redol 2003] As for the cylinder glass the globe is elongated into a cylinder, which is then cut lengthwise and separated from the blowpipe. After being cut, the cylinder is reheated to allow it to open and flatten into a glass sheet, later on smoothed with a piece of wood. This method allows obtaining much larger glass panes, with a more homogeneous surface. In both production techniques, the glass sheets need to be reheated and left to cool down slowly, to reduce tensions and avoid cracking. [Redol 2003, Navarro 2003]

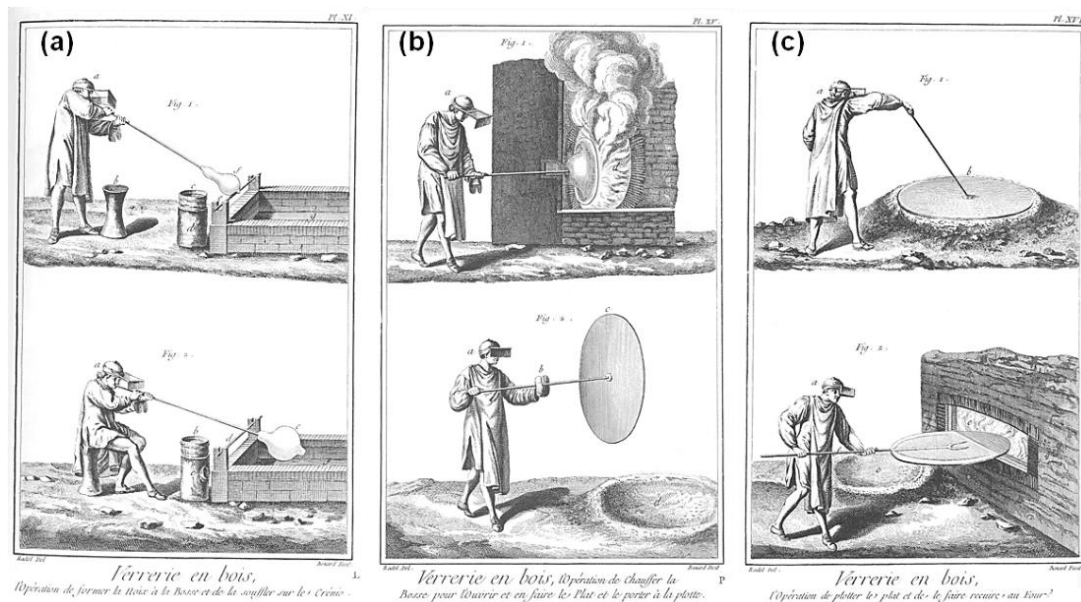


Figure 1.4: Different phases of the production of a crown glass plate. **(a)** Plate XI: Wood Glass Making, Operation of Shaping the Tip of the Ball and Blowing it over the Trough, **(b)** Plate XV: Wood Glass Making, Operation of Heating the Ball to Open it and Make the Pane and Carry it to the Embers Pit, **(c)** Plate XVI: Wood Glass Making, Operation of Placing the Pane in the Pit and of Refiring it in the Furnace. From *Planches d'Encyclopedie or Dictionnaire raisonnée des Arts et Metiers* by Diderot and D'Alembert [d'Ambert 2002].

1.3 – Nature and structure of medieval stained-glass

In *De diversis artibus*, Theophilus describes in what consists a stained glass window. These are produced by binding several colored glass pieces – some painted with *grisaille* – with a lead frame, which holds the pieces together and works as part of the composition as well. [Carmona 2009] *Grisaille* was the most used technique in stained-glass painting, and it was applied on the front – surface of the

glass facing the interior of the building. It is essentially a mixture of a flux (glass and lead oxide or lead rich glass) with metal powders of metal oxides (iron or copper), a mixture that is usually dark in color (brown or black) and highly pigmented. [Debitus 1991, Redol 2003, Schalm 2003] Then, the powder is mixed with a small amount of water and some binding compound – Arabic gum, for example – in order to obtain a paste that can be used to paint the glass. [Debitus 1991, Redol 2003, Schalm 2003] After dried, the fragments are fired at temperatures between 600 and 750° C in order to obtain the vitrification of the painting material, resulting in a connection between the glass surface and the flux (glass and lead oxide or lead rich glass), with the pigments in suspension [Debitus 1991, Redol 2003, Schalm 2003] (scheme presented in figure 1.5 (a)).

So ultimately, the final result is a lead reach glass, with particles of metals oxide (mainly iron or copper) in suspension in the matrix. [Debitus 1991] The ratio between the flux and the pigment may determine the adherence of the *grisaille* to the glass surface underneath [Veritá 1996, Schalm 2003], being the deterioration of the glass or of the flux one of the factors that can lead to the detachment of the paint layers. The decoration of the surface consisted mainly in dark trace lines combined with shades, used to depict faces and garments, architectural elements and landscapes, for example [Redol 2003]. The color and level of detail were variable, as in the examples presented in figure 1.5.

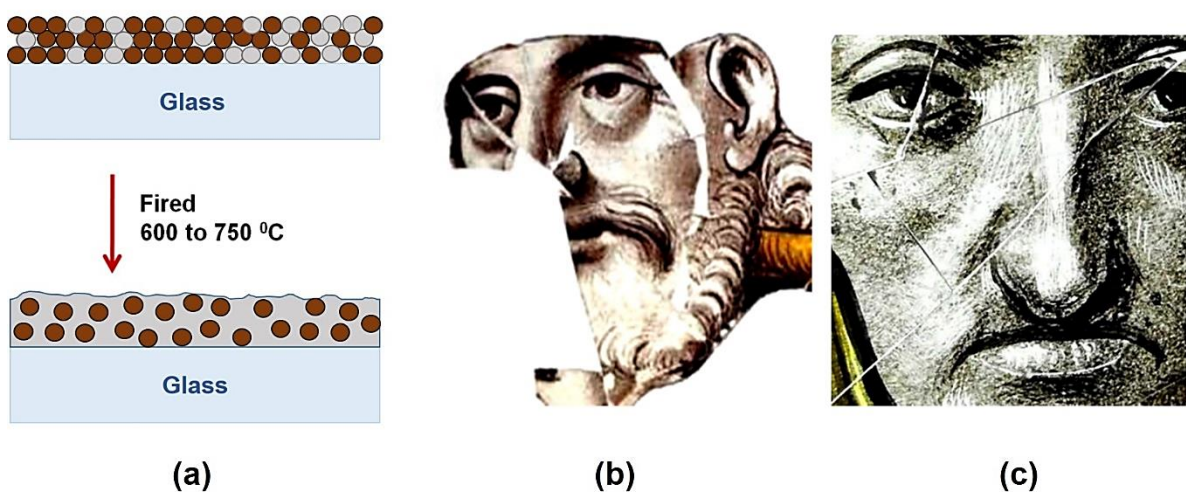


Figure 1.5: (a) Simplified scheme of the grisaille layer before and after the firing of the glass fragment (adapted from O. Schalm et al. [Schalm 2003]). (b) *Saint Joseph*, 16th c., Monastery of Batalha, Portugal (Paula Fernandes©) and (c) *Face detail*, 16th c., Convento de Cristo, Tomar, Portugal (Joana Delgado©).

In figure 1.6, a simplified methodology for the production of a stained glass panel following the technique used since the Middle Ages is presented, from creating the project to the assemblage of the panel, passing through the glass cutting and painting stages. A more detailed explanation of each step of the process can be found in the figure's description.



Figure 1.6: Methodology for making a stained glass panel. **(a)** In the first place, a full size cartoon is made, showing the lead lines around each glass fragment, as well as the colors and details to be painted on the glass; **(b)** then, the glass – colored or transparent – is cut to size, following the cut-lines from the cartoon; **(c)** also according to the cartoon, the *grisaille* painting is made, **(d)** using different tools and brushes, some of the details being made after the paint is dry. The fragments are fired in a kiln, for the paint – *grisaille*, yellow silver staining or, later on, enamels – to adhere to the glass surface. **(e)** By the time all the glass pieces are prepared, they are gathered on the cartoon, over a usually wooden base, and set together by lead came cut to size. **(f)** After completing this process, each junction is soldered, **(g)** and cemented on both sides in order to make the panel more resistant and waterproof, being left for a few days to harden. **(h)** Finally, the panel is complete. [Redol, 2003] These images are stills from the video “Making a stained glass panel”, that can be seen on the Victoria and Albert Museum website [<http://www.vam.ac.uk/content/videos/m/video-making-a-stained-glass-panel/>], V&A©.

1.4 – But what is glass?

James E. Shelby defines glass as “an amorphous solid completely lacking in long range, periodic atomic structure, and exhibiting a region of glass transformation behavior”. [Shelby 2005, p.3] Here, glass is an amorphous inorganic material that can be cooled below its super-cooling temperature and re-heated above it, without this causing the appearance of crystalline phases [Janssens 2013, p.8].

In the context of medieval stained glass, the main component of glass is silica, the network former (figure 1.7). The fusion temperature of pure silica is too high to allow a workable glass, and the energy needed to achieve such temperatures would be too expensive. As so, it is necessary to add a flux and a stabilizer – network modifiers, such as alkali and earth alkali compounds – (figure 1.7), that have a strong effect on the alteration of the glass final structure and properties. [Navarro 2003, Janssens 2013] The flux, usually a soda or potash ash traditionally made from burning marine plants, trees or ferns, helps to lower the fusion temperature; while the stabilizer – calcium oxide being one of the most common, in the form of limestone – will prevent the dissolution of the glass, as well as the formation of crystals, by avoiding phase separation/crystallization, conveying a better durability. [Navarro 2003, Shelby 2005]

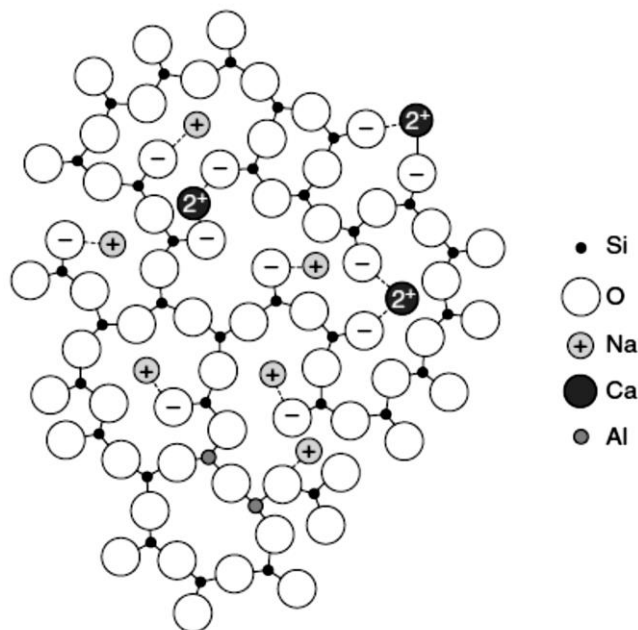


Figure 1.7: Example of a two dimensional structure of a soda-lime glass with a low content of Al_2O_3 . [Janssens 2013, p. 9]

However, if a glass has a higher amount of network modifiers, its stability is compromised; the higher the content of silica in a glass matrix, the higher the chemical stability and durability of the glass. [Navarro 2003] And from the 15th up to the mid-16th century, in Europe, the most commonly used glass in stained-glass windows was potash glass [Caen 2009]¹, which contains a high content of Na_2O (see figure 1.8).

¹ Though this work is focused on the Low Countries, it was a similar situation to the one in the Western Countries, where the most common glass used in the production of stained-glass windows was also potash glass.

In figure 1.8, a scheme is presented with a stratification of glass types according to composition. This was adapted from a O. Schalm et al. publication, being based on several published classifications² [Schalm 2010]. The first criteria to consider is the amount of PbO in the glass, if being superior to 15 wt%, the glass can be classified as lead glass. If it is inferior to 15 wt%, the wt% of Na₂O will be the next parameter to take into consideration, followed by the ratio of K₂O/Na₂O, depending on which the glass will be classified as: soda glass, mixed-alkali glass, potash glass or high lime low alkali (HLLA) glass.

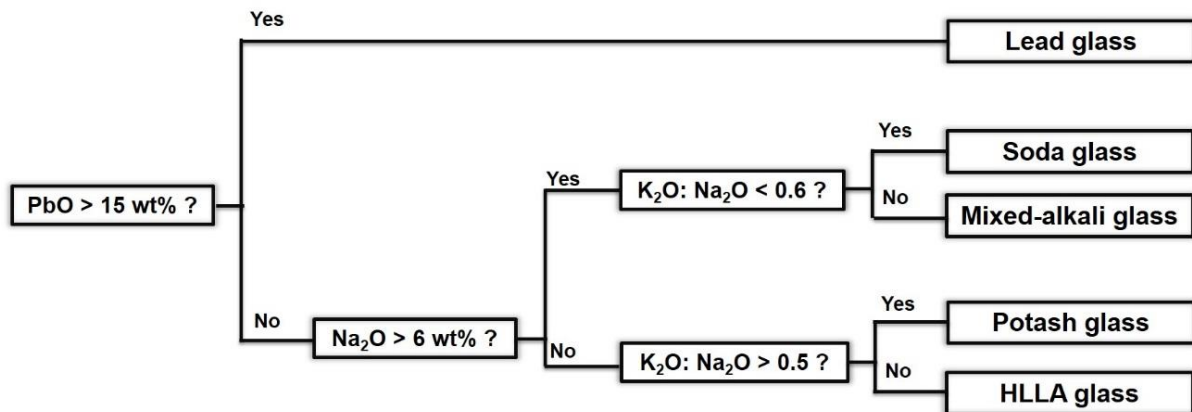


Figure 1.8: Classification of glass used in the production of window glass panes, based on their major composition [adapted from O. Schalm et al. 2010] Note: HLLA stands for High Lime Low Alkali glass.

In figure 1.9, the evolution of the most commonly used types of glass in the production of stained glass windows in Europe is presented. Potash and HLLA glass were the most common types of glass from the 15th to mid-18th century [Caen 2009], both types containing less than 6 wt% of Na₂O in its composition, and a wt% of CaO varying from 16 to 22 for potash glass and from 21 to 28 for HLLA glass [Schalm 2010].

² For more detailed information about the compositions and classifications used, some examples of publications referred in O. Schalm et al. are:

- Gratuze B., 1994, *Le verre : les éléments de réponses que peuvent proposer les méthodes de caractérisation physico-chimiques aux problématiques archéologiques posées par ce matériau*, Revue d'Archéométrie, 18 (1994) 75-87.
- Müller W., Torge M., Adam K., *Ratio of CaO/K₂O > 2 as evidence of a special Rhenish type of medieval stained glass*, Glasstechnische Berichte Glass Science and Technology, 67 (2) (1994) 45-48.
- Barrera J., Velde B., *A study of French medieval glass composition*, Archéologie médiévale, 19 (1989) 81-130.

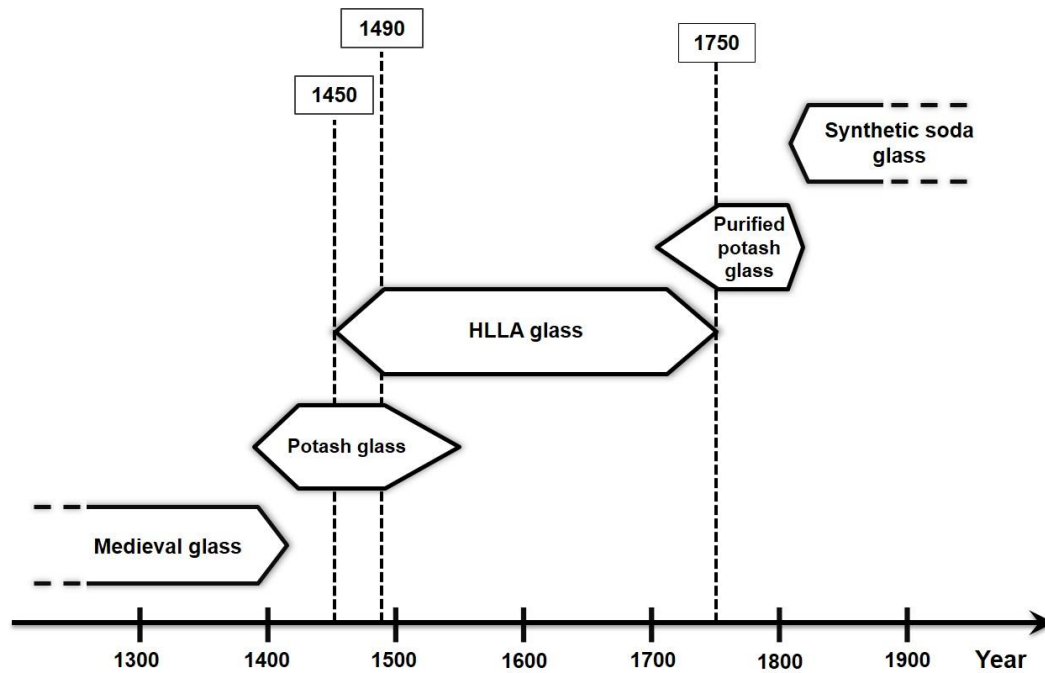


Figure 1.9: Types of glass more commonly used in the production of stained glass windows in Europe, from the 13th to the 20th century (image adapted from J. Caen, *The Production of stained glass in the county of Flanders and the Duchy of Brabant from the XVth to the XVIIIth centuries: materials and techniques*. Brepols, Antwerpen, 2009. Copyright © 2009 Brepols [Caen 2009]).

1.5 – Glass corrosion: mechanism of formation

The medieval stained-glass is composed by a high concentration of alkaline and alkaline-earth ions – mainly potassium, calcium and sodium – and low contents of silica compared with contemporary glass, being the chemical composition of medieval glass one of the main causes for its deterioration. [Newton 1989, Vilarigues 2004, De Bardi 2013, De Bardi 2013i] The other main cause is the presence of water, being temperature fluctuations, polluting agents and microorganism's effects other important factors. [Redol 2003, Vilarigues 2009]

The existence of water, whether in liquid or gaseous form, is enough to trigger the mechanism that will initiate glass corrosion formation. [Newton 1989, Clark 1992, Melcher 2010, Dohmen 2013, Janssens 2013] In figure 1.10, adapted from Melcher et al. [Melcher 2010], a proposed simplified mechanism is presented.

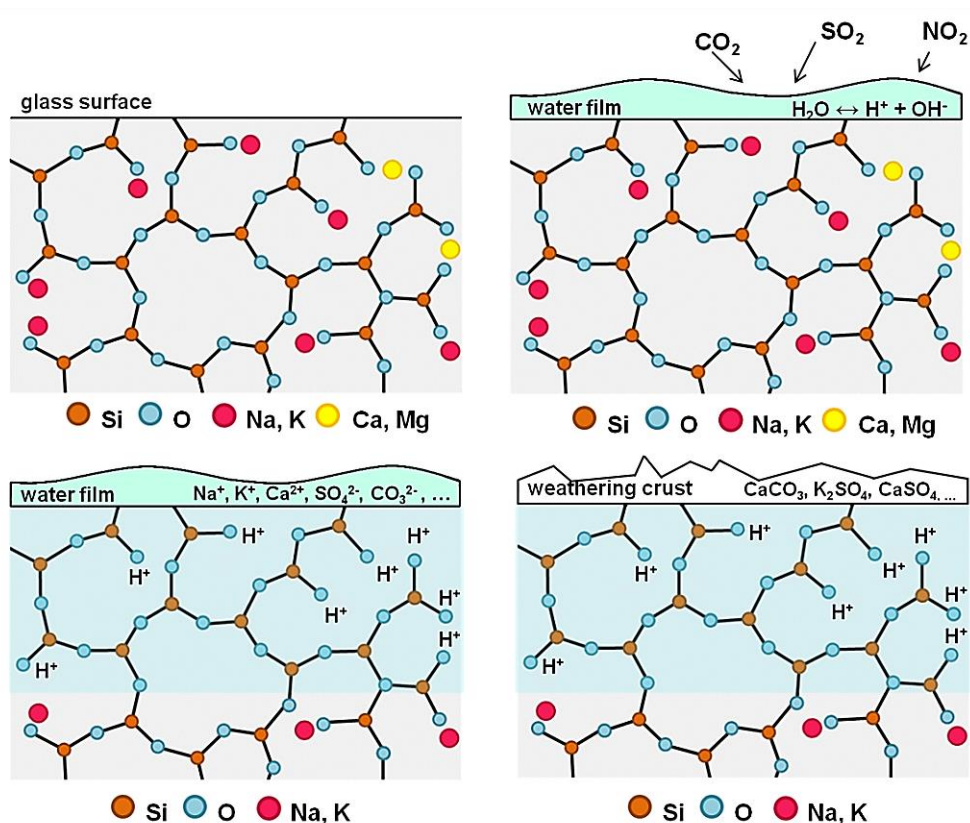


Figure 1.10: (a) Glass corrosion mechanism (weathering) starts with a clean and un-corroded surface. (b) The formation of a water film occurs, due to the atmospheric conditions, allowing ionic exchange between the ions H^+ and H_3O^+ of water and the alkaline ions present in glass, which may be reinforced by the presence of acid gases. (c) This lixiviation reaction starts slowly, but accelerates overtime; after the formation of a hydrated layer (light blue in the figure), rich in silica and alkaline oxides, (d) the glass surface becomes more resistant to the attack of water and the surface pH increases. The crystalline corrosion products (salts) stay in the glass surface after the water evaporates (adapted with permission from M. Melcher et al., *Degradation of Glass Artifacts: Application of Modern Surface Analytical Techniques*, Accounts of Chemical Research (2010), Copyright © 2010 American Chemical Society [Melcher 2010]).

In the presence of water, corrosion of glass will occur with the formation of a hydrated layer and lixiviation of ions of Ca^{2+} and K^+ . The presence of pollutant agents, such as CO_2 and SO_2 , will accelerate this process, and corrosion crusts are formed at the surface. These crusts are composed by insoluble salts, such as calcium carbonate ($CaCO_3$), calcium sulphate ($CaSO_4$) and calcium oxalate (CaC_2O_4), and others, which are very difficult to remove from the glass surfaces. [Newton 1989, Clark 1992, Carmona 2006, Cailleteau 2008, Vilarigues 2009] As can be seen in figure 1.10, where we can observe a simplified scheme of a proposed glass corrosion mechanism (weathering), in the presence of water, an ionic exchange between the ions H^+ and H_3O^+ and the alkaline and alkaline-earth ions present in glass will occur. In medieval glasses, where the percentage of potassium ions is high, this process is more intense than in soda-glasses. [Newton 1989, Clark 1992, Vilarigues 2006, Vilarigues 2009, Melcher 2010] The most common effects that corrosion can cause on the glass are the loss of transparency, the

loss of paint layers – such as *grisaille* –, and the loss of the glass material itself. [Romich 2000] The hydrated layer formed in the surface presents mechanical properties different from the original glass matrix, and with the fluctuation of relative humidity and temperature, tensions between both occur, which may lead to the formation of micro fissures that can develop through the entire glass surface. [Carmona 2006] In some cases there is also the formation of syngenite ($K_2Ca(SO_4)_2 \cdot H_2O$) and arcanite (K_2SO_4) [Tournié 2008, Machado 2010, Machado 2011].

In the figure below (figure 1.11), elementary maps of a cross-sectioned archaeological sample present a good example of the final stage of the corrosion process explained in figure 1.10. The hydrated layer, rich in Si and O, is clearly visible below the grisaille painting layer, rich in Fe, and right above this one there is a calcium corrosion crust, very noticeable as well.³

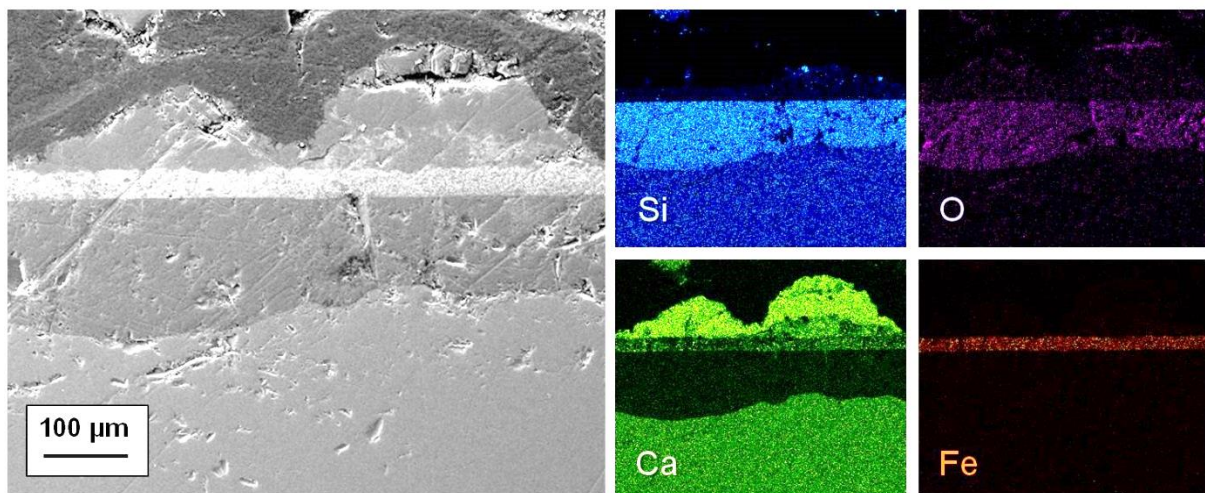


Figure 1.11: SEM-EDS elementary maps of a cross-sectioned archeological sample, presenting Si, O, Ca and Fe elementary maps. 150x magnification.

These corrosion crusts that cover the surface of the glass can be perceived as a protective layer [Romich 2003, Murcia-Mascarós 2008, Abd-Allah 2013], but, at the same time, are blocking the passage of light, one of the most important elements for a stained-glass panel. In figure 1.12 an example of a heavily corroded panel is presented. Having this into consideration, as well as the fact that the corrosion crust is, in essence, original material deteriorated and, as so, part of the history of the object itself, there is a balance that needs to be obtained between the preservation of the original material and

³ Note: this map and other similar ones will be presented and further discussed in Chapter 5, and more examples can also be found in Attachment III.

the preservation of the original essence of the stained-glass panel. It is very important to remember that any cleaning procedure should remove the corrosion deposits only as far as necessary to improve the transparency, without damaging the hydrated glass surface underneath as the gel-layer protects the glass beneath. A thin residual layer should be left on the surface, rather than removing the crust down to the bulk glass, which would trigger further degradation. Special attention is necessary when cleaning painted areas, since the loss of paint would irreversibly damage the artistic integrity of the stained-glass. [Romich 2000, Romich 2003, Murcia-Mascarós 2008, Abd-Allah 2013]



Figure 1.12: *Figura aureolada*, 15th century stained-glass panel from the Monastery of Batalha, Portugal. Exterior side, reflected and transmitted light (left) and reflected light (right) (Joana Delgado ©). Dimensions: 70 x 31.2 cm².

The stained-glass panel presented in the figure above (1.12) is one of several from the collection of 15th century stained-glass panels from the Monastery of Batalha, some of the earliest examples of this type of object known in Portugal [Barros 1988, Redol 2003]. Most of the fragments in this panel are corroded: in some areas the corrosion crusts are rendering the visibility of the painted layer quite difficult, and in general these end up disturbing the global observation of this panel in all its splendor.

1.6 – Glass cleaning: State of the art in cleaning technology

One of the most important, but also delicate, phases in the conservation practice is the cleaning process, no matter what is the material **[Murcia-Mascarós 2008]**. It is essential to maintain or increase the chemical stability of the treated object. It is very important to remember that any cleaning procedure should remove the corrosion deposits only as far as necessary to improve the transparency, without damaging the hydrated glass surface underneath. A thin residual layer should be left on the surface, rather than removing the crust down to the bulk glass, which would trigger further degradation. The gel-layer must not be damaged, as it can protect the glass beneath. **[Romich 2000]** Special attention is necessary when cleaning painted areas, since the loss of paint would irreversibly damage the artistic integrity of the stained-glass. As so, the objective is to reduce or stabilize the weathering process and to improve the readability of the object.

A variety of mechanical and chemical methods is currently used in restoration practice. The mechanical methods include the scalpel, bristle brushes and glass-fiber brushes, among others, and the chemical methods go from the use of water, usually in combination with ethanol (water:ethanol, 1:1 [v/v]), to organic solutions. However, those that present a higher efficiency in removing or diminishing the corrosion crusts are the same that may induce damage or long-term risks to the glass surface. These are the application of chelant agents, such as ethylenediaminetetraacetic acid (EDTA), weak acids and ionic resins. **[Romich 2000, Altavilla 2008, Abd-Allah 2013]** Depending on the conditions of the glass surface, these products may cause irreversible damage. The consequences of the application are also difficult to control, and it is complicated to evaluate if all the remains of product are completely removed after the treatment, presenting an aggravated risk to the glass surface. **[Romich 2000]**

Previous studies describe the use of an excimer-laser (operating at 248 nm) for cleaning stained glass windows **[Klein 1999, Romich 2000i, Romich 2003, Hildenhagen 2003, Hildenhagen 2003i, Sokhan 2003, Fekrsanati 2000]**. Of particular interest is the good results presented regarding the removal of corrosion crusts without damaging the glass surface or the gel-layer **[Romich 2003]**, which was confirmed by light microscopy, electron microscopy and infrared spectroscopy **[Romich 2000i, Romich 2003]**. The conclusion of these studies was that this method could, indeed, be used for stained glass cleaning, although within limits. **[Romich 2003]** However, the papers describing these results were an outcome of a European project in the early 2000's. Either because of the high cost of the equipment, that also needs a qualified technician for handling, or for the requirement of more extensive short and long-term tests, this method does not seem to be as generally used nowadays as its promising results would indicate.

1.7 – Ionic liquids: Introducing a new alternative

The development of cleaning methods that are effective and harmless for the work of art but also less harmful to health and the environment are major concerns of conservators/restorers. Therefore, the possibility of replacing volatile and toxic organic solvents by ionic liquids (ILs) could contribute to safer procedures.

A more detailed description on ILs and its characteristics will be given in Chapter 2. However, these compounds possess interesting characteristics, such as the possibility to tune their solubility and viscosity depending on the polarity and functional groups of cation/anion combinations, which make them attractive for many different applications [Branco 2002]. Preliminary studies showed some efficiency of ILs for the gentle cleaning of the corrosion products from the surface of the glass, without damage, through control of its viscosity and solubility properties. [Machado 2010]

New approaches provided by modern chemistry were explored during this project, such as the use of ILs as an alternative non-toxic solvent. ILs are defined as organic salts formed by a combination of an organic cation and organic or inorganic anion with a melting point below 100°C. [Johnson 2007] Recently, patents describing the use of ionic liquids for surface cleaning were published [Patent A1 2006, Patent A2 2006, Patent 2010] Of special importance is patent WO2010040917A1 [Patent 2010] that describes the use of a protic imidazolium room temperature ionic liquid (RTIL) for the cleaning of surfaces such as metals, ceramics and glass contaminated with oil, grease or soil.

Organic aromatic compounds often exhibit fluorescence emission when irradiated with UV light. Some of those compounds are sensitive to the environment, responding to effects such as temperature or the presence of metal cations such as calcium. Examples of several fluorescent compounds (e.g., coumarins, rhodamines and fluoresceins molecules) are described in the literature for the sequestration of calcium cations in biomedical applications [Silva 1997]. Some of these molecules allow the possibility to have negative charge (anionic), and therefore they may be combined with organic cations that are known to give rise to ILs. These intrinsic luminescent ILs are a new type of luminescent material that was described recently [Tang 2008], but to best of our knowledge there are still no published examples of luminescent ionic liquids able to dissolve inorganic salts such as CaCO₃.

So being, luminescent ILs designed for removing stained glass calcium corrosion crusts were developed and tested, being imperative that these ILs are both effective in removing the crusts and harmless for the glass surface. The development and characterization of these ILs, as well as the tests performed in model glass samples and archaeological stained glass fragments, is described in the following chapters.

Chapter 2

Ionic Liquids

As explained before, the intention of this project is to develop a new task specific luminescent ionic liquid for the removal of insoluble stained glass corrosion crusts. Being these crusts mainly composed by calcium salts, enabling the solubilization of the corrosion crusts soluble and consequently an easy removal from of easily removed from the glass surface. That is also what happens with EDTA, a strong chelating agent, which will not only bind with the calcium ions present in the corrosion crusts, but also with the calcium present in the glass surface, as a composing element of this material (see Chapter 1.5).

So being, the selected molecules must have a weaker chelating power than EDTA, in order to have a milder effect on corrosion crusts, and especially on the glass surface. It is also important to have intrinsically luminescent ionic liquids allowing the detection of their presence after the cleaning procedure. The viscosity is also of extreme importance, as compound with a low viscosity is more difficult to situate and control during the treatment. Another important requested characteristic is related to the solubility of ionic liquid (IL) in water or in a less toxic organic solvent (e.g. ethanol), making the removal of the ILs from the glass surface after the treatment harmless for the conservator, for the object and for the environment

In this chapter, a brief introduction about ionic liquid topic including their peculiar properties and potential applications will be given, in order to put into context and justify why these class of compounds have been chosen for the specific purpose of this project. Then, a general description of the synthetic methodology and characterization of the intrinsically luminescent ILs, in particular: trihexyltetradecylphosphonium 1-anilino-naphthalene 8-sulfonate, $[P_{6,6,6,14}][ANS]$, 1-[2-(2-Methoxyethoxy)ethyl]-3-methylimidazolium 1-anilino-naphthalene 8-sulfonate, $[C_5O_2MIM][ANS]$, and trihexyltetradecylphosphonium 1-pyrene carboxylate, $[P_{6,6,6,14}][PyrCOO]$, will be presented. These ILs were considered the ones with the most promising characteristics – good viscosity, chemical stability and bright fluorescence – in order to perform the tests in the glass samples, described in Chapters 4 and 5.

2.1 – What is an ionic liquid? Ionic liquids properties and advantages

In the past few years, ionic liquids have been largely studied, and their large range of possible applications was widely explored. Ionic liquids are composed by an organic cation and an organic or inorganic anion, they are liquid at temperatures under 100 °C and present some peculiar and tunable characteristics, such as their negligible vapour pressure, a high ionic conductivity, higher chemical and thermal stability and a considerable capacity to solubilise organic, inorganic and polymeric materials. [Freemantle 2009, Branco 2011, Wasserscheid 2007]

Recently, novel generations of ILs were developed, in which a cation or anion is chosen in order to obtain ILs with specific physical, chemical or biological functions, usually called task specific ionic liquids. **[Kulkarni 2007, Wasserscheid 2007, Branco 2009, Freemantle 2009, Branco 2011, Branco 2011i, Ferraz 2011, Hallett 2011, Kokorin 2011, Branco 2013]**

The first known IL was reported by Walden in 1914 and was an ethylammonium nitrate **[Walden 1914]**. The main composition of the first generation of ILs was cations like dialkylimidazolium and alkylpyridinium, and toxic and non-biodegradable anions such as metal halides (e.g. chloroaluminate). **[Tavares 2013]** This first generation was mostly focused on substituting organic solvents, toxic and volatile, by an alternative solvent to be used in synthesis and catalysis operations. **[Tavares 2013]** The first room temperature IL (RTIL) was reported in 1982 by Wilkes et al. **[Wilkes 1982, Faridbod 2011]**, and since then a big variety of ILs containing various cations and anions has been synthesized.

Consequently, a second generation of ILs appeared, composed by more biocompatible cations and anions **[Bogel-Lukasik 2015]** and presenting lower melting points and other interesting tunable properties that lead to the widespread of their use in many different fields, facing a significant boost in the 1990's. This second generation still presents a level of toxicity comparable to aromatic solvents, which is a disadvantage. **[Tavares 2013, Bogel-Lukasik 2015]**

A last generation of ILs, the third, can be defined by the use of biocompatible cations and anions, which allowed the exploration of the possibilities of its use for pharmaceutical and biological purposes **[Sekhon 2011, Marrucho 2014]**. This is based in more hydrophobic and stable anions, also characterized by its biodegradability and low toxicity. **[Tavares 2013]**

ILs are mostly used as solvents, but its applications are vast, spreading through different fields, from electrochemistry to engineering, analytic techniques to biological uses, and the field is growing exponentially, partially thanks to a positively close cooperation between academia and industry. **[Wilkes 2002, Pechkova 2008]**

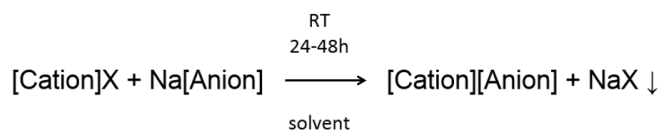
Within this framework, intrinsically luminescent ionic liquids were also developed, where usually the anion is the luminescent molecule. These ILs represent a new approach for the development of photochemically active materials. The common method would be to dissolve photochromic **[Pina 2007, Pina 2011]** or photoluminescent compounds **[Karmakar 2002, Hu 2006]** in neat ILs. However, some groups have described the possible combination of specific molecules such as metal complexes **[Tang 2008, Gago 2013, Pereira 2013]**, fluorescein **[Rodrigues 2013]** and anthracene derivatives **[Babu 2013]** with appropriate organic cations giving intrinsic luminescent ILs. Potentially these ILs may have applications in, e.g., foldable light emitting devices, solar cells or fluorescence sensors. **[Gago 2013]**

To sum up, ILs are organic salts composed by a variety of possible cation/anion combinations which can influence their physical, chemical and thermal properties as well as their range of applications. For the specific purpose of this project, their solubility in water and other organic solvents and viscosity can be modulated according our final interest.

2.2 – Ionic liquids synthesis

2.2.1 – Synthesis method

The method used to synthesize the ILs was a traditional ionic exchange method, as illustrated and described below. In general, the selected cation was dissolved in an appropriate solvent, such as dichloromethane (or another solvent that can be efficient to solubilize the starting materials and simplify the final purification of the product) in slight defect (1:1.1 mol) in relation to anion, in order to force the reaction to occur. Then, this solution is added to a room temperature (RT) solution of the anion using the same solvent and left stirring during at least 24 hours at room temperature. Then, the solution is purified by simple filtration of insoluble inorganic salts (e.g. ammonia chloride or sodium chloride) using the same organic solvent. After this purification, the solvent is removed in rotary evaporator and the final product is dried in vacuum for 24 hours.



2.2.2 – Equipment and methods

Nuclear Magnetic Resonance (NMR) spectra were done on a Bruker AMX 400 instrument operating at 400.13 MHz (1H) and 100.61 MHz (13C). Temperature effects were monitored submitting the sample to successive heating steps up to 85°C followed by similar stepwise cooling. Temperatures quoted were those presented in the spectrometer temperature control unit.

Fourier Transform InfraRed (FTIR) spectra were recorded on a Buker Tensor 27, using NaCl cells for the deposition of RTIL as a stable film.

Elemental Analysis (C, H, N) analysis was obtained on a Thermofinnigan Flash EA 1112 Series instrument by the Laboratório de Análises at REQUIMTE, FCT/UNL.

Differential Scanning Calorimetry (DSC) analysis was carried out using a Setaram, model DSC 131 with a refrigerated cooling system. The temperature range was from -100 to 100 °C and the scanning rates were 10 °C/min. The resolution is ±0.2 μW. The sample is continuously purged with 50 ml/min nitrogen. About 5-10mg of salt was crimped in an aluminium standard sample pan with lid. Glass transition temperature (T_g) were determinate in the second heating.

Spectroscopic measurements. UV/Vis absorbance spectra were performed using a UV-Vis-NIR spectrophotometer Varian Cary 5000 (spectral range from 300 to 800 nm). Luminescence spectra were measured using a SPEX Fluorolog-3 Model FL3-22 spectrofluorimeter, with 2 nm slits with controlled temperature with an external bath. Phosphorescence lifetime measurement was run on a LKS.60 nanosecond laser photolysis spectrometer from Applied Photophysics, with a Brilliant Q-Switch Nd-YAG

laser from Quantel, using the second harmonic ($\lambda_{exc}=355$ nm, laser pulse half-width equal to 6 ns). An optical cut-off filter (570 nm) for the emitted light was used in order to avoid scattering light contamination. Fluorescence lifetimes (τ) were measured via time correlated single photon counting technique (TCSPC) using a home-built equipment. The samples were excited at 373 nm using a nanoled (IBH). The electronic start pulses were shaped in a constant fraction discriminator (Canberra 2126) and directed to a time to amplitude converter (TAC, Canberra 2145). Emission wavelength was selected by a monochromator (Oriel 77250) imaged in a fast photomultiplier (9814B Electron Tubes Inc.), the PM signal was shaped as before and delayed before entering the TAC as stop pulses. The analogue TAC signals were digitized (ADC, ND582) and stored in multichannel analyzer installed in a PC. Temperature control was performed with a water bath connected to the spectrophotometer, with an approximate accuracy of ± 1 °C.

2.2.3 – Ionic liquids synthesized

A wide range of non-luminescent ionic liquids was synthesized during the course of this project. The tables 2.1 and 2.2 include information about the cations and anions used in the synthesis of the ILs that were tested in the course of this project, being the results presented in chapters 4 and 5. The prices of each compound are also presented, because this was one of the factors taken into consideration, as having a relatively cheap alternative was also one of the goals.

Table 2.1: Detailed information about the cations used.

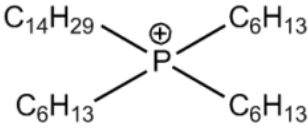
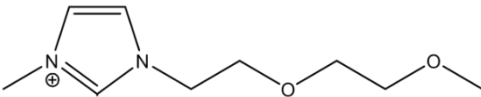
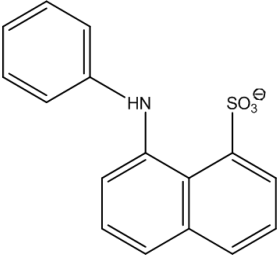
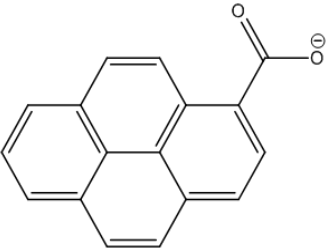
Cation, commercial name and molecular formula	Chemical structure (without Cl ⁻)	Brand, reference and price (in 25 th January 2016)
<p>[P_{6,6,6,14}][Cl]</p> <p>[CH₃(CH₂)₅]₃P(CH₂)₁₃CH₃Cl Trihexyltetradecylphosphonium chloride</p> <p>MW= 519.31 g/mol</p>		<p>Cytec Sigma-Aldrich CAS number 258864-54-9</p> <p>5 g / 16.5 €</p>
<p>[C₅O₂MIM][Cl] or [C₅O₂MIM][BF₄]</p> <p>C₂₅H₂₉N₃O₅ 1-[2-(2-Methoxyethoxy)ethyl]-3-methylimidazolium</p> <p>MW= 220.70 g/mol (Cl) MW= 272.05 g/mol (BF₄)</p>		<p>Solchemar</p> <p>25g / 85 € (Cl) 5g / 79 € (BF₄)</p>

Table 2.2: Detailed information about the anions used.

Anion, commercial name and molecular formula	Chemical structure (without H⁺/NH₄⁺)	Brand, reference and price (in 25th January 2016)
<p>[ANS] C₁₆H₁₃NO₃S · NH₃</p> <p>8-Anilino-1-naphthalenesulfonic acid ammonium salt</p> <p>MW= 316.37 g/mol</p>		<p>Fluka (purchased at Sigma) CAS number 28836-03-5</p> <p>100 g / 38.90 €</p>
<p>[PyrCOO]</p> <p>C₁₇H₁₀O₂</p> <p>1-Pyrenecarboxylic acid</p> <p>MW= 246.26 g/mol</p>		<p>Sigma-Aldrich CAS number 19694-02-1</p> <p>1 g / 67.60 €</p>

The ionic liquid that presented the characteristics that seemed to suit better the purposes of this project was the [P_{6,6,6,14}][ANS] ionic liquid, that was extensively characterized, and later used in several tests, presented in Chapters 4 and 5. In these tests, the [P_{6,6,6,14}][ANS] IL was also compared to [P_{6,6,6,14}][PyrCOO] and [C₅O₂MIM][ANS], and so these three ionic liquids are characterized in the following points.

2.3.3 – Why these molecules?

All the molecules chosen as anions have a fluorescent molecular component and a molecular component to interact with ions, such as calcium cations, Ca²⁺. The purpose was to have a slight chelating effect, but assuring that the ions would not have a quenching effect on the luminescence of the compound. In figure 2.1, the two anions selected are presented, with the functional groups that interact with ions highlighted.

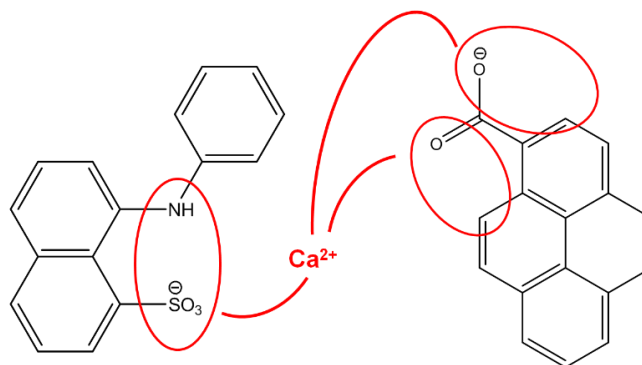


Figure 2.1: Functional groups from [ANS] and [PyrCOO] anions molecules where the calcium ions will likely bind.

Looking at the cation molecules, the phosphonium cation, [P_{6,6,6,14}] is not expected to interact with Ca²⁺, unlike the [C₅O₂MIM] molecule (see figure 2.2), which is an indicator that an IL that contains this molecule as a cation will probably be more efficient removing calcium corrosion crusts, having a higher chelating power. However, sulfonate groups generally have relatively low formation constants, especially when compared with EDTA. [Harris 2007] An ionic liquid with the [C₅O₂MIM] molecule will also be more easily dissolved in water than one using the hydrophobic [P_{6,6,6,14}] molecule.

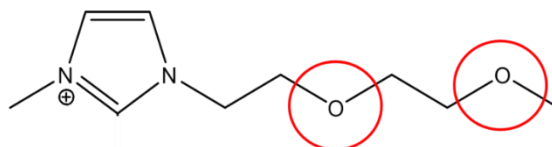


Figure 2.2: Functional groups in the [C₅O₂MIM] cation molecule more probable to form a link with calcium ions.

On the contrary, EDTA has a very high formation constant, namely with Ca²⁺ ions – 10.65 log K_f⁴ [Harris 2007]. Below it is presented the EDTA molecule (figure 2.3), for comparative purposes. This is a chelating agent used to remove corrosion crusts from glass objects, as mentioned in chapter 1.6.

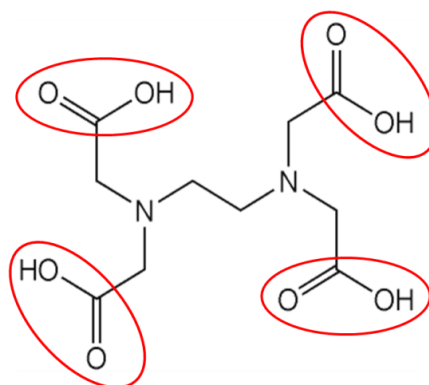


Figure 2.3: EDTA molecule with the indication of the areas likely to bind with calcium ions.

⁴ Note from the author D.C. Harris: the stability constant is the equilibrium constant for the reaction: $M^{n+} + Y^{4-} \leftrightarrow MY^{n-4}$ at 25 °C and ionic strength 0.1 M. [Harris 2007]

2.3 – [P_{6,6,6,14}][ANS] characterization

An intrinsically luminescent room temperature ionic liquid (RTIL) was prepared by adequate combination of phosphonium cation with a very common and largely studied fluorescent molecule, 8-anilinonaphthalene-1-sulfonate; ANS (figure 2.4). [P_{6,6,6,14}] cation is hydrophobic aliphatic molecule and presents a localized charge in the phosphorus atom. ANS is used as fluorescence probe of biological macromolecules such as proteins [Brand 1972], due to its sensitivity to solvent effects such as polarity and viscosity [Seliskar 1971, Kosower 1975, DeToma 1976, Robinson 1978, Sadkowski 1980, Huppert 1981, Nakamura 1981, Kosower 1982, Drew 1983, Kosower 1983, Ebbesen 1989, Upadhyay 1995, Tong 1996]. A charge-transfer emission band shifts strongly the ANS fluorescence to red by increasing the solvent polarity, namely from about 463.2 nm in solvents such as dioxane to 530 nm in water. [Huppert 1981, Kosower 1982, Drew 1983, Kosower 1983] This also results in a loss of visibility of the fluorescence with the increase of the polarity of the solvent where the ANS is dissolved due to a decrease of the fluorescence efficiency.

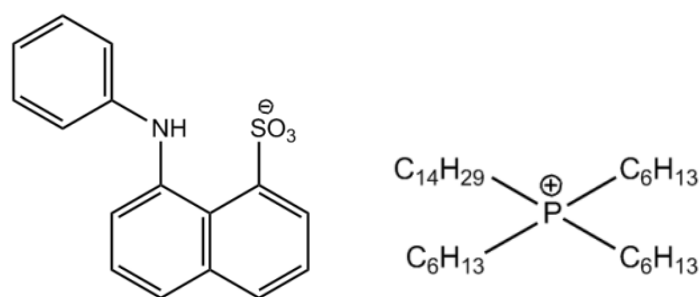


Figure 2.4: Molecular structures of [ANS] anion and [P_{6,6,6,14}] cation.

As the fluorescent quantum yield, excited-state lifetimes also decrease with increasing solvent polarity. ANS was previously used as solvation dynamics probes by studying the shifts of the emission spectra with time-resolved fluorescence techniques. [Bagchi 1984, Castner 1987] The excited-state dynamics is dominated by a locally excited state (LE) with rather low Stokes Shift dominant in non-polar solvents and a charge-transfer (CT) emission dominant in polar solvents responsible for the solvatochromic effect of the fluorescence. [Huppert 1981, Nakamura 1981, Drew 1983, Kosower 1983] Nevertheless, single-exponential fluorescence decays are only observed in low viscous solvents, otherwise solvation dynamics is in the nanosecond timescale, analogous to the ANS excited-state lifetime giving non-exponential decays. The fluorescence decays and rheology of this IL, amongst other characteristics, were more extensively explored in the published paper by Delgado *et al.* [Delgado 2015], but not all will be described here, as for this specific project and purposes these developments and characteristics are not as relevant.

Therefore, *a priori* a luminescent ionic liquid with ANS as anion may reveal some of the general properties of ILs such as viscosity or polarity. In order to illustrate the potential of this new luminescent RTIL, detailed photochemical studies, complementary temperature dependence $^1\text{H-NMR}$ and rheological studies were performed in order to better understand the ion-ion interactions (such as electrostatic or hydrogen bonding) and its impact on either macroscopic properties (viscosity) or molecular properties (in this case, ANS photophysics behaviour).

2.3.1 – Synthesis of $[\text{P}_{6,6,6,14}][\text{ANS}]$

A novel room temperature ionic liquid (RTIL), based on the combination of $[\text{P}_{6,6,6,14}]\text{Cl}$ as a cation and luminescent compound, $\text{NH}_4[\text{ANS}]$, as an anion was efficiently prepared and purified. $[\text{P}_{6,6,6,14}][\text{ANS}]$ as RTIL was obtained in quantitative yield using an optimized ion exchange methodology.

In particular, 1-anilino-sulfonate ammonia ($\text{NH}_4[\text{ANS}]$) was dissolved in appropriate solvent (e.g. dichloromethane or dry acetone) and then added to a trihexyltetradecylphosphonium chloride ($[\text{P}_{6,6,6,14}]\text{Cl}$) solution at room temperature. The purification method is efficient by simple filtration of unsolved inorganic salts (e.g. ammonia chloride) in the same organic solvent. The selection of an appropriate organic solvent that solubilize both starting salts and precipitate the inorganic salt (ammonium chloride) is relevant in order to obtain a high pure product. The desired pure product was obtained as a dark green and viscous RTIL displaying turquoise blue photoluminescence under UV light as shown in figure 2.5.

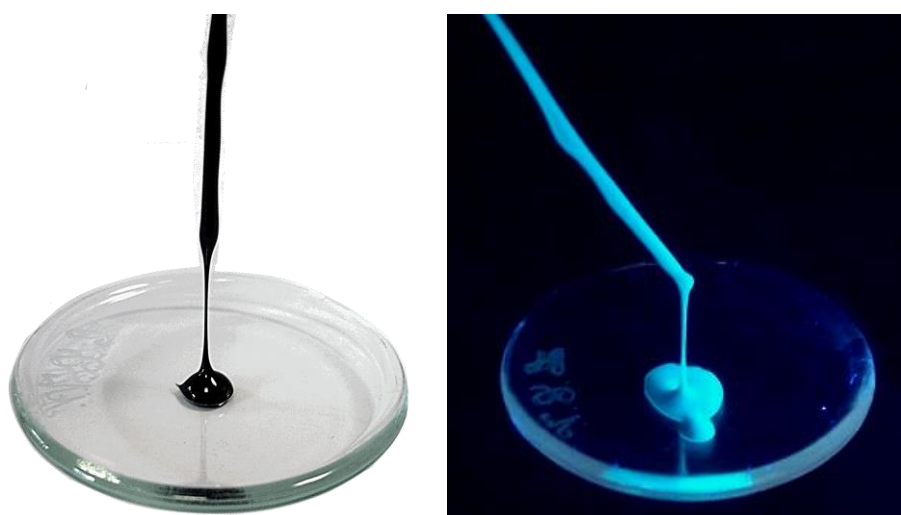


Figure 2.5: $[\text{P}_{6,6,6,14}][\text{ANS}]$ in daylight and under UV light, 365 nm.

Experimental Procedure of RTIL [P_{6,6,6,14}][ANS]: [P_{6,6,6,14}][Cl] (1.376 g; 3.85*10⁻³ mol) was dissolved in dichloromethane (20 mL) and then 8-anilino-1-naphthalenesulfonic acid ammonium salt, [NH₄][ANS] (1.00 g, 3.16*10⁻³ mol) was added to the reaction mixture. The reaction mixture was stirred at room temperature for 24 hours. Then, resulted mixture was filtered and the solvent was removed using the rotary evaporator. The final desired pure product was dried in vacuum for 24 hours and obtained as a dark green viscous liquid (2.21 g; 99%). The purity of the final product was verified by NMR and FTIR analysis.⁵

2.3.2 – Characterization of the IL [P_{6,6,6,14}][ANS]

The refraction index at 26.85 °C (300 K) is 1.534 and the density is 0.9984 g.cm⁻³ at 25.25 °C (298.4 K). ¹H or ¹³C NMR and FTIR techniques as well as elemental analysis were used in order to characterize the novel luminescent RTIL. NMR spectra allowed to proof the expected purity and chemical stability of the RTIL as well as the adequate cation:anion (1:1) proportion. FTIR spectra identify some characteristic bands such as the one located at 1238 cm⁻¹ attributed to the sulfonated group from anion, pointing out to specific electrostatic interactions with cations.

2.3.3 – DSC and rheology studies

DSC measurements reveal a clear glass transition temperature at T_g = 223.7 K in both cooling and heating cycles with a rate of 10 °C/min (figure 2.6 (a)). It is important to note that no crystallization (or melting temperature) was observed for different measurement experiments. In this context, [P_{6,6,6,14}][ANS] can be defined as a room temperature ionic liquid. On the other hand, the rheological studies revealed some interesting features. The [P_{6,6,6,14}][ANS] exhibit a Newtonian behaviour (n=1, from power law equation), corresponding a viscosity value of 4.87x10⁻⁴ Pa.s, at 25°C. The heating experiments from -5 °C to 80 °C (figure 2.6 (b)) showed the usual viscosity profile as a glass forming liquids and the data could be fitted with the Vogel-Tammann-Fulcher (VTF) equation [Bohmer 1993]:

$$\eta = \eta_0 \exp\left(\frac{B'}{T - T_0}\right) \quad (1)$$

⁵ Note: ¹H-NMR (400.13 MHz, CDCl₃) δ= 8.48 (d, J=8.00 Hz,1H), 7.81 (d, J = 8.00 Hz, 1H), 7.61 (d, J = 8.01 Hz, 1H), 7.44 (d, J = 4.02 Hz,1H), 7.32 (t, J = 4.00 Hz, 2H), 7.27 (t, J = 8.00 Hz, 2H), 7.17 (t, J = 8.01 Hz, 2H), 6.80 (t, J = 8.01 Hz, 1H),2.02 (m, 8H), 1.32-1.28 (m, 48H), 0.86 (m,12H); ¹³C-NMR (100.62 MHz, CDCl₃) δ=144.57, 141.55, 136.88, 132.02, 128.86, 128.09, 125.81, 124.11, 123.30, 122.84, 120.03, 118.06, 31.86, 31.06, 30.35, 30.15, 29.64, 29.37, 28.93, 22.74, 22.32, 21.79, 19.06, 18.53, 14.13, 13.94 ppm; FTIR (NaCl): 3267, 3052, 2926, 2858, 2361, 1927, 1599, 1561, 1497, 1452, 1350, 1309, 1234, 1181, 1109, 1033, 873, 819, 751, 700, 636, 581 cm⁻¹.

where η is the liquid viscosity, η_0 , B' and T_0 are empirical parameters. The fitting parameters gives T_g - $T_0=29.1$ K, which is nicely in fair agreement with the general empirical expectation for this value (40 K). The RTIL displays a Newtonian behaviour as well. However the cooling cycle yielded an unexpected result: around 20°C the measured viscosities diverged from the heating cycle reaching values one order of magnitude greater than those from the heating cycle at 0°C and clearly away from the VTF equation. This experiment was repeated three times, giving exactly the same results for both cycles, while DSC measurements do not offer an explanation for this odd result.

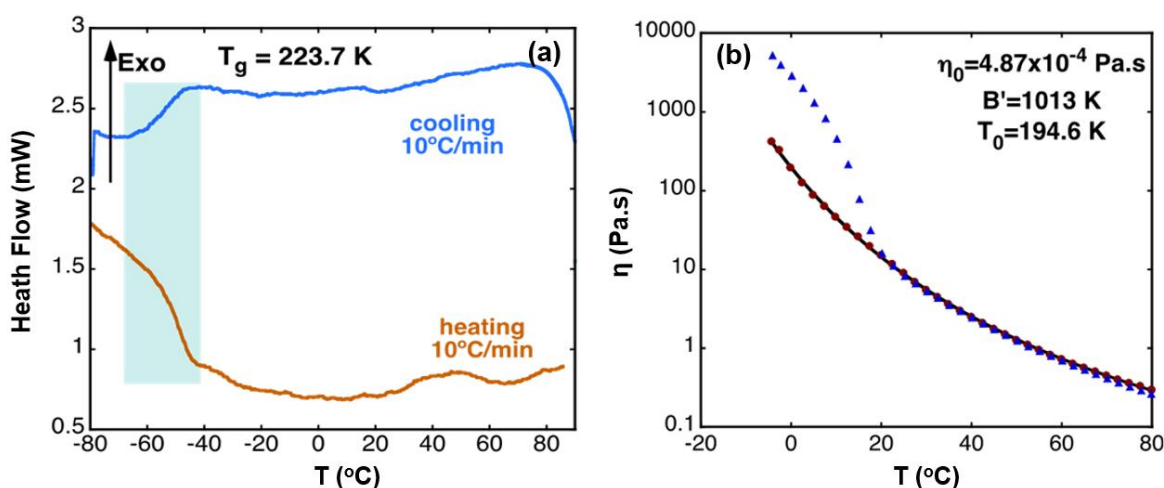


Figure 2.6: (a) DSC measurements of [P_{6,6,6,14}][ANS] and (b) viscosity of [P_{6,6,6,14}][ANS] in heating (circles) and cooling (triangles) cycle. Viscosity values of the heating cycle were fitted with the VTF equation (see text) giving the parameters inserted in the figure.

2.3.4 – Contact angle

The contact angle of the IL on a glass surface was measured over time. A small drop was placed on the surface of a model glass sample (the composition and characteristics of this glass will be described in chapter 3), and the contact angle of the drop with the glass sample was measured, being taken a measurement every 2 seconds during 118 seconds (60 measurements in total). The contact angle presented is the average between the right and left contact angles. This experiment was repeated four times, always with the same results.

In figure 2.7, this kinetic is presented. It is possible to observe that in the first thirty seconds after the application of the drop on the surface, the contact angle decreases more than half (from 64° to 28°), starting to stabilize, which eventually happens after 80 seconds at about 16°. On the images in figure 2.7, this variation becomes clearer.

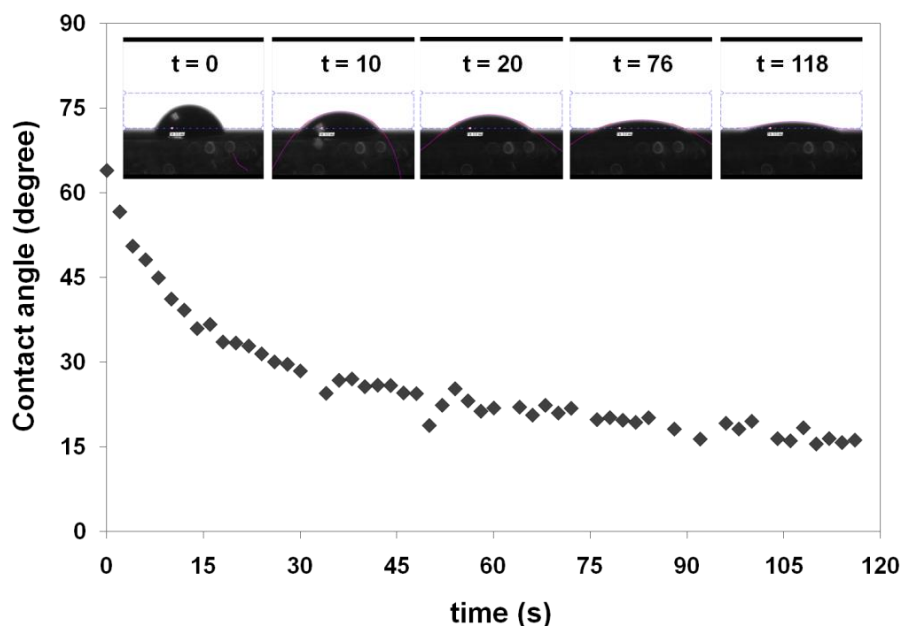


Figure 2.7: Contact angle variation over time of a $[P_{6,6,6,14}][ANS]$ IL drop on a clean glass surface, and images of this drop at a given time (0, 10, 20, 76 and 118 seconds).

The affinity with the glass surface is an important characteristic for the purposes for which this IL was developed: it is easy to apply and spread, at the same time being possible to control the area of application due to its high viscosity.

2.3.5 – NMR studies

1H -NMR spectra of the RTIL $[P_{6,6,6,14}][ANS]$ in deuterated chloroform ($CDCl_3$) showed two separate spectral windows: one (region of 0.5 to 4 ppm) containing peaks from aliphatic protons from long alkyl chains of $[P_{6,6,6,14}]$ cation with a pattern which was, in all samples, similar to that appearing for starting pure $[P_{6,6,6,14}][Cl]$; and the other (region of 6 to 9 ppm) displaying the aromatic protons from ANS anion structure. The ratio of the integrated intensities of the 1H (aliphatic/aromatic) signals was approximately 1:1, as predicted, although in chloroform the value was somewhat affected by putative resonances hiding under the solvent peak.

Very broad signals in 1H -NMR spectra of the pure IL are observed below 25 °C. The peaks become narrower by increasing temperature, with concomitant shift of the chemical shifts downfield of both aromatic and aliphatic regions. This chemical shift is as large as 0.5 ppm from 25 to 85 °C and, as rheological measurements, a hysteresis is observed when comparing heating and cooling cycles. Figure 2.8 shows 1H -NMR spectra of pure $[P_{6,6,6,14}][ANS]$ for heating (black lines) and cooling (grey lines) cycles comparing aromatic resonance (figure 2.8 (a); from ANS anion) and aliphatic resonances (figure 2.8 (b); from $[P_{6,6,6,14}]$ cation). In the case of pure $[P_{6,6,6,14}][ANS]$ electrostatic cation/anion interactions are mainly expected. H-bonding or π - π interactions characteristics of many classes of ILs are not presented in this case.

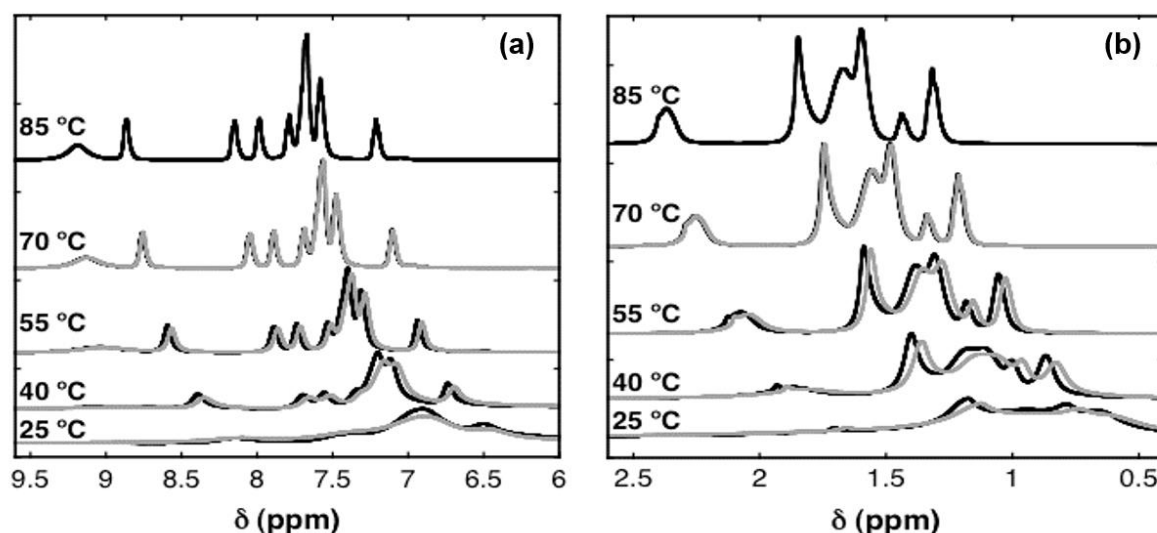


Figure 2.8: $^1\text{H-NMR}$ spectra of pure $[\text{P}_{6,6,6,14}][\text{ANS}]$ for heating (black lines) and cooling (grey lines) cycle containing (a) aromatic and (b) aliphatic resonances.

While the peak widths are readily correlated with solvent viscosity, the position of the peaks when increasing the temperature indicates a decreasing electron density of all protons from both cation and anion.

2.3.6 – UV/vis. Absorption Spectroscopy and Emission Spectroscopy Studies

$[\text{P}_{6,6,6,14}][\text{ANS}]$ was dissolved in acetonitrile and methanol, enabling the measurement of the absorption spectra (see Table 2.3 and figure 2.9). The results are similar to those previously reported for ANS sodium salts. [Sadkowski 1980, Kosower 1983, Drew 1983, Ebbesen 1989, Upadhyay 1995] The emission spectra are also similar to other ANS salts, which indicates that ANS spectra are not significantly affected by the counter-ion when dissolved in those polar solvents (i.e., there is no indication for the formation of ion pairs). As an IL, a red shift is observed for the absorption spectra, rendering a significantly smaller Stokes shift (Table 2.3). The presence of aggregates (such as ANS dimers) could partially explain the result. The emission spectrum also indicates a polarity similar to those molecular solvents. [Sadkowski 1980]

Table 2.3. UV/vis spectroscopy measurements of $[\text{P}_{6,6,6,14}][\text{ANS}]$

	$\lambda_{\text{abs max}} / \text{nm}$	$\lambda_{\text{em max}} / \text{nm}$	Stokes Shift / cm^{-1}
Acetonitrile	364	477	6510
Methanol	370	481	6240
Ionic liquid	376	479	5720

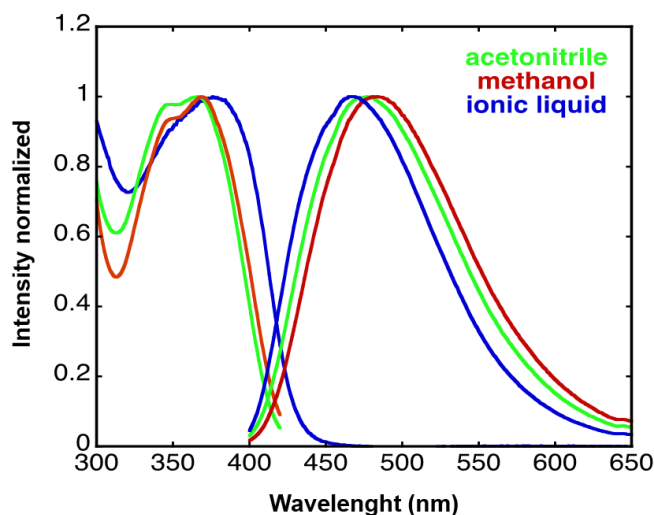


Figure 2.9: [P_{6,6,6,14}][ANS] UV/vis absorption and fluorescence spectra ($\lambda_{\text{ex}}=370$ nm).

[P_{6,6,6,14}][ANS] emission spectra shows some temperature dependence (see fig. 2.10), namely in its intensity which drops by about 50% from 15 °C to 80 °C. The band shape does not change with temperature, in fact the normalized spectra completely overlap at all temperatures of this study. Therefore there is no indication for, e.g., changes of the local polarity in the IL with temperature. The activation energy from the intensity decrease is rather low (about 670 cm^{-1} , comparable with values obtained by Nakamura and Tanaka in molecular solvents [Nakamura 1981]). There is no indication for effects related with those described in rheology and NMR studies in these temperature studies. However, in the temperature range of 15 to 30 °C, which can be considered as the temperature range of usage for the specific purpose of this project, there is no substantial difference in the intensity of the emission spectra.

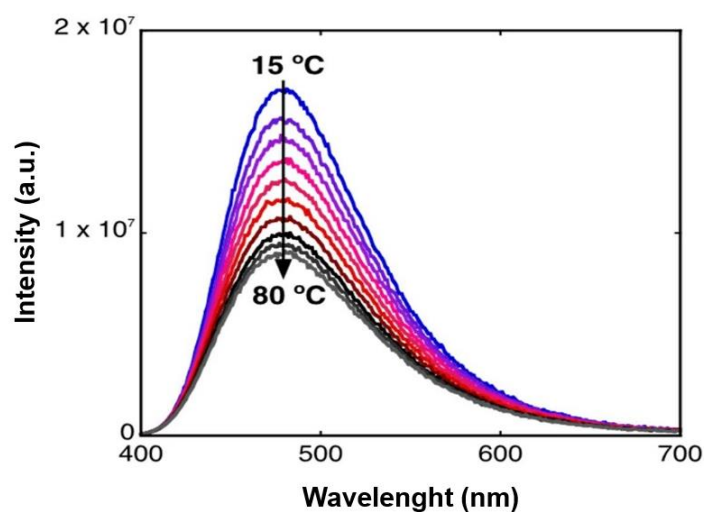


Figure 2.10: [P_{6,6,6,14}][ANS] temperature dependence of the fluorescence spectra ($\lambda_{\text{ex}}=370$ nm).

2.4 – Characterization of other intrinsically luminescent room temperature ionic liquids

After the promising characteristics presented by the IL [P_{6,6,6,14}][ANS], it seemed interesting to compare it to other ILs, namely the consequence of changing the cation and anion and study the resulting characteristics and effects on the glass and glass corrosion surfaces in the following chapters. With this in mind, several ILs were synthesized and characterized by Mani Hosseinzadeh within an Applied Chemistry project. From the 12 different ILs synthesized, 2 room temperature ILs were selected for the comparison studies: changing the cation phosphonium to methylimidazolium, the IL [C₅O₂MIM][ANS], and changing the anion, ANS to pyrenecarboxylate, the IL [P_{6,6,6,14}][PyrCOO]. A more detailed characterization of the two ILs presented below can be found in Attachment I.

2.4.1 – [C₅O₂MIM][ANS]

Using the same luminescent compound as an anion, NH₄[ANS], but replacing the cation for [C₅O₂MIM] – see figure 2.11 –, another room temperature ionic liquid was synthesized. The [C₅O₂MIM] molecule is aromatic and has a delocalized positive charge. The synthesis method used, described above (2.2.1), was an ionic exchange method.

A RTIL, based on the combination of [C₅O₂MIM] as a cation and a luminescent compound, [ANS] as an anion was prepared, with a 92.2% yield (unpublished results). The synthesis method was the same as described above, for the [P_{6,6,6,14}][ANS] IL (2.3.1), and the pure product is very similar to the later, a dark green and viscous RTIL displaying a turquoise blue (slightly greenish) photoluminescence under UV light. The purity of the IL was also confirmed by NMR spectroscopy (see appendix I).

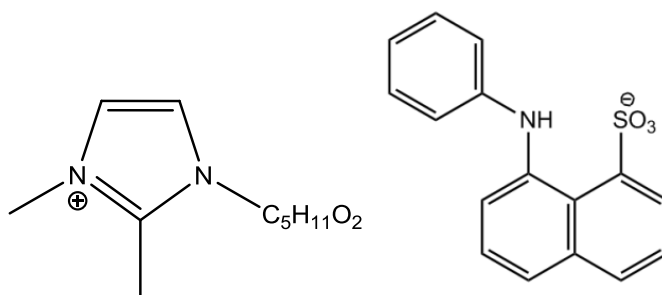


Figure 2.11: Molecular structures of [C₅O₂MIM] cation and [ANS] anion.

2.4.2 – [P_{6,6,6,14}][PyrCOO]

[P_{6,6,6,14}][PyrCOO] IL was synthesised also by ionic exchange method. To do so, it was necessary to transform previously the carboxylic acid form of pyrene in its respective carboxylate salt of sodium. The carboxylic form has a very low solubility in the majority of common organic

solvents, so a small amount – 0.25 g – was dispersed in about 250 ml of methanol by the action of ultrasound at ~40 °C, and then one equivalent of sodium hydroxyl dissolved in methanol was added, originating a soluble sodium salt. Then, 0.48 g of $[P_{6,6,6,14}]Cl$, already dissolved in methanol, was added to the previous mixture, that had been left stirring for 24 hours at room temperature. In order to separate the NaCl as sub product of the ionic exchange, after evaporating the solvent, the obtained product was redissolved in dichloromethane p.a, provoking the precipitation of the NaCl salt by use of ice bath. After separating the solid phase by filtering, the dichloromethane was evaporated and the compound was dried it in vacuum during 24h.

The synthesis of $[P_{6,6,6,14}][PyrCOO]$ (molecular structure presented in figure 2.12) rendered an viscous transparent yellowish liquid with high yield and apparently pure in NMR spectroscopy (see appendix I). However there is a possibility of interaction with water or other material that would produce protonated forms of the fluorophore ($PyrCOOH$). Some experiments demonstrated that the IL contains pyrene units in the anionic state displaying large aggregation effects and the presence of water (also confirmed in elemental analysis – unpublished results).

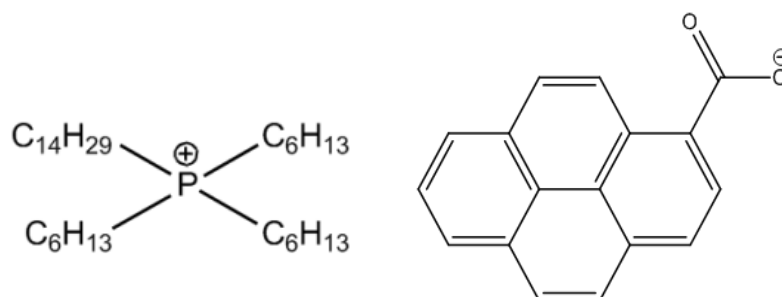


Figure 2.12: Molecular structures of $[P_{6,6,6,14}]$ cation and $[PyrCOO]$ anion.

The RTIL was obtained with a 92% yield. Unlike the previous ILs described, this is a viscous transparent yellowish IL, also with a turquoise blue photoluminescence (see figure 2.13), though less intense than the ILs with $[ANS]$. The purity of the IL was also confirmed by NMR spectroscopy.

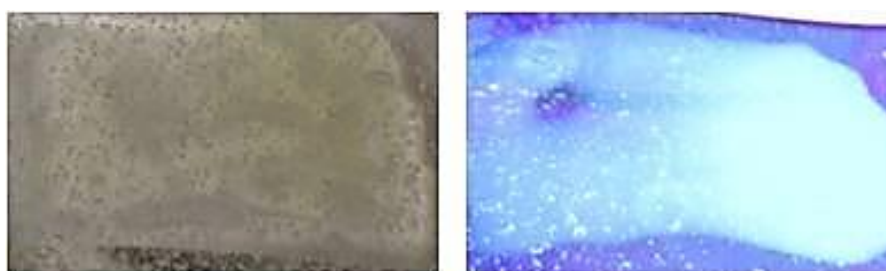


Figure 2.13: $[P_{6,6,6,14}][PyrCOO]$ IL under natural light (transparent yellowish IL) and under UV light (blue photoluminescence, not as intense as the IL containing $[ANS]$).

2.5 – Potential applications

Three of the ILs synthesized, described above, present characteristics of interest for the specific purpose of this project. They present a viscosity that allows a slower penetration in the substrate, as well as the application of a thin film of product in stained glass windows displayed vertically, *in situ*; the molecules selected have a high probability of forming complexes with calcium ions due to the presence of anionic groups, present in the corrosion crusts that are intended to be removed from the glass surface; these ILs are also miscible in water or in less toxic organic solvents, making the removal of the ILs from the glass surface after the treatment harmless for the conservator / user and for the environment.

The fluorescence is not highly sensitive to effects such as temperature, especially in the range of temperatures in which these ILs will most likely be used, between 15 to 30 °C. The luminescence is very intense and perfectly visible at day light, even under a weaker UV-lamp, not being necessary to have darker surroundings during the application or for the detection of the presence of the IL after the cleaning procedure. The high intensity of luminescence also allows the detection of the most negligible amounts of these ILs.

Chapter 3

Experimental procedure and techniques

In this chapter, the experimental procedure followed to develop the study of the ionic liquids selected to apply on the glass samples is described. The following chapters will be divided according to the different features under study: the effect of the ILs on the surface of model glass samples and on the surface of *grisaille* painting in model samples (chapter 4) and the effectiveness of the ILs in removing glass corrosion and its effect on the surface of archaeological stained-glass and on the corrosion layers (chapter 5).

Analysis were performed in order to verify if there were any morphological or chemical alterations in the surface of the glass samples provoked by the use of one of the ILs. The samples have been characterized before and after the cleaning treatment, to allow detection of impurities and surface alterations. The characterization was performed using microscopy techniques – such as Optical Microscopy and Scanning Electron Microscopy with X-ray microanalysis (SEM-EDS) and Fourier Transform Infrared Spectroscopy (FTIR), for both elementary maps and linescan profiles. Optical microscopy (OM) and SEM-EDS were performed on the samples' surface and in cross-section of the samples casted in epoxy resin.

The tests in model glass samples can be divided in two categories:

1. Comparison between the effects of three different ILs, high relative humidity (RH) and EDTA on the glass surface;
2. Long-term effect of the [P_{6,6,6,14}][ANS] IL on the surface of un-corroded and artificially corroded model glass samples.

As for the archaeological samples, a comparison between the efficiency of [P_{6,6,6,14}][ANS] IL, [C₅O₂MIM][ANS] IL and EDTA for the corrosion crusts removal was made. A more extensive study on the effects of the [P_{6,6,6,14}][ANS] IL on the glass and corrosion surfaces was performed. The tests on the *grisaille* painted model glass samples were performed in order to detect if there were any alterations on the substrate. Only the [P_{6,6,6,14}][ANS] IL was tested and the samples were analyzed simply by optical microscopy.

The archaeological samples are medieval stained-glass fragments from a Franciscan friar in Canterbury. The set provided has dozens of fragments, each with different colors and thickness, some painted, with *grisaille* and yellow silver stain. Six samples were selected for these particular tests, with different colors, with and without *grisaille* painting, all presenting a thick corrosion layer constitute of several compounds and a size exceeding 2 x 1 cm² to allow performing the tests described. In Attachment III is presented the full catalogue of the fragments.

3.1 Production of model glass

Model glass with compositions similar to those typically found in stained-glass from Mosteiro da Batalha [Vilarigues 2004, Fernandes 2008, Vilarigues 2009] (Table 3.1) – the main example of international Gothic architecture in Portugal, and where can be found the oldest examples of Portuguese stained-glass in the country, from the 15th century [Redol 2003] – was produced with laboratory reagents p.a. (SiO_2 and CaCO_3 , Sigma-Aldrich; K_2O and P_2O_5 , Panreac; MgO , BDH; Al_2O_3 , Merck). The reagents were put in the kiln at $1300\text{ }^\circ\text{C}$, in an Al_2O_3 crucible, for 24 hours.

Table 3.1: Composition of the glass produced.

Oxide	MgO	Al_2O_3	SiO_2	CaO	K_2O	P_2O_5
% weight	2	2	52	20	22	2
% molar	2.68	1.06	63.66	19.24	12.60	0.76

After being taken out of the kiln, the glass was blown into a glass roundel, and left to cool down slowly from $\sim 500\text{ }^\circ\text{C}$ to room temperature. Some of the steps of production and shown below, in figure 3.1, as well as the final result, where it is also possible to observe that the rondel is quite thick – $\sim 0.5\text{ cm}$ –, having the characteristic variation of thickness from the center to the edges. The glass obtained was blown by Robert Wiley – an artist and Invited Professor at Vicarte – using traditional off-hand glass tools and techniques analogous to the production period of the original samples.

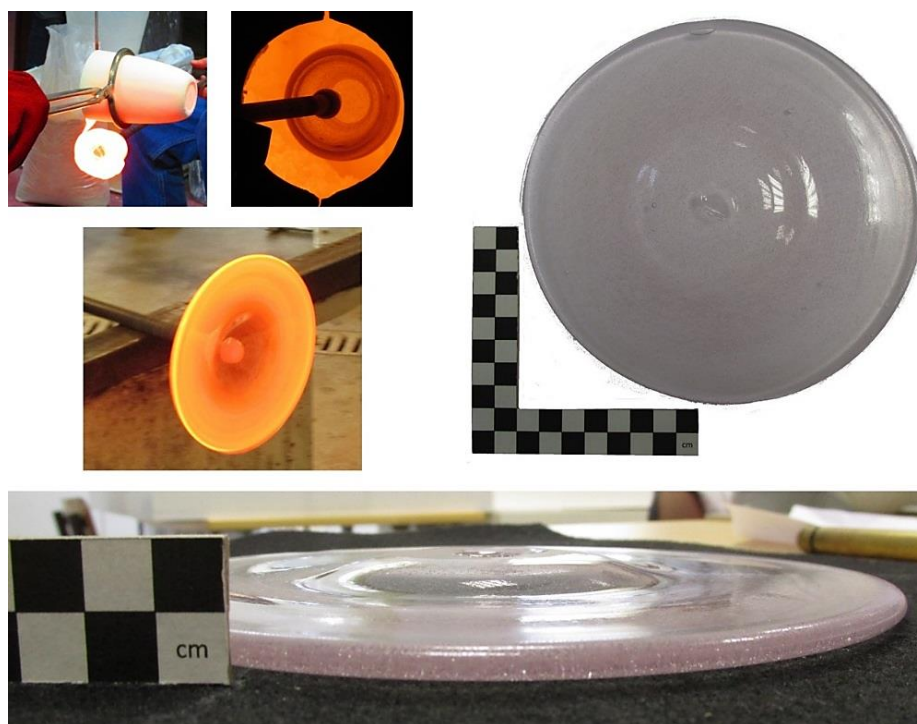


Figure 3.1: Stages of production of the glass roundel and final result (Joana Delgado ©).

The roundel was later cut into samples of about 1.5 cm², using a diamond tipped glass cutter, and each sample was identified with a serial number using a laser engraving printer.

For the tests in *grisaille* painted model glass samples, black and brown *grisaille* paint from Debitus® was used. According to the brand, these paints have a composition similar to the medieval *grisaille*⁶ [**in website www.debitus.com, and Debitus 1991**]. The model glass samples were painted using a *grisaille* and Arabic gum paint, and then fired at 650 °C for 1 hour.

3.2 Corrosion essays: artificial corrosion

Model glass samples were divided in three groups, according to the environment used to promote the formation of corrosion products. The group A samples were not subjected to corrosion, being the control group. Each sample from group B was put in a plastic container with distilled water for 3 months, in order to promote the formation of calcium carbonate corrosion crusts. There was no control of the pH of the water, and after this period the container was opened for the water to evaporate and allow the corrosion products to remain deposited in the surface of the glass sample. The same process was followed for the samples from group C, except these were put in distilled water with sulfuric acid (H₂SO₄), to promote the formation of calcium sulfate on the glass surface.

3.3 Archaeological stained glass samples

In table 3.2, the composition of each of the archaeological stained glass samples is presented. This was obtained after analyzing 3 points for each sample's cross-section casted in epoxy resin with Particle-induced X-ray emission (μ-PIXE).

The highlighted oxides – SiO₂, K₂O and CaO – represent the main components of these fragments' composition. All the glass fragments analyzed present a low SiO₂ content and very high CaO and K₂O contents. This is characteristic of potassium-rich glasses of low chemical durability and may justify the extent of corrosion observed in the surface of these fragments [**Newton 1989, Veritá 1996, Redol 2003, Janssens 2013**], also offering good models for the tests to be performed.

⁶ Note: these were recipes originally developed in the late 19th century. Though they do mention that the composition is similar to medieval *grisaille*, that is not entirely truthful, according to some recent studies. The known composition [**Debitus 1991**] of these *grisailles* is the following:

- **Noir Ordinaire:** 41.18% Fe₃O₄ + 58.82% 5SiO₂.4PbO
- **Brun XIII:** 37.04% Noir Ordinaire (composition above) + 37.04% Rouge n° 2 (33.33% Fe₂O₃ + 66.66% 5SiO₂.4PbO) + 25.93% Brun Claire (41.18% (2Fe₂O₃.ZnO) + 58.82% (5SiO₂.4PbO))

In recent analysis it was also detected the presence of MnO and some impurities in these *grisailles*. Though the composition is not completely similar to medieval *grisailles* composition, this is still the most similar available in the market.

Table 3.2 – Composition of the archaeological stained-glass samples (% mol and % weight).

	Cant 001 green		Cant 002 no color		Cant 003 blue		Cant 004 brown		Cant 005 yellow		Cant 006 no color		Cant 028		Cant 033		Cant 034	
	%mol	%wt	%mol	%wt	%mol	%wt	%mol	%wt	%mol	%wt	%mol	%wt	%mol	%wt	%mol	%wt	%mol	%wt
Na₂O	1.37	1.6	1.35	1.6	1.11	1.3	1.42	1.7	1.28	1.5	0.35	0.4	1.01	1.22	-	-	-	-
MgO	5.28	4	6.08	4.7	5.39	4.1	9.01	7	5.51	4.2	6.27	4.6	5.84	4.58	4.93	3.78	5.14	3.93
Al₂O₃	1.1	2.1	1.18	2.3	1.2	2.3	0.92	1.8	1.14	2.2	0.65	1.2	1.03	2.05	0.74	1.43	0.62	1.19
SiO₂	65.01	53.9	66.56	56.3	66.71	55.5	63.45	53.9	66.21	55.2	56.09	45	68.55	58.8	60.41	50.7	58.88	49.2
P₂O₅	1.27	3.4	1.36	3.7	1.23	3.3	1.72	4.7	1.49	4	1.74	4.5	-	-	-	-	-	-
S	-	-	0.13	0.08	0.12	0.07	0.13	0.08	0.03	0.02	0.19	0.11	-	-	0.16	0.1	0.16	0.1
Cl	0.63	0.42	0.66	0.45	0.61	0.41	0.57	0.39	0.69	0.46	0.08	0.05	0.57	0.39	-	-	-	-
K₂O	6.6	11.7	6.97	12.6	7.26	12.9	6.39	11.6	8.64	15.4	10.62	18.2	9.71	17.8	9.81	17.6	9.8	17.5
CaO	13.37	14.1	14.22	15.3	13.7	14.5	14.53	15.7	13.58	14.4	21.65	22.1	12.46	13.6	22.57	24.1	23.71	25.2
TiO₂	0.09	0.13	0.09	0.14	0.1	0.15	0.07	0.11	0.09	0.14	0.08	0.12	0.06	0.1	0.08	0.12	0.11	0.17
MnO	0.66	0.88	0.79	1.08	0.79	1.06	1.37	1.87	0.86	1.16	1.57	2.03	0.47	0.65	0.96	1.3	1.09	1.46
Fe₂O₃	0.35	1.04	0.36	1.09	0.7	2.1	0.21	0.66	0.29	0.89	0.24	0.71	0.17	0.52	0.1	0.3	0.16	0.49
CoO	-	-	-	-	0.14	0.2	-	-	-	-	-	-	-	-	-	-	0.03	0.04
NiO	-	-	-	-	0.01	0.01	-	-	-	-	0.01	0.02	-	-	0.01	0.01	0.01	0.01
CuO	3.72	5.57	0.06	0.09	0.48	0.72	0.03	0.05	0.03	0.05	0.04	0.06	0.02	0.03	0.01	0.01	0.04	0.06
ZnO	0.36	0.55	0.03	0.05	0.14	0.21	0.04	0.07	0.03	0.05	0.05	0.08	0.02	0.03	0.02	0.03	0.03	0.04
Rb₂O	0.01	0.04	0.01	0.04	0.01	0.05	0.01	0.05	0.01	0.04	0.04	0.13	0.01	0.04	0.01	0.04	0.01	0.05
SrO	0.05	0.1	0.06	0.12	0.06	0.12	0.04	0.07	0.05	0.09	0.13	0.25	0.02	0.05	0.05	0.09	0.06	0.11
ZrO₂	-	-	-	-	-	-	-	-	-	-	0.04	0.08	-	-	-	-	-	-
BaO	0.08	0.24	0.07	0.22	0.07	0.19	0.07	0.22	0.05	0.14	0.14	0.4	0.06	0.17	0.15	0.43	0.15	0.45
PbO	0.05	0.19	0.03	0.13	0.19	0.78	0.01	0.03	0.01	0.03	-	-	-	-	-	-	-	-

3.4 Experimental design for the comparison of the ionic liquids effect on glass

At this stage, three ILs were selected: based on the $[P_{6,6,6,14}][ANS]$ IL, changing the anion – $[P_{6,6,6,14}][Pyr]$ –, and changing the cation – $[C_5O_2MIM][ANS]$. The samples where these ILs were applied were also compared with samples that were in a high RH environment and with samples in contact with an EDTA solution. This experiment was performed according to the scheme presented in figure 3.2.

The purpose was to compare the effect of the ILs and EDTA with the effect of a high level of humidity on the glass surface, from a short period (1 hour) to a longer period of contact (28 days), in order to have a better idea of the mid-term effect of these compounds.

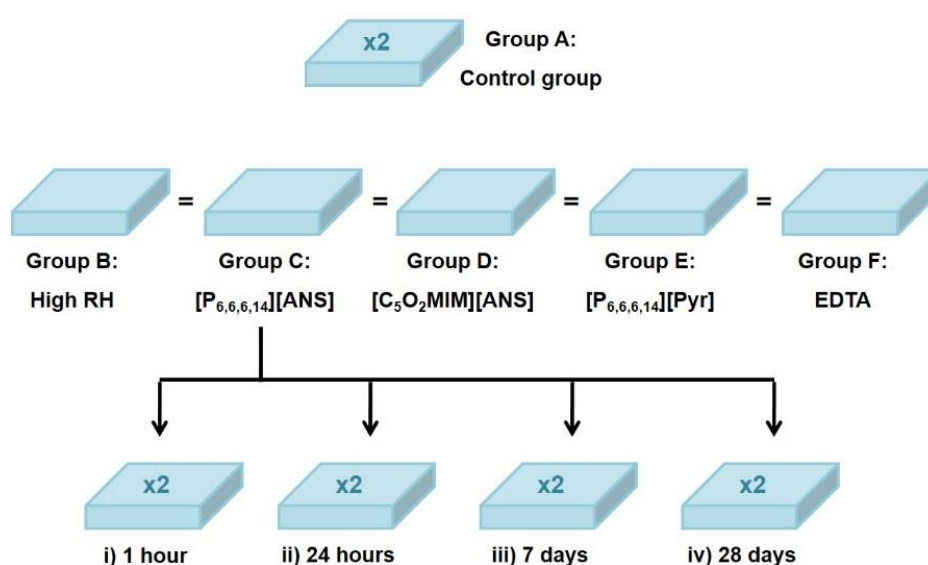


Figure 3.2: Experimental design for the experiments comparing the effects of different environment and compounds on model glass samples. Each parameter was tested in 2 samples.

The samples from group A were vacuum sealed for the 28 days in order to avoid at most any kind of alteration provoked by atmospheric conditions. Group B samples were placed in a desiccator with a constant high RH (between 80 and 90%) at ~ 22 °C. A drop of IL was deposited on the samples of groups C, D and E. After the due time, the ILs were removed using a swab impregnated with a solution of water:ethanol (1:1/v:v), and its complete removal was always controlled using an UV-light lamp (365 nm). For the group F samples, a solution of 3% EDTA + 3% NH_4HCO_3 in distilled water, pH 8.26 was used [Romich 2000]; the samples were put in a closed plastic container and covered with the EDTA solution during 1 hour to 28 days, then removed and rinsed with distilled water several times. All the samples were then cut, casted in epoxy resin and polished with Micro-Mesh™ sanding sheets, up to 12000 mesh, for the examination of the cross section.

Regarding the archaeological samples, and as the $[P_{6,6,6,14}][Pyr]$ IL was found to be unstable on the tests performed on the model glass samples, the comparison focused on $[P_{6,6,6,14}][ANS]$ IL, $[C_5O_2MIM][ANS]$ IL and EDTA. Considering that the mid-term effect of these compounds on the glass was tested using model glass samples, here the purpose was to compare the efficiency of the ILs and EDTA removing corrosion crusts. Three archaeological samples were selected and cut in four sections, as shown in figure 3.3. After the cleaning tests, these samples sections were cut, casted in epoxy resin and polished with Micro-Mesh™ sanding sheets, up to 12000 *mesh*, for the examination of the cross section.

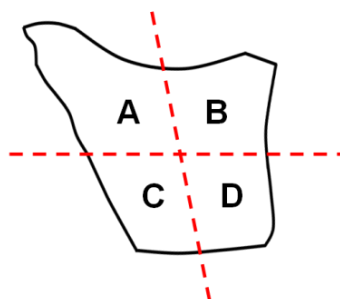


Figure 3.3: Scheme of division of an archaeological sample: Section A (control group), section B ($[P_{6,6,6,14}][ANS]$), section C ($[C_5O_2MIM][ANS]$) and section D (EDTA solution).

3.5 Experimental design for the mid-term effects of the $[P_{6,6,6,14}][ANS]$ IL

At this stage, model glass samples were divided in three groups: a control group, a group subjected to induced corrosion using distilled water (to promote the formation of $CaCO_3$) and a third group subjected to induced corrosion using distilled water with H_2SO_4 (to promote the formation of $CaSO_4$). For the study of the mid-term effect on the IL on the glass surface – schematized in figure 3.4 –, a drop of IL was deposited on 3 samples of each group, being a fourth sample left without IL.

An emission spectrum was obtained for each sample. Then, the 12 samples were put in a desiccator under vacuum. Every 4 weeks until the twelfth week, the IL was removed from 1 sample from each group, after measuring the emission spectrum. The emission spectra were measured in all samples, in order to control the intensity of the emission of the IL over time. Upon the removal of the IL, using a swab impregnated with a solution of water:ethanol (1:1/v:v), its complete removal was always controlled using an UV-light lamp (365 nm) and emission spectroscopy. All the samples were then cut, casted in epoxy resin and polished with Micro-Mesh™ sanding sheets, up to 12000 *mesh*, for the examination of the cross section.

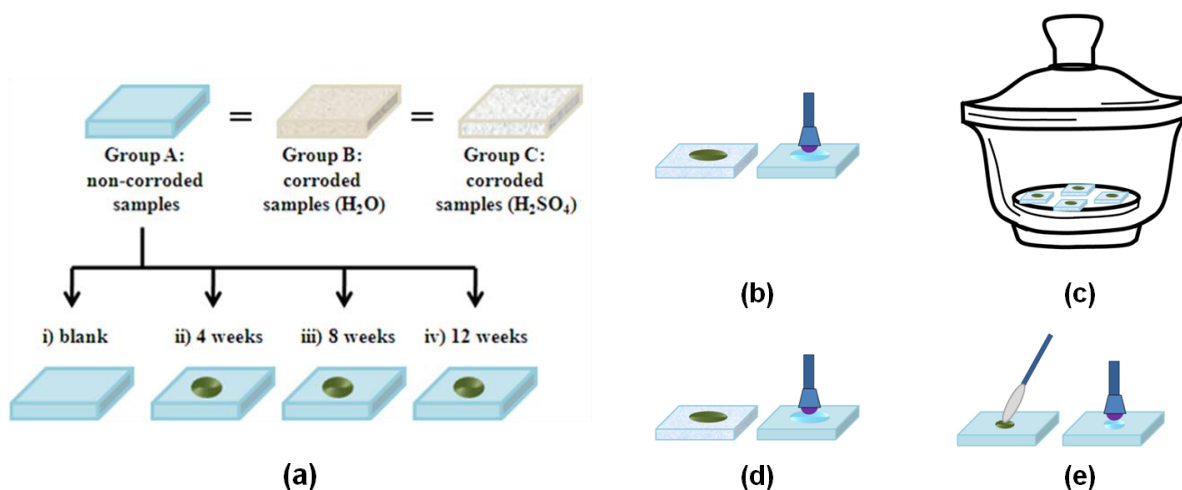


Figure 3.4: Experimental procedure for testing the long term effect of the ionic liquid [P_{6,6,6,14}][ANS] on the glass. **(a)** One sample was left without any IL, being the control sample. A drop of IL was deposited on 3 samples of each group. **(b)** An emission spectra was measured for each sample. **(c)** The samples were put in a desiccator under vacuum. **(d)** The emission spectra was measured, **(e)** and the IL was removed using a swab impregnated with a solution of water:ethanol (1:1/v:v). Its complete removal was always controlled using an UV-light lamp and by the emission spectra.

The same process was followed for 6 archaeological samples. Each of the 6 archaeological samples was cut in half, using a diamond tipped glass cutter, to proceed to 2 different types of test: one half was used for the cleaning tests – analyzing the amount of corrosion removed using the IL –, and the other half was used in the mid-term effect tests on the glass surface. These were cut in 2, one half being used as control sample. However, the IL was not removed every 4 weeks, as it was only applied to one fragment of each sample. The emission spectra were measured every 4 weeks, but the IL was only removed in the end of the experiment, after 12 weeks. All the samples were then cut, casted in epoxy resin and polished with Micro-Mesh™ sanding sheets, up to 12000 *mesh*, for the examination of the cross section.

3.6 Morphologic analysis

Optical microscope. The images of surfaces of the non-corroded and corroded glass samples, before and after the cleaning procedure, were obtained with an optical microscope Axioplan 2, Zeiss®, coupled with a Nikon DMX digital camera, using different filters.

SEM observations were carried out using a Carl Zeiss AURIGA CrossBeam (FIB-SEM) workstation, equipped for Energy dispersive spectroscopy (EDS) measurements. The samples were previously coated with a ~15 nm Au/Pd conductive film for avoiding charge effects.

3.7 Chemical analysis

FTIR. For the characterization of the corrosion products, before and after the application of the ILs, infrared spectra were acquired with a Nicolet Nexus spectrophotometer interfaced with a Continuum microscope (15x objective), with a MCT-A Thermo Nicolet detector cooled by liquid nitrogen. The spectra presented were obtained in reflectance mode, with an ATR Si slide on accessory. The spectra were obtained with a resolution of 4 cm^{-1} and 128 scans.

μ -Raman. Analyses were performed with a Labram 300 Jobin Yvon spectrometer, equipped with a solid state laser of 50 mW power operating at 532 nm. The laser beam was focused either with 50x or 100x Olympus objective lenses. The laser power was filtered to 10% incident power using a neutral density filter for all analyses. Analyses were performed on the surface of the glass. Spectra were recorded as an extended scan. A mixed Gaussian-Lorentzian curve-fit provided by the LabSpec software (v 5.15.25) was used to determine the exact peak wavenumbers.

SEM-EDS. In the model glass samples, linescan were performed in 20 point analysis, covering $\sim 100\text{ }\mu\text{m}$, to verify if there were any changes in the composition of the glass after the application of the IL. In the archaeological stained-glass samples, elementary maps were made in cross-sectioned samples casted into epoxy resin. The samples were previously coated with a $\sim 15\text{ nm}$ Au/Pd conductive film for avoiding charge effects.

Luminescence spectra were measured using a SPEX Fluorolog-3 Model FL3-22 spectrofluorimeter, with an optical fiber attached, to control the IL's emission during and after the cleaning procedure. The excitation wavelength was always 370 nm and the spectra were corrected in both the emission spectra and lamp light intensity. The slits were the same for both excitation and emission (2 nm). The detection limits of this device are $\sim 10^{-7}\text{ M}$.

μ -PIXE. Quantitative results were achieved with μ -PIXE ion beam analytical technique using an Oxford Microbeams OM150 type scanning nuclear microprobe setup, either with the in-vacuum or with the external beam configuration. To allow efficient detection of low energy X-rays such as the ones of Na, all the glass fragments were irradiated in vacuum with a focused 1 MeV proton beam. The X-rays were collected by an 8 μm thick Be windowed SDD detector with 145 eV resolution. In order to avoid or detect possible local glass heterogeneities, X-ray imaging (2D elemental distribution) and spectra were obtained from an irradiated sample area of $750 \times 750\text{ }\mu\text{m}^2$. For trace elements quantification (typically elements with atomic number above the one of Fe), a higher energy was needed and a 2 MeV proton beam was used. In this case, the external beam setup was chosen in order to prevent sample beam-charging and consequently X-ray spectra degradation. X-rays were collected with a SDD detector with 145 eV resolution from a sample area of $800 \times 800\text{ }\mu\text{m}^2$. Operation and basic data manipulation, including elemental distribution mapping, was achieved through the OMDAQ software code (Grime and Dawson 1995), and quantitative analysis with GUPIX program (Campbell et al. 2010). The results are expressed in weight percentage of oxides and were normalized to 100%. In order to validate the obtained concentration results, a glass reference standard, Corning B, was also analyzed.

Chapter 4

Corrosion crusts removal: model glass

In this chapter, the results of all the trials performed using model glass samples will be presented and discussed. The main aim of these trials was to determine if there were any alterations – morphological and chemical – on the glass surface induced by the various cleaning materials. For this purpose, a model glass was produced, with a simplified composition and blown into a glass roundel (as described in chapter 3.1) to have a production technique as similar to the original as possible. This procedure has a major impact on the surface of the glass.

These trials can be divided in two categories:

1. Comparison between the effects of three different ILs - [P_{6,6,6,14}][ANS] IL, [C₅O₂MIM][ANS] and [P_{6,6,6,14}][PyrCOO] – and the effect of EDTA deposition on the glass surface with the effect of high relative humidity (RH)⁷;
2. Long-term effect of the [P_{6,6,6,14}][ANS] IL on the surface of un-corroded and artificially corroded model glass samples.

The samples have been characterized before and after the cleaning treatment, to allow the detection of impurities and surface alterations. The characterization was performed using microscopy techniques – such as Optical Microscopy (OM) and Scanning Electron Microscopy (SEM) –, Raman Spectroscopy, Fourier transform infrared spectroscopy (FTIR) and Scanning Electron Microscopy with Energy Dispersive Scattering (SEM-EDS), for linescan profiles.

4.1 Samples characterization

Before performing the tests, the samples were characterized using the analytical techniques mentioned above: OM, SEM, Raman, FTIR and SEM-EDS. All the technical features and conditions of the devices and analysis can be found in Chapter 3 – Morphological analysis (3.6) and Chemical analysis (3.7).

For the morphological characterization, the samples were analyzed using OM and SEM. These analyses were important to allow the comparison between the model glass surface before and after being subjected to the different products or conditions. Chemically, the samples' surface was characterized using Raman and SEM-EDS, the later was also used to analyze cross-sections of the samples. The objective was, once again, to compare and verify if there were any chemical alterations on the surface – or in depth – of the model glass samples after the application of the ILs, also comparing these results to those of the samples submitted to a very high RH environment – between 85 and 90% – and with

⁷ Note: apart from the EDTA solutions, there are other “Bettembourg-methods”, such as ammonium-bicarbonate and sodium-thiosulfate, that could have been used in this comparison. However, for this particular project only the EDTA solution was tested, as it is one of the most commonly mentioned and used [Abd-Allah 2013], despite being considered a method that may induce damage to the glass surface [Romich 2000].

samples in contact with an EDTA solution. The results presented compare directly the samples before and after the exposure to the external agent.

4.2 Comparison of the effect of ILs and EDTA with high RH on the model glass surface

Based on the $[P_{6,6,6,14}][ANS]$ IL, two additional ILs were designed by changing the anion – $[P_{6,6,6,14}][Pyr]$ – and changing the cation – $[C_5O_2MIM][ANS]$ in order to expand different possibilities to study the effects of those cleaning materials in the glass surface. The samples where those ILs were applied were also compared with samples that were submitted to a high RH environment and with samples in contact with an EDTA solution. The experimental design is described more exhaustively in chapter 3.3.

Starting with the alterations in the ILs themselves, the first difference that was possible to observe by comparing the deposition in a glass surface between those with $[ANS]$ and that with $[PyrCOO^-]$ as an anion was the color change developing a greenish hue of the $[P_{6,6,6,14}][PyrCOO]$ IL over time. This color change also leads to a decrease of intensity of its luminescence as it is shown in figure 4.1. Regarding $[P_{6,6,6,14}][ANS]$ and $[C_5O_2MIM][ANS]$ ILs, the dark green color remains unchanged. In conformity with this observation, the luminescence intensity the ANS ILs remains very intense 1 week after deposition on the glass surface. The $[P_{6,6,6,14}][PyrCOO]$ IL was a transparent – slightly yellow – compound at the moment of its application (remaining so after 1 hour), developing the green color after 1 week. The intensity of the luminescence degrades drastically, which makes it difficult to detect its presence on the glass surface a few days after the deposition.

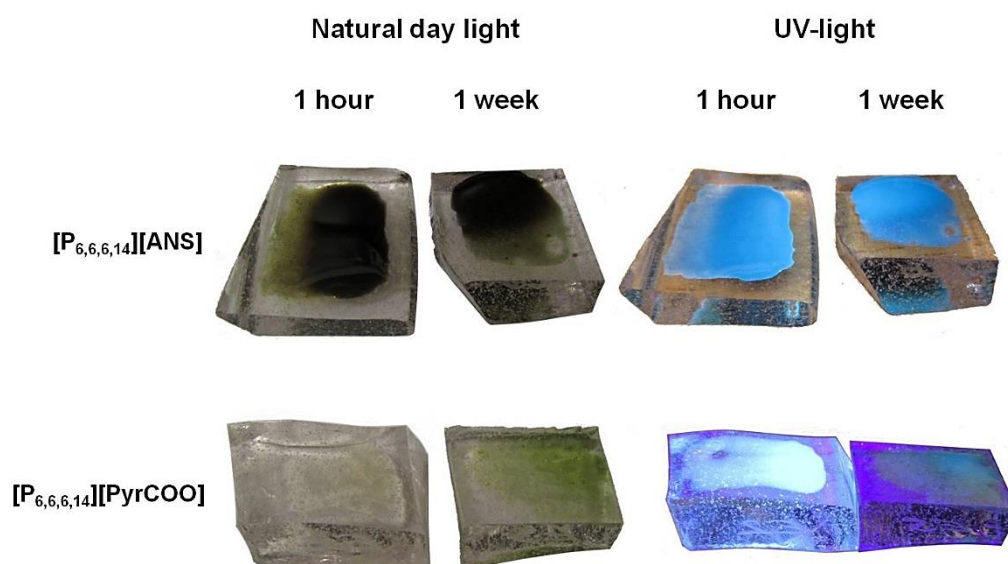


Figure 4.1: Comparison between the $[P_{6,6,6,14}][ANS]$ and the $[P_{6,6,6,14}][PyrCOO]$ ILs applied on a transparent model glass sample after 1 hour and after 1 week, under natural day light and under UV-light. The visual behavior of the other IL, $[C_5O_2MIM][ANS]$ is similar to $[P_{6,6,6,14}][ANS]$.

It is also important to refer that the luminescence of the ILs with [ANS] is rather intense using a low power UV light source (365 nm), being very easy to see and photograph even in an illuminated environment, whilst the $[P_{6,6,6,14}][\text{PyrCOO}]$ IL has a low luminescence that requires a dark environment in order to be visible. This characteristic is evident in figure 4.1; the purple light scattering of the UV-light on the glass is only noticeable on the model glass where $[P_{6,6,6,14}][\text{PyrCOO}]$ IL was applied, as the image was taken in a slightly darker surroundings and with the UV-light irradiating closer to the samples in order to ensure a stronger UV-light absorption by the IL and consequently a brighter photoluminescence.

Now when it comes to the sample' surface alterations, the morphology of the surface of the samples were compared using optical microscope (OM) and scanning electron microscopy (SEM). In figure 4.2, optical microscope images of model samples are displayed for comparison. In particular we show images selected from the control group (A), the group that was in a high RH atmosphere (B) – in this case during 4 weeks –, and from the group that was in a solution of EDTA, pH 8.26 (F) – also during 4 weeks. A more complete collection of optical microscope images can be found in Appendix II.

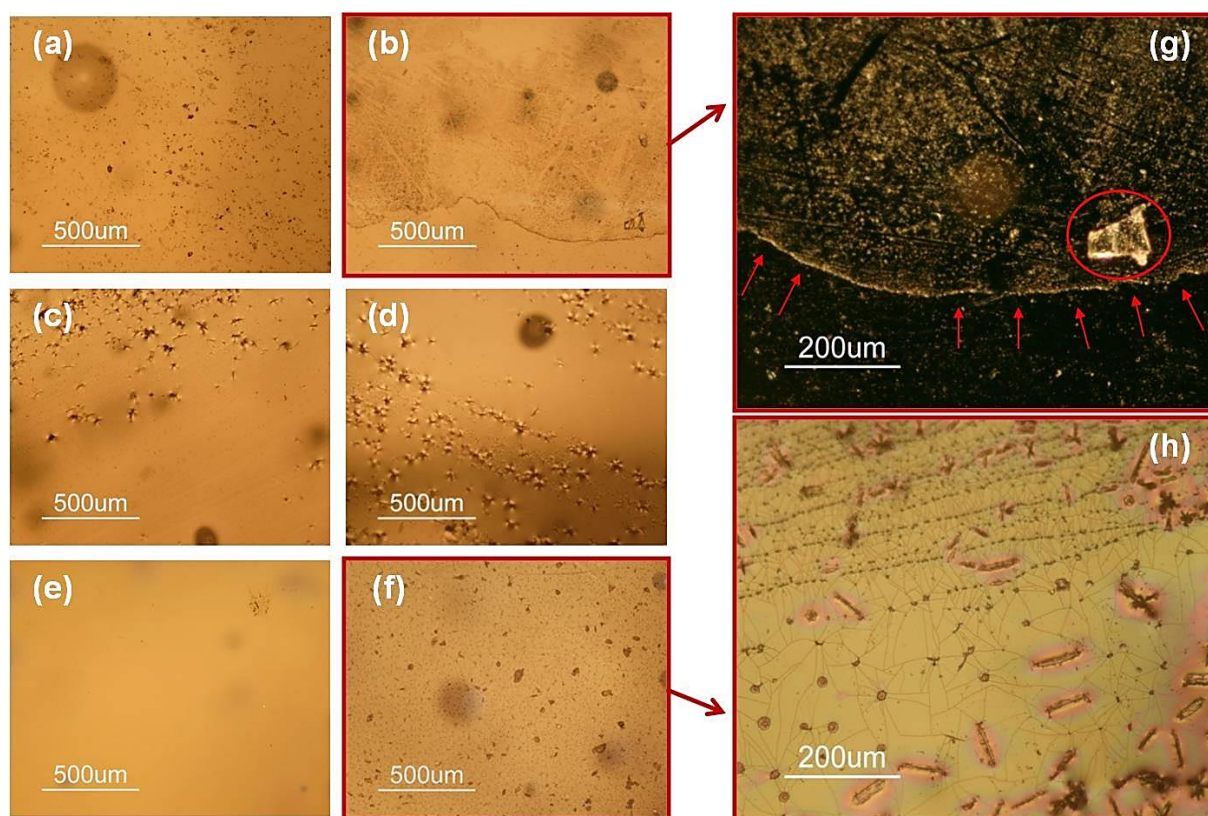


Figure 4.2: Optical microscope images of the surface of the model glass samples, with a 5x magnification (a) of a control sample, from group A, (b) a sample from group B, left for 4 weeks in a high RH atmosphere, (c) a sample from group C, that was in contact with $[P_{6,6,6,14}][\text{ANS}]$ IL for 4 weeks, (d) a sample from group D, that was in contact with $[\text{C}_5\text{O}_2\text{MIM}][\text{ANS}]$ IL for 4 weeks, (e) a sample from group E, that was in contact with $[P_{6,6,6,14}][\text{PyrCOO}]$ IL for 4 weeks and (f) a sample from group F, that was in a solution of 3% EDTA + 3% NH_4HCO_3 in distilled water, pH 8.26, for 1 week. Optical microscope image with 10 x magnification (g) of the surface of a sample from group B, left for 4 weeks in a high RH atmosphere and (h) of a sample from group F, left for 1 day in a solution of 3% EDTA + 3% NH_4HCO_3 in distilled water, pH 8.26.

The small marks observed on the surface of the control sample are attributed to production defects, taking into account that, as explained in chapter 3.3, these samples were vacuum sealed and, so, protected from the influence of the atmosphere. These marks appear in some other samples, with no apparent relation with the environment conditions to which they were submitted, reinforcing the idea that they are formed during the glass production, most likely when the glass crown is being formed and flattened (chapter 1.1), being sleeked with wooden tools.

In figure 4.2 (g), a higher magnification of the area of a sample from group B, displayed in figure 4.2 (b) is shown. The main changes on the surface are highlighted in red, such as the presence of a crystal – probably a calcium salt crystal –, and a hydrated layer, which corresponds the first stage for the formation of a corrosion crust. This was the expected result, illustrating the effect of water reacting with the ions present in the glass matrix causing alterations on the sample surface.

The corrosion induced by EDTA, however, is more evident. After one day, the samples from group F – immersed in a solution of 3% EDTA + 3% NH_4HCO_3 in distilled water (pH 8.26) – already present a leached surface with multiple micro-cracks [figure 4.2 (h)].

In figure 4.2 (c,d,e), the optical microscope images of the model samples where the ILs ($[\text{P}_{6,6,6,14}][\text{ANS}]$, $[\text{C}_5\text{O}_2\text{MIM}][\text{ANS}]$ and $[\text{P}_{6,6,6,14}][\text{PyrCOO}]$, respectively), were applied and left in contact with the glass for 4 weeks are shown. As in the model sample images [figure 4.2 (a)], there are some marks on the surface of some of these samples [figure 4.2 (c,d)]. However, the surface appears to be clear and unaltered, even after 4 weeks of direct contact with the ILs, indicating rather small effects on the glass surface when compared with the cases of an 88% RH atmosphere during the same period of contact, 4 weeks, and of an EDTA solution for an even shorter period, 1 week.

The morphology of the surface of model glass samples from groups B (high RH) and F (EDTA) was observed by SEM, being the results presented to comparison in figure 4.3. In the upper images – Figure 1.3 (a,b) – are the samples from group B; here the crystals that were present all over the surface can be observed in more detail, and their analysis determined the main component of these crystals is Ca, as expected. Bellow, in the samples that were in contact with an EDTA solution for 7 and 28 days (Figure 1.3 (c) and (d), respectively), it is possible to observe that the surface has been damaged, presenting the micro-fissures characteristic of the formation of a silica-gel layer on the surface, that could eventually lead to the formation of a corrosion layer [Melcher 2010].

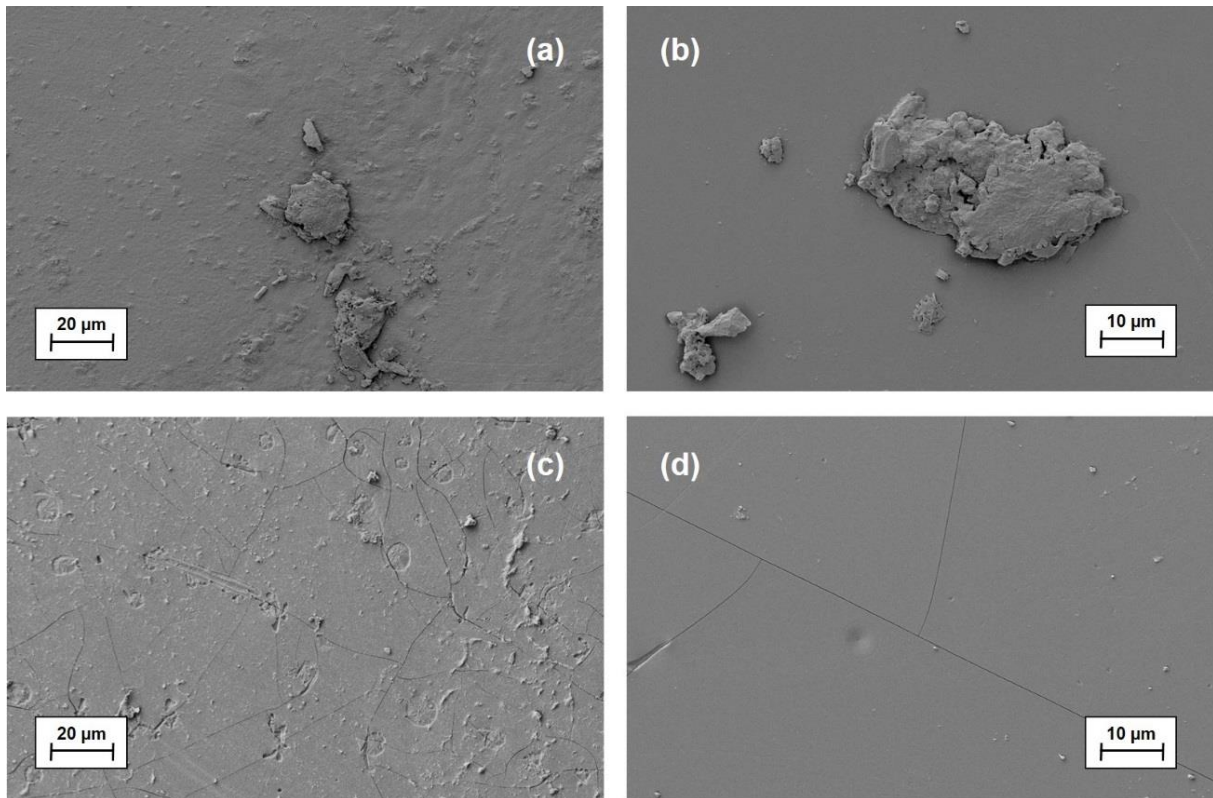


Figure 4.3: SEM image of the surface of a model glass sample from group B after being for 7 days in a high RH environment **(a)** 500x magnification and **(b)** 1000x magnification. SEM image of the surface of a model glass sample from group F after being for **(c)** 7 days in an EDTA solution, 500x magnification, **(d)** and for 28 days in an EDTA solution, 1000x magnification.

Being a product to be used in glass conservation, it is essential to assure that the ILs did not induce any alteration to the glass surface. To verify this, Raman spectra from the surface of model glass samples from all the groups were acquired. Three spectra were acquired in each sample, and as these spectra showed no differences between them, an average was made and is presented to each sample. In addition, in figure 4.4 it is possible to observe that the spectra of the surface of the control sample matches exactly the spectra of the samples of groups B, C, D and E – high RH, IL 1, IL 2 and IL 3, respectively – that were in contact with the respective IL or in a high RH atmosphere for 28 days. The same does not happen with the spectra of the samples immersed in a solution of 3% EDTA + 3% NH_4HCO_3 in distilled water, pH 8.26, for 7 and 28 days.

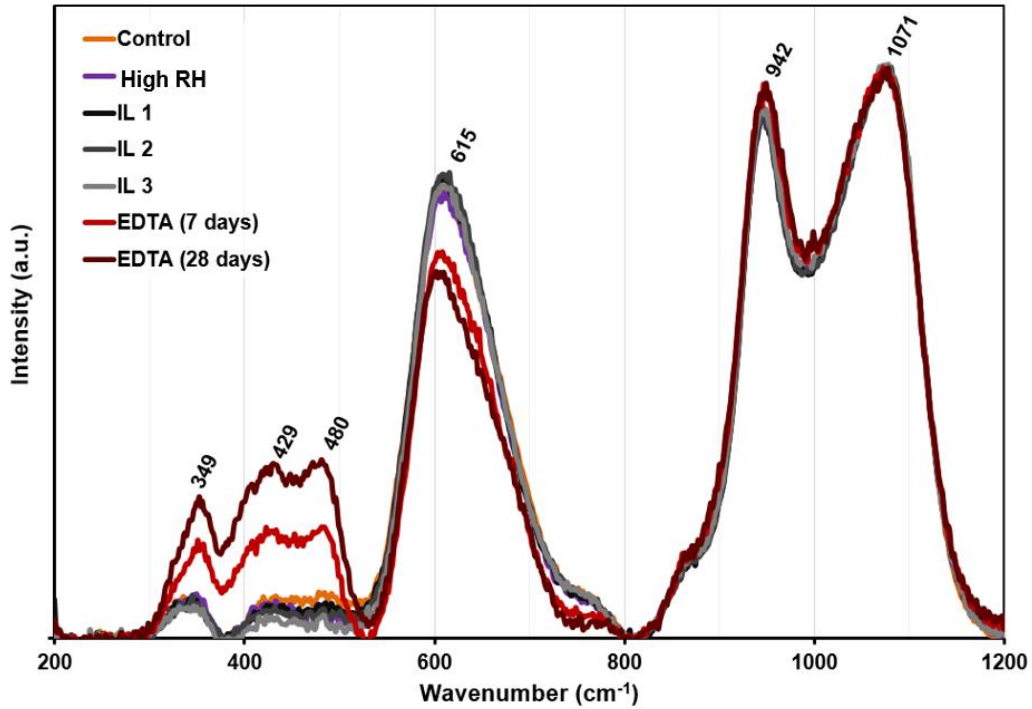


Figure 4.4: Raman spectra, range 200 to 1200 cm^{-1} , of the model glass samples of all groups.

The highest intensity bands, at 942 and $\sim 1071 \text{ cm}^{-1}$, remain unaltered. However, both the band at $\sim 615 \text{ cm}^{-1}$ and those between 349 and 480 cm^{-1} , though coinciding in the spectra of the control samples, high RH and ILs 1 to 3, present a clear alteration for the samples in contact with the EDTA solution. The intensity of the peaks between 349 and 480 cm^{-1} tends to increase with the time of contact with the EDTA solution.

Table 4.1 – Identification of the Raman bands associated with the components of the Si–O stretching and bending modes [Colomban 2003].

Oxygen	Structure	Q^n	$Q^{n'}$
zero	SiO_4	$\sim 800\text{-}850 \text{ cm}^{-1}$	$\sim 260 \text{ cm}^{-1}$
one	Si_2O_7	$\sim 900 \text{ cm}^{-1}$	$\sim 300 \text{ cm}^{-1}$
two	Si chains	$\sim 1050\text{-}1100 \text{ cm}^{-1}$	$\sim 470 \text{ cm}^{-1}$
three	sheet-like	$\sim 1100 \text{ cm}^{-1}$	$\sim 500 \text{ cm}^{-1}$
four	tectosilicate	$\sim 1150\text{-}1250 \text{ cm}^{-1}$	$\sim 570 \text{ cm}^{-1}$

On the contrary, the intensity of the peak at $\sim 615\text{ cm}^{-1}$ decrease, being attributed to bending vibrations of Si-O-Si bonds, which can indicate that some of these bonds are breaking [Colomban 2003, Colomban 2006, Colomban 2006i].

In order to verify if there was any migration of the Ca to the surface – or any other kind of chemical alteration of the samples in depth, some linescan profiles (intensities of Ca, Si and K) were measured on cross-sectioned model glass samples from all groups. The purpose was to observe if there would be changes of the composition of the glass after a long contact with the IL. When cutting the samples to cast them in epoxy resin, the alteration of the surface of the samples from group F (EDTA) was very evident; the mechanical properties were very different from those of the samples from all the other groups, as the group F samples were easily shattered during the cutting and polishing. This difference also influenced the linescan results, as it was not possible to obtain a clear and relatively homogeneous cross-section surface [figure 4.5 (c)].

The linescans are presented in figures 4.5 and 4.6. Observing the linescans, it is possible to verify that these are consistent with the Raman results. Meaning, the linescan of the control sample – figure 4.5 (a) – is very similar to those of the samples from groups B to E (high RH and ILs 1, 2 and 3) – figure 4.5 (b) and figure 4.6. In the first one [figure 4.5 (a)], it is possible to observe a slight increase of the Ca levels at the sample's surface – as the control sample was under vacuum in a controlled environment, most likely this occurs naturally during the production –, but the opposite is occurring on the other linescans mentioned. This would indicate that the Ca is being “captured”; however, this possible migration of Ca to the surface would be happening on a very small depth scale ($5\text{ }\mu\text{m}$) and only after a relatively long period of contact with the IL (7 days). Having into consideration the fact that the IL will be in contact with the glass surface only for a few minutes and that it can be completely removed from the surface of a glass that presents no corrosion, this effect on the Ca leaching is almost negligible for the time-scale of the IL/surface physical contact, specially having into consideration that the IL is being applied pure and un-diluted.

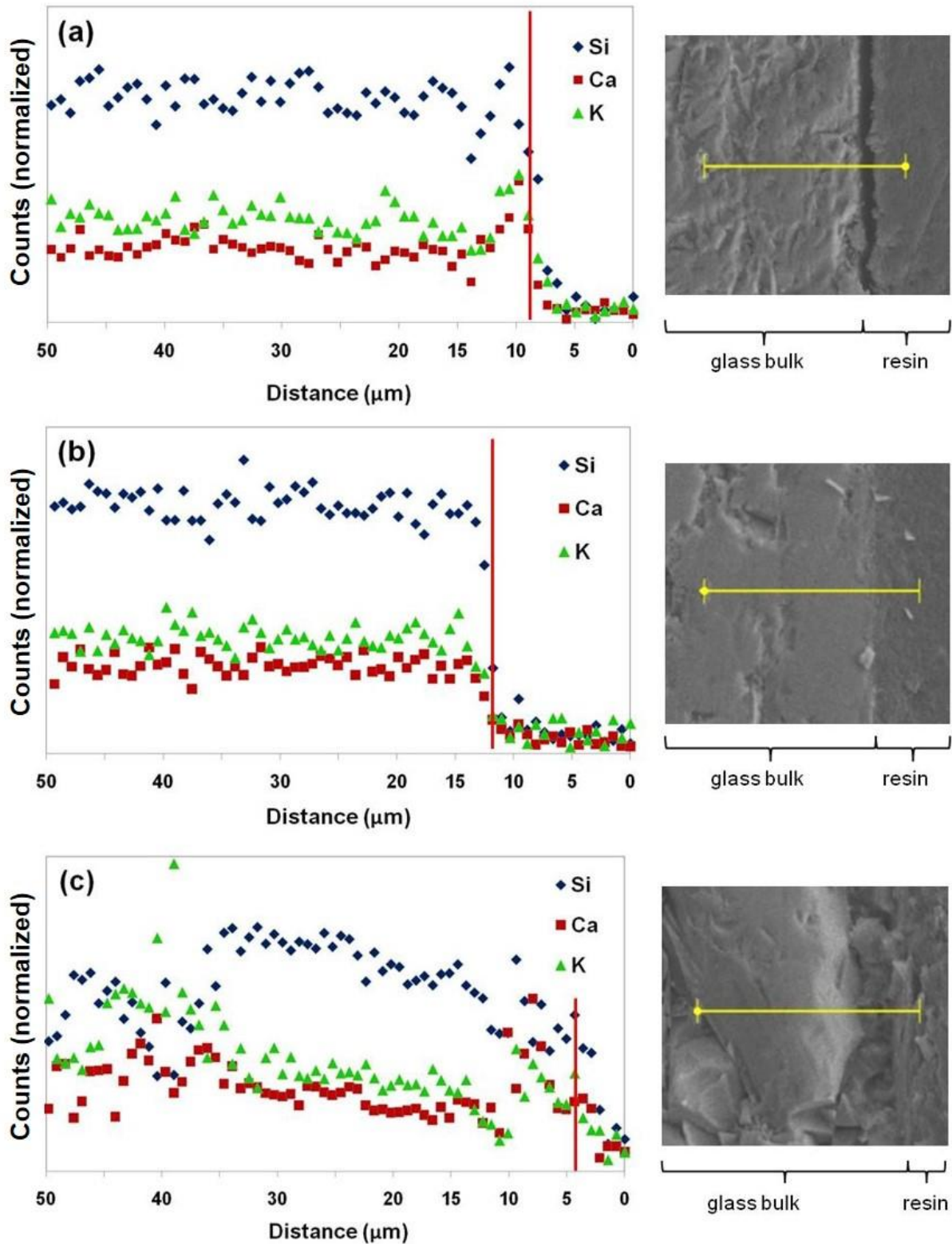


Figure 4.5: Linescan profile (intensities of Ca, Si and K) measured on a cross-sectioned (a) model glass sample from the control group (group A), (b) model glass sample left for 1 week in a high RH atmosphere (group B) and (c) model glass sample immersed in an EDTA solution for 1 week (group F). The red line in the linescan indicates where the glass bulk starts. On the right of each linescan profile, there is the correspondent image of the line where the measure was made, marked as a yellow line with 50 μm .

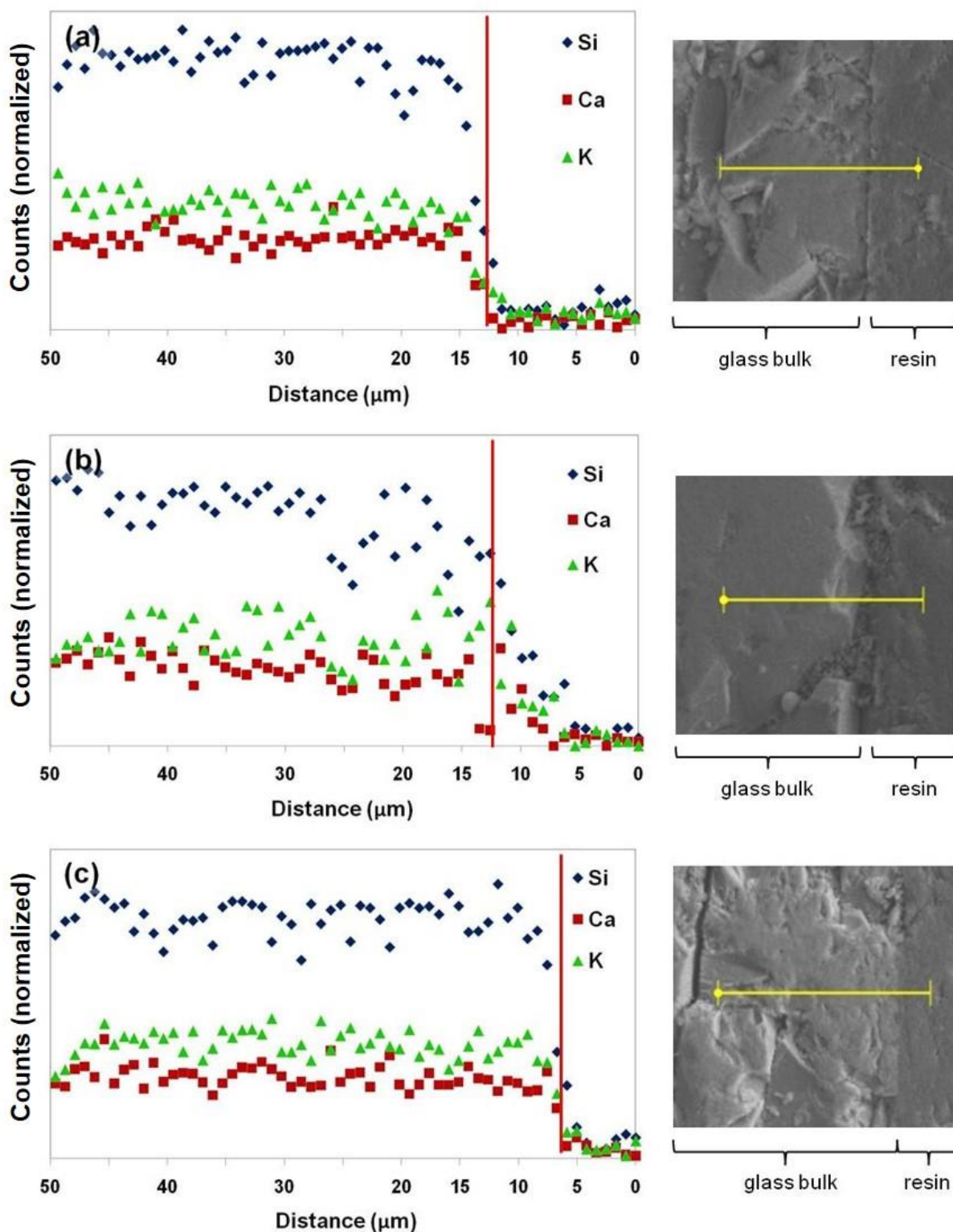


Figure 4.6: Line scan profile (intensities of Ca, Si and K) measured on a cross-sectioned **(a)** model glass sample after the application of the $[P_{6,6,6,14}][ANS]$ IL for 1 week (group C), **(b)** model glass sample after the application of the $[C_{5}O_{2}MIM][ANS]$ IL for 1 week (group D) and **(c)** model glass sample after the application of the $[P_{6,6,6,14}][PyrCOO]$ IL for 1 week (group E). The red line in the linescan indicates where the glass bulk starts. On the right of each linescan profile, there is the correspondent image of the line where the measure was made, marked as a yellow line with 50 μm .

4.3 Mid-term effect of the [P_{6,6,6,14}][ANS] IL on the glass surface

Considering that the [P_{6,6,6,14}][ANS] IL was the one presenting the most promising results in the tests performed on archaeological stained glass samples⁸, another set of tests was carried out using this IL on another group of model glass samples.

The experimental design, more detailed in Chapter 3.5, consisted in dividing the samples in three groups: a control group, a group subjected to induced corrosion using distilled water (to promote the formation of CaCO₃) and a third group subjected to induced corrosion using distilled water with H₂SO₄ (to promote the formation of CaSO₄). A drop of IL was deposited on 3 samples of each group, being a fourth sample left without IL. The emission spectra were measured in all samples, in order to control the intensity of the emission of the IL over time. Upon the removal of the IL, using a swab impregnated with a solution of water:ethanol (1:1/v:v), its complete removal was always controlled using an UV-light lamp (365 nm) and emission spectroscopy. Then each sample was analyzed to verify if there were any morphological and chemical alterations.

An emission spectra of the IL on the surface of an un-corroded sample was measured after 4 weeks to verify that the IL retains its fluorescent properties after deposition for a long time. Figure 4.7 demonstrates that ANS fluorescence remains intense 4 weeks after deposition [figure 4.7 (a)]. On the other hand, after the removal of the IL using a swab impregnated with ethanol, the emission is residual [figure 4.7 (b)], proving that the IL was almost completely removed from the un-corroded glass surface – the possible residues left on the surface are below the detection limit of about 10⁻⁷ M, which is a very low quantity⁹.

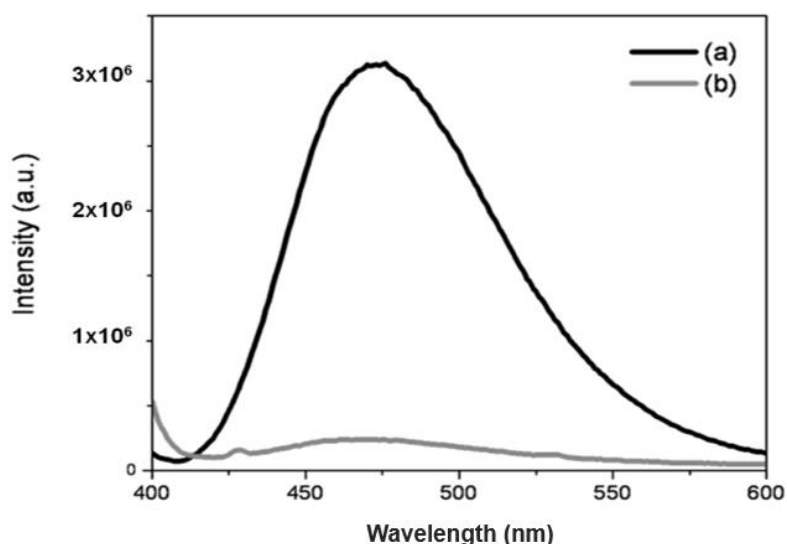


Figure 4.7: Emission spectra of the IL (a) 4 weeks after the application of the IL on a model glass sample and (b) after the removal of the IL.

⁸ Results presented and discussed in Chapter 5 - Corrosion crusts removal: archaeological stained-glass.

⁹ The detection limit for ANS fluorescence is estimated to be below 0.1 µg/cm².

The morphology of the surface of the non-corroded and corroded samples, before and after the application of the IL for 12 weeks, was observed by SEM – figure 4.8. On the non-corroded sample, there are no changes of the morphology of the glass surface after the application of the IL (figure 4.8 [a,b]). On the corroded sample, it is clear that the corrosion layers in the sample were removed. As can be observed in figure 4.8 (d), the surface of the sample appears much smoother than before the application of the IL – figure 4.8 (c) –, indicating that the insoluble salts were removed but a gel layer on the glass surface is still present.

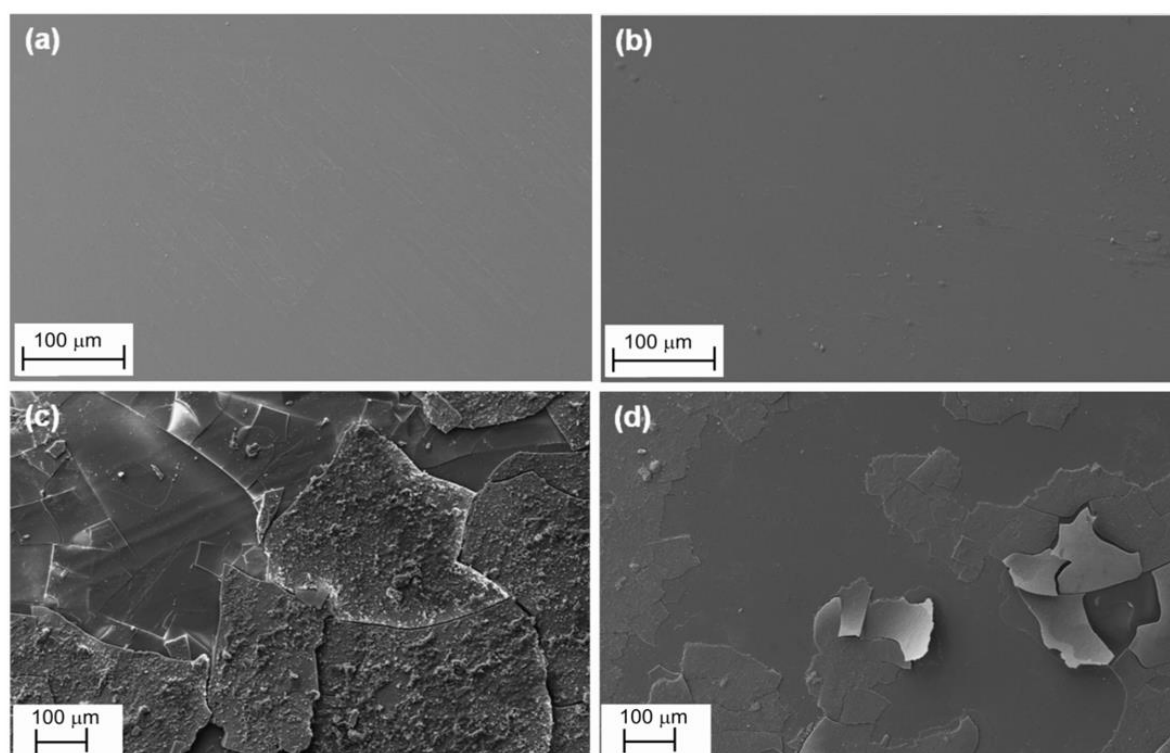


Figure 4.8: SEM image of the surface of an un-corroded sample – Group A – (a) before and (b) after the application of $[P_{6,6,6,14}][ANS]$ IL for 12 weeks, 200x magnification. SEM image of the surface of an artificially corroded sample from Group B (c) before and (d) after the application of $[P_{6,6,6,14}][ANS]$ IL for 12 weeks, 100x magnification.

4.4. – *Grisaille*: Application of the IL $[P_{6,6,6,14}][ANS]$ on *grisaille* painted model glass

Model glass samples from the same roundel as the one used for the experiences previously described was painted with brown and black *grisaille* paint from Debitus®. According to the brand, these paints have a composition similar to the medieval *grisaille* [in website www.debitus.com, Debitus 1991]¹⁰. The model glass samples were painted using a *grisaille* and Arabic gum paint, and then fired at 650 °C for 1 hour.

¹⁰ See Chapter 3.1, p.35, for more details on this matter.

The samples were distributed by 5 groups, each with one sample of each color or *grisaille*. The first group has the control samples, then a small amount of [P_{6,6,6,14}][ANS] IL was applied in the other samples and left for 15 min, 1 day, 7 days and 28 days. The goal was to determine if there were any alterations caused by the IL in the *grisaille* painted surface.

During the time that the IL was in contact with the samples' surface, there was no apparent alteration of the IL's physical characteristics, regardless of the time range. The viscosity remained quite similar, it did not seem to be more or less adhered to the surface, and the process of removal was not more nor less difficult for the samples of longer time ranges, and the IL luminescence remained very intense. This observations are based on the experience and no measures or further analysis were performed in this case.

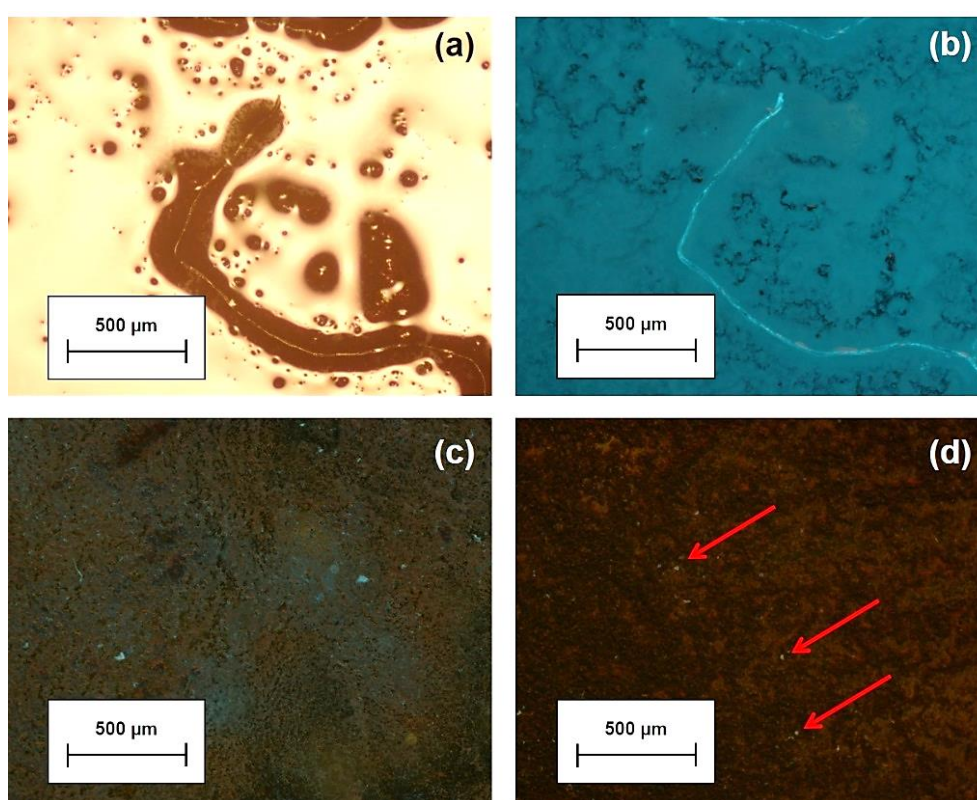


Figure 4.9: Optical microscope images of the surface of the model glass samples, with a 5x magnification (a) of a *grisaille* painted sample, after the removal of the [P_{6,6,6,14}][ANS] IL using a dry swab, bright field filter, (b) and the same sample under UV-light filter (c) after the removal of the IL using a swab impregnated with a water:ethanol (1:1) solution once, and (d) after another passage with a swab impregnated in the same solution.

The removal process, however, was more complicated when compared with the model glass samples without any *grisaille*, which is understandable as the painted surface is more rough [Schalm 2003]. When trying to remove the IL with a dry swab – almost enough in the case of the non-painted model glass samples, though it was always used one impregnated with a water:ethanol (1:1) solution to guarantee the complete removal of the IL –, there was still a very thick layer of IL left on the surface. This is clear when observing figure 4.9 (a), and even more when looking at the same sample under the

UV-light filter in figure 4.9 (b). For this same sample, two more images are presented, representing two more stages in the cleaning process, always using an impregnated swab as mentioned above, and though in figure 4.9 (c) some traces of the IL are still visible (only under UV-light, using other filters it is not possible to observe the presence of the IL at this scale), in figure 4.9 (d) the IL has been removed almost entirely, with the exception of the small traces pointed in the figure. Photo-degradation tests performed in archaeological stained glass fragments with traces of $[P_{6,6,6,14}][ANS]$ IL, described and discussed in Chapter 5, present a solution to minimize this risk.

4.4.1 – Effect of the IL on the *grisaille* layer

The morphology of the surface of the model glass samples painted with *grisaille* was analyzed by optical microscopy before and after the deposition of the $[P_{6,6,6,14}][ANS]$ IL for different time ranges. As can be seen in figure 4.10, the IL does not seem to have affected the surface's morphology.

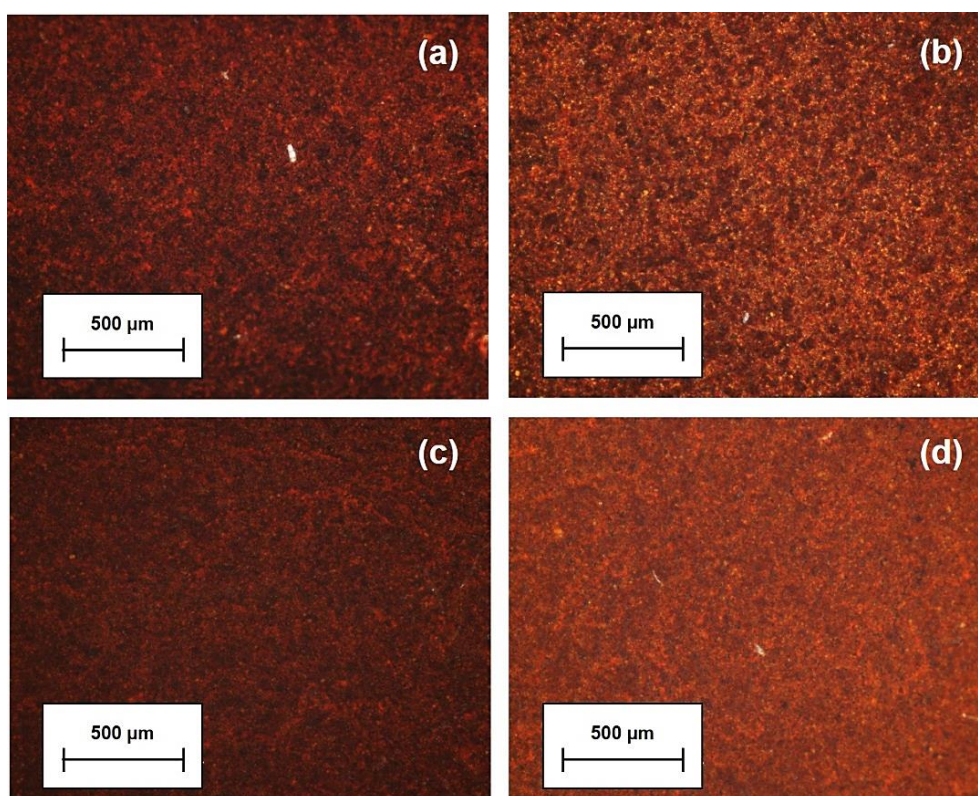


Figure 4.10: Optical microscope images of the surface of the model glass samples, with a 5x magnification of *grisaille* painted model glass samples that were in contact with $[P_{6,6,6,14}][ANS]$ IL for: **(a)** 15 minutes, **(b)** 1 day, **(c)** 1 week and **(d)** 28 days, all after the removal of the IL using a swab impregnated with a water:ethanol (1:1).

As the samples were painted and fired, and not subjected to any induced corrosion or degradation processes previously, the *grisaille* layer is in a very good condition. It would be necessary to have a substance with a very high chelating power, which is not the case of the IL tested, that did not present indications of damaging the *grisaille* layer even when in permanent contact for a long period of time.

4.5 – Conclusions

After the application of the ILs, there were no apparent changes neither on the surface of the glass nor in the glass composition. However, the same type of glass samples that were subjected to 88% RH and an EDTA solution exhibited both chemical and morphological changes on the glass surface, confirming that these chemical stress is damaging the glass, even when in contact for a relatively short period of time.

The results described and discussed above, seem to indicate that the ILs tested – [P_{6,6,6,14}][ANS], [C₅O₂MIM][ANS] and [P_{6,6,6,14}][PyrCOO] – will not cause any detectable morphological or chemical alterations on the glass surface, even when in direct contact for longer periods of time. The preliminary tests in some *grisaille* painted model glass samples also did not present any evidence of damage induced by the [P_{6,6,6,14}][ANS] IL, even when in direct contact with the samples' surface for a long period of time.

Provided that the [P_{6,6,6,14}][PyrCOO] IL did not present enough physical and chemical stability, even though there were no evidence of this IL provoking changes on the glass composition or surface morphology, it was decided not to use this compound in further tests – specifically on archaeological samples –, not only because the results might not be reliable and reproducible, but especially because any product used in the conservation practice must be chemically stable.

Chapter 5

Corrosion crusts removal: archaeological stained-glass

5.1 – Archaeological stained-glass samples

In this chapter, the results of all the tests performed using archaeological stained glass samples will be presented and discussed. The main aim of these tests was to determine the effectiveness of the ionic liquids (ILs) produced and if there were any alterations – morphological and chemical – on the corrosion crusts, on the glass surface and on the painting caused by the different products tested. The archaeological samples are medieval stained-glass fragments from a Franciscan friar in Canterbury. The set provided has dozens of fragments, each with different colors and thickness, some painted with *grisaille* and yellow silver stain. The composition of the samples used is described in chapter 3.3.

The tests can be divided in two categories (experimental design described in chapter 3):

1. Comparison between the efficiency of two different ILs – [P_{6,6,6,14}][ANS] and [C₅O₂MIM][ANS] – and EDTA in the removal of corrosion crusts, as well as the effect of such products on these crusts;
2. Long-term effect of the [P_{6,6,6,14}][ANS] IL on the corrosion crusts, on the glass surface and on the painting.

On a first stage, three archaeological samples were selected and cut in four sections – one remained a control fragment, and to the others [P_{6,6,6,14}][ANS] IL, [C₅O₂MIM][ANS] IL and EDTA were applied for comparison (see chapter 3.4).

For the second category of tests, six samples were selected, with different colors, with and without *grisaille* painting, all presenting a thick corrosion layer constituted of several compounds and a size exceeding 2 x 1 cm² to allow performing the tests described; each of the 6 archaeological samples was cut in half, to proceed to 2 different types of test: one half was used for the cleaning tests – analyzing the amount of corrosion removed using the IL –, and the other half was used in the mid-term effect tests on the glass surface (see chapter 3.5).

The samples have been characterized before and after the cleaning treatment and the characterization was performed using microscopy techniques – such as Optical Microscopy and Scanning Electron Microscopy (SEM) –, Fourier transform infrared spectroscopy (FTIR) and Scanning Electron Microscopy with Energy Dispersive Scattering (SEM-EDS), for elementary maps.

Finally, two samples were clean using only the [P_{6,6,6,14}][ANS] IL, for a more general view of its effect on the surface.

5.2 – Comparison of the effect of ILs and EDTA on the glass surface

On a first stage, three archaeological samples were selected and cut in four sections – one remained a control fragment, and to the others [P_{6,6,6,14}][ANS] IL, [C₅O₂MIM][ANS] IL and EDTA were applied for comparison (see figure 5.1 and chapter 3.4 for more details). After the application of the respective IL or EDTA, each section was cut in half: one part had its surface analyzed, and the other was casted in epoxy resin for a cross-section analysis.

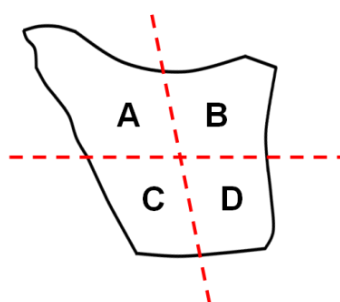


Figure 5.1: Scheme of division of an archaeological sample: Section A (control group), section B ([P_{6,6,6,14}][ANS]), section C ([C₅O₂MIM][ANS]) and section D (EDTA solution).

When comparing the surface cleaned using the [C₅O₂MIM][ANS] IL with the one cleaned with [P_{6,6,6,14}][ANS], there is a very small difference indicating that the first might be slightly more effective in the removal of corrosion crusts, which could be explained by the functional groups in the cation molecule (see Chapter 2.3.3). However, this difference is not very significant, and both ILs appeared to leave a smoother surface in the fragment than the EDTA solution used. This observations are based on the experience performed in the three archaeological stained glass samples, in small fractions of the fragments.

Elementary maps of each cross-section were made using Scanning Electron Microscopy. An example of all four sections of a sample is presented in figure 5.2. The hydrated layer, rich in Si and O is clearly visible below the grisaille painting layer, rich in Fe, and right above this one there is a calcium corrosion crust, very evident.

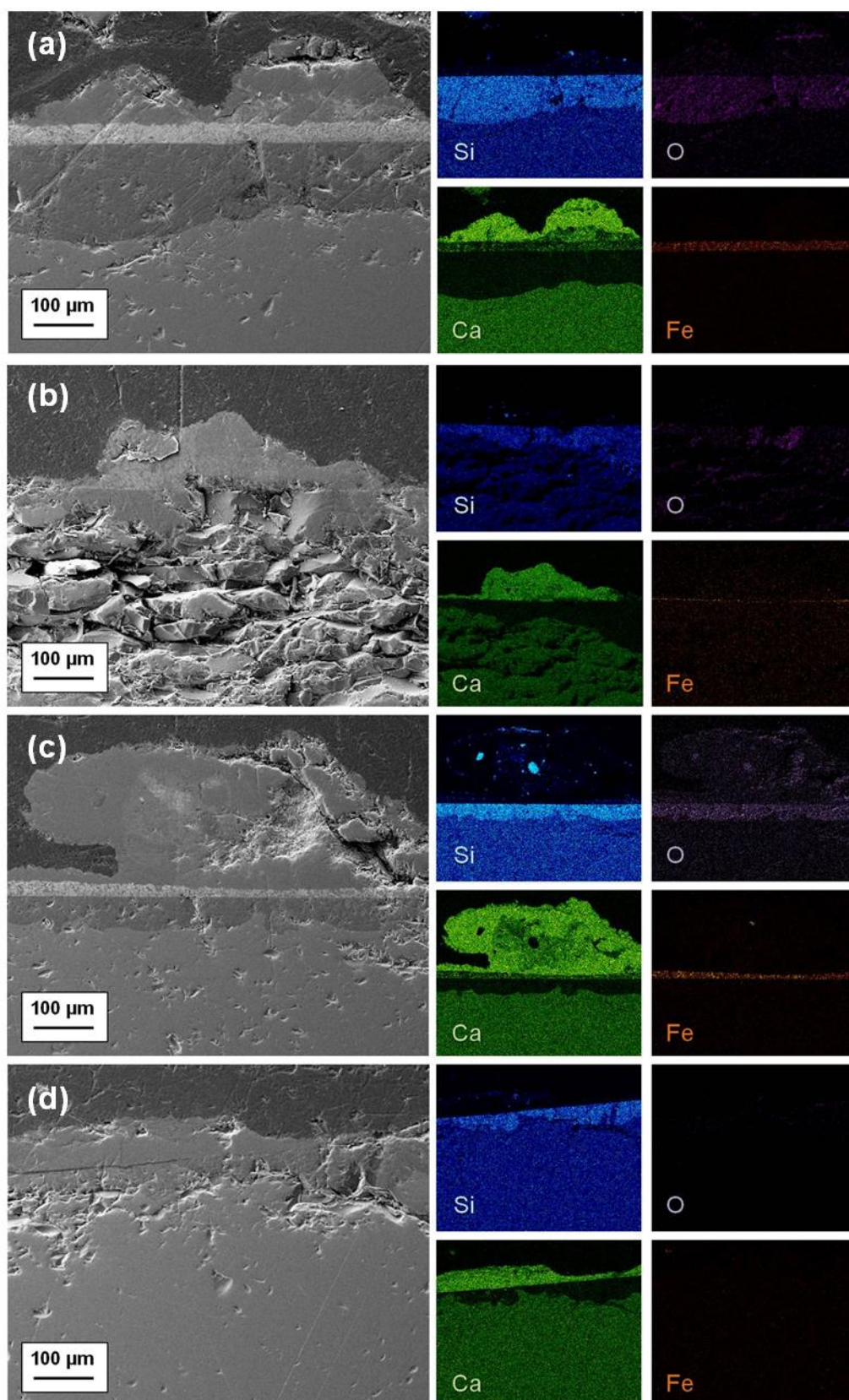


Figure 5.2: SEM images and EDS maps of a cross-sectioned archaeological sample **(a)** before and **(b)** after the application of the $[P_{6,6,6,14}][ANS]$ IL, **(c)** after the application of the $[C_5O_2MIM][ANS]$ IL and **(d)** after the application of the and EDTA solution. The corresponding EDS maps for Si, O, Ca and Fe are presented. In these images it is possible to see a layer very rich in Si (hydrated layer), and another above very rich in Ca (corrosion layer), as well as the Fe (corresponding to the *grisaille* layer).

There is no apparent alteration between the control section and the others where the ILs and EDTA were applied, being the difference in the thickness of the Ca and Fe layers due to the fact that the areas analyzed are different; naturally, both the corrosion layer and the *grisaille* painting are heterogeneous layers. The shattering, more clear in figure 5.2 (b), is a result of the cutting process, though does not seem to interfere with the elementary maps obtained. These elementary maps (more examples can be seen in appendix III) suggest that the ILs tested and the EDTA are not affecting the Ca nor the hydrated layers of the samples in which they were applied, even in areas where the porous corrosion layer is thinner and more easily permeable to these compounds.

All the samples were also analyzed by FTIR to determine if the composition of the corrosion crusts suffered any alteration after the application of the ILs and EDTA solutions. In the spectra presented in figure 5.3. The significant decrease of intensity of the bands $\sim 1400\text{ cm}^{-1}$ and $\sim 870\text{ cm}^{-1}$, that correspond to calcium carbonate [Machado 2010], is associated with the removal of these calcium salts during the cleaning procedure, though there are still traces of these compounds. It is also possible to observe the presence of SiO-O band (1035 cm^{-1}) [Machado 2010], which remains relatively unaltered – within the experimental background – on the spectra of the samples where the IL and EDTA were applied.

The fact that these corrosion species are still present, as well as the SiO-O band, indicates that neither the IL nor the EDTA solution altered the corrosion composition in these samples in a way that would be detectable by FTIR. However, a more exhaustive study would be recommended in order to exclude this possibility entirely.

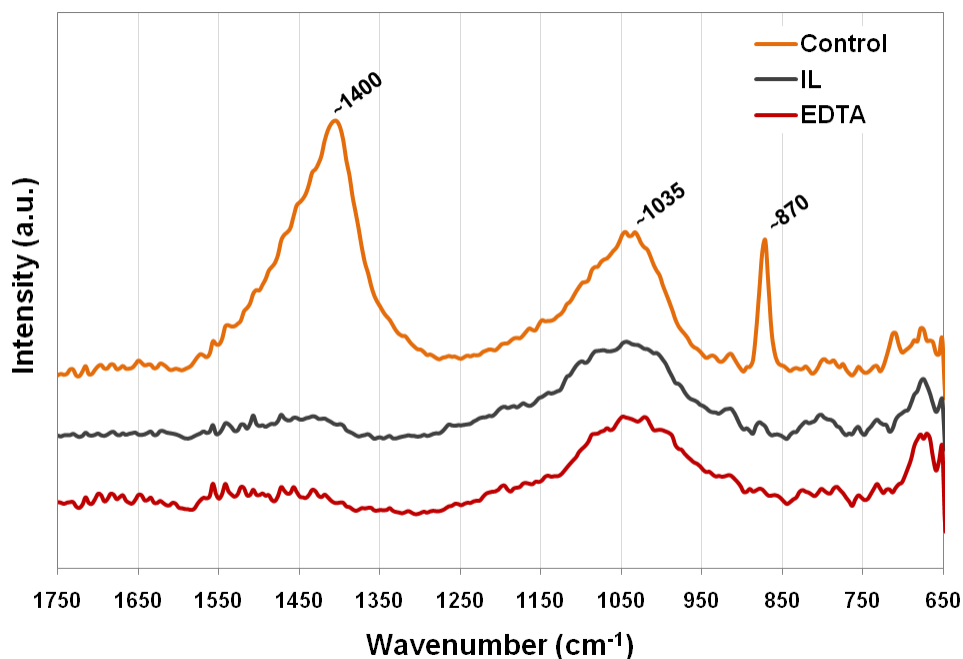


Figure 5.3: FTIR spectra of archeological samples, before and after the application of the IL and EDTA, with the indication of the most representative peaks.

The pH of the surface of the samples was measured in order to determine if there were alterations after the application of the ILs or EDTA. This is very important, as pH has a strong influence on the glass degradation and development of further corrosion, being essential to keep the pH stabilized [Janssens 2013]. As showed in figure 5.4, there was a significant increase of the pH value after the application of an EDTA solution, especially in the case of the samples Cant 033 and Cant 034, that are either close of above the pH level of 9, that is considered as a safety pH limit, above which the Si-O bonds start breaking [Clark 1979]. The ILs did not seem to alter the surface's pH.

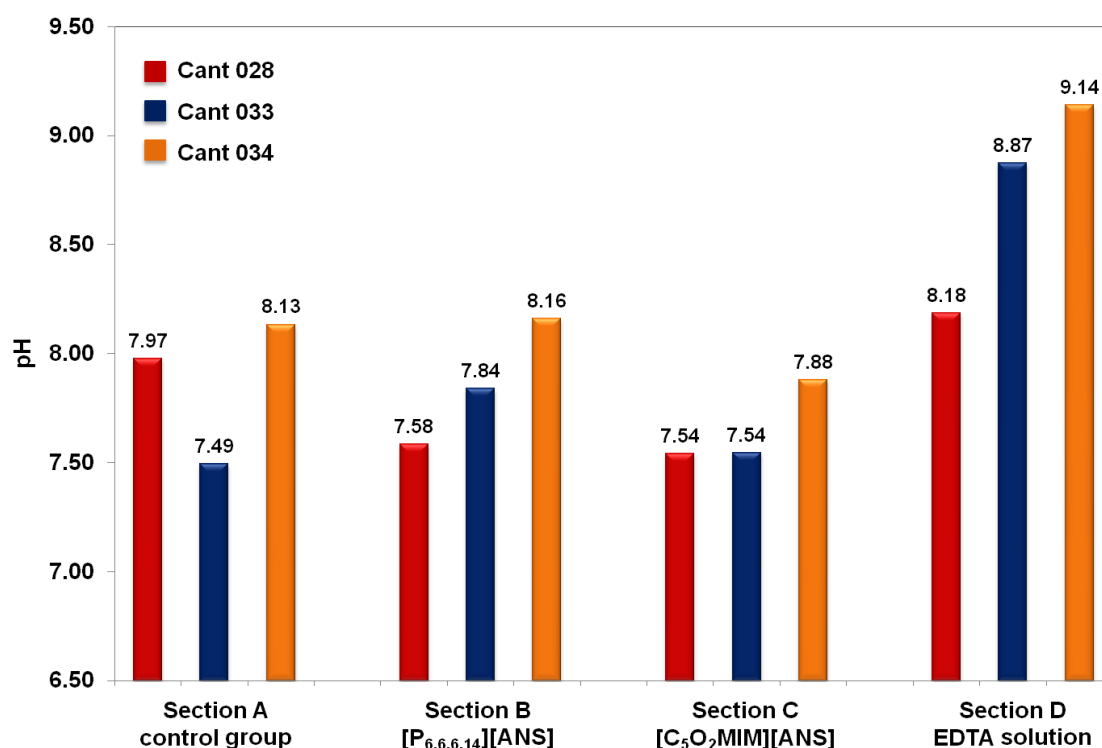


Figure 5.4: pH of the surface of samples Cant 028, Cant 033 and Cant 034, before and after the application of [P_{6,6,6,14}][ANS] IL, [C₅O₂MIM][ANS] IL and an EDTA solution. For every sample, three measurements were made, and the average is presented in the chart above, with the respective value indicated. The standard deviation is <0.07 for all samples except Cant 028 A (0.19) and Cant 033 C (0.14).

The [P_{6,6,6,14}][ANS] IL is more hydrophobic than the [C₅O₂MIM][ANS] IL, which can be an asset in a compound to be applied on a glass surface, as water is one of the main causes of the formation of corrosion crusts. Having this into consideration, as well as the fact that the [C₅O₂MIM][ANS] IL more likely has a stronger chelating power, the [P_{6,6,6,14}][ANS] IL was selected to be further tested in archaeological stained glass samples.

5.3 – Effect of the [P_{6,6,6,14}][ANS] IL on the glass surface

The IL effectively removed most of the corrosion crusts, as presented in figure 5.5. There are no significant differences when applying the IL for 5 minutes or 4 hours, which indicates the IL has a relatively fast action, removing the crusts after a few minutes, while its effect is also limited as it does not eliminate the corrosion layer completely. The IL is easily removed from the clean glass surface, simply using a swab impregnated with a water:ethanol (1:1) solution. However, it is difficult to completely remove the IL from the corrosion crusts, as can be observed in figure 5.5 (c). It is also possible to observe than in the thinner corrosion layer, highlighted in figure 5.5, the IL was easily removed after the cleaning procedure.

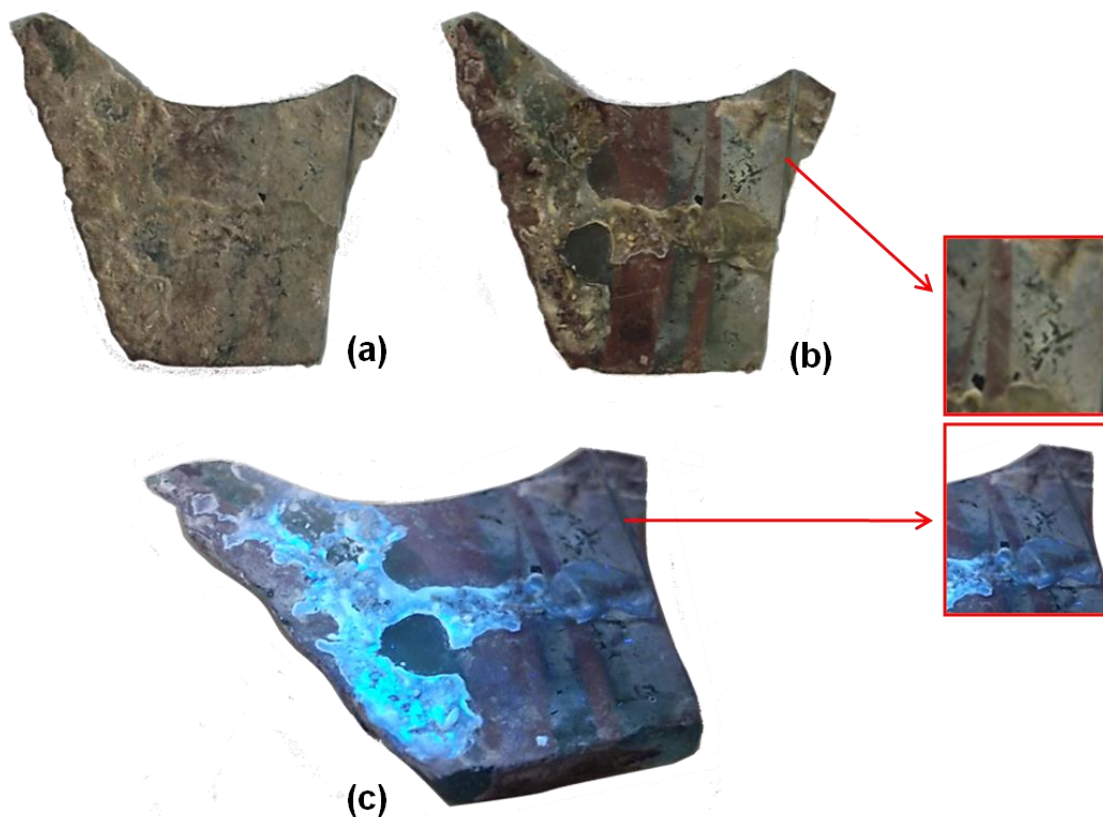


Figure 5.5: Archaeological sample (a) before and (b) after cleaning tests using [P_{6,6,6,14}][ANS] IL, under natural light, (c) and after the cleaning tests, under 365 nm UV-light.

The emission remains intense 8 weeks after the IL deposition (Figure 5.6 (a)). Photodegradation tests show that after 10 minutes of exposure to a Solar Lamp, the emission of the IL is drastically reduced (Figure 5.6 (b)). This indicates a possible photo-oxidative degradation of the IL and, most likely, this degradation will inhibit its effectiveness on reacting with the calcium ions, forming essentially calcium carbonates – and sulfates, in smaller quantities –, which is similar to the composition of the glass corrosion. [Chen 2010, p. 4207-08]

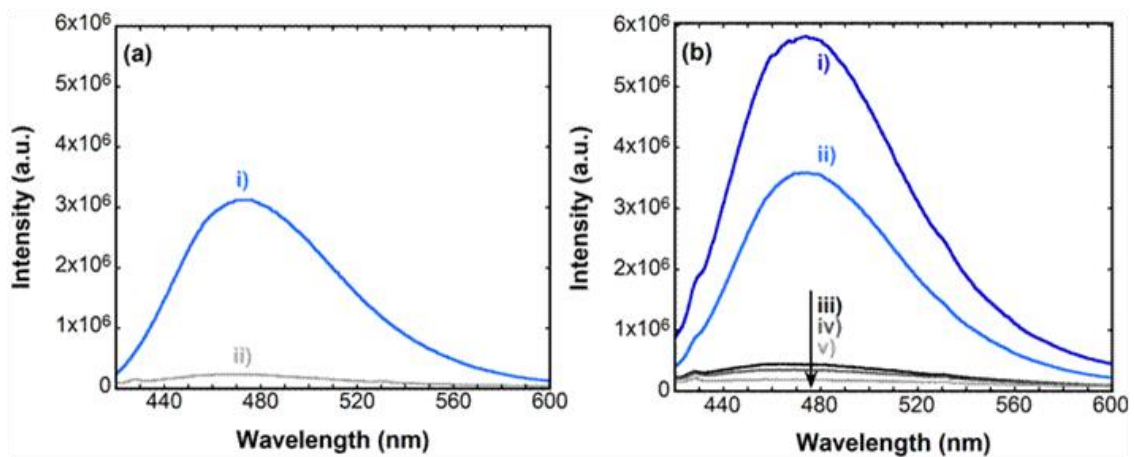


Figure 5.6: (a) Emission spectra of the IL (i) 4 weeks after the application of the IL on a model glass sample and (ii) after the removal of the IL. (b) Emission spectra of the IL (i) when it is applied on an archaeological sample, (ii) after 4 weeks, (iii) after the removal of the IL (iv) and after being photodegraded using a Solar lamp for 1 minute and (v) 10 minutes.

The morphology of the corroded surface of the samples, before and after the application of the IL, was observed by optical microscopy – figure 5.7 (a,b) – and by SEM – figure 5.7 (c,d). White opaque crystalline forms were observed, and the corrosion products showed a great adhesion to the surface. The images were taken in different areas of the samples. It is possible to observe that the morphology of the corrosion and of the area without corrosion has not been altered after the application of the IL. The corrosion layer on figure 5.7(b) seems only slightly smoother than the same on figure 5.7(a).

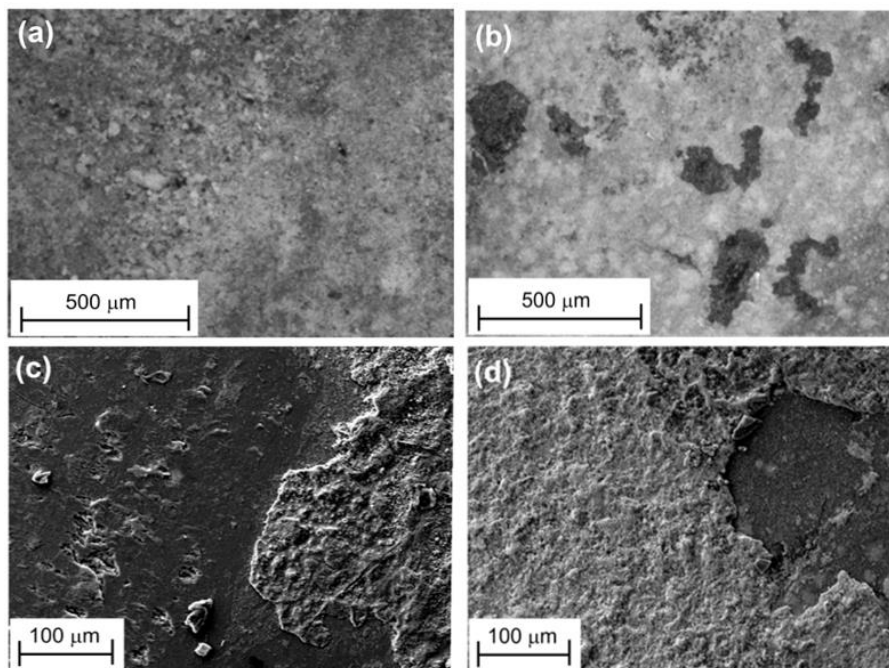


Figure 5.7: Optical microscope image of the surface of an archaeological sample (a) before and (b) after cleaning tests using [P_{6,6,6,14}][ANS] IL. 5x magnification, dark field filter. SEM image of the surface of an archaeological sample (c) before (d) and after the application of [P_{6,6,6,14}][ANS] IL for 12 weeks, 200x magnification.

In the FTIR spectra presented in figure 5.8, the presence of calcium salts as a combination of calcium carbonate, calcium sulfate and calcium oxalate is confirmed. It is also possible to observe that these corrosion species are present even after the cleaning procedure, proving that the IL does not alter the corrosion composition. In the FTIR spectra presented in figure 5.8, the presence of Si-O-O band (1030 cm^{-1} , 1038 cm^{-1}) [Machado 2010] and of calcium salts, such as calcium carbonate (1423 cm^{-1} , 1419 cm^{-1} , 876 cm^{-1} , 714 cm^{-1}) [Machado 2010] is confirmed.

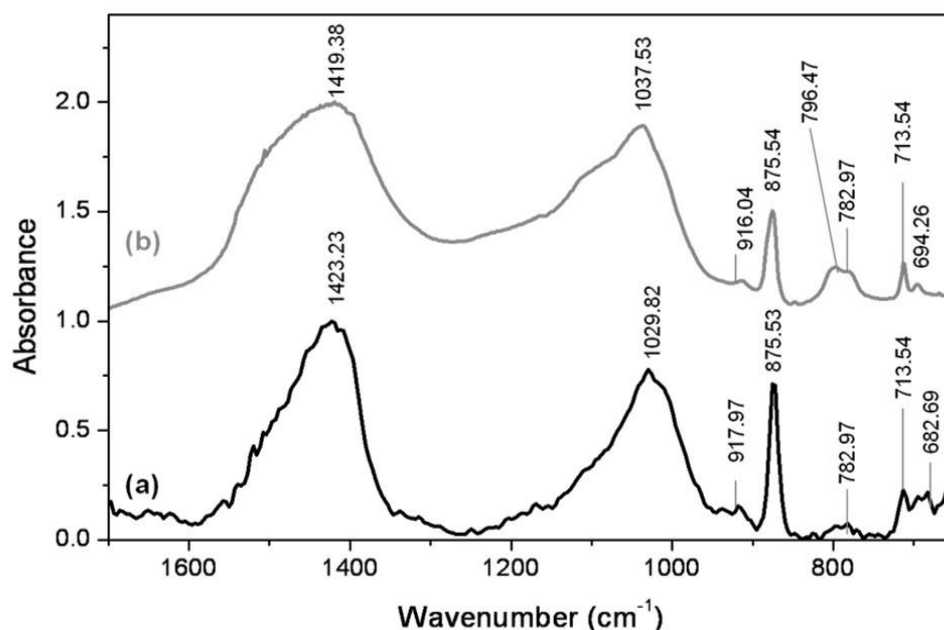


Figure 5.8: FTIR spectra of the corrosion present in the surface of an archaeological sample (a) before and (b) after the application of the [P_{6,6,6,14}][ANS] IL.

SEM-EDS elementary maps of a cross-sectioned sample were performed for the following elements: Si, O, Ca, P, C, Na, Mg, K. It is important to refer that the lack of cohesion of the corrosion layer, observable on the sample without IL, is due to the cutting process – using a diamond tipped glass cutter –, which sometimes lead to the chipping of the corrosion layer. On these maps, represented in figure 5.9, the Ca from the corrosion crust is clearly visible on the surface of the sample, as well as lack of Si on the area rich in Ca. It is possible to observe a rich layer of Si and O right under the corrosion layer, corresponding to the hydrated layer. On the elementary map that corresponds to the unclean sample, the Si rich layer is not visible, as in this sample the surface is more heterogeneous. However, the O rich layer is evident in that area, which can indicate that a hydrated layer is present. The differences between the composition before and after the cleaning process are not evident. Besides the Ca layer, that seems to get thinner after the application of the IL, the other elements appear to maintain their distributions.

The P maps presented were included as a more intense concentration of P on the surface could be indicative of the presence of IL on a larger scale, having into consideration that most elements in its

chemical composition – $([\text{CH}_3(\text{CH}_2)_5]_3\text{P}(\text{CH}_2)_{13}\text{CH}_3\text{Cl}) \cdot (\text{C}_{16}\text{H}_{13}\text{NO}_3\text{S} \cdot \text{NH}_3)$ – might be confused with the glass chemical composition. There is no apparent concentration of P on the surface of the sample suggesting this.

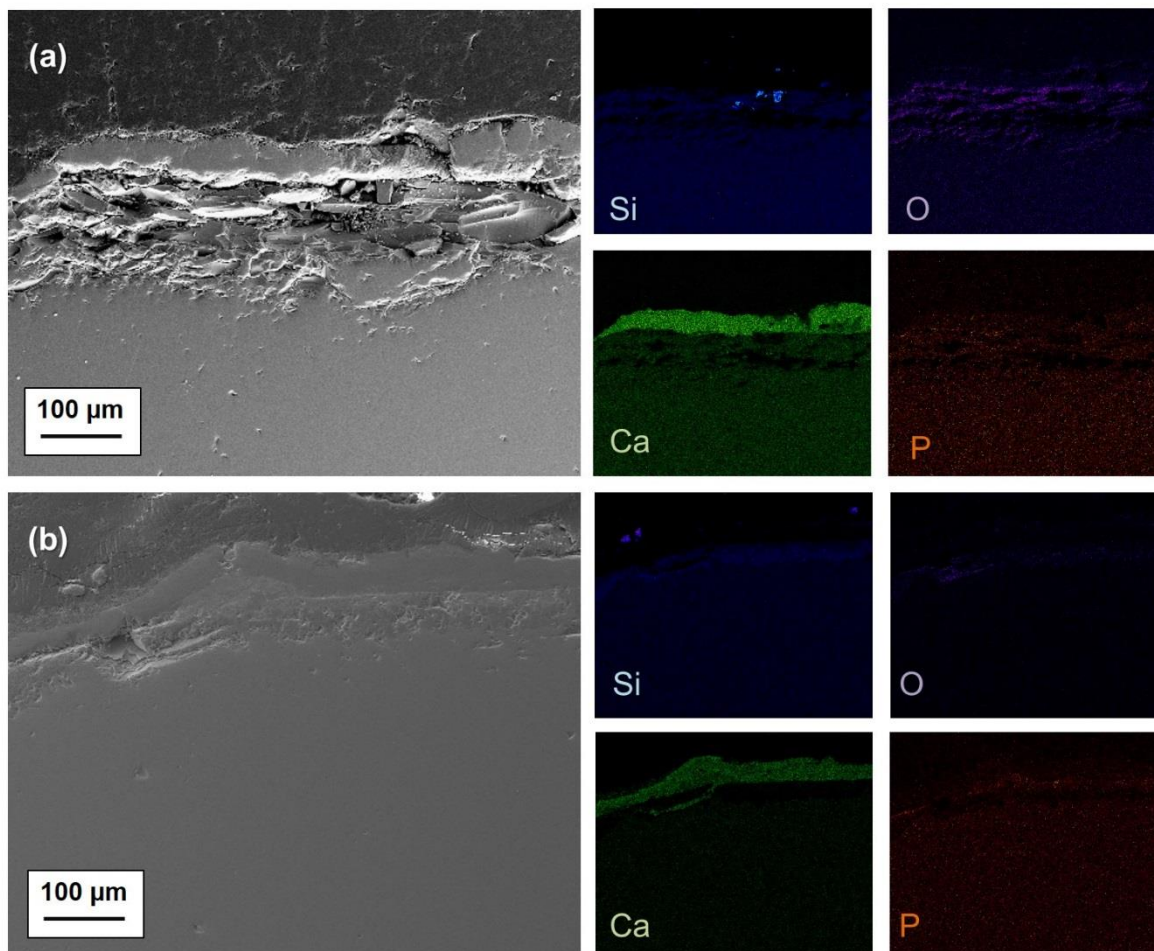


Figure 5.9: SEM-EDS elementary maps of a cross-sectioned archeological sample (a) before and (b) after the application of the IL $[\text{P}_{6,6,6,14}][\text{ANS}]$. 100x magnification.

5.4 – Before and after [P_{6,6,6,14}][ANS]

Other archaeological stained glass samples were selected to test the effect of the [P_{6,6,6,14}][ANS] IL. These samples were photographed before and after the cleaning procedure, in reflected and transmitted light, and the results can be seen bellow, in figures 5.10 and 5.11. It is important to mention that before the application of the IL – and before taking the photos –, the samples were clean with a swab impregnated with a water:ethanol (1:1, v:v) solution.

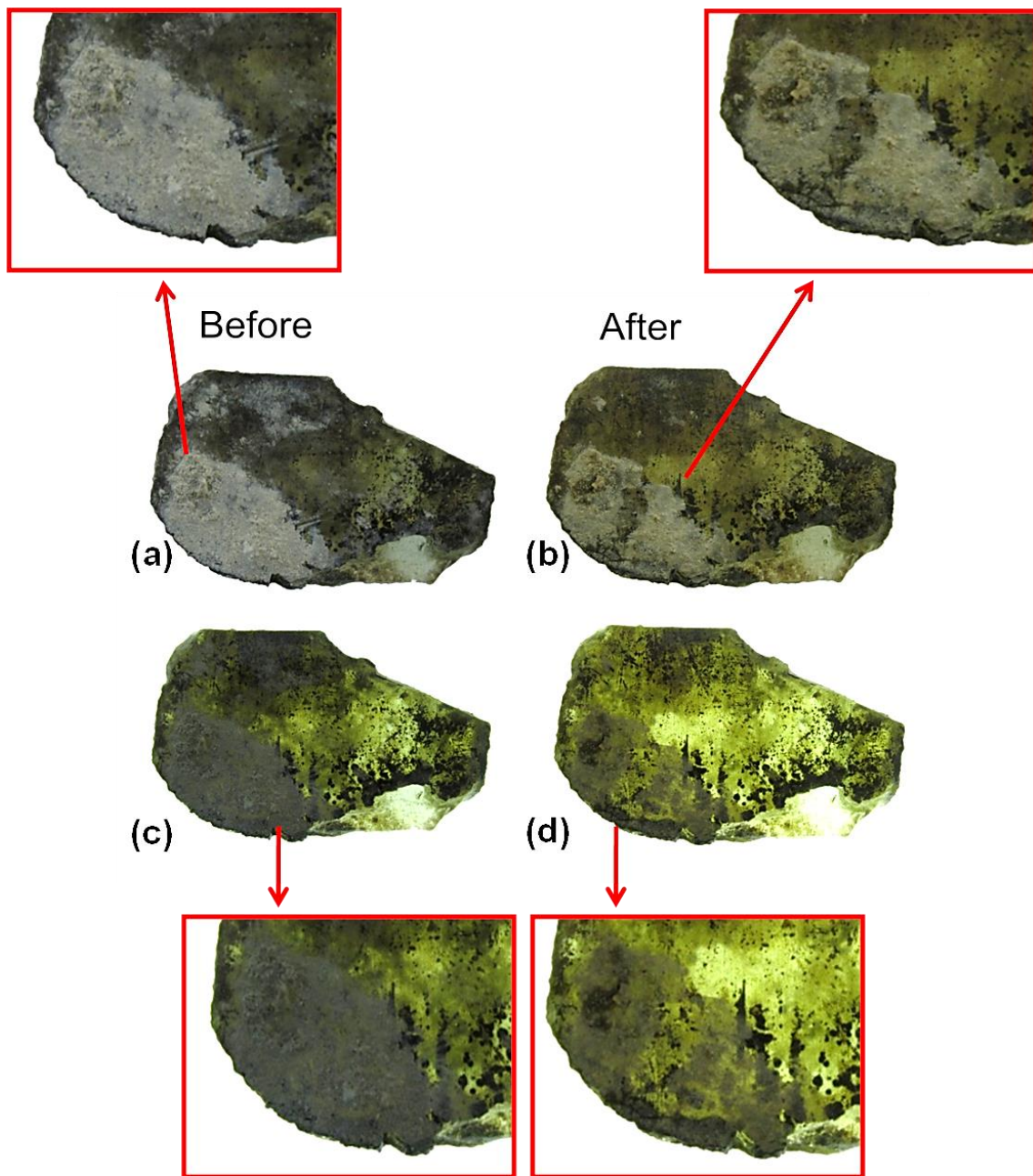


Figure 5.10: Archaeological stained glass fragment before and after the application of [P_{6,6,6,14}][ANS] IL, with reflected light (a,b) and transmitted light (c,d).

In general, the transparency of the fragment significantly increased. It is also possible to see that larger corrosion crust – highlighted in figure 5.10 – was not entirely removed, but enough to increase considerably the transparency on that area of the fragment, leaving the *grisaille* painting below visible.

A similar result was obtained after applying the IL on the surface of another sample. The results can be seen in figure 5.11, and the transparency increase is significant, being now the painting layer clearer and the silver staining brighter, though there is still a visible corrosion layer. As it was previously mentioned, the intention was not to remove the corrosion completely, only to increase the transparency and visibility of the stained glass fragments, and this objective has been achieved.

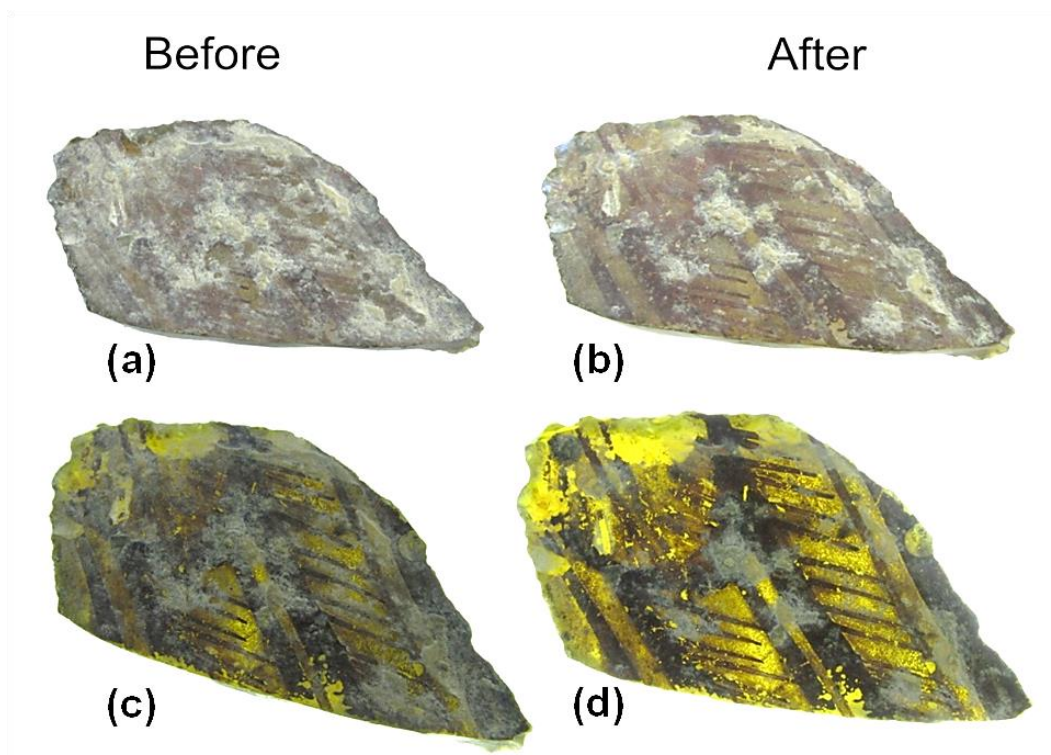


Figure 5.11: Archaeological stained glass fragment before and after the application of [P_{6,6,6,14}][ANS] IL, with reflected light (a,b) and transmitted light (c,d).

Another example of an archaeological fragment before, during and after the cleaning procedure using the [P_{6,6,6,14}][ANS] IL can be found in Attachment III, as well as a table with all archaeological samples from the set from Canterbury.

5.5 – Possible mechanisms and effects: a general comparison between the IL and EDTA

As discussed previously, and looking at the molecules of the [P_{6,6,6,14}][ANS] IL and EDTA (Chapter 2.3.3), it is clear that the latest has a stronger chelating power. Depending on its concentration, pH and time of application, EDTA might bind not only with the Ca²⁺ present in the corrosion crusts, but also with the Ca from the glass surface, as well as other metal ions – as, for example, from painted layers in the glass.

One important difference between the two might rely on their viscosity. While EDTA is usually prepared and applied as an aqueous solution, quickly penetrating in the porous and micro-cracks on the glass surface. On the contrary, the IL is applied pure, as a concentrated viscous liquid that will penetrate slower on the surface – and most likely not entirely –, being more easily removed as it remains in more superficial layers, not to mention that the complete removal may always be controlled using a UV-lamp.

5.6 – Conclusions

As expected, the success of the cleaning procedure, as a larger scale removal of the corrosion crusts, depends on the specific composition and thickness of such layer. ILs may be considered a new alternative to conventional cleaning methods for corrosion crusts. The [P_{6,6,6,14}][ANS] IL is very effective, and relatively fast, removing corrosion crusts from the glass surface. There are no apparent changes neither on the surface of the glass, nor in the glass and corrosion crusts' composition, and the pH of the samples' surface seemed to remain stable, especially when compared with the samples treated with the EDTA solution. This seems to be an effective and safe method for the removal of corrosion crusts, both for the object and for the conservator/user – due not only to a low toxicity, but also for its non-volatile nature, preventing the user from being in contact with possibly harmful vapors, during the application of the IL and its removal, that can be done using a water:ethanol (1:1) solution.

The IL is easily removed from the clean glass surface and from thin corrosion layers, but it is difficult to completely remove the IL from the corrosion crusts. The IL is photodegradable and, most likely, this degradation will inhibit its effectiveness on reacting with the calcium ions. The composition and morphology of the corrosion and of the glass has not been altered after the application of the IL.

Any cleaning procedure should remove the corrosion deposits only as far as necessary to improve the transparency, without damaging the hydrated glass surface underneath. A thin – protective – residual layer should be left on the surface, rather than removing the crust down to the bulk glass, which would trigger further degradation. Special attention is necessary when cleaning painted areas, since the loss of paint would irreversibly damage the artistic integrity of the stained-glass. Preliminary tests show that the IL [P_{6,6,6,14}][ANS] does not damage or remove the *grisaille* painting.

Conclusions

First of all, it is important to emphasize once again that any cleaning procedure should remove the corrosion deposits only as far as necessary to improve the transparency, without damaging the hydrated glass surface underneath. A thin – protective – residual layer should be left on the surface, rather than removing the crust down to the bulk glass, which would trigger further degradation. Special attention is necessary when cleaning painted areas, since the loss of paint would irreversibly damage the artistic integrity of the stained-glass.

After the tests and analysis performed, it is secure to affirm that ILs may be considered a new alternative to conventional cleaning methods for corrosion crusts. The [P_{6,6,6,14}][ANS] IL is very effective, and relatively fast, removing corrosion crusts from the glass surface. There are no apparent alterations neither on the morphology of the glass surface nor in the glass composition, which was clearly demonstrated by tests performed in model glass samples.

The IL is easily removed from the clean glass surface and from thin corrosion layers, but it is difficult to completely remove the IL from thicker corrosion crusts. However, the IL is photodegradable (under a Solar Lamp) and, most likely, this degradation will inhibit its effectiveness on reacting with the calcium ions. The composition and morphology of the corrosion and of the glass has not been altered after the application of the IL. This seems to be an effective and safe method for the removal of corrosion crusts.

It is also important to mention the safety of this method for the conservator/user, not only due to a low toxicity of the ILs, but also for its non-volatile nature, preventing the user from being in contact with possibly harmful vapors during the application of the IL and its removal may be done using a water:ethanol (1:1) solution.

The synthesis process of the [P_{6,6,6,14}][ANS] IL is relatively simple and it has been published already [Delgado 2015], which allows an easy access to its potential uses to whomever might be interested. However, this does not exclude the possibility of a production at a larger scale, to be marketed and traded specifically for the conservation-restoration market (as well as other finalities). For this purpose, the synthesis and production of this IL needed to be developed and perfected by a chemical engineer. Other concerns such as the packaging – opaque, to protect the IL from light, for example – would also have to be taken into consideration. This possibility might allow obtaining the product at a lower cost, assuring its purity and proper conditioning.

What comes next? Further suggestions to be developed in the future

Despite the promising results obtained, already described and discussed in the previous chapters, there are still some tests that need to be performed in order to assure the complete safety of this cleaning method for the object – and the user. Most were not made during this project due to time restrictions, as well as because, in some cases, it would not be completely under this project's scope.

It would be very interesting to compare the effect of these ILs with other “Bettembourg-methods” other than EDTA solution, for example ammonium-bicarbonate and sodium-thiosulfate. But more important would be to determine more exhaustively the long-term effects of the ILs, namely:

- In glasses with a bigger variety of compositions;
- In the corrosion layer, determining if there are long-term alterations of its chemical and physical characteristics;
- In enamels;
- In altered *grisaille* painted layers.

The characterization of the IL [P_{6,6,6,14}][ANS] at different temperatures was made (see Chapter 2). However, it would be of interest to study the cleaning efficiency of this IL at different temperatures, especially temperatures lower than the average room temperature (~21 °C), to verify if there is any alteration in the IL's cleaning capability, which would be important for the *in situ* application of this product.

Of interest would also be to discuss the utility and, thus, the possibility of using the IL [P_{6,6,6,14}][ANS] for cleaning enameled stained glass panels. All things considered, it will also be important to determine exactly which species are forming after the photo-degradation of the IL [P_{6,6,6,14}][ANS], again to guarantee the safety of this method for application in the stained glass conservation practice. It is also important to determine the expiration date of this IL, hence, to define for how long after the synthesis will the IL maintain its properties.

And finally, it is important to remember that even though the ionic liquids developed and studied during the course of this project had a very specific goal, its potentialities are much more extensive, not only in the conservation-restoration field – were it would be of great use in cleaning optical materials, such as microscopes or telescopes and telescope mirrors, and glass objects other than stained glass –, but in other areas as well. This type of ILs may be used in oLEDs: the viscosity effects here reported are rather large, which may have an impact in the future design of those devices employing this type of materials. Other possible applications include the conversion of UV light into visible light, important for phosphors or solar cells. The presence of anionic groups may also be used in the future as sensors for dissolution of cations in ILs and/or in other applications such cleaning fluids for surfaces. Chelating agents, including EDTA, are also used as medicine, for example to treat lead poisoning or to treat calcium deposits in the eye. To attain the interest of researchers from different fields of knowledge would only increase the possibilities of having these ILs further studied and maybe of finding new applications. Nonetheless, the main purpose of this project has been achieved: to restore medieval stained-glass transparency using new task specific luminescent ionic liquids for the removal of corrosion crusts.

References

- [Abd-Allah 2013] R. Abd-Allah, *Chemical cleaning of soiled deposits and encrustations on archaeological glass: A diagnostic and practical study*, Journal of Cultural Heritage 14 (2013), 97–108.
- [Alcaide 1969] V. N. Alcaide, *Las Vidrieras de la Catedral de Sevilla*; Laboratório de Arte de la Universidad de Sevilla – Instituto Diego Velazquez del C.S.I.C., Madrid, 1969.
- [Altavilla 2008] C. Altavilla, E. Ciliberto, S. Ladelfa, S. Panarello, A. Scandurra, *The cleaning of early glasses: investigation about the reactivity of different chemical treatments on the surface of ancient glasses*. Applied Physics A, Materials Science & Processing 92 (2008), 251-255.
- [Aubert 1983] Aubert, M., *O Gótico no seu apogeu*. Editorial Verbo, Lisboa, 1983.
- [Babu 2013] S. S. Babu, M. J. Hollamby, J. Aimi, H. Ozawa, A. Saeki, S. Seki, K. Kobayashi, K. Hagiwara, M. Yoshizawa, H. Möhwald, Takashi Nakanishi, *Nonvolatile liquid anthracenes for facile full-colour luminescence tuning at single blue-light excitation*, Nature Communications 4 (2013), Article number: 1969.
- [Bagchi 1984] B. Bagchi; D.W. Oxtoby; G.R. Fleming, *Theory of the time development of the stokes shift in polar media*, Chemical Physics 86 (1984), 257-267.
- [Barroca 2002] M.J. Barroca, C.A. Ferreira, *História da Arte em Portugal. O Gótico*, Editorial Presença, Lisboa, 2002.
- [Barros 1988] C. V. Barros, *O Vitral em Portugal - Séculos XV-XVI*, Imprensa Nacional - Casa da Moeda, Lisboa, 1988.
- [Bogel-Lukasik 2015] R. Bogel-Lukasik (ed.), *Ionic Liquids in the Biorefinery Concept : Challenges and Perspectives*, RSC (The Royal Society of Chemistry) Publishing, 2015.
- [Bohmer 1993] R. Böhmer; K.L. Ngai; C.A. Angell; D.J. Plazek, *Nonexponential relaxations in strong and fragile glass formers*, The Journal of Chemical Physics 99 (1993), 4201-4209.

- [Branco 2002]** L.C. Branco, J.N. Rosa, J.J. Moura Ramos, C.A.M. Afonso, *Preparation and Characterization of New Room Temperature Ionic Liquids*. Chemistry European Journal 8 (2002), 3671- 3677.
- [Branco 2009]** L.C. Branco, F. Pina, *Intrinsically photochromic ionic liquids*, Chemical Communications (2009), 6204-6206.
- [Branco 2011]** A. Branco, L.C. Branco, F. Pina, *Electrochromic and magnetic ionic liquids*, Chemical Communications 47 (2011), 2300-2302.
- [Branco 2011i]** L.C. Branco, G.V.S.M. Carrera, J. Aires-de-Sousa, I. L.Martin, R. Frade, C.A.M. Afonso. *Physico-Chemical Properties of Task-Specific Ionic Liquid* in Ionic Liquids, Theory and Applications (Chapter 3), InTech Press, 2011.
- [Branco 2013]** A. Branco, J. Belchior, L. C. Branco, F. Pina, *Intrinsically electrochromic ionic liquids based on vanadium oxides: illustrating liquid electrochromic cells*, RSC Advances 3 (2013), 25627-25630.
- [Brand 1972]** L. Brand, J.R. Gohlke, *Fluorescence Probes for Structure*, Annual Review of Biochemistry 41 (1972), 843-868.
- [Caen 2009]** J. M. Caen, *The Production of stained glass in the county of Flanders and the Duchy of Brabant from the XVth to the XVIIIth centuries: materials and techniques*. Brepols, Antwerpen, 2009.
- [Cailleteau 2008]** C. Cailleteau, F. Angeli, F. Devreux, S. Gin, J. Jestin, P. Jollivet, O. Spalla. *Insight into silicate-glass corrosion mechanisms*, Nature Materials 7 (2008) 978-983.
- [Carmona 2006]** N. Carmona, M. A. Villegas, J. M. Fernández Navarro, *Characterisation of an intermediate decay phenomenon of historical glasses*, Journal of Materials Science 41 (2006) 2339-2346.
- [Castner 1987]** E.W. Castner, M. Maroncelli, G.R. Fleming, *Subpicosecond resolution studies of solvation dynamics in polar aprotic and alcohol solvents*, The Journal of Chemical Physics 86 (1987), 1090-1097.

- [Caviness 1985]** M. Caviness, *Stained Glass, Dictionary of the Middle Ages 5*, Joseph Strayer (Ed.), Scribner, New York, 1985.
- [Chen 2010]** C. Chen, W. Ma, J. Zhao, *Semiconductor-mediated photodegradation of pollutants under visible-light irradiation*, *Chemical Society Reviews* 39 (2010), 4206-4219.
- [Clark 1979]** D.E. Clark, C.G. Pantano, L.L. Hench, *Corrosion of Glass*, Books for Industry, New York, 1979.
- [Clark 1992]** D.E. Clark, B.K. Zoitos, *Corrosion of Glass, Ceramics and Ceramic superconductors*. Noyes Publications, New Jersey, 1992.
- [Colomban 2003]** P. Colomban, *Polymerization degree and Raman identification of ancient glasses used for jewelry, ceramic enamels and mosaics*, *Journal of Non-Crystalline Solids* 323 (2003), 180–187.
- [Colomban 2006]** P. Colomban, A. Tournié, L. Bellot-Gurlet, *Raman identification of glassy silicates used in ceramics, glass and jewellery: a tentative differentiation guide*, *Journal of Raman Spectroscopy* 37(8) (2006), 841-852.
- [Colomban 2006i]** P. Colomban, M.-P. Etcheverry, M. Asquier, M. Bounichou, A. Tournié, *Raman identification of ancient stained glasses and their degree of deterioration*, *Journal of Raman Spectroscopy* 37(5) (2006), 555-626.
- [Custódio 2000]** J. Custódio, *A Problemática do Fabrico da Vidraça em Portugal entre os séculos XV e XIX*, in *O Vitral. História, Conservação e Restauro* (pp. 94-121). Ministério da Cultura. IPPAR, Lisboa, 2000.
- [d'Alembert 2002]** D. d'Alembert, J. Diderot, *L'Encyclopedie Diderot & d'Alembert: Art Du Verre Fabrication Des Glaces*, Bibliotheque de l'Image, Paris, 2002.
- Note: originally published as "Verrerie – verrerie en bois ou grande verrerie à vitres ou en plats," *Encyclopédie ou Dictionnaire raisonné des sciences, des arts et des métiers*, vol. 10 (plates), Paris, 1772.

- [De Bardi 2013]** M. De Bardi, R. Wiesinger, M. Schreiner, *Leaching studies of potash–lime–silica glass with medieval composition by IRRAS*, Journal of Non-Crystalline Solids 360 (2013), 57–63.
- [De Bardi 2013i]** M. De Bardi, H. Hutter, M. Schreiner, *ToF-SIMS analysis for leaching studies of potash–lime–silica glass*, Applied Surface Science 282 (2013), 195– 201.
- [Debitus 1991]** H. Debitus, *Recherche pour une formulation nouvelle de grisailles*, Science et Technologie de la Conservation et de la Restauration des oeuvres d’art et du patrimoine (2) (1991), 24-29.
- [Delgado 2015]** J.M. Delgado, A. Raymundo, M. Vilarigues, L.C. Branco, C.A.T. Laia, *Characterization of a Novel Intrinsic Luminescent Room-Temperature Ionic Liquid Based on $[P_{6,6,6,14}][ANS]$* , Chemistry - A European Journal 21 (2015), 726-732.
- [DeToma 1976]** R.P. DeToma; J.H. Easter; L. Brand, *Dynamic interactions of fluorescence probes with the solvent environment*, Journal of the American Chemical Society 98(16) (1976), 5001-5007.
- [Dohmen 2013]** L. Dohmen, C. Lenting, R.O.C. Fonseca, T. Nagel, A. Heuser, T. Geisler. *Pattern Formation in Silicate Glass Corrosion Zones*, International Journal of Applied Glass Science, 4(4) (2013), 357–370.
- [Drew 1983]** J. Drew; P. Thistlethwaite; G. Woolfe, *Excited-state relaxation in 1-amino-8-naphthalene sulphonate*, Chemical Physics Letters 96(3) (1983), 296-301.
- [Duby 1993]** G. Duby, *O Tempo das Catedrais. A arte e a sociedade 980-1420*, Editorial Estampa, Lisboa, 1993.
- [Ebbesen 1989]** T.W. Ebbesen; C.A. Ghiron, *Role of specific solvation in the fluorescence sensitivity of 1,8-ANS to water*, Journal of Physical Chemistry 93 (1989), 7139-7143.
- [Eco 1989]** H. Eco, *Arte e Beleza na Estética Medieval*, Coleção Dimensões, Editorial Presença, Lisboa, 1989.

- [Faridbod 2011]** F. Faridbod, M.R. Ganjali, P. Norouzi, S. Riahi, H. Rashedi, *Application of Room Temperature Ionic Liquids in Electrochemical Sensors and Biosensors in Ionic Liquids: Applications and Perspectives*, Chapter 29, A. Kokorin (ed.), InTech, 2011.
- [Fekrsanati 2000]** F. Fekrsanati, J. Hildenhagen, K. Dickmann, C. Troll, U. Drewello, C. Olainck, *UV-laser radiation: basic research of the potential for cleaning stained glass*, Journal of Cultural Heritage 1 (2000), 155-160.
- [Fernandes 2008]** P. Fernandes, M. Vilarigues, L.C. Alves, R.C. da Silva, *Stained-glass from Monastery of Batalha: non-destructive characterization of glass and paintings*, Journal of Cultural Heritage 9, Supplement 1 (2008), e5-e9.
- [Ferraz 2011]** R. Ferraz, L.C. Branco, C. Prudêncio, J.P. Noronha, Z. Petrovski, *Ionic liquids as active pharmaceutical ingredients*, ChemMedChem 6(6) (2011), 975-985.
- [Freemantle 2009]** M. Freemantle, *An Introduction to Ionic Liquids*, Royal Society of Chemistry, United Kingdom, 2009.
- [Gago 2013]** S. Gago, L. Cabrita, J.C. Lima, L.C. Branco, F. Pina, *Synthesis and Characterization of luminescent room temperature ionic liquids based on Ru(bpy)(CN)₄²⁻*, Dalton Transactions 42 (2013), 6213-6218.
- [Hallett 2011]** J.P. Hallett, T. Welton, *Room-temperature ionic liquids: solvents for synthesis and catalysis 2*, Chemical Reviews 111(5) (2011), 3508-3576.
- [Harris 2007]** D. C. Harris, *Quantitative Chemical Analysis*, 7th Edition, W. H. Freeman and Company, United States of America, 2007.
- [Hildenhagen 2003]** J. Hildenhagen, K. Dickmann, *Excimer laser for fundamental studies in cleaning hewn stone and medieval glass*, Journal of Cultural Heritage 4 (2003), 118s–122s.
- [Hildenhagen 2003i]** J. Hildenhagen, K. Dickmann, *Low-cost sensor system for online monitoring during laser cleaning*, Journal of Cultural Heritage 4 (2003), 343s–346s

- [Hu 2006]** Z. Hu, C.J. Margulis, *Heterogeneity in a room-temperature ionic liquid: Persistent local environments and the red-edge effect*, Proceedings of the National Academy of Sciences (USA) 103 (2006), 831-836.
- [Huppert 1981]** D. Huppert, H. Kanety, E.M. Kosower, *Kinetic studies on intramolecular electron transfer in solution*, Chemical Physics Letters 84 (1981), 48-53.
- [Janssens 2013]** K.H.A. Janssens (Ed.), *Modern Methods for Analysing Archaeological and Historical Glass*, Wiley, 2013.
- [Johnson 2007]** K.E. Johnson, *What's an Ionic Liquid?*, The Electrochemical Society Interface 16(1) (2007).
- [Karmakar 2002]** R. Karmakar, A. Samanta, *Solvation Dynamics of Coumarin-153 in a Room-Temperature Ionic Liquid*, The Journal of Physical Chemistry A 106 (18) (2002), 4447-4452;
- [Klein 1999]** S. Klein, T. Stratoudaki, V. Zafirooulos, J. Hildenhagen, K. Dickmann, Th. Lehmkuhl, *Laser-induced breakdown spectroscopy for on-line control of laser cleaning of sandstone and stained glass*, Applied Physics A 69 (1999), 441–444.
- [Kokorin 2011]** A. Kokorin (Ed.), *Ionic Liquids: Applications and Perspectives*, InTech, 2011.
- [Kosower 1975]** E.M. Kosower; H. Dodiuk; K. Tanizawa; M. Ottolenghi; N. Orbach, *Intramolecular donor-acceptor systems. Radiative and nonradiative processes for the excited states of 2-N-Arylamino-6-naphthalenesulfonates*, Journal of the American Chemistry Society 97 (1975), 2167-2178.
- [Kosower 1982]** E.M. Kosower, *Intramolecular donor-acceptor systems. 9. Photophysics of (Pheny1amino)naphthalenesulfonates: a paradigm for excited-state intramolecular charge transfer*, Accounts of Chemical Research 15 (1982), 259-266.

- [Kosower 1983]** E.M. Kosower; H. Kanety, *Intramolecular donor-acceptor systems. 10. Multiple fluorescence from 8-(phenylamino)-1-naphthalenesulfonates*, Journal of the American Chemistry Society 105 (1983), 6236-6243.
- [Kulkarni 2007]** P.S. Kulkarni, L.C. Branco, J.G. Crespo, M.C. Nunes, A. Raymundo, C.A. Afonso, *Comparison of Physicochemical Properties of New Ionic Liquids Based on Imidazolium, Quaternary Ammonium, and Guanidinium Cations*, Chemistry European Journal 13 (2007), 8478-8488.
- [Kurmman-Schwarz 2000]** B. Kurmman-Schwarz, *O Vitral Gótico* in, *O Gótico. Arquitectura, Escultura e Pintura* (pp. 468-483), R. T. (Ed.), Konemann, Cologne, 2000.
- [Machado 2010]** A. Machado, P. Redol, L. Branco, M. Vilarigues. *Medieval stained-glass cleaning with Ionic liquids cleaning*. Proceedings of ICC 2010 congress – Conservation and the Eastern, Istanbul, 2010.
- [Machado 2011]** A. Machado, P. Redol, L. Branco, M. Vilarigues, *Ionic liquids for medieval stained glass cleaning: a new frontier*, ICOM-CC Lisbon 2011: Sixteenth Triennial Conference, International Council of Museums – Committee for Conservation, Preprints CD, ISBN: 978-98997522-0-7, 2011.
- [Murcia-Mascarós 2008]** S. Murcia-Mascarós, P. Foglia, M.L. Santarelli, C. Roldán, R. Ibañez, A. Muñoz, P. Muñoz, *A new cleaning method for historic stained glass windows*, Journal of Cultural Heritage 9 (2008), 73-80.
- [Marrucho 2014]** I.M. Marrucho, L.C. Branco, L.P.N. Rebelo, *Ionic Liquids in Pharmaceutical Applications*, Annual Review of Chemical and Biomolecular Engineering 5 (2014), 527-546.
- [Melcher 2010]** M. Melcher, R. Wiesinger, M. Schreiner, *Degradation of Glass Artifacts: Application of Modern Surface Analytical Techniques*. Accounts of Chemical Research 43 (2010), 916-926.
- [Nakamura 1981]** H. Nakamura; J. Tanaka, *Temperature dependence of fluorescence lifetimes of 8-anilino-1-naphthalene sulfonate and solvent isotope effect*, Chemical Physics Letters 78 (1981), 57-60.

- [Navarro 2003]** J. M. Navarro, *El Vidrio*, Consejo Superior de Investigaciones Científicas - Sociedad Española de Cerámica y Vidrio, Madrid, 2003.
- [Newton 1989]** R.G. Newton, S. Davison, *Conservation of glass*, Butterworths, London, 1989.
- [Pacheco 2013]** M.F. Pacheco, A.I. Pereira, L.C. Branco, A.J. Parola, *Varnish removal from paintings using ionic liquids*, *Journal of Materials Chemistry A* 24 (2013), 7016-7018.
- [Patent A1 2006]** Patent US 2006/183654 A1.
- [Patent A2 2006]** Patent WO 2006/050308 A2.
- [Patent 2010]** Patent WO 2010/040917 A1.
- [Plechkova 2008]** N.V. Plechkova, K.R. Seddon, *Applications of ionic liquids in the chemical industry*, *Chemical Society Reviews* 37(1) (2008), 123-150.
- [Pereira 2013]** C.C.L. Pereira, S. Dias, I. Coutinho, J.P. Leal, L.C. Branco, C.A.T. Laia, *Europium (III) tetrakis (β -diketonate) complex as an ionic liquid: a calorimetric and spectroscopic study*, *Inorganic Chemistry* 52(7) (2013), 3755-3764.
- [Pina 2007]** F. Pina, A. J. Parola, M. J. Melo, C. A. T. Laia, C. A. M. Afonso, *Photochromism of 7-(N,N-diethylamino)-4-hydroxyflavylium in a water-ionic liquid biphasic system*, *Chemical Communications* (2007), 1608-1610.
- [Pina 2011]** F. Pina, L. C. Branco, *Photochromism in Ionic Liquids. Theory and Applications in Ionic Liquids: Theory, Properties, New Approaches* (Chapter 6), Prof. Alexander Kokorin (Ed.), ISBN: 978-953-307-349-1, InTech Press, 2011.
- [Presbyter 1979]** T. Presbyter, C.S. Smith, J.G. Hawthorne, *On divers arts: the foremost medieval treatise on painting, glassmaking, and metalwork*, Dover Publications, New York, 1979.
- [Raguin 2003]** V.C. Raguin, *The History of Stained Glass: the Art of Light – Medieval to Contemporary*, Thames & Hudson, London, 2003.

- [Redol 2000]** P. Redol, *O Vitral em Portugal nos séculos XV e XVI*, in *O Vitral. História, Conservação e Restauro* (pp. 12-43). Ministério da Cultura. IPPAR, Lisboa, 2000.
- [Redol 2003]** P. Redol, *O Mosteiro da Batalha e o Vitral em Portugal nos Séculos XV e XVI*, Câmara Municipal da Batalha, Batalha, 2003.
- [Robinson 1978]** G.W. Robinson; R.J. Robbins; G.R. Fleming; J.M. Morris; A.E.W. Knight; R.J.S. Morrison. *J. Am. Chem. Soc.* 1978, 100, 7145-7150.
- [Romich 2000]** H. Römich, E. Jägers, M. Torge, W. Müller, K. Adam., *Cleaning: A Balancing Act*. English version available in Corpus Vitrearum Medii Aevi website.
- Note: English version translated from *Restaurierung und Konservierung historischer Glasmalereien* (pp. 65-99), edited by Arnold Wolff, P. von Zabern, Mainz, 2000. Printed version in German.
- [Romich 2000i]** H. Römich, A. Weinmann, *Laser cleaning of stained glass windows. Overview of an interdisciplinary project*, *Journal of Cultural Heritage* 1(2) (2000), 151-154.
- [Romich 2003]** H. Römich, K. Dickmann, P. Mottner, J. Hildenhagen, E. Müller, *Laser cleaning of stained glass windows – Final results of a research project*, *Journal of Cultural Heritage* 4 (2003), 112-117.
- [Rodrigues 2013]** C.A.B. Rodrigues, C. Graça, E. Maçôas, A. Fedorov, C.A.M. Afonso, J.M.G. Martinho, *Excited-State Proton Transfer of Fluorescein Anion as an Ionic Liquid Component*, *Journal of Physical Chemistry B* 117(45) (2013), 14108-14114.
- [Sadkowsky 1980]** P.J. Sadkowsky, G.R. Fleming, *The influence of solvent-solute interaction on radiationless processes: Excited state dynamics of 1,8-anilinonaphthalene sulphonate and related molecules*, *Chemical Physics* 54 (1980), 79-89.
- [Sekhon 2011]** B.S. Sekhon, *Ionic liquids: Pharmaceutical and Biotechnological Applications*, *Asian Journal of Pharmaceutical and Biological Research* (2011), 395-411.
- [Seliskar 1971]** C.J. Seliskar, L. Brand, *Electronic spectra of 2-aminonaphthalene-6-sulfonate and related molecules. I. General properties and excited-state reactions*, *Journal of American Chemistry Society* 93(21) (1971), 5405-5414.

- [Schalm 2003]** O. Schalm, K. Janssens, J. Caen, *Characterization of the main causes of deterioration of grisaille paint layers in 19th century stained-glass windows by J.-B. Capronnier*, *Spectrochimica Acta Part B* 58 (2003), 589–607.
- [Schalm 2010]** O. Schalm, I. De Raedt, J. Caen, K. Janssens. *A methodology for the identification of glass panes of different origin in a single stained glass window: Application on two 13th century windows*. *Journal of Cultural Heritage* 11 (2010) 487–492.
- [Shelby 2005]** J.E. Shelby, *Introduction to Glass Science and Technology*, 2nd Edition, The Royal Society of Chemistry, Cambridge, 2005.
- [Silva 1997]** A. de Silva et al., *Signaling Recognition Events with Fluorescent Sensors and Switches*. *Chem. Rev.* 97 (1997), 1515-1566.
- [Sokhan 2003]** M. Sokhan, P. Gaspar, D.S. McPhail, A. Cummings, L. Cornish, D. Pullen, F. Hartog, C. Hubbard, V. Oakley, J.F. Merkel, *Initial results on laser cleaning at the Victoria & Albert Museum*, Natural History Museum and Tate Gallery, *Journal of Cultural Heritage* 4 (2003), 230-236.
- [Tang 2008]** S. Tang; A. Babai; A.-V. Mudring, *Europium-Based Ionic Liquids as Luminescent Soft Materials*, *Angewandte Chemie International Edition* 47(40) (2008), 7631– 7634.
- [Tavares 2013]** A.P.M. Tavares, O. Rodríguez, E.A. Macedo, *New Generations of Ionic Liquids Applied to Enzymatic Biocatalysis in Ionic Liquids - New Aspects for the Future* – Chapter 20, J. Kadokawa (ed.), InTech, 2013.
- [Tong 1996]** A.-J. Tong; Y.-G. Wu; L.-D. Li, *Solid-substrate and micellar-stabilized room-Temperature Phosphorescence of 2 anilino-naphthalenesulfonates*, *Analytica Chimica Acta* 322(1-2) (1996), 91-97.
- [Tournié 2008]** A. Tournié, P. Ricciardi, Ph. Colomban, *Glass corrosion mechanisms: A multiscale analysis*. *Solid State Ionics* 179 (2008), 2142–2154.

- [Upadhyay 1995]** A. Upadhyay; T. Bhatt; H.B. Tripathi; D.D. Pant, *Photophysics of 8-anilinonaphthalene-1-sulphonate*, Journal of Photochemistry and Photobiology A 89(3) (1995), 201-207.
- [Veritá 1996]** M. Veritá, *Composition, structure et mécanisme de détérioration des grisailles*, in *Grisaille, jaune d'argent, sanguine, émail et peinture à froid. Techniques et conservation* (pp. 61-68). Commission royale des Monuments, Sites et Fouilles de la Région wallonne, Liège, 1996.
- [Vilarigues 2004]** M. Vilarigues, R.C. da Silva, *Ion beam and Infrared analysis of medieval stained-glass*, Applied Physics A 79 (2004), 373-378.
- [Vilarigues 2006]** M. Vilarigues, R. C. da Silva, *Characterization of potash-glass corrosion in aqueous solution by Ion Beam and IR Spectroscopy*, Journal of Non-crystalline Solids 352 (2006) 5368-5375.
- [Vilarigues 2009]** M. Vilarigues, R.C. da Silva, *The effect of Mn, Fe and Cu ions on potash-glass corrosion*, Journal of Non-crystalline Solids 355 (2009), 1630-1637.
- [Walden 1914]** P. Walden, *Ueber die Molekulargrösse und elektrische Leitfähigkeit einiger geschmolzenen Salze*, Bulletin de l'Académie Impériale des Sciences de St.-Pétersbourg. VI série, 8:6 (1914), 405–422.
- [Wasserscheid 2007]** P. Wasserscheid, T. Welton, *Ionic Liquids in Synthesis*, Wiley-VCH, 2007.
- [Wilkes 1982]** J.S. Wilkes, J.A. Levisky, R.A. Wilson, L.H. Charles, *Diaklyimidazolium chloroaluminate melts: A new class of room-temperature ionic liquids for electrochemistry, spectroscopy, and synthesis*, Inorganic Chemistry 21 (1982), 1263–1264.
- [Wilkes 2002]** J.S. Wilkes, *A short history of ionic liquids—from molten salts to neoteric solvents*, Green Chemistry 2(4) (2002), 73-80.
- [Worringer 1992]** W. Worringer, *A Arte Gótica*, Edições 70, Lisboa, 1992.

Attachment I – Complementary data related to Chapter 2

- i) Nuclear Magnetic Resonance (NMR) of the [P_{6,6,6,14}][ANS], [C₅O₂MIM][ANS] and [P_{6,6,6,14}][PyrCOO] ionic liquids**
- ii) [C₅O₂MIM][ANS] IL complementary data**
- iii) [P_{6,6,6,14}][PyrCOO] IL complementary data**

i) Nuclear Magnetic Resonance (NMR) of the [P_{6,6,6,14}][ANS], [C₅O₂MIM][ANS] and [P_{6,6,6,14}][PyrCOO] ionic liquids

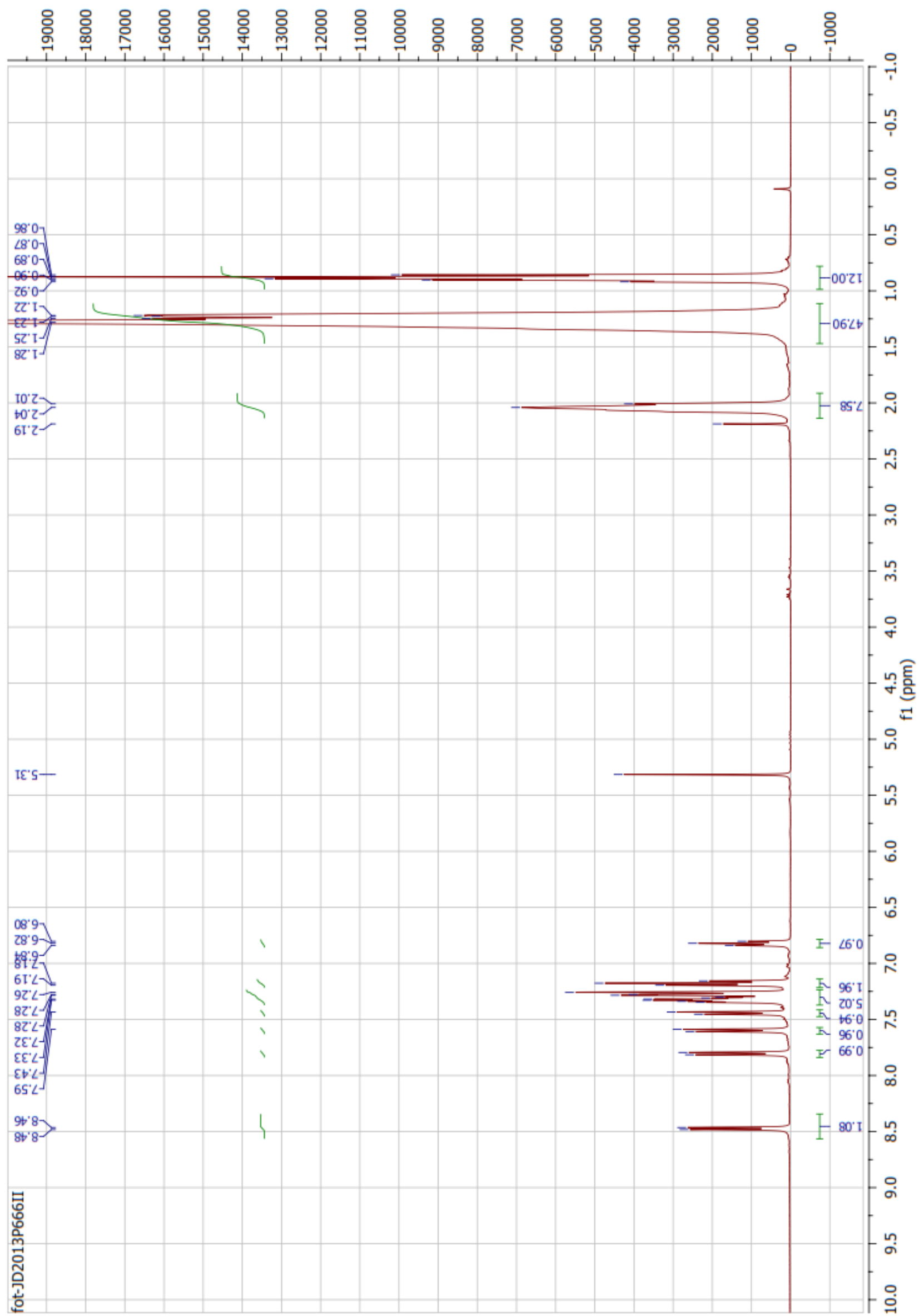


Figure: ¹H-NMR spectra of the of the [P_{6,6,6,14}][ANS] IL.

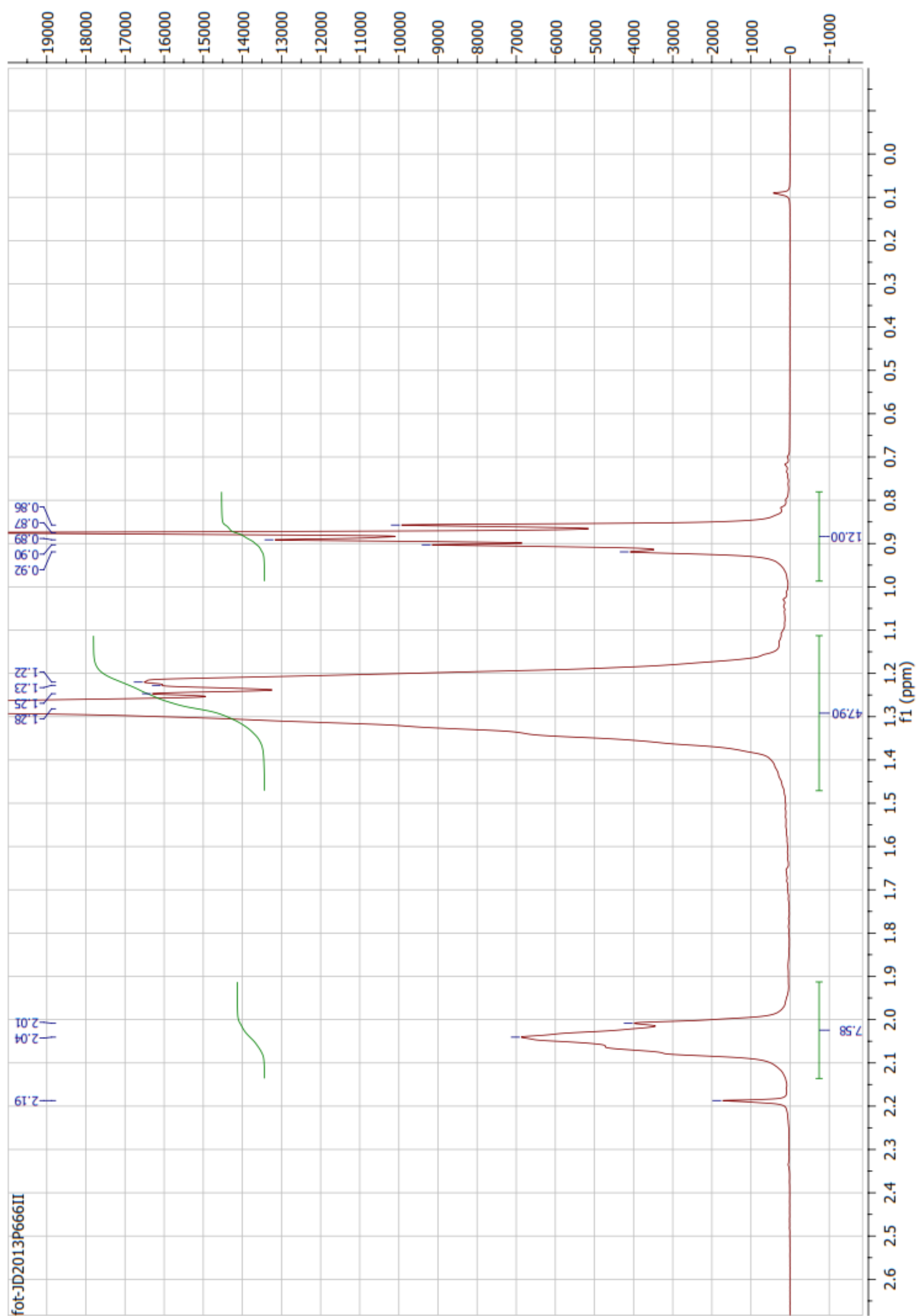


Figure: $^1\text{H-NMR}$ spectra of the of the $[\text{P}_{6,6,6,14}]\text{ANS}$ IL, aliphatic resonance.

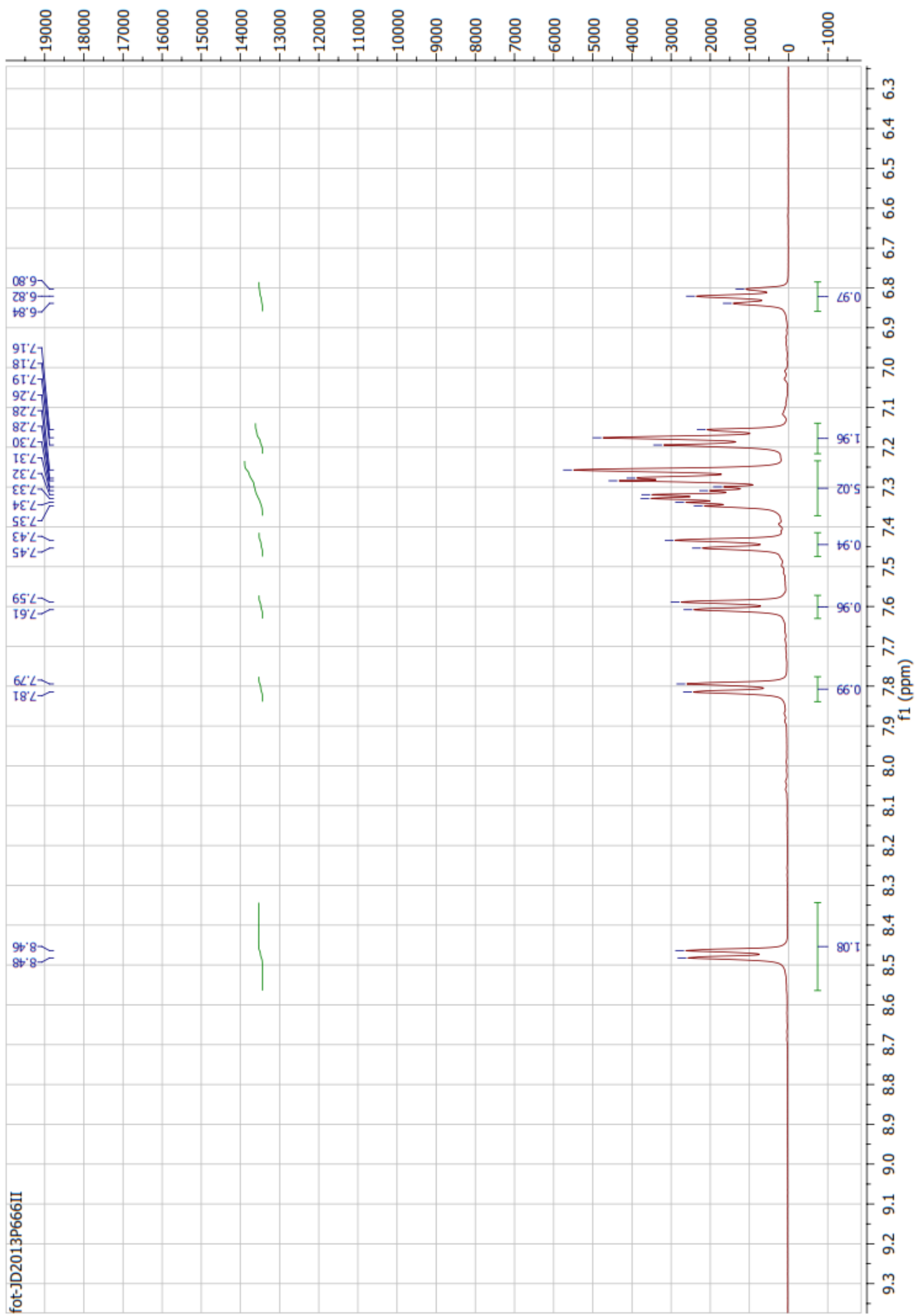


Figure: ¹H-NMR spectra of the of the [P_{6,6,14}][ANS] IL, aromatic resonance.

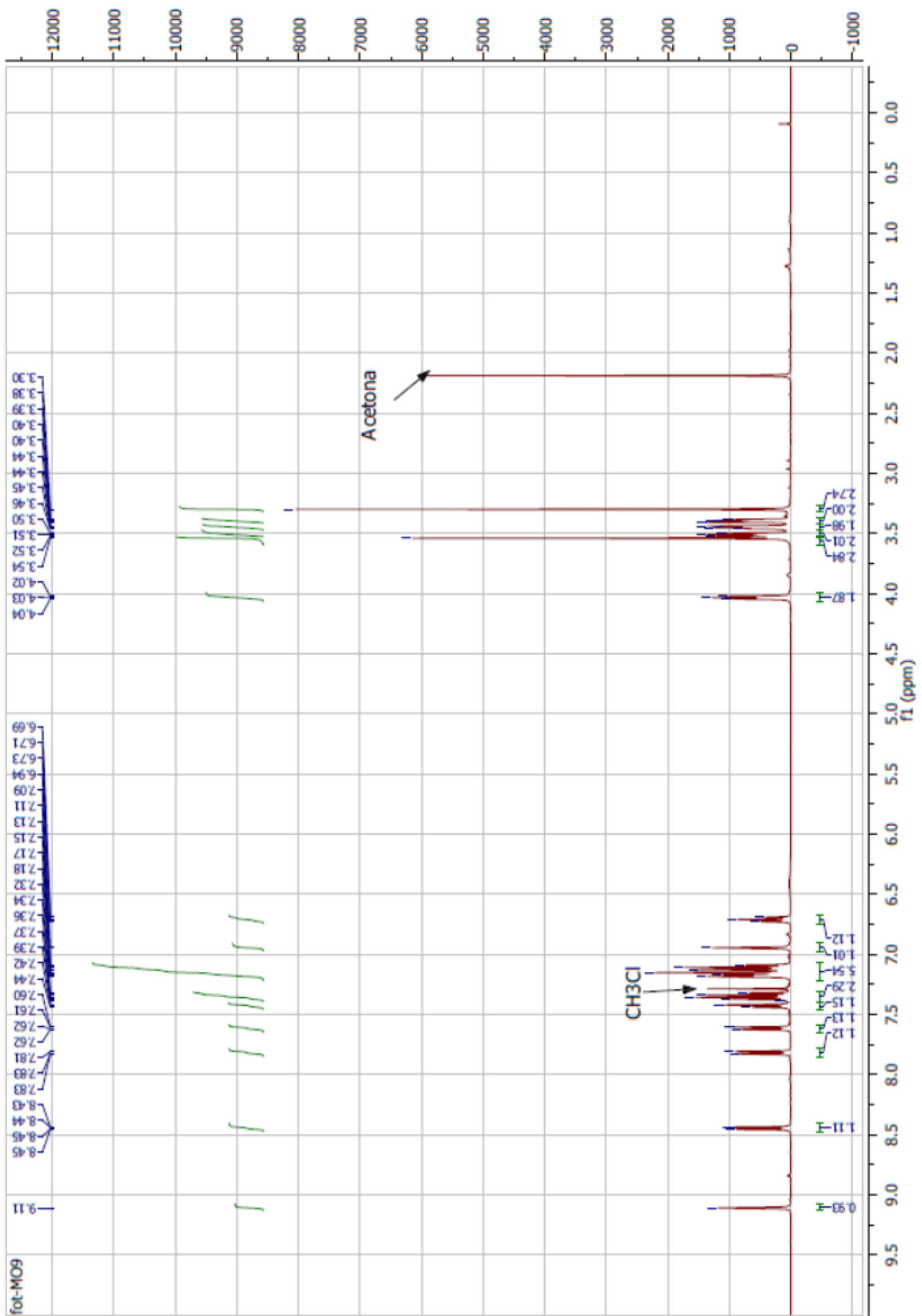


Figure: $^1\text{H-NMR}$ spectra of the of the $[\text{C}_5\text{O}_2\text{MIM}][\text{ANS}]$ IL.

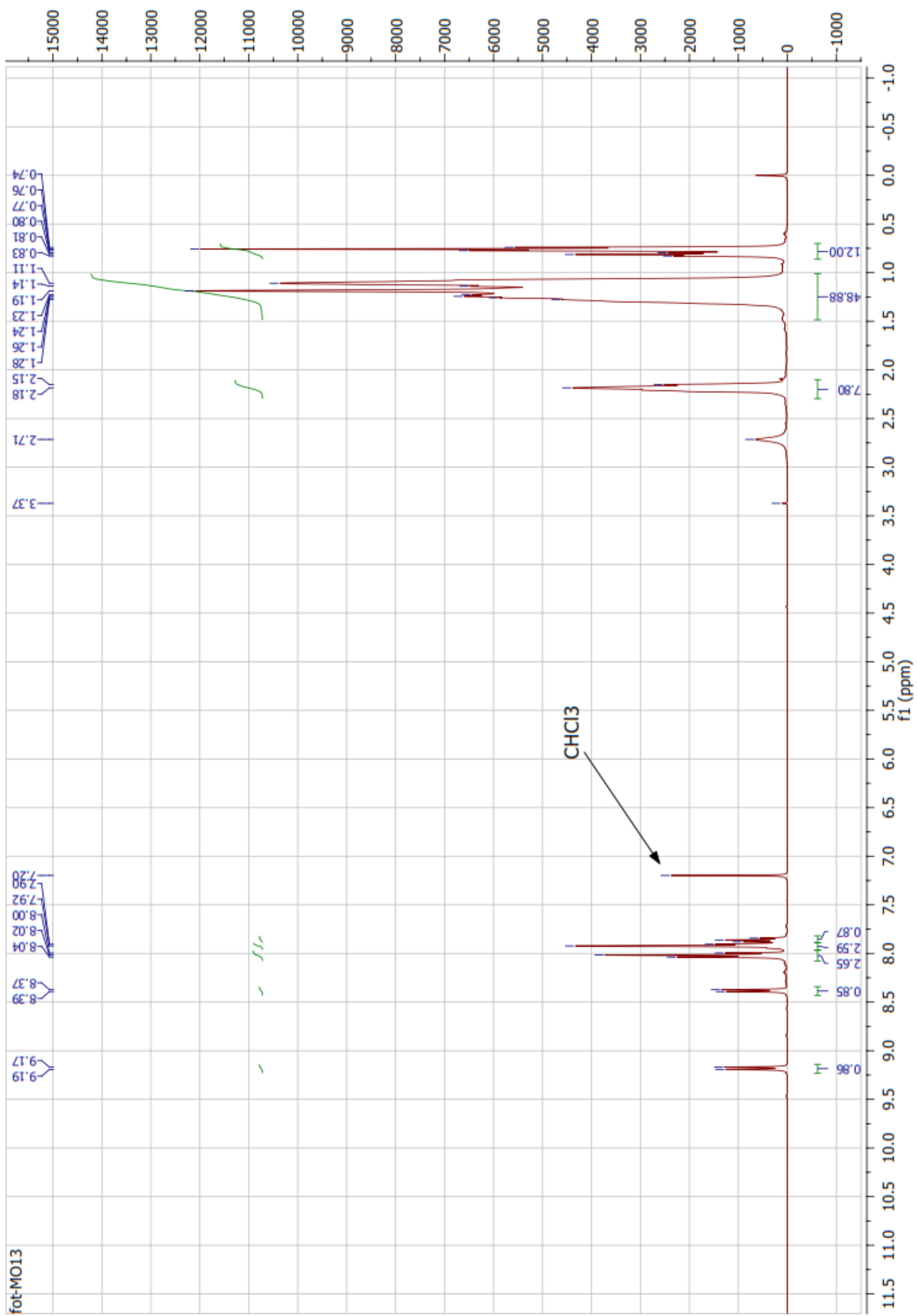


Figure: ¹H-NMR spectra of the of the [P_{6,6,6,14}][PyrcOO] IL

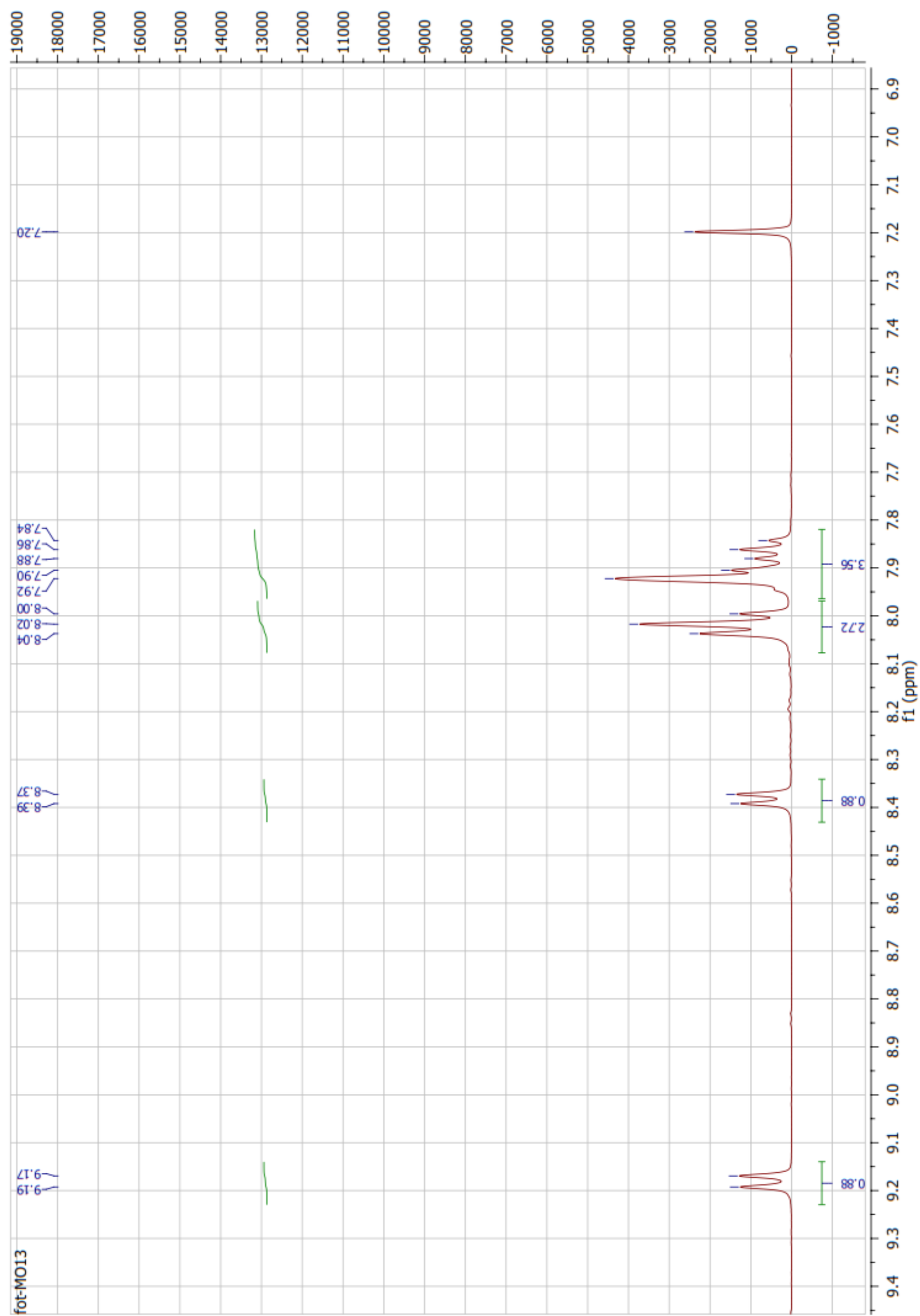


Figure: ¹H-NMR spectra of the of the [P_{6,6,6,14}][PyrCOO] IL, aromatic resonance.

ii) **[C₅O₂MIM][ANS] IL complementary data**

Note: this IL has been characterized by Mani Hosseinzadeh. The results here presented are of his authorship and are not yet published.

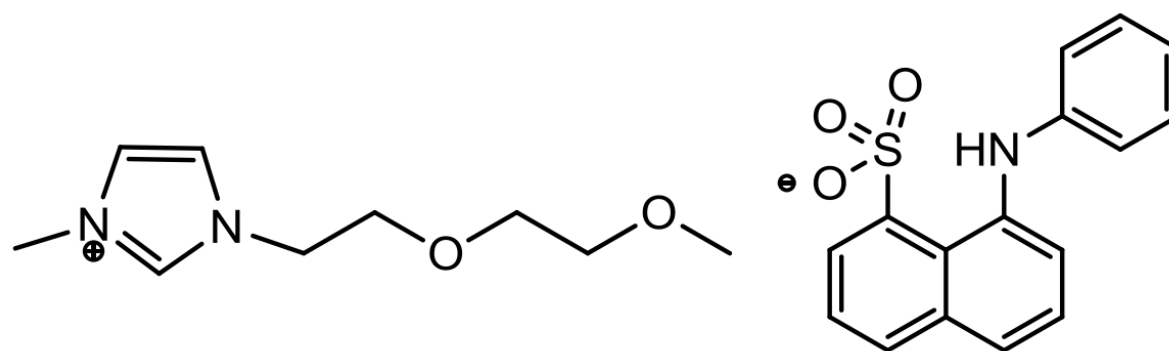


Figure: Molecular structure of the cation and anion of [C₅O₂MIM][ANS] IL.

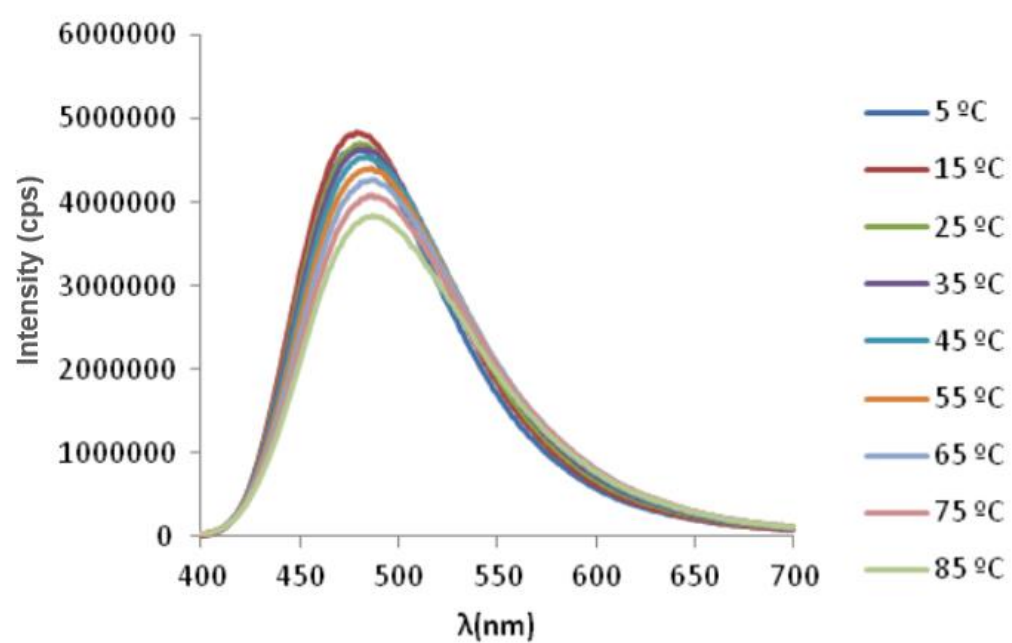


Figure: Evolution of the emission spectra of the IL exciting at 370 nm in a temperature range of 10 to 85°C.

iii) $[P_{6,6,6,14}][PyrCOO]$ IL complementary data

Note: this IL has been characterized by Mani Hosseinzadeh. The results here presented are of his authorship and are not yet published.

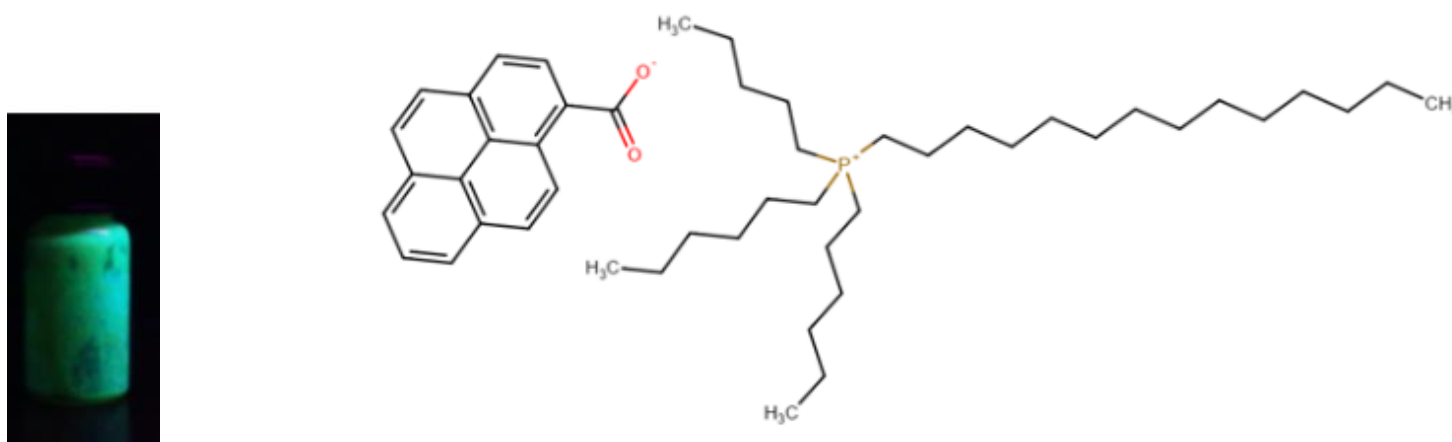


Figure: $[P_{6,6,6,14}][PyrCOO]$ IL under UV-light and the molecular structure of the IL anion and cation.

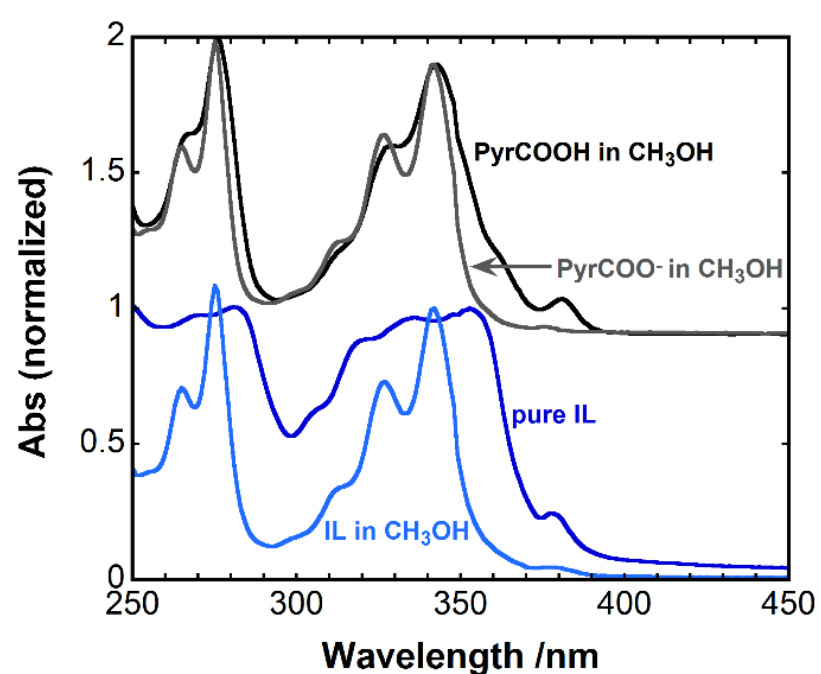


Figure: Absorption spectra of the pyrene derivative in the acidic and anionic form in methanol, of the ionic liquid dissolved in methanol and of the pure ionic liquid.

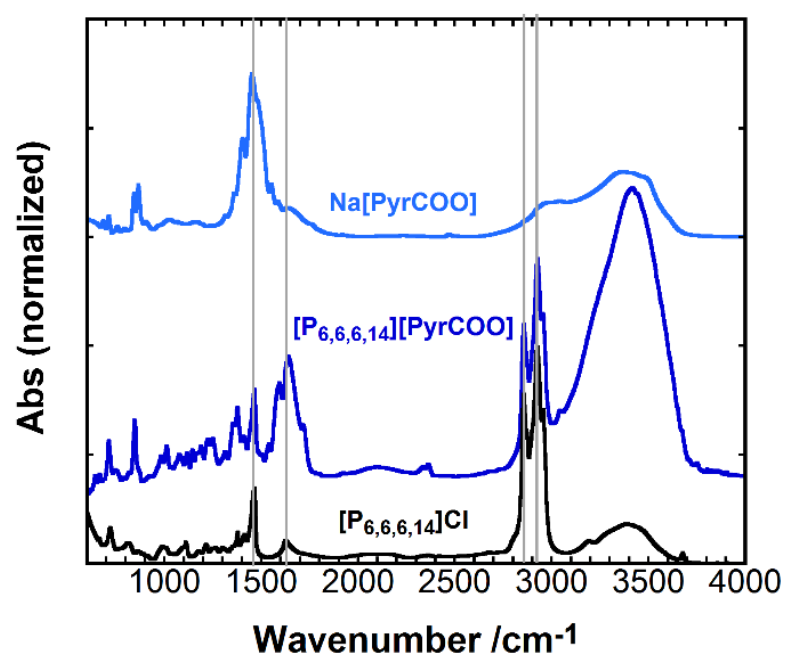


Figure: FTIR spectra of the cation, anion and pure $[P_{6,6,6,14}][PyrCOO]$ ionic liquid.

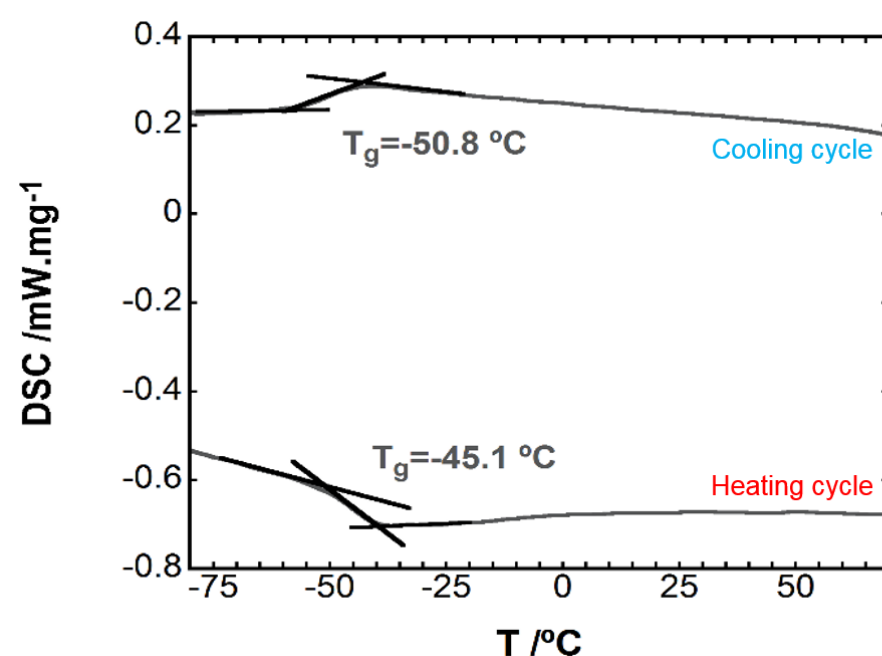


Figure: DSC scanning of $[P_{6,6,6,14}][\text{PyrCOO}]$, with a glass transition temperature around -50°C (upon cooling). The absence of a melting point probably indicates a high thermal barrier for the solid/liquid transition, as it is completely unobserved in our samples. Still it might be in the 0 to 100°C temperature window, which would make this RTIL a supercooled liquid at room temperature.

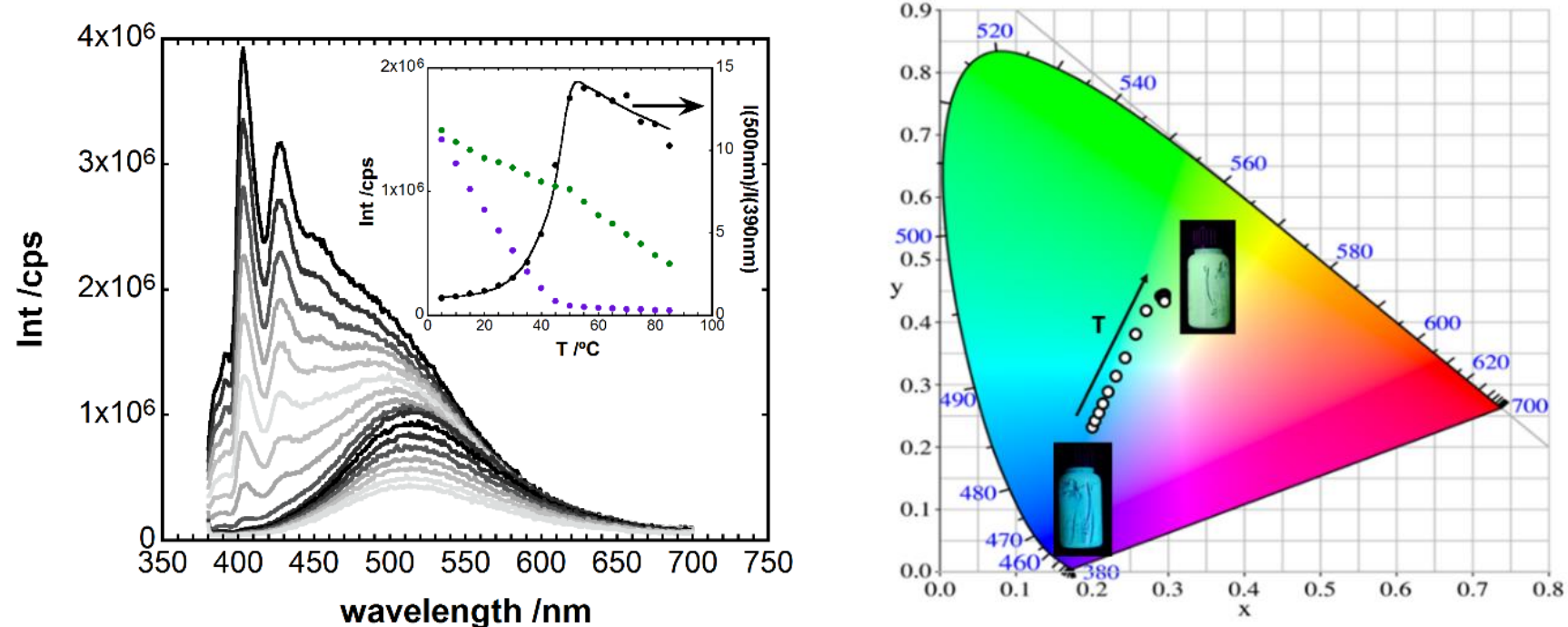


Figure: (left) Evolution of the emission spectra of the IL exciting at 370 nm in a temperature range from 10 to 85°C . At low temperatures the spectra exhibits the vibronic bands of M, along with the broad excimeric emission. But at high temperatures (above 55°C), the M emission completely disappears and only excimeric emission is present. **(right)** Such a strong variation with temperature actually leads to interesting emission color changes. While at low temperatures (below 20°C) the fluorescence is blue, at temperatures above 55°C one observes a green/yellow fluorescence. The effect narrowly passes the center of the color diagram (white light emission), opening the intriguing possibility of generating such emission by tuning the substituents in the pyrene ring.

Attachment II – Complementary data to Chapter 4

- i) Optical Microscope images of model glass samples**
- ii) SEM images of model glass samples' surface**

i) Optical Microscope images of model glass samples

In the next tables, the images of optical microscopy from model glass samples from all groups are presented. The discussion of the observed effects can be found in Chapter 2. Please note that the marks on the glass surface, highlighted in the figure below and present in many samples, regardless of the group, are very likely production defects/characteristics. These do not seem to have any relation to the presence application of ILs, EDTA or a high RH environment, being observable even on the control samples (group A).

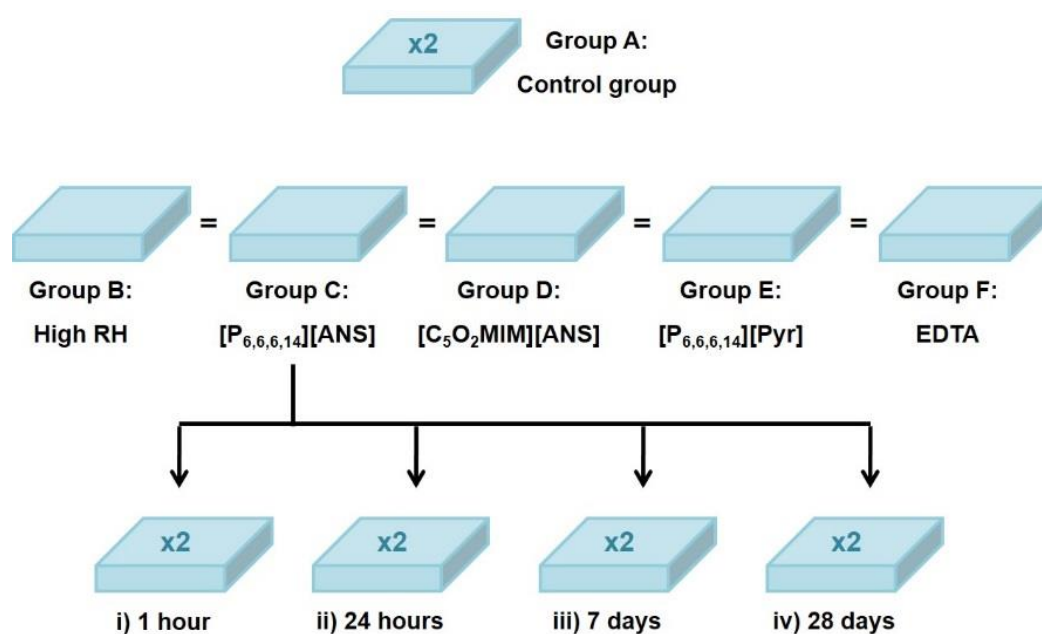
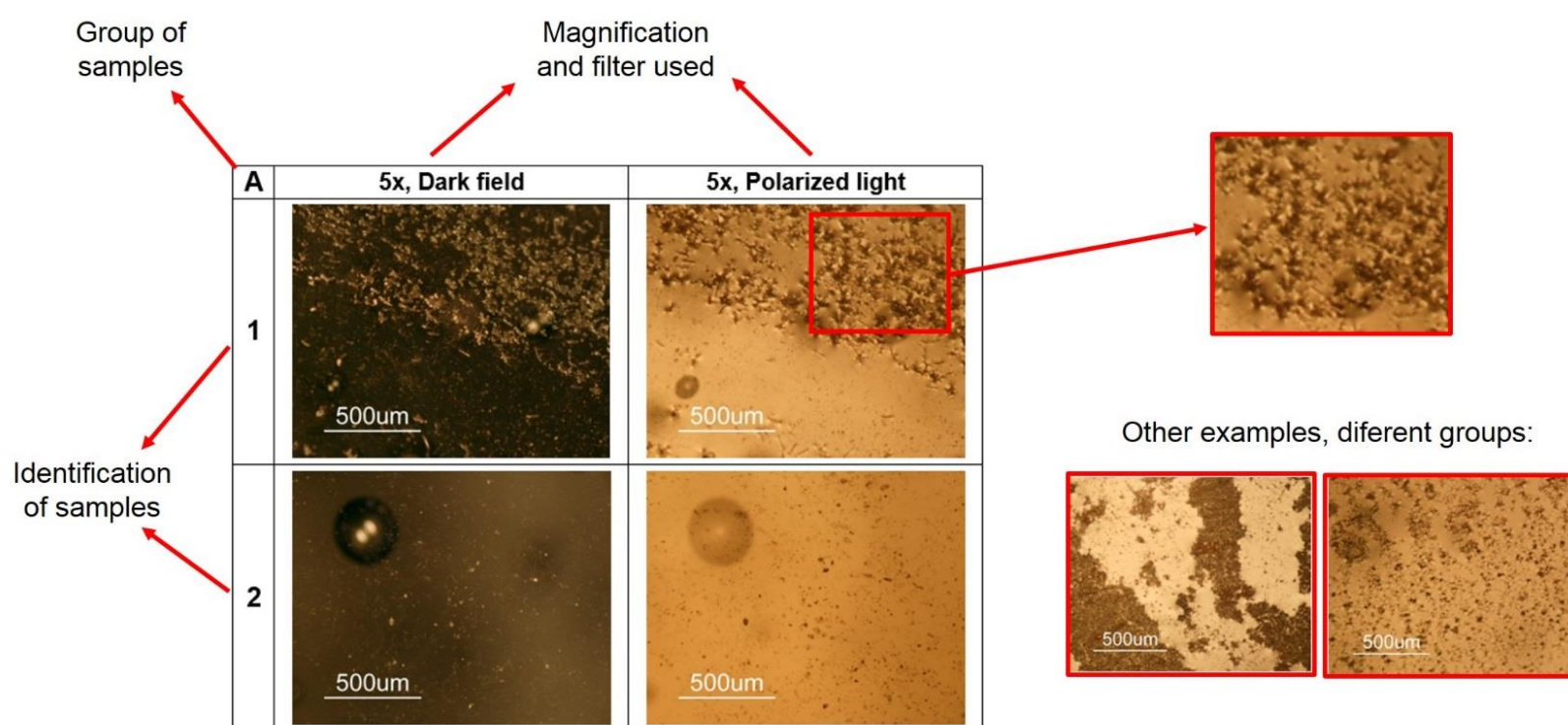
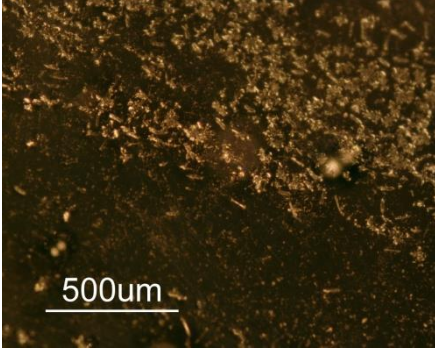
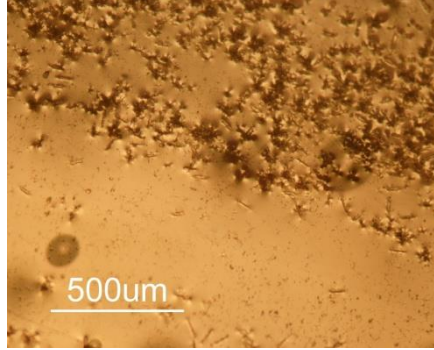
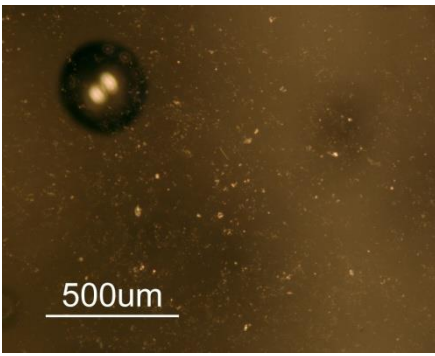
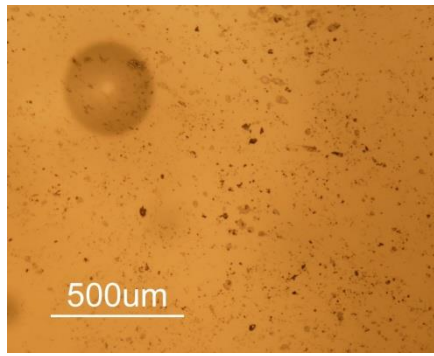
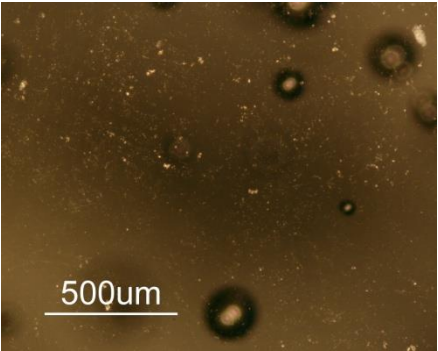
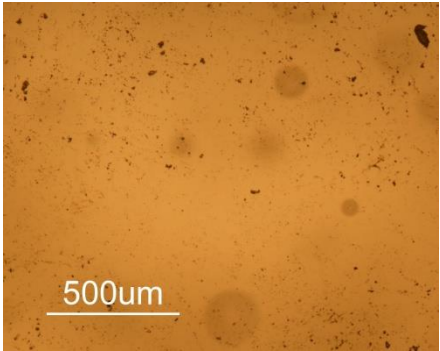
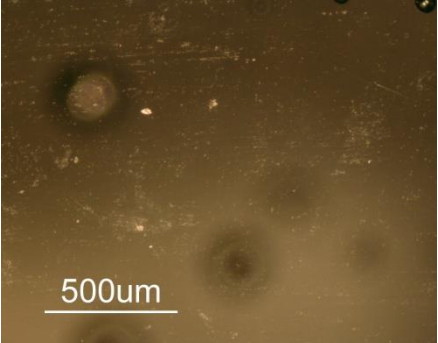
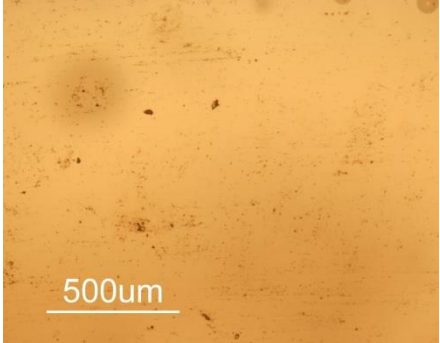
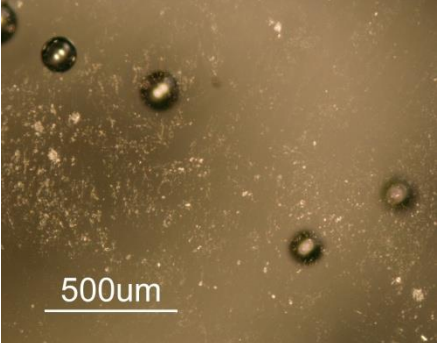
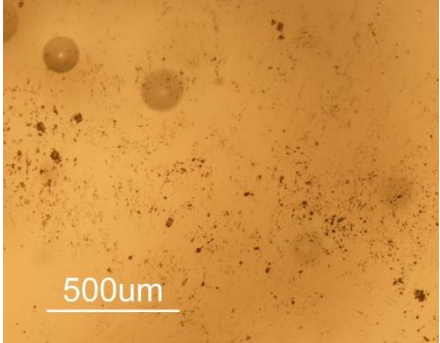
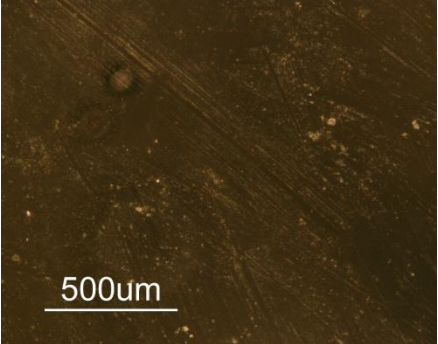
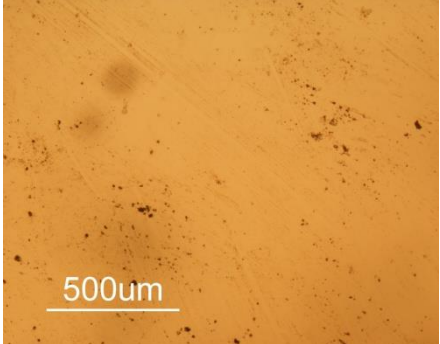
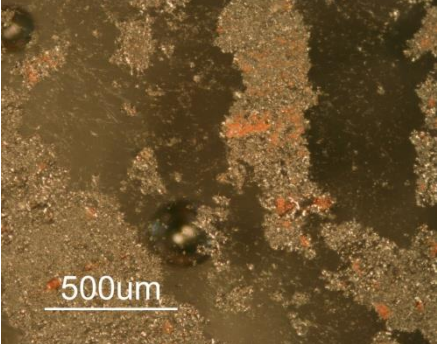
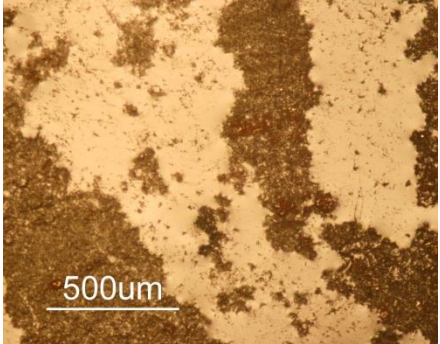
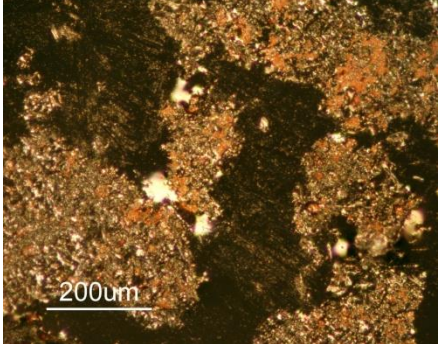
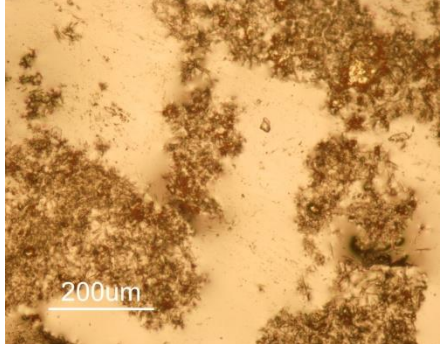
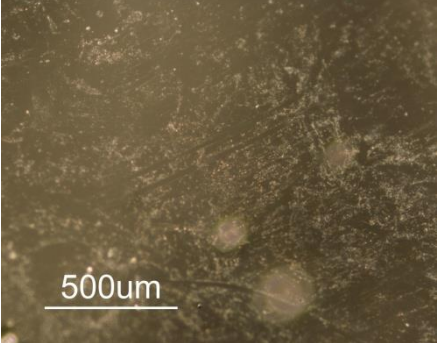
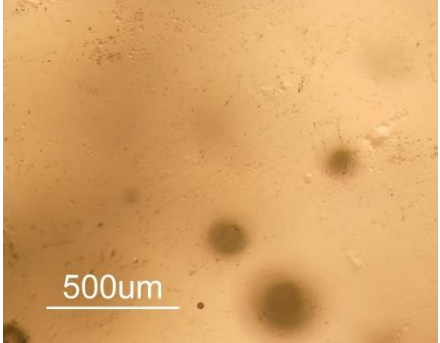
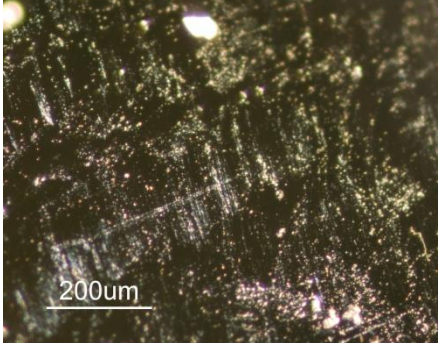
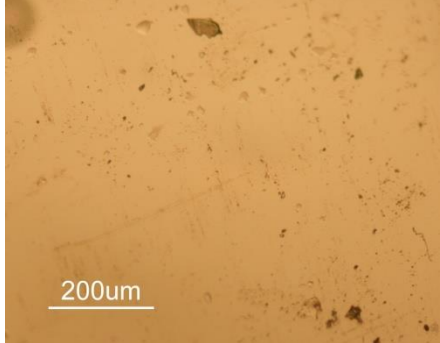
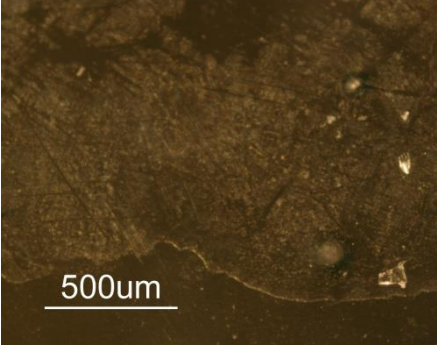
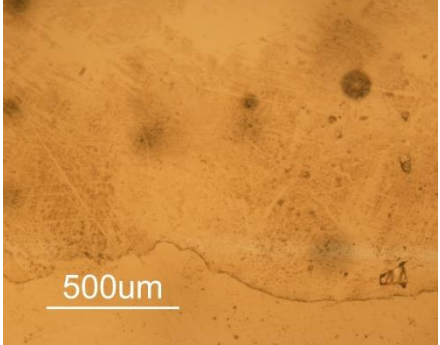
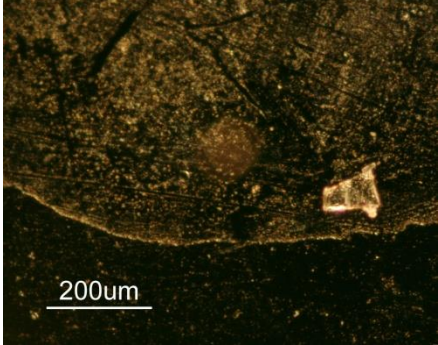
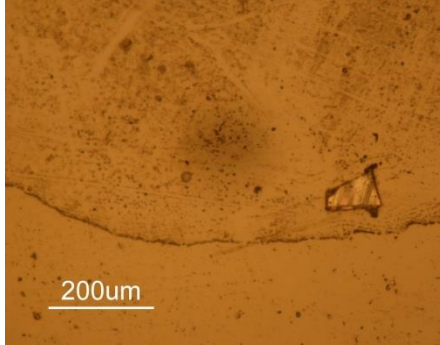
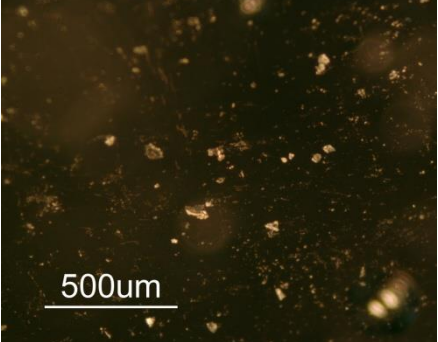
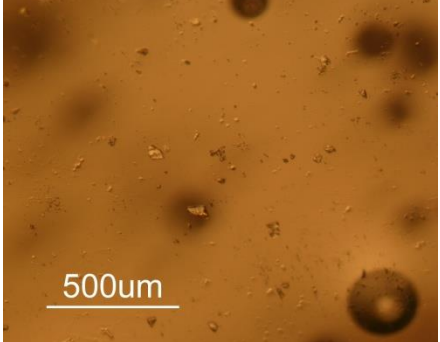
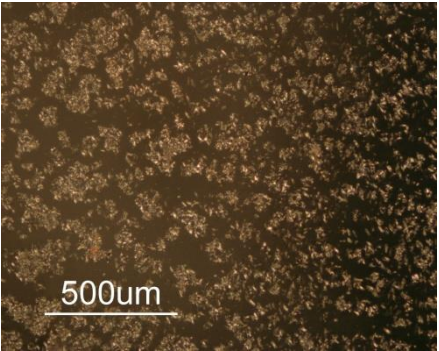
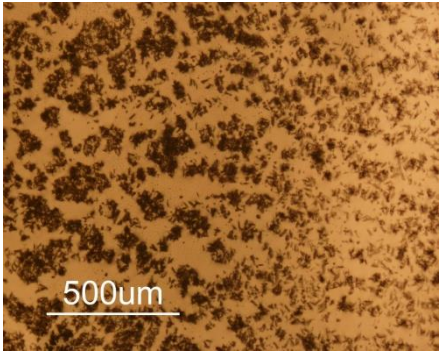
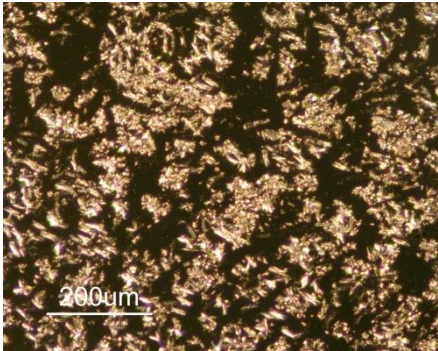
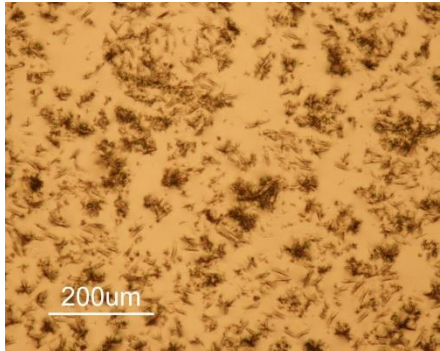
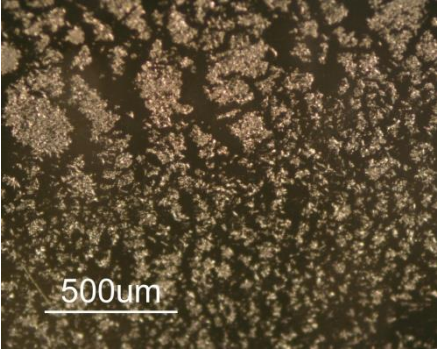
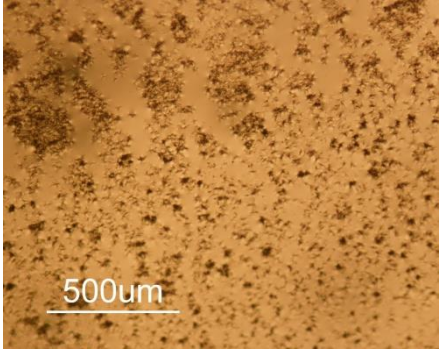
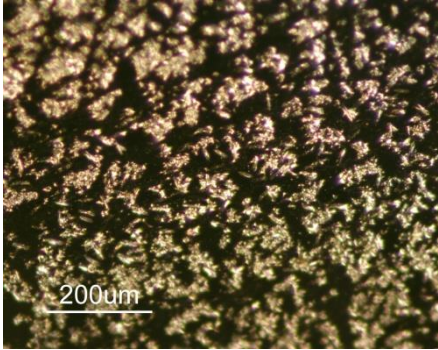
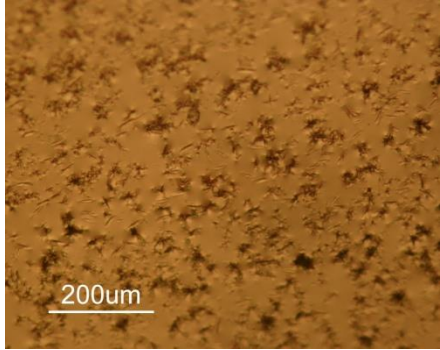
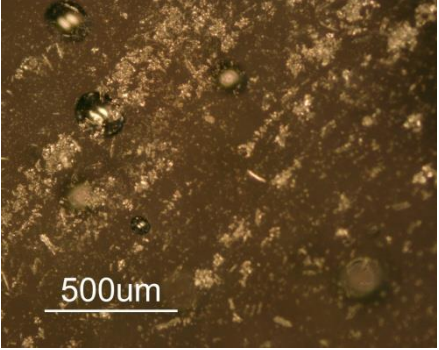
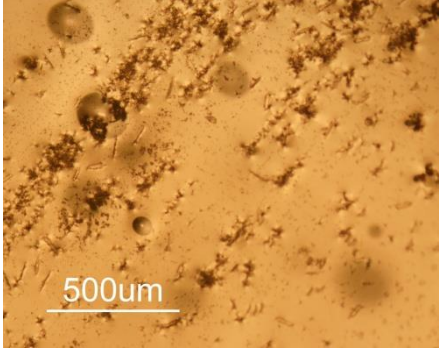
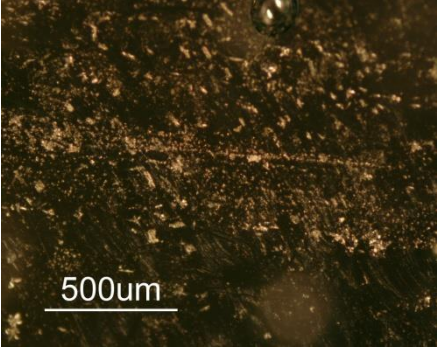
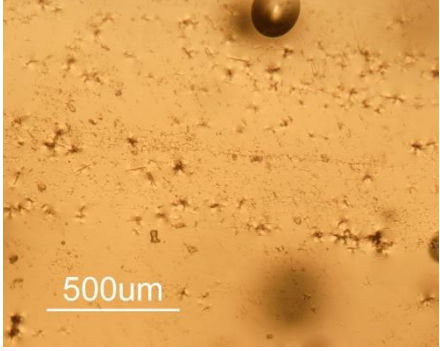
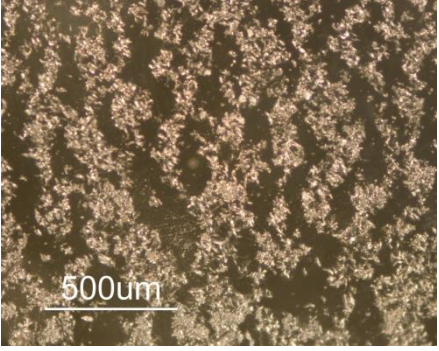
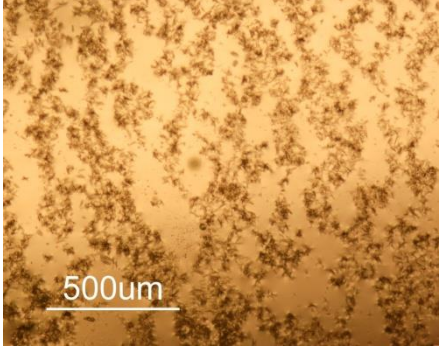
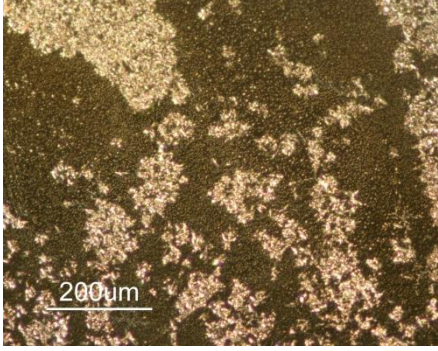
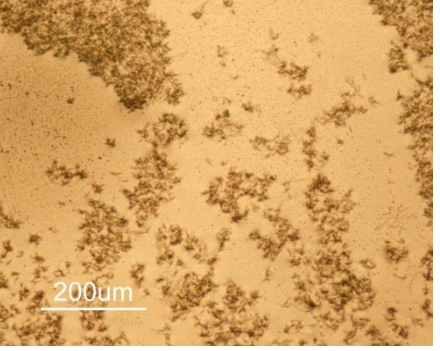
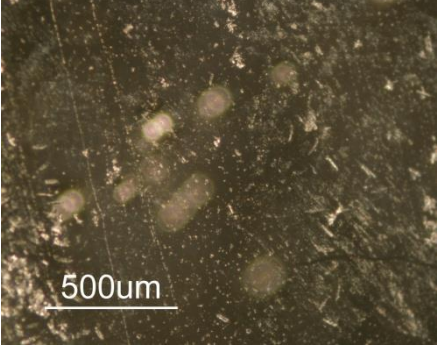
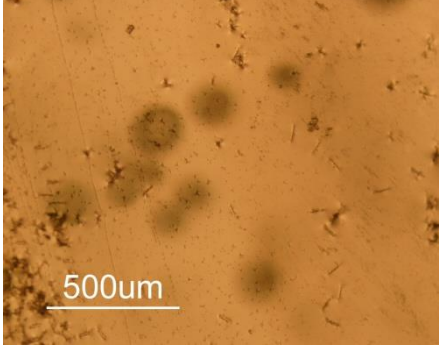
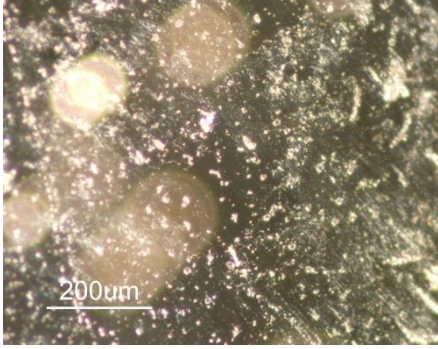
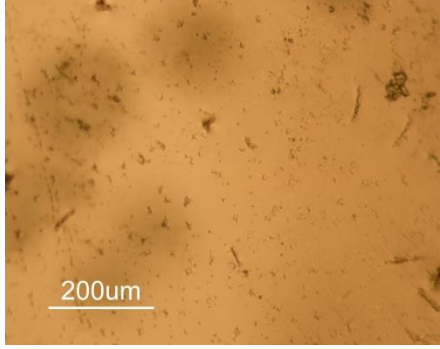
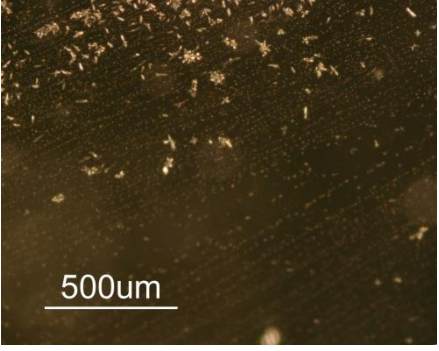
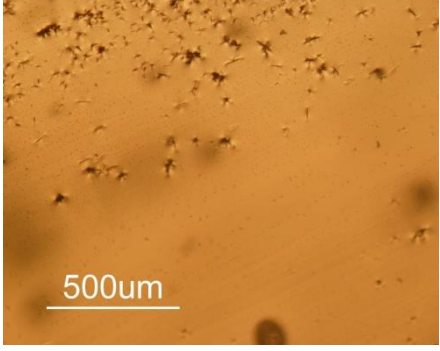
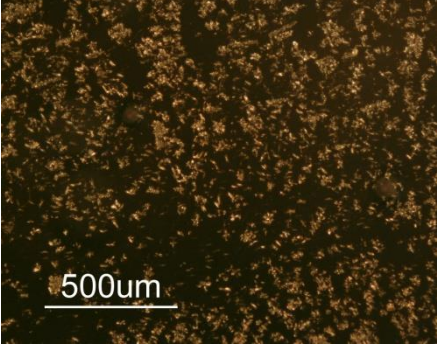
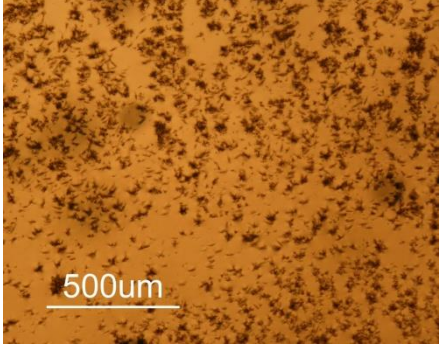
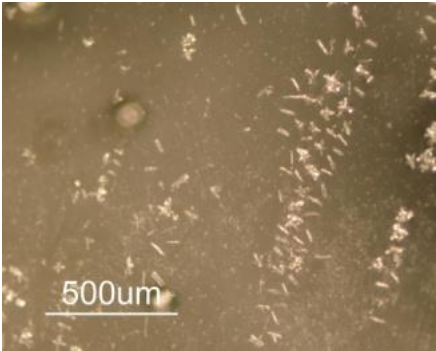
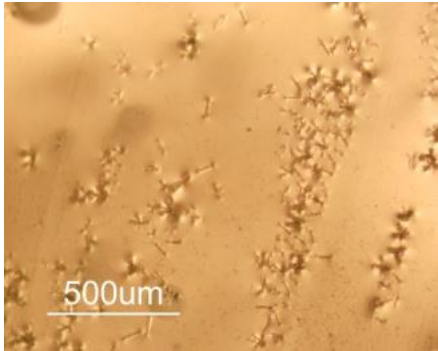
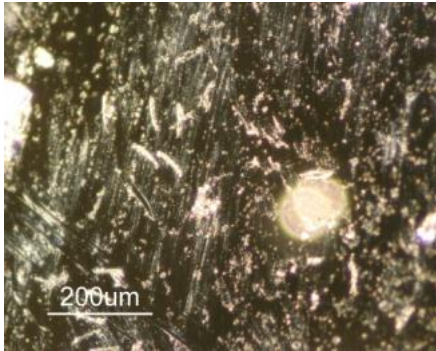
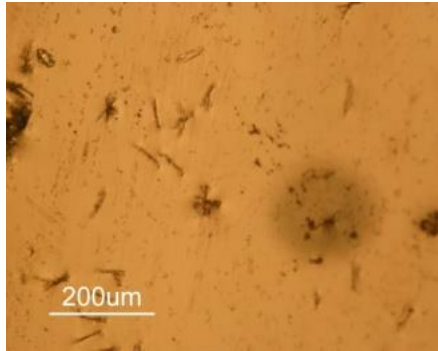
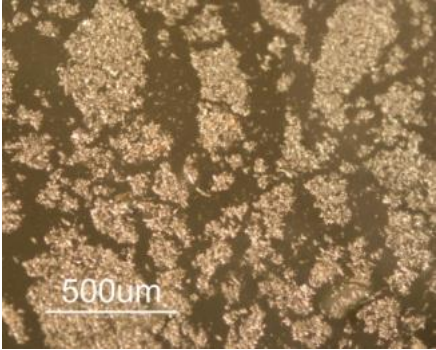
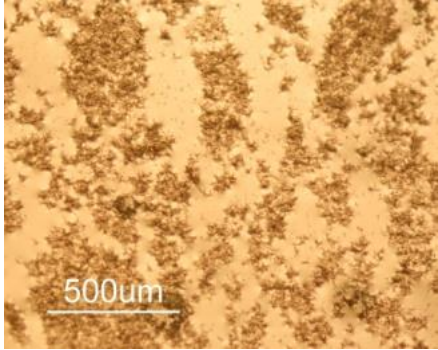
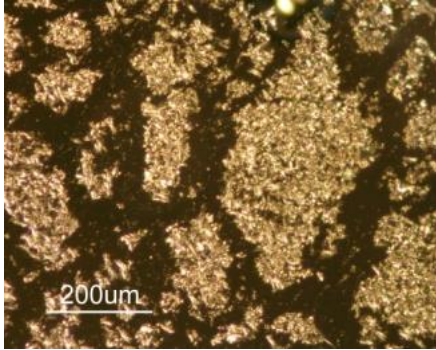
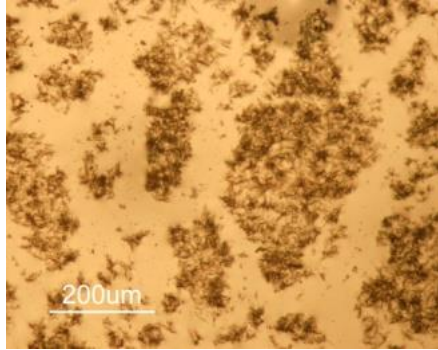
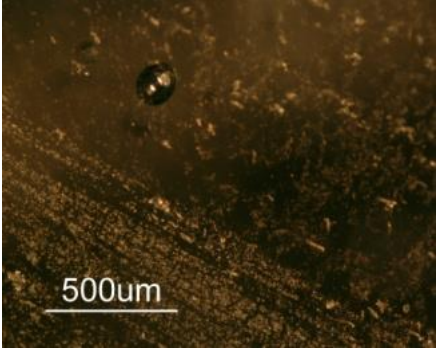
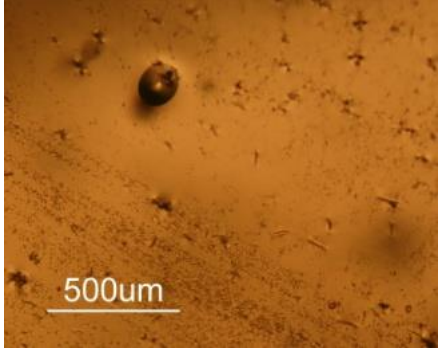
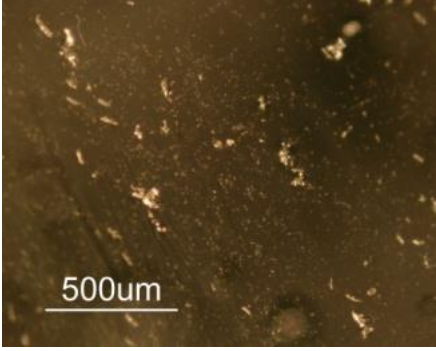
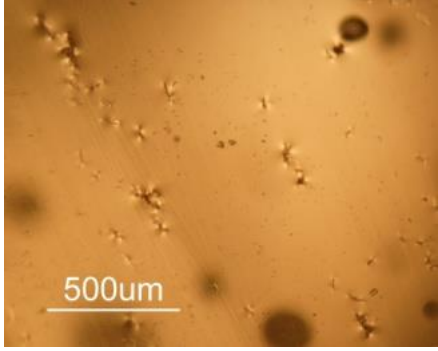
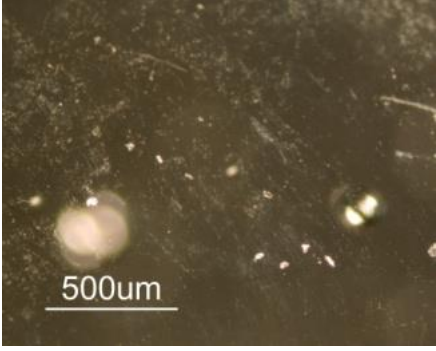
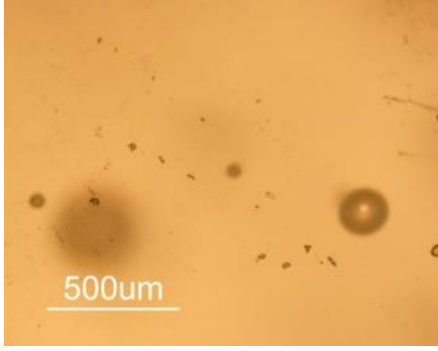
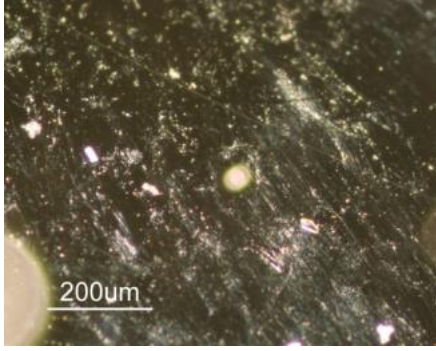
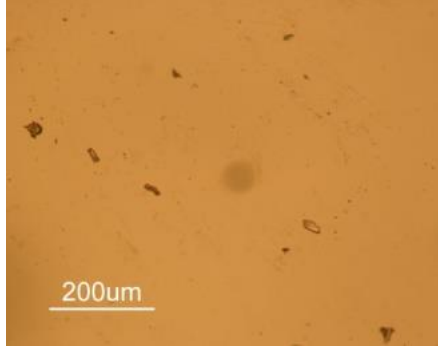
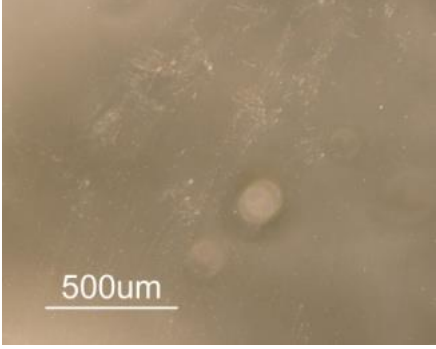
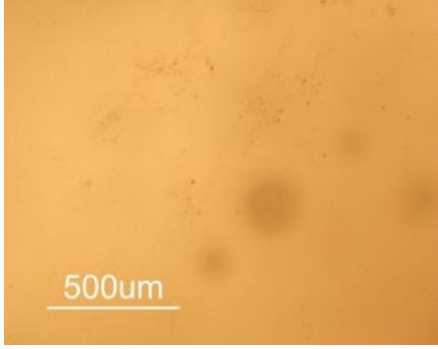
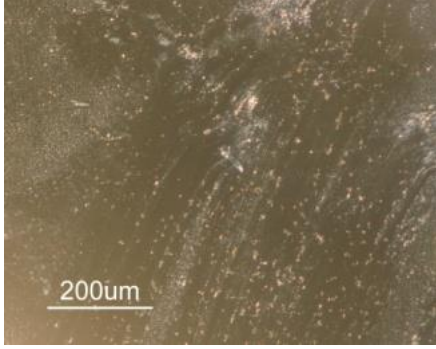
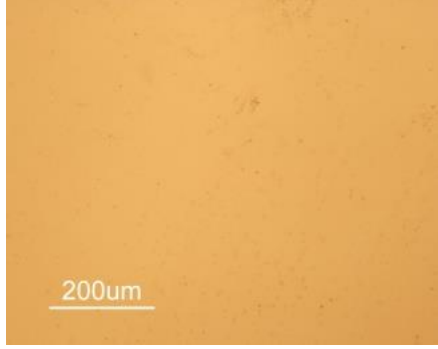
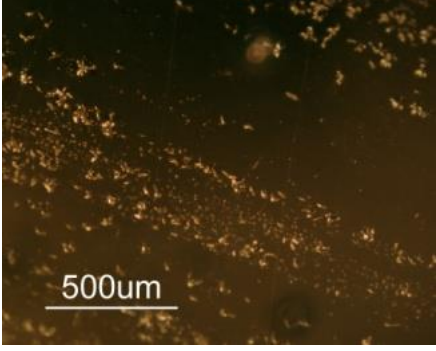
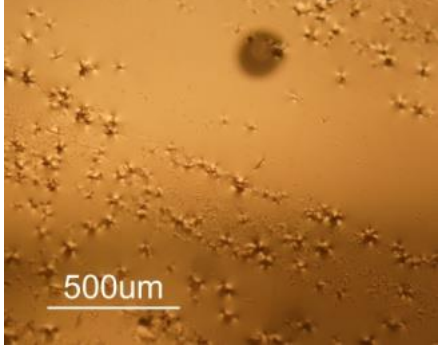
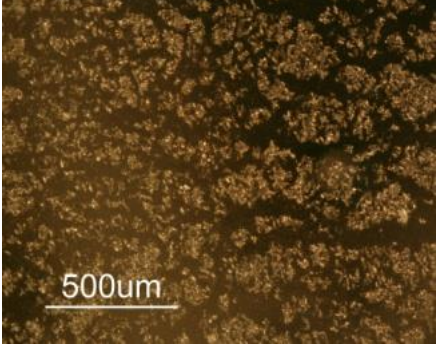
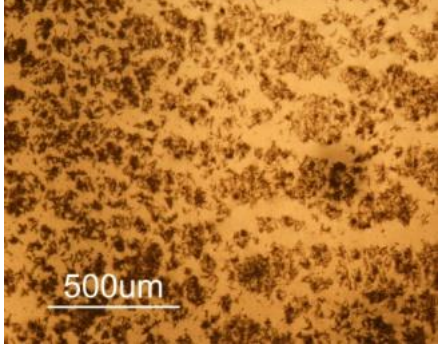


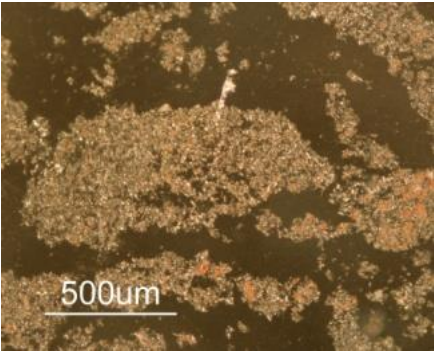
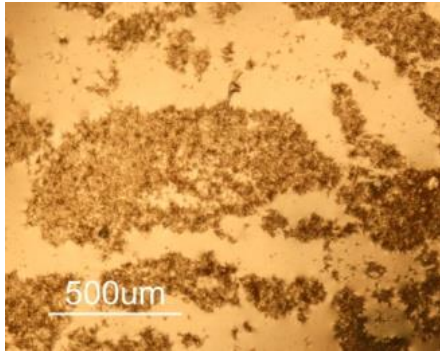
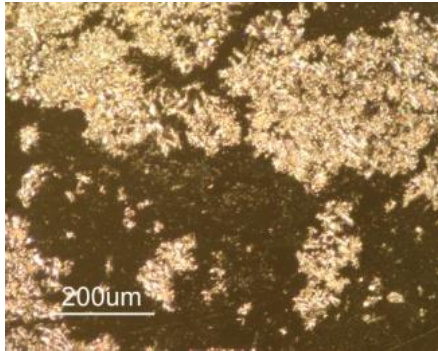
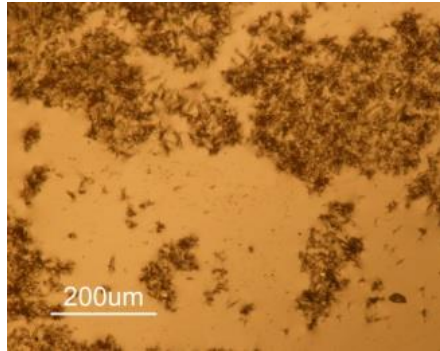
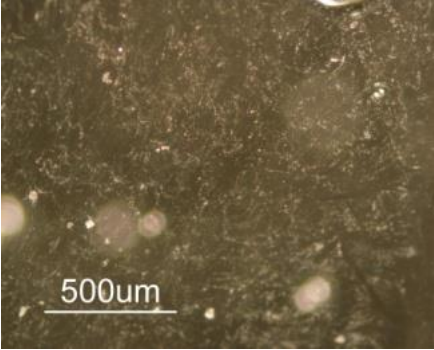
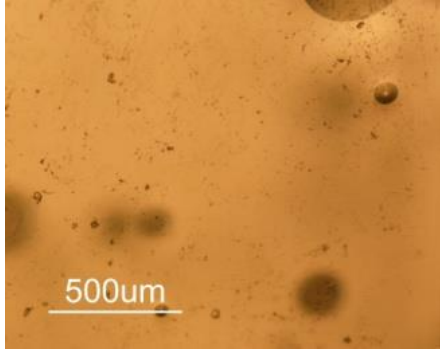
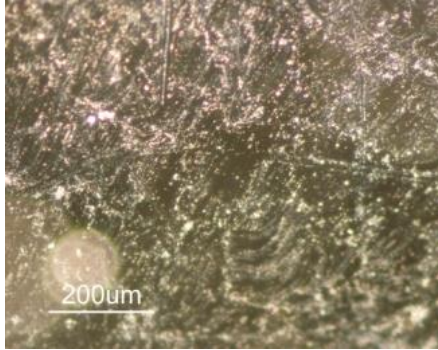
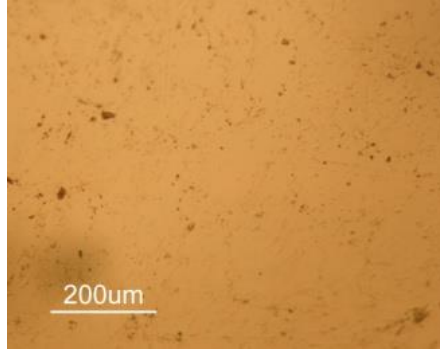
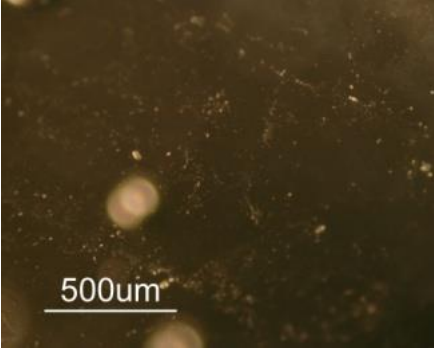
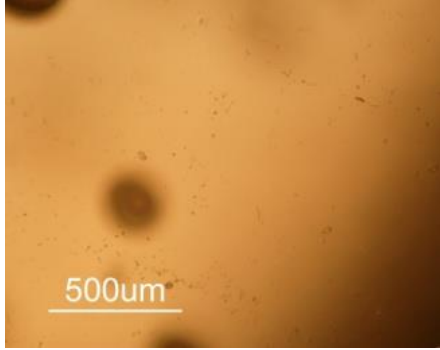
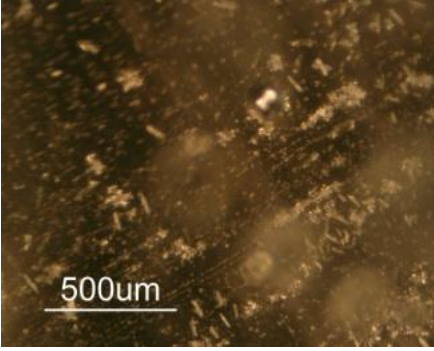
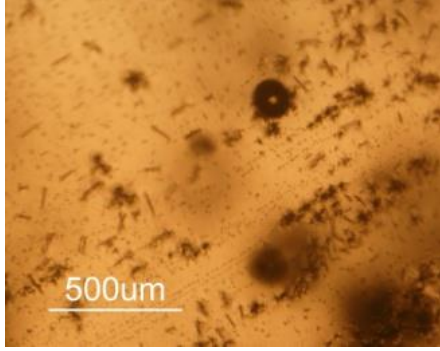
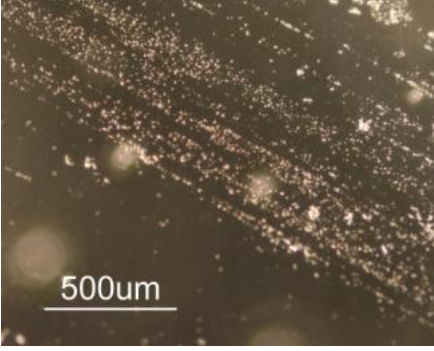
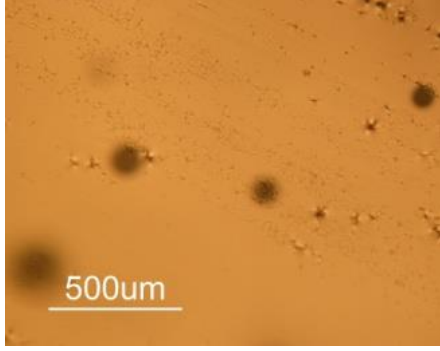
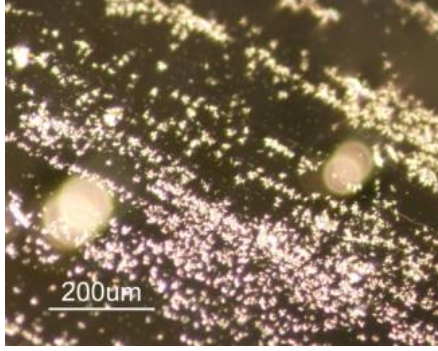
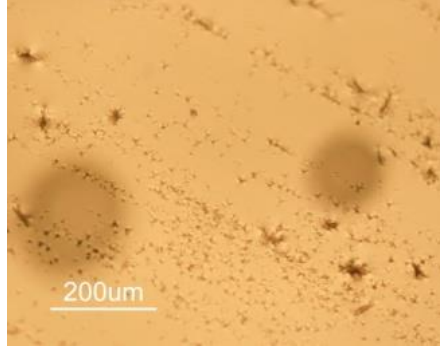
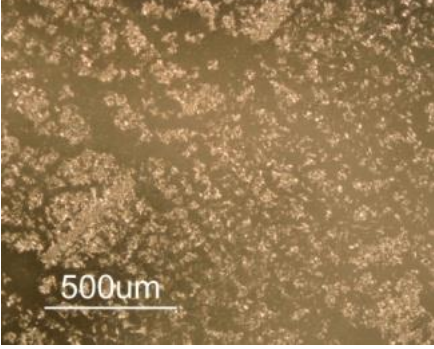
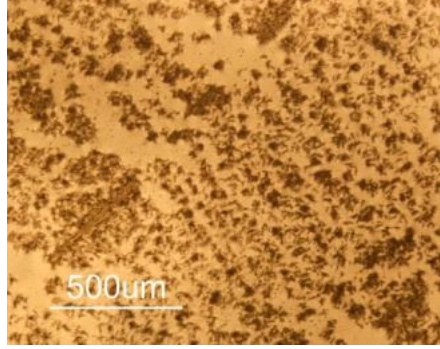
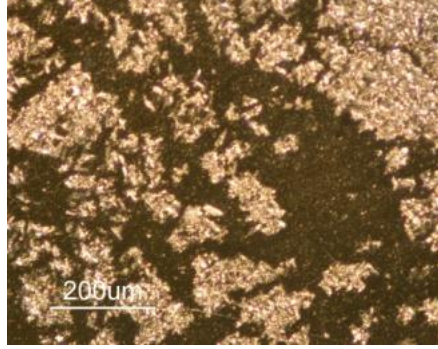
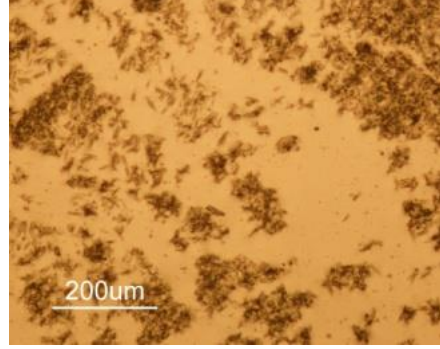
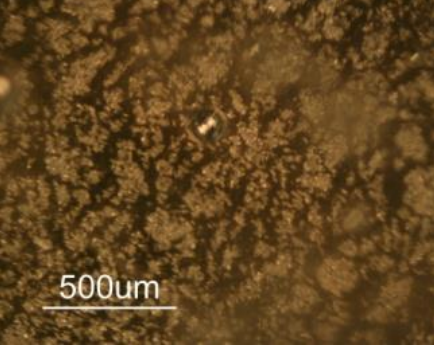
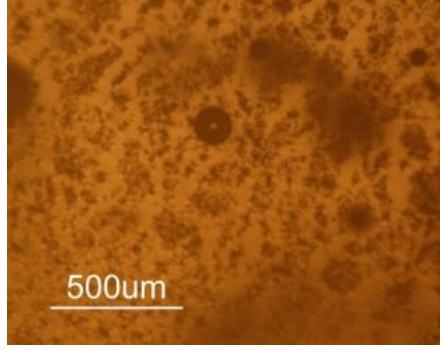
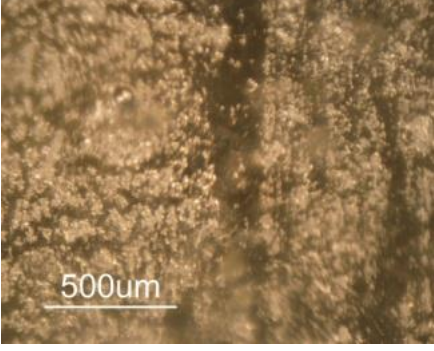
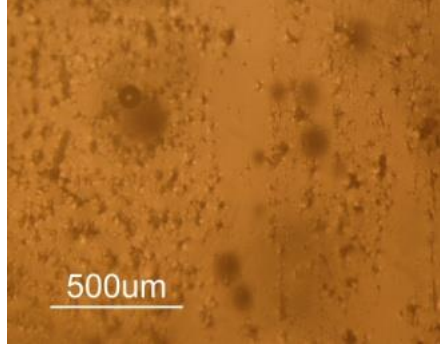
Figure: (above) Indication of what represents each label on the tables that will be presented in the next pages of this section and **(below)** experimental design for the experiments comparing the effects of different environment and compounds on model glass samples (each parameter was tested in 2 samples). This last figure and consequent explanation can be found in Chapter 3.

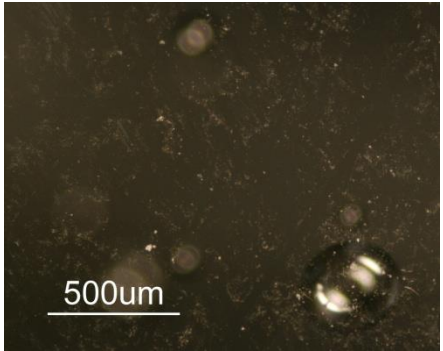
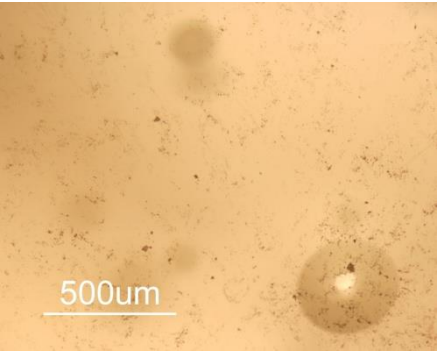
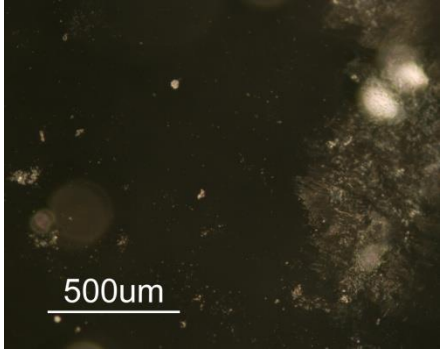
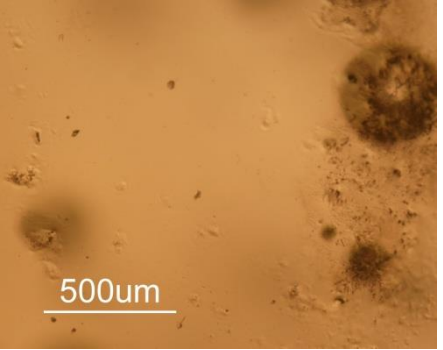
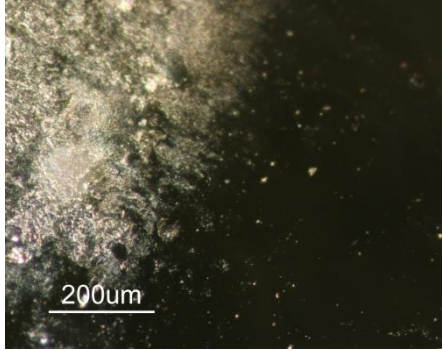
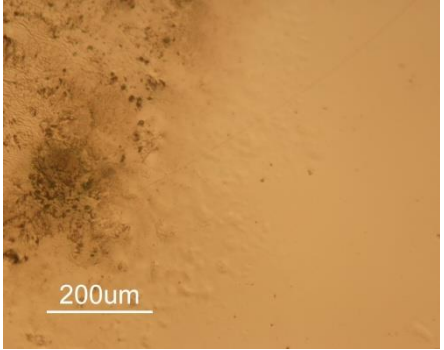
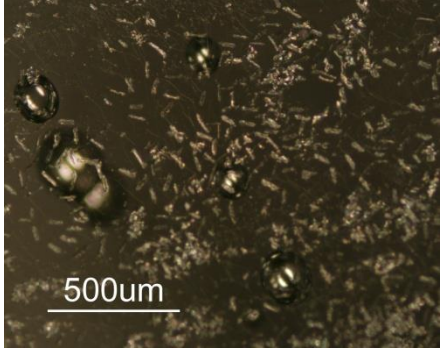
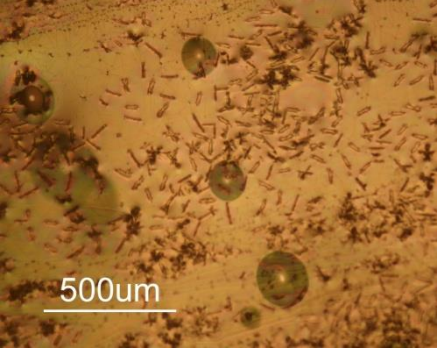
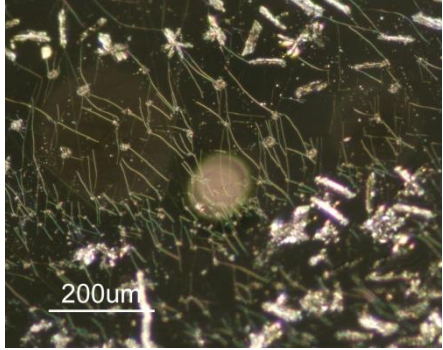
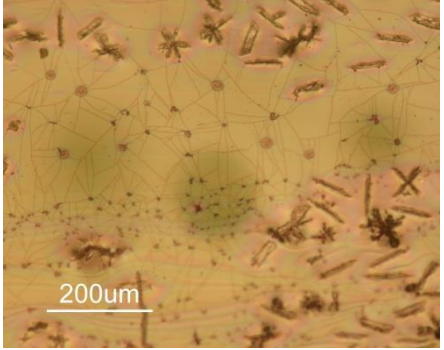
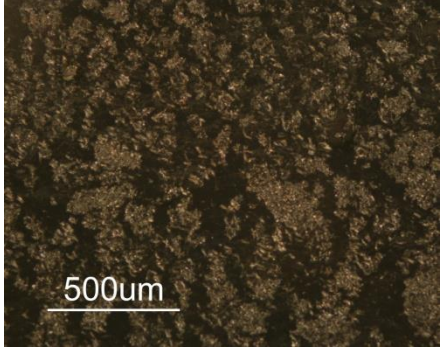
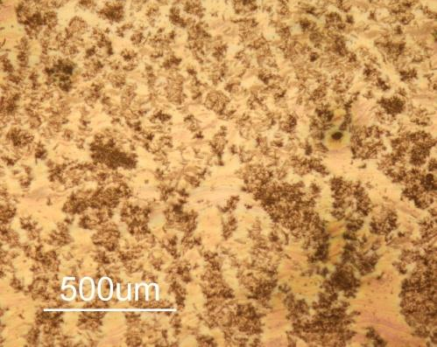
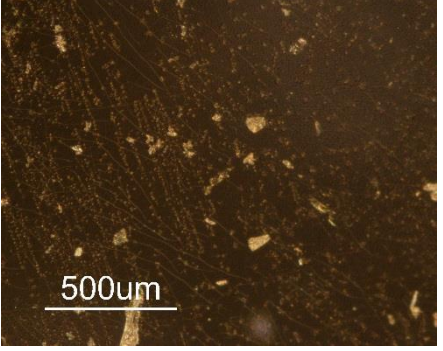
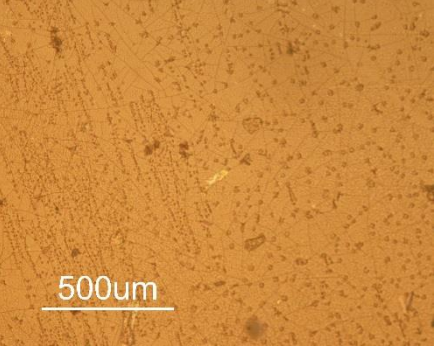
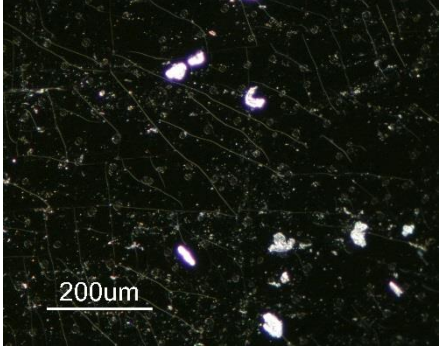
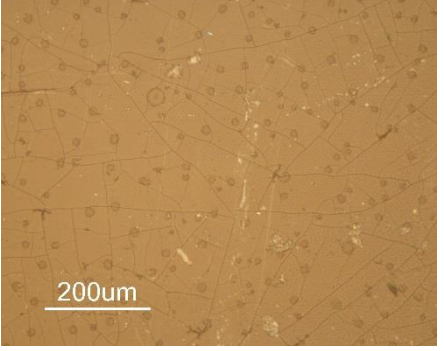
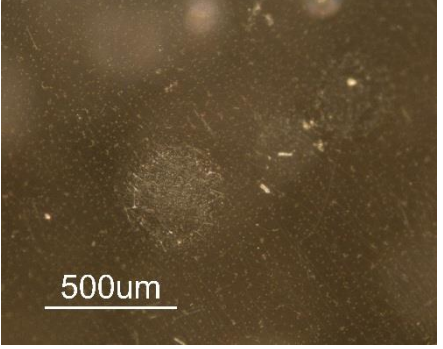
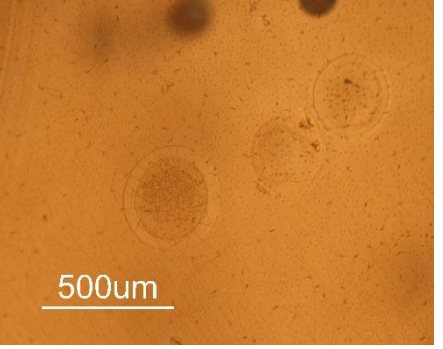
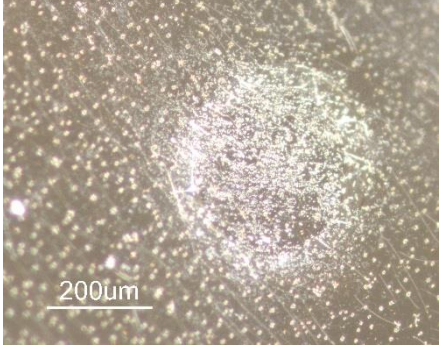
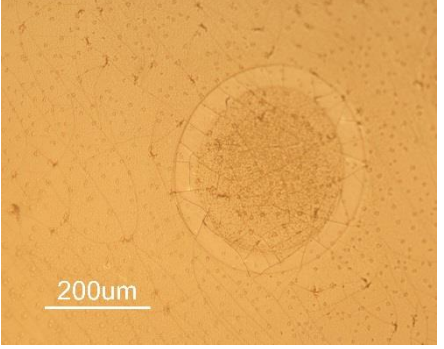
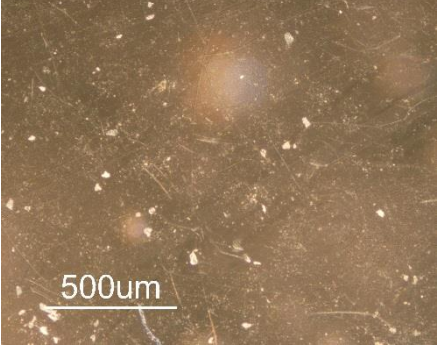
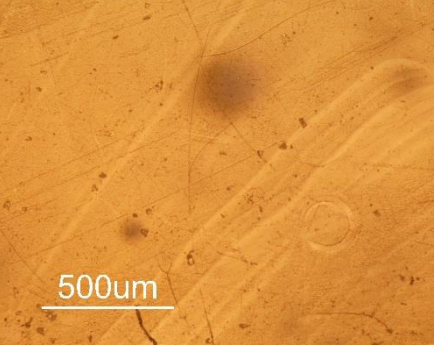
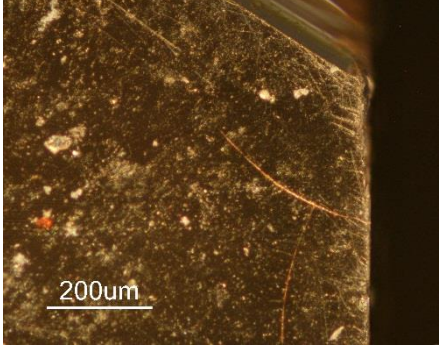
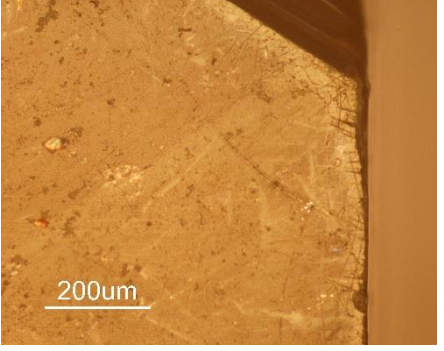
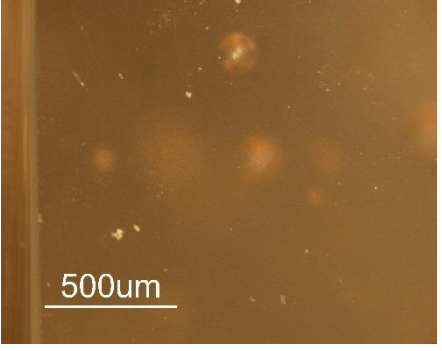
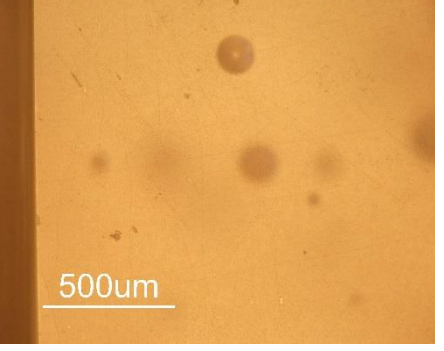
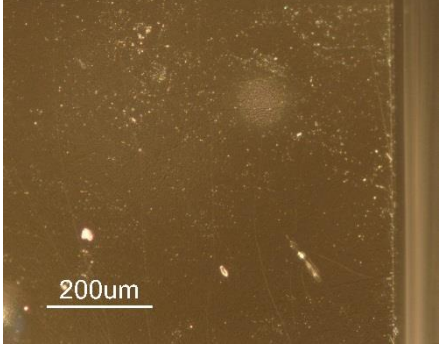
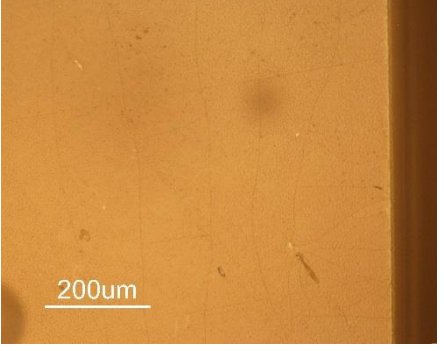
A	5x, Dark field	5x, Polarized light
1		
2		

B	5x, Dark field	5x, Polarized light	10x, Dark field	10x, Polarized light
1				
2				
3				
4				
5				
6				
7				
8				

C	5x, Dark field	5x, Polarized light	10x, Dark field	10x, Polarized light
1				
2				
3				
4				
5				
6				
7				
8				

D	5x, Dark field	5x, Polarized light	10x, Dark field	10x, Polarized light
1				
2				
3				
4				
5				
6				
7				
8				

E	5x, Dark field	5x, Polarized light	10x, Dark field	10x, Polarized light
1				
2				
3				
4				
5				
6				
7				
8				

F	5x, Dark field	5x, Bright field	10x, Dark field	10x, Bright field
1				
2				
3				
4				
5				
6				
7				
8				

Below is presented a comparative figure of samples from all groups.

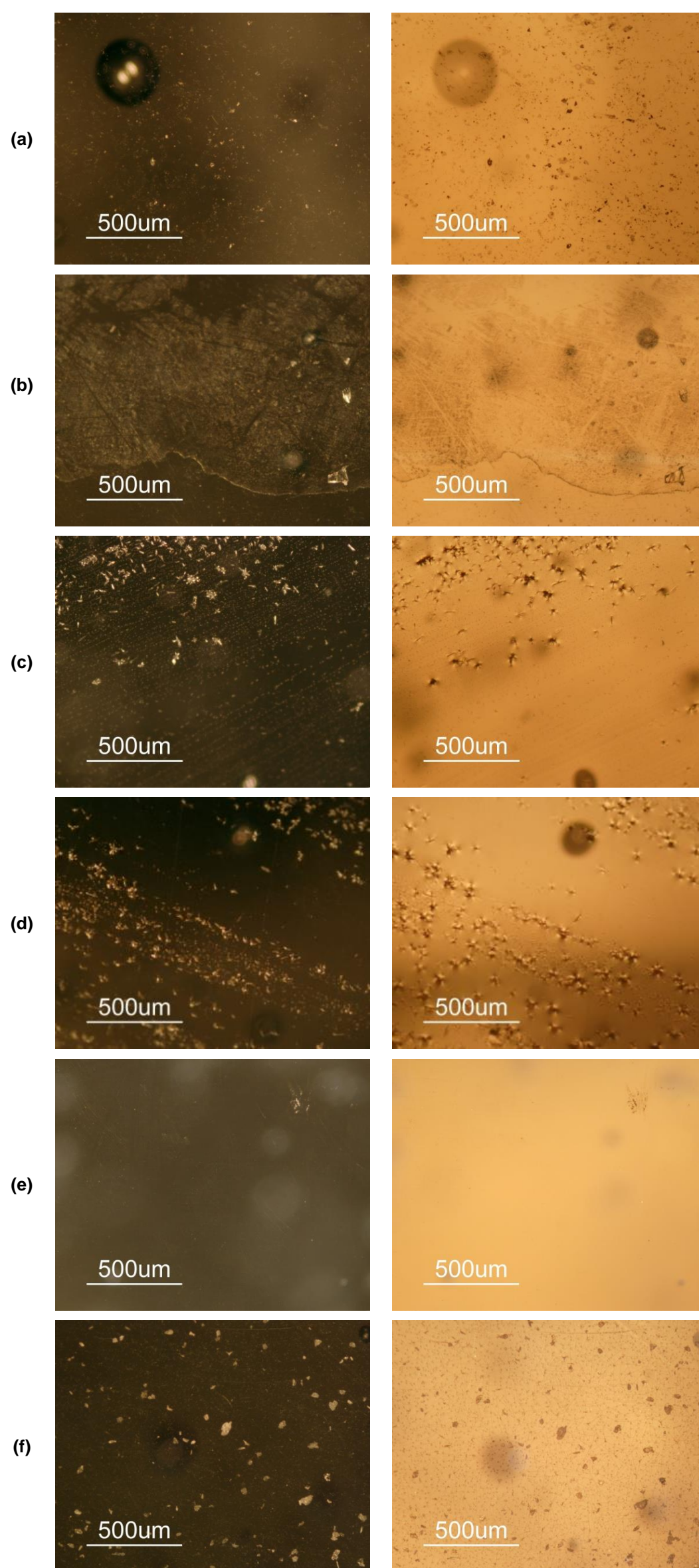


Figure: Optical microscope images of the surface of the model glass samples, with the dark field images on the left, and polarized light images on the right, all with a 5x lens magnification. **(a)** Control sample, from group A, **(b)** a sample from group B, left for 4 weeks in an 88% RH atmosphere, **(c)** a sample from group C, that was in contact with $[P_{6,6,6,14}][ANS]$ IL for 4 weeks, **(d)** a sample from group D, that was in contact with $[C_5O_2MIM][ANS]$ IL for 4 weeks, **(e)** a sample from group E, that was in contact with $[P_{6,6,6,14}][PyrCOO]$ IL for 4 weeks, and **(f)** a sample from group F, that was in a solution of 3% EDTA + 3% NH_4HCO_3 in distilled water, pH 8.26, for 1 week.

Below is presented a comparative figure of samples from group F, showing an altered surface even after being in contact with a solution of 3% EDTA + 3% NH_4HCO_3 in distilled water, pH 8.26, for only 1 hour.

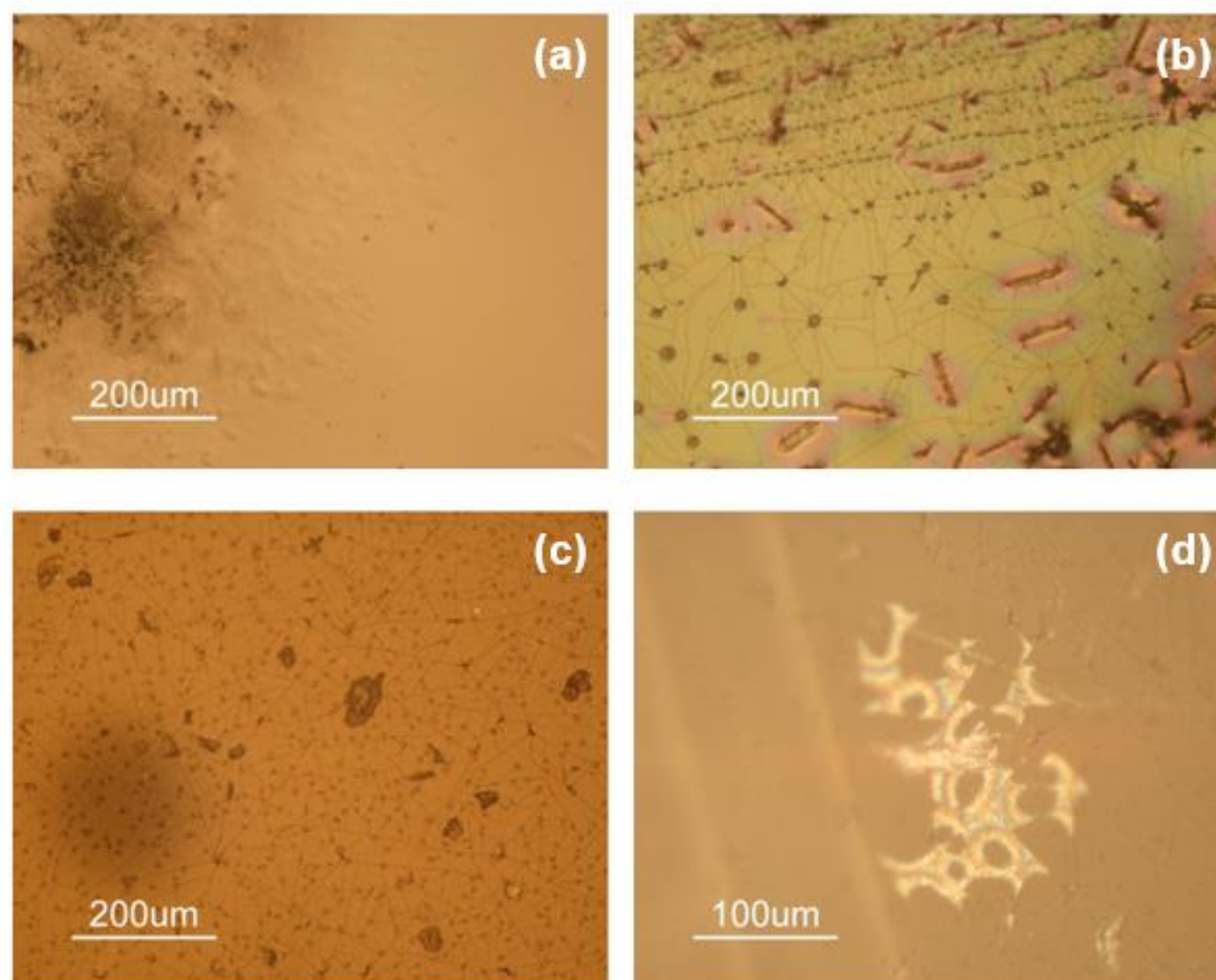
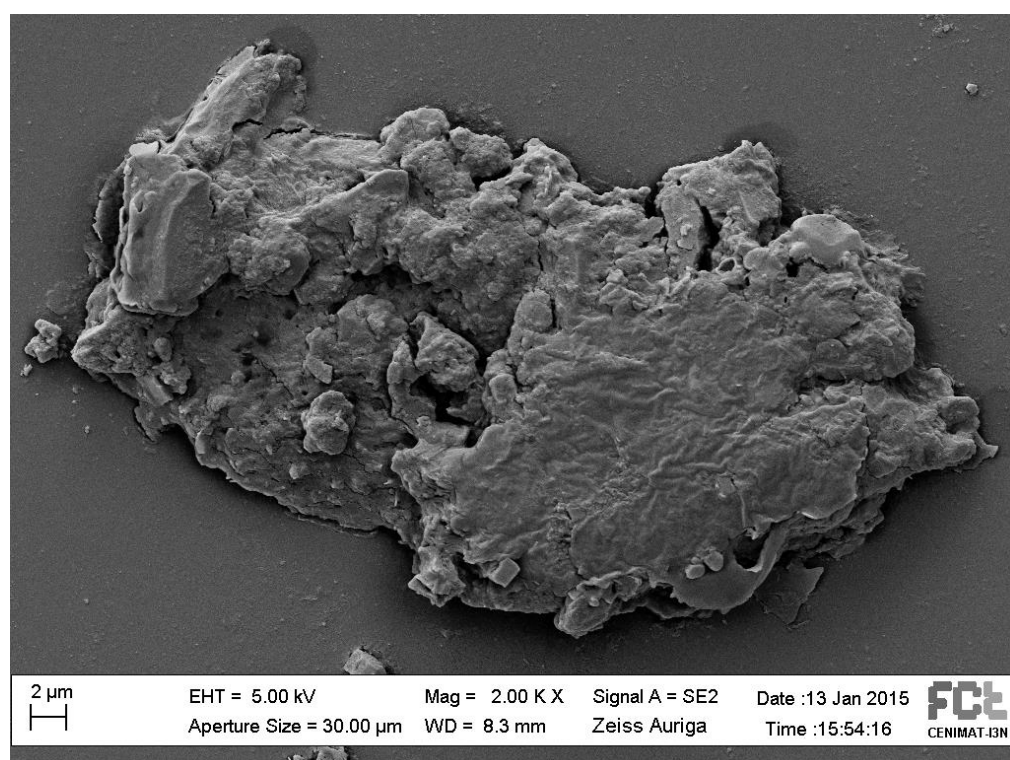
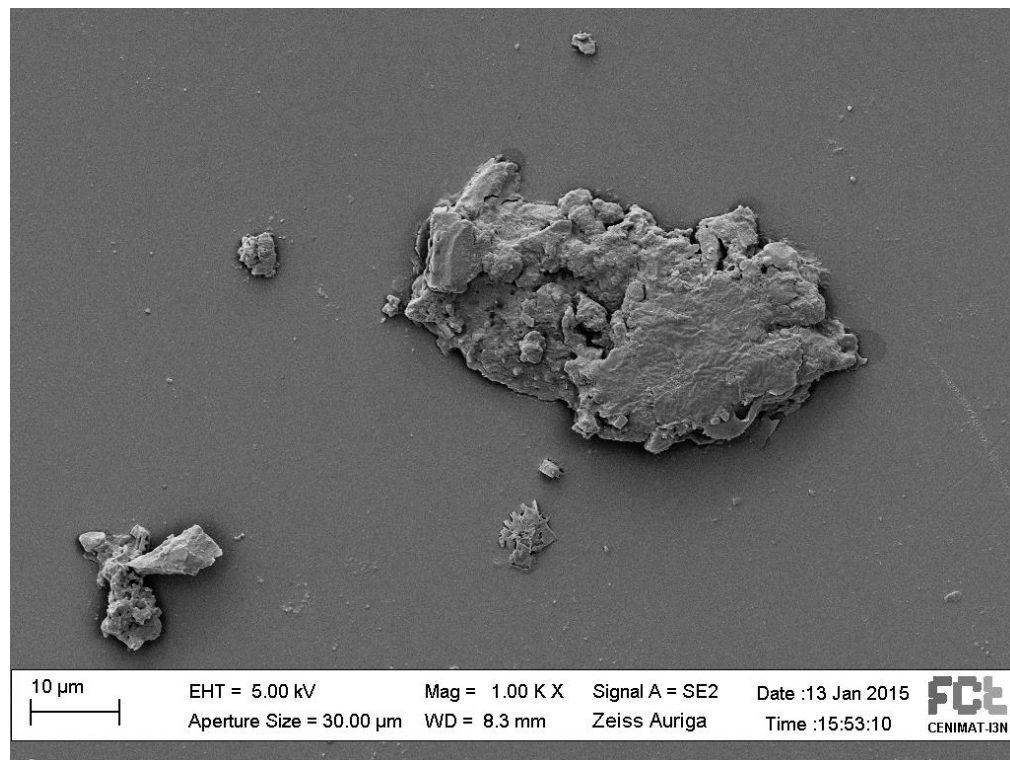
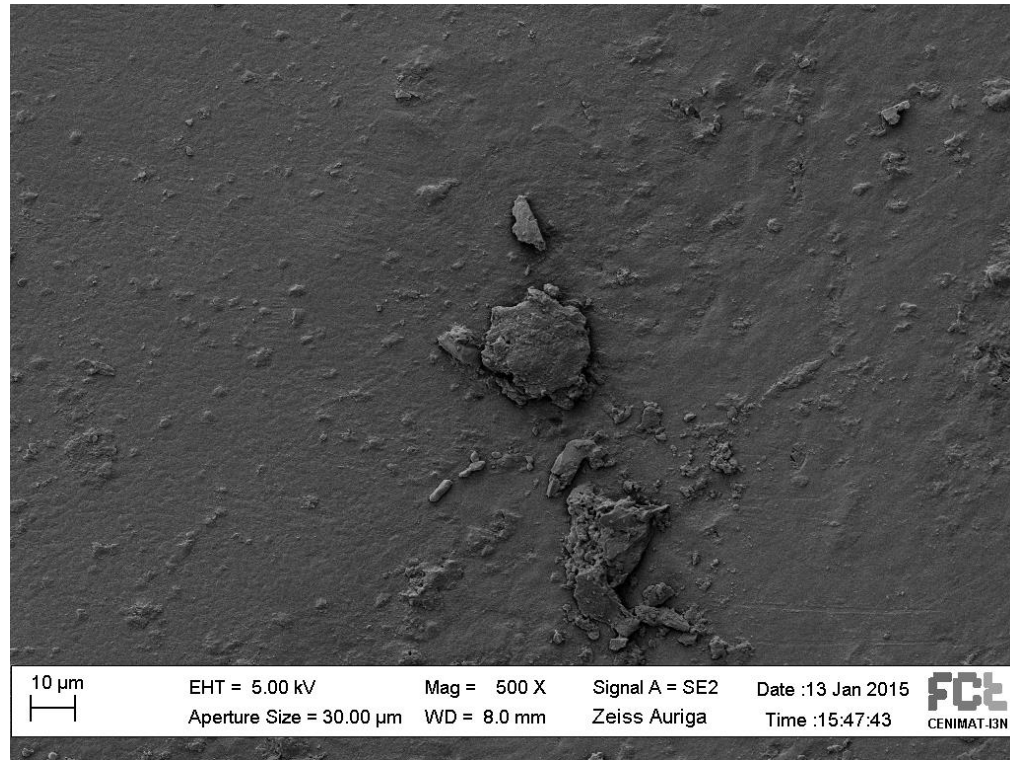


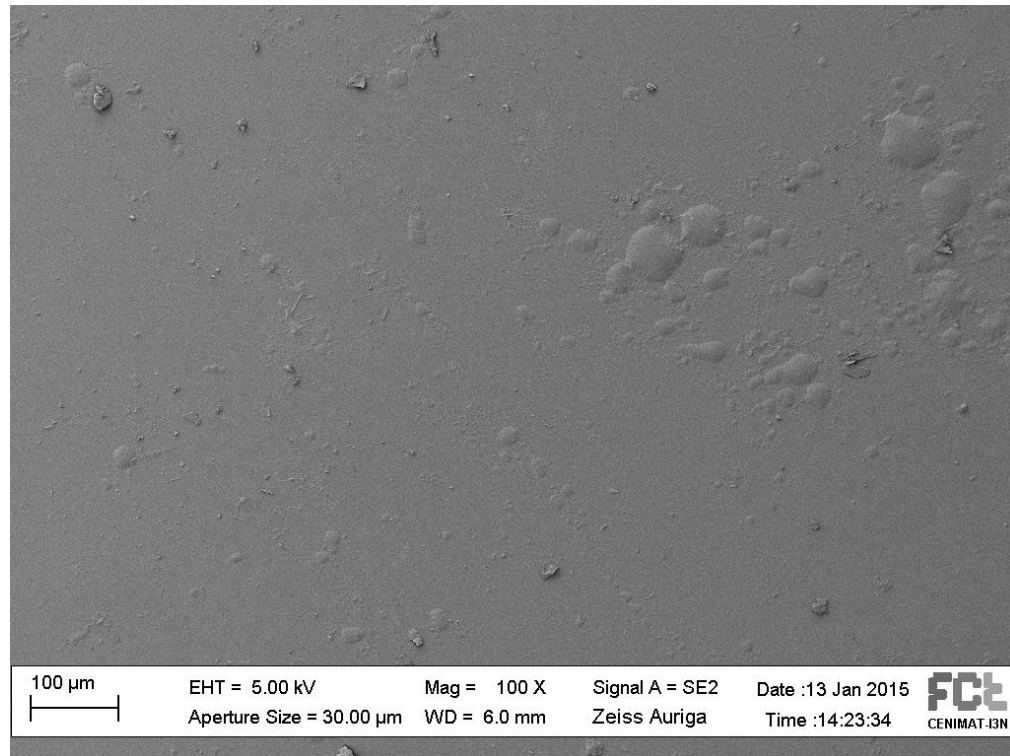
Figure: Optical microscope image of the surface of a sample from group F, **(a)** left for 1 hour in a solution of 3% EDTA + 3% NH_4HCO_3 in distilled water, pH 8.26, 10 x magnification, bright field. **(b)** A model sample left for 1 day in the same solution, 10 x magnification, bright field. Model glass sample left for 1 week **(c)** 10 x magnification, bright field and **(d)** 20 x magnification, polarized light.

ii) SEM images of model glass samples' surface;

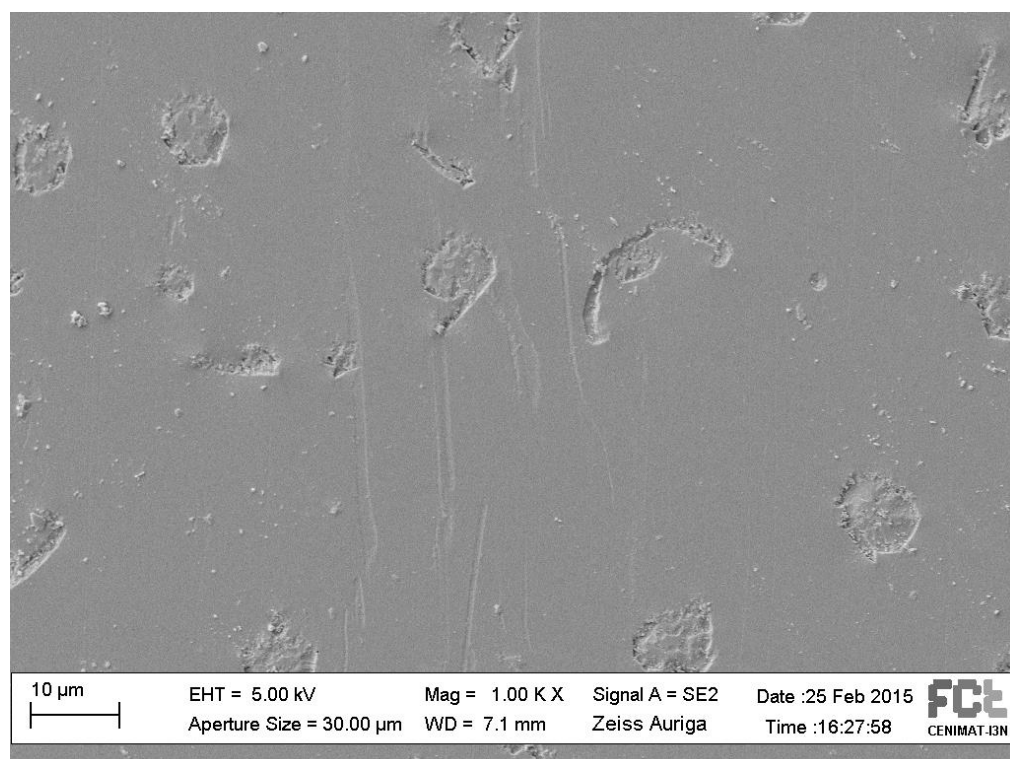
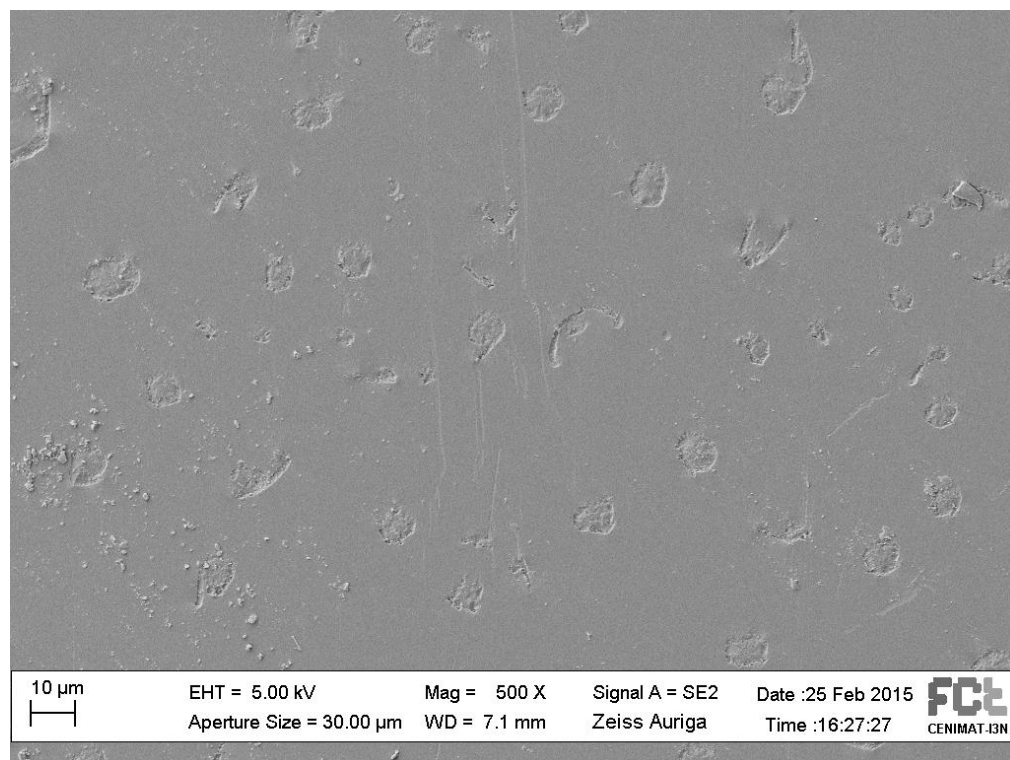
Group B (high RH) – 7 days



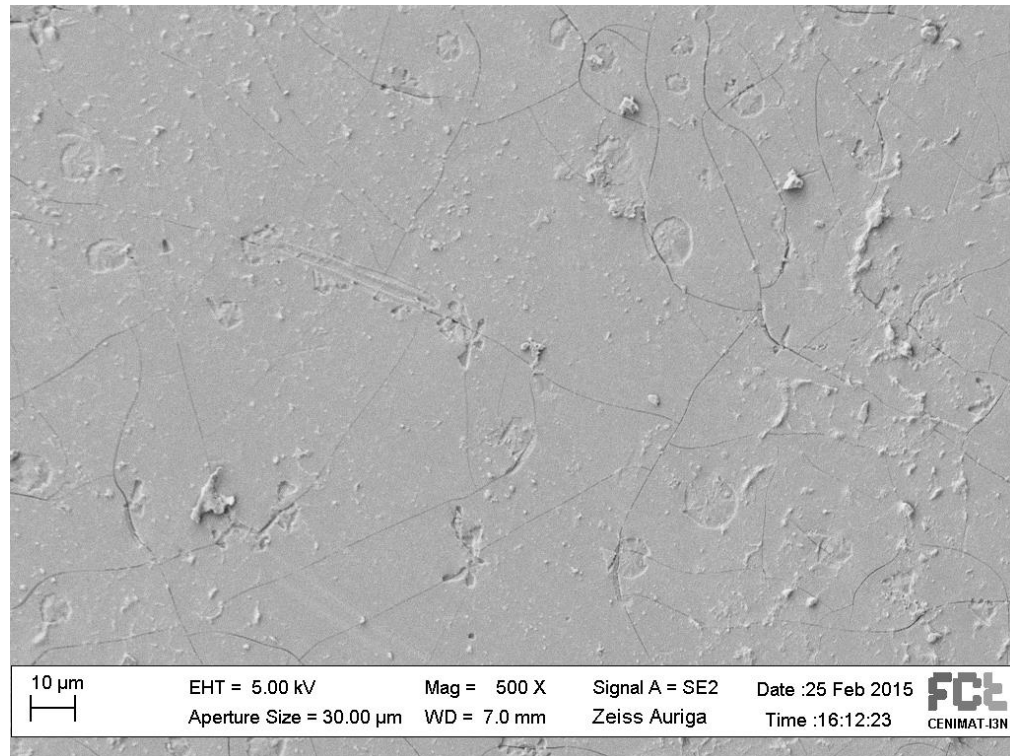
Group B (high RH) – 28 days



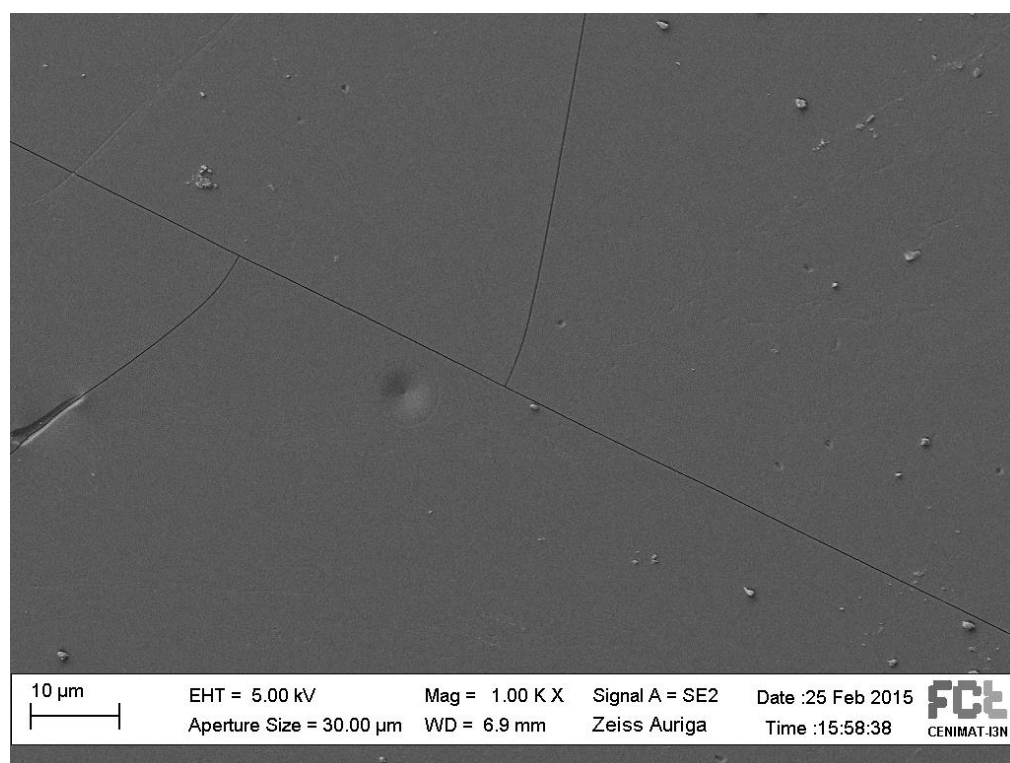
Group F (EDTA) – 1 hour



Group F (EDTA) – 7 days



Group F (EDTA) – 28 days



Attachment III – Complementary data related to Chapter 5

- i) Archaeological stained-glass fragments: images of the interior and exterior surfaces of the samples.**

- ii) SEM-EDS elementary mapping of archaeological stained glass samples Cant 001, 002, 003, 004, 005, 006, 028, 033 and 034.**

- iii) Cant 042 before and after the application of [P_{6,6,6,14}][ANS] IL**

i) **Archaeological stained-glass fragments: images of the interior and exterior surfaces of the samples.**

Note: The scale included on the side of each fragment has 1 x 1 cm².

Cant 007 – reflected light, interior face



Cant 007 – reflected light, exterior face



Cant 007 – reflected and transmitted light



Cant 008 – reflected light, interior face



Cant 008 – reflected light, exterior face



Cant 009 – reflected light, interior face



Cant 009 – reflected light, exterior face



Cant 010 – reflected light, interior face



Cant 010 – reflected light, exterior face



Cant 011 – reflected light, interior face



Cant 011 – reflected light, exterior face



Cant 012 – reflected light, interior face



Cant 012 – reflected light, exterior face



Cant 013 – reflected light, interior face



Cant 013 – reflected light, exterior face



Cant 014 – reflected light, interior face



Cant 014 – reflected light, exterior face



Cant 014 – reflected and transmitted light



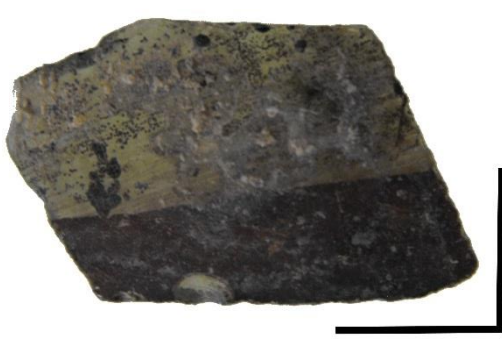
Cant 015 – reflected light, interior face



Cant 015 – reflected light, exterior face



Cant 016 – reflected light, interior face



Cant 016 – reflected light, exterior face



Cant 017 – reflected light, interior face



Cant 017 – reflected light, exterior face



Cant 017 – reflected and transmitted light



Cant 018 – reflected light, interior face



Cant 018 – reflected light, exterior face



Cant 019 – reflected light, interior face



Cant 019 – reflected light, exterior face



Cant 020 – reflected light, interior face



Cant 020 – reflected light, exterior face



Cant 020 – reflected and transmitted light



Cant 021 – reflected light, interior face



Cant 021 – reflected light, exterior face



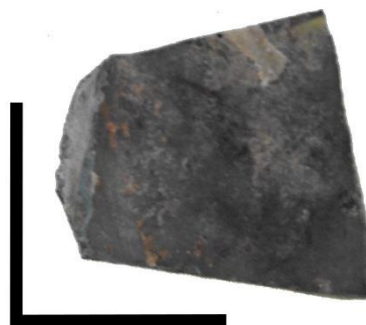
Cant 021 - curvature



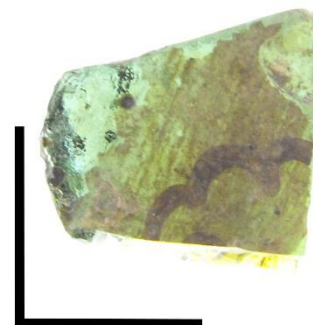
Cant 022 – reflected light, interior face



Cant 022 – reflected light, exterior face



Cant 022 – reflected and transmitted light



Cant 023 – reflected light, interior face



Cant 023 – reflected light, exterior face



Cant 024 – reflected light, interior face



Cant 024 – reflected light, exterior face



Cant 025 – reflected light, interior face



Cant 025 – reflected light, exterior face



Cant 025 – reflected and transmitted light



Cant 026 – reflected light, interior face



Cant 026 – reflected light, exterior face



Cant 027 – reflected light, interior face



Cant 027 – reflected light, exterior face



Cant 028 – reflected light, interior face



Cant 028 – reflected light, exterior face



Cant 028 – reflected and transmitted light



Cant 029 – reflected light, interior face



Cant 029 – reflected light, exterior face



Cant 030 – reflected light, interior face



Cant 030 – reflected light, exterior face



Cant 030 – reflected and transmitted light



Cant 031 – reflected light, interior face



Cant 031 – reflected light, exterior face



Cant 030 – reflected and transmitted light



Cant 032 – reflected light, interior face



Cant 032 – reflected light, exterior face



Cant 033 – reflected light, interior face



Cant 033 – reflected light, exterior face



Cant 034 – reflected light, interior face



Cant 034 – reflected light, exterior face



Cant 035 – reflected light, interior face



Cant 035 – reflected light, exterior face



Cant 036 – reflected light, interior face



Cant 036 – reflected light, exterior face



Cant 036 – reflected and transmitted light



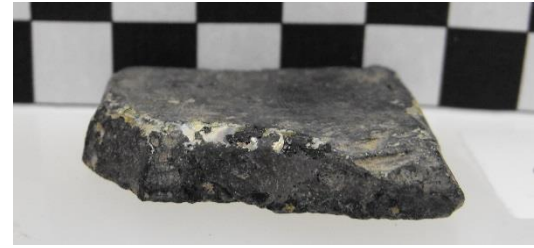
Cant 037 – reflected light, interior face



Cant 037 – reflected light, exterior face



Cant 037



Note: each square in the scale has 1 x 1 cm²

Cant 038 – reflected light, interior face



Cant 038 – reflected light, exterior face



Cant 038 – reflected and transmitted light



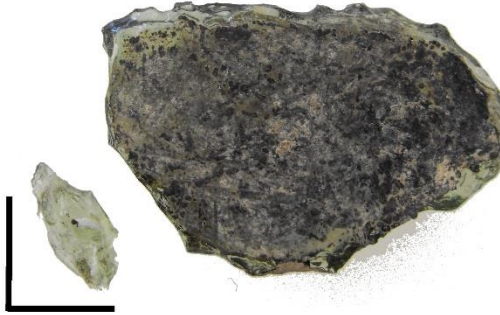
Cant 039 – reflected light, interior face



Cant 039 – reflected light, exterior face



Cant 040 – reflected light, interior face



Cant 040 – reflected light, exterior face



Cant 041 – reflected light



Cant 041



Cant 042 – reflected light, interior face



Cant 042 – reflected light, exterior face



Cant 042 – reflected and transmitted light



Cant 043 – reflected light, interior face

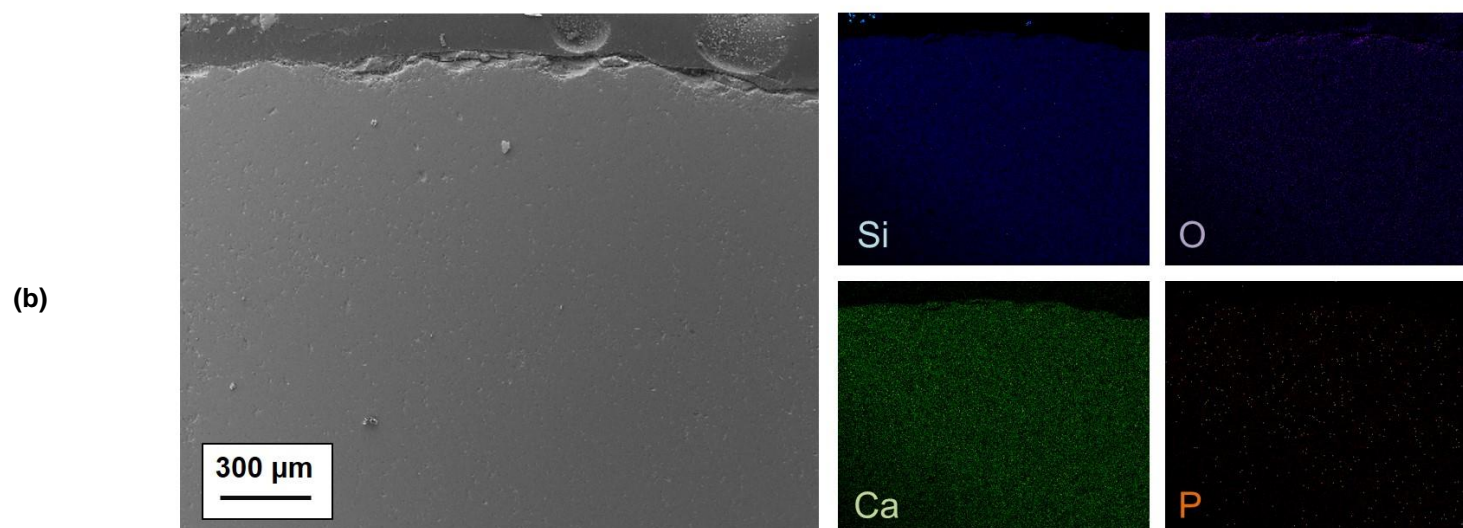
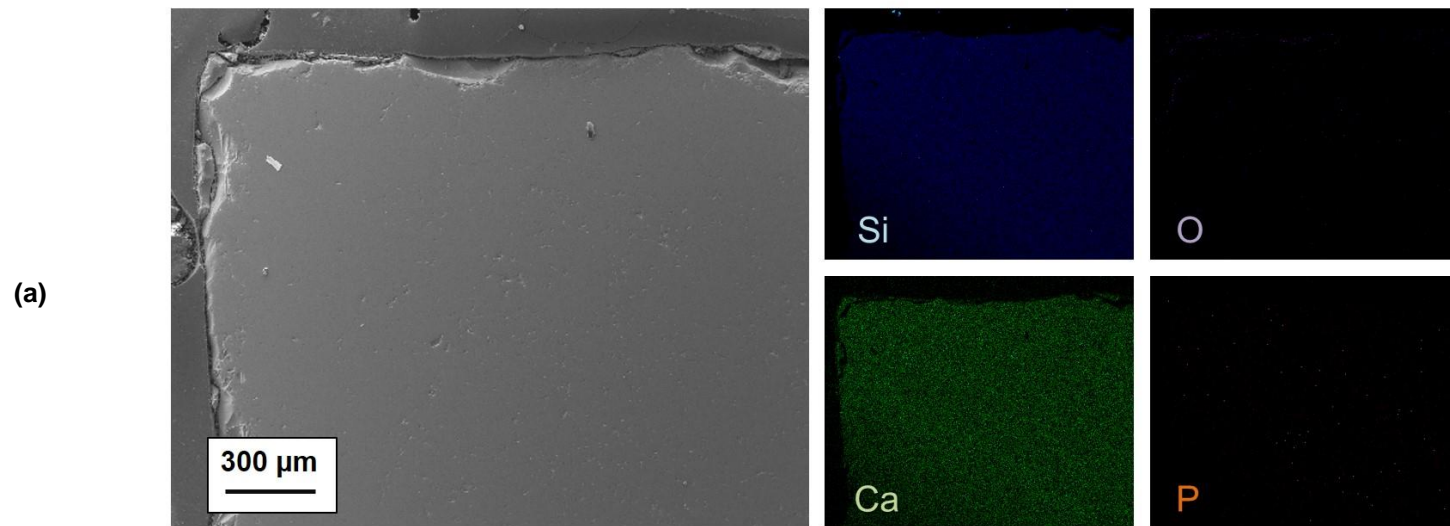


Cant 043 – reflected light, exterior face

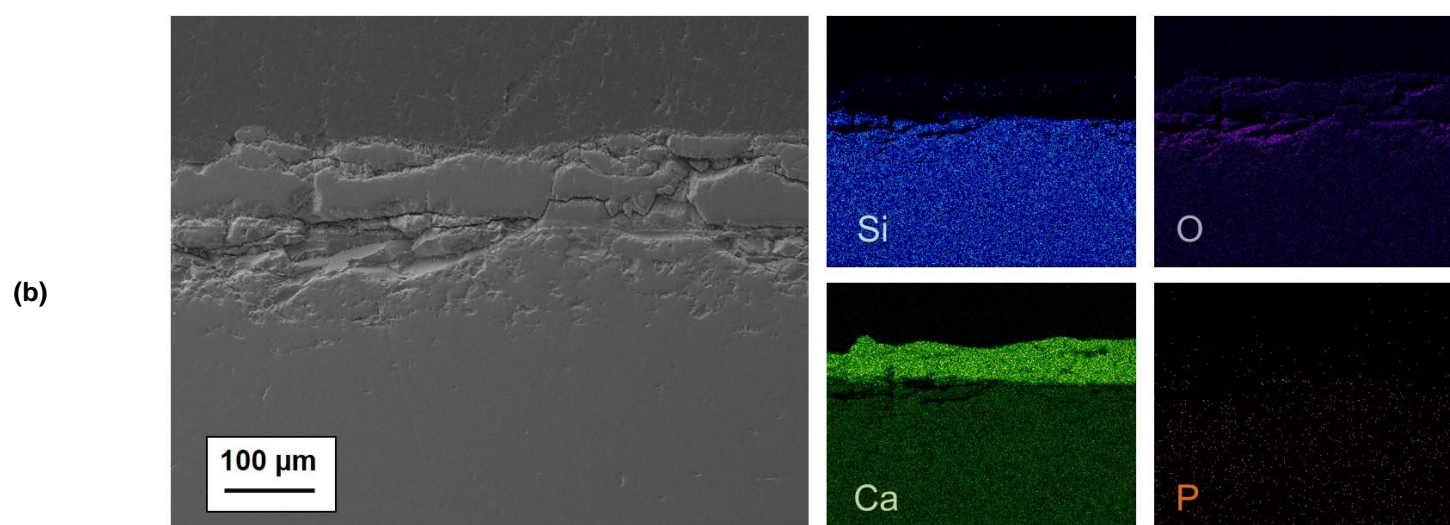
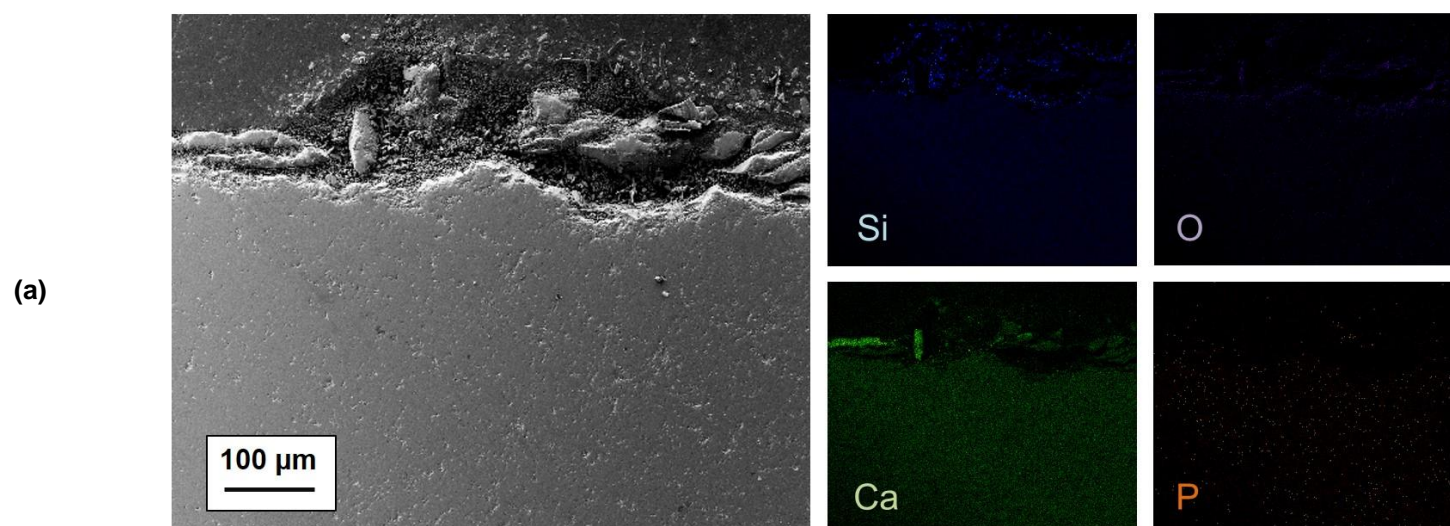


- ii) SEM-EDS elementary mapping of archaeological stained glass samples Cant 001, 002, 003, 004, 005, 006, 028, 033 and 034, (a) before and (b) after the application of $[P_{6,6,6,14}][ANS]$ IL.

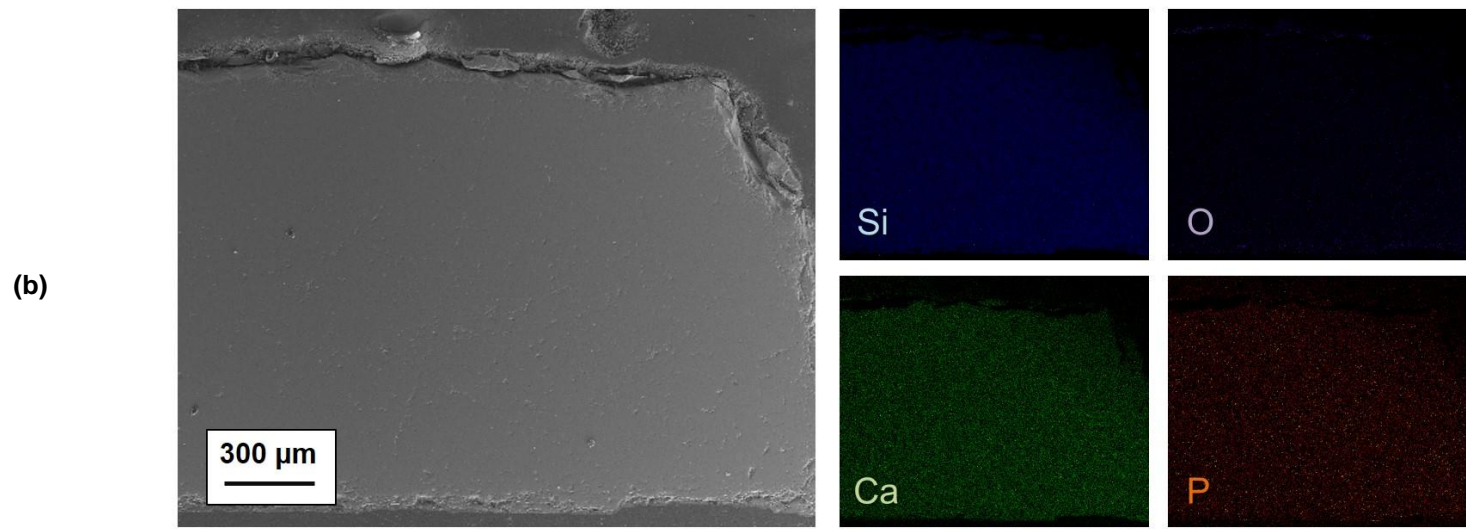
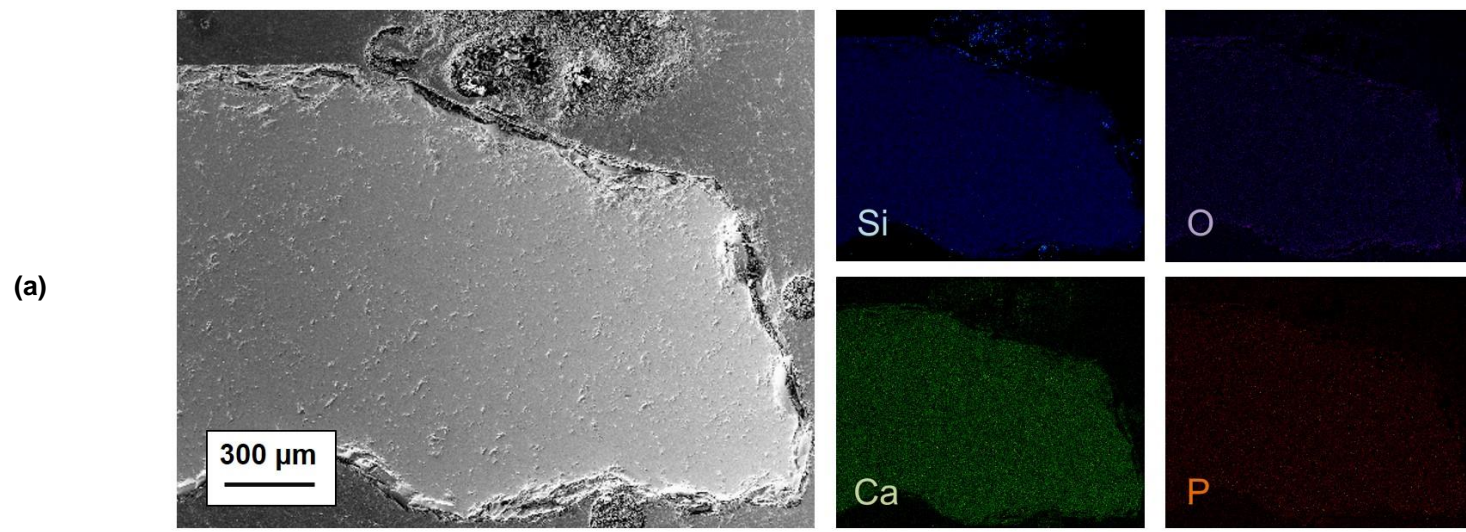
Cant 001



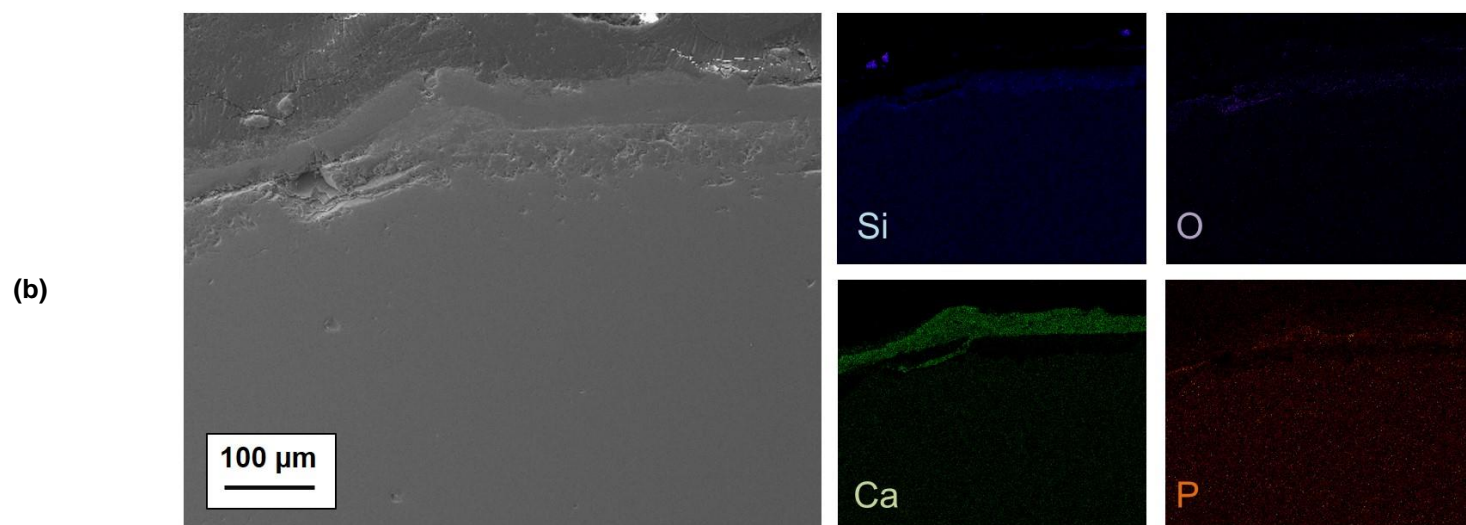
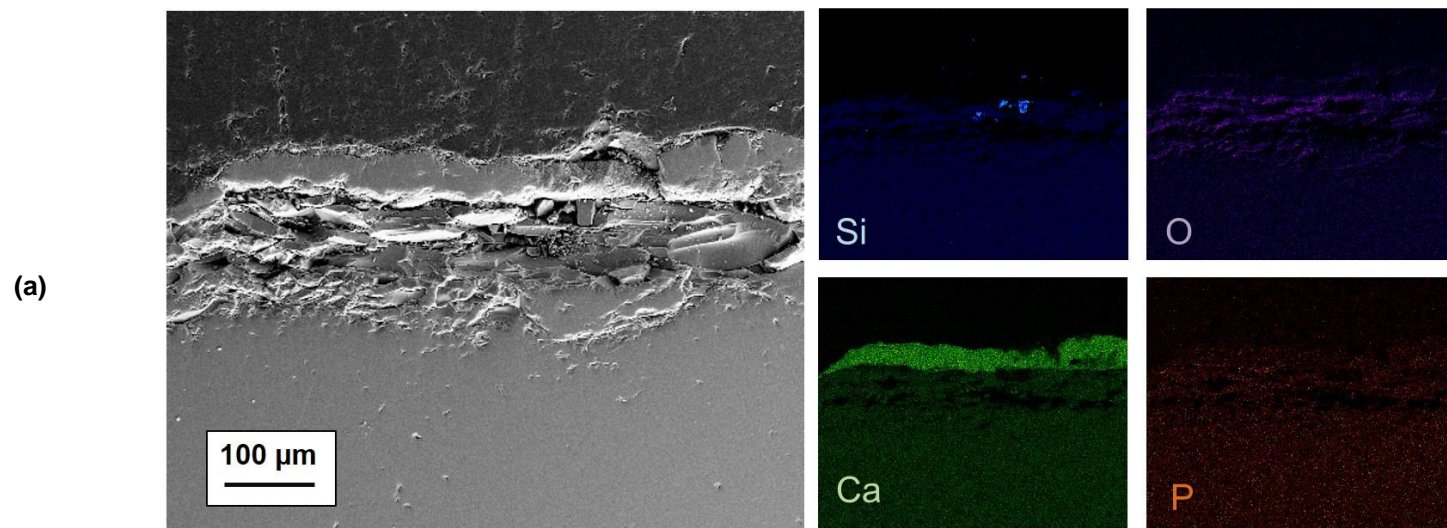
Cant 002



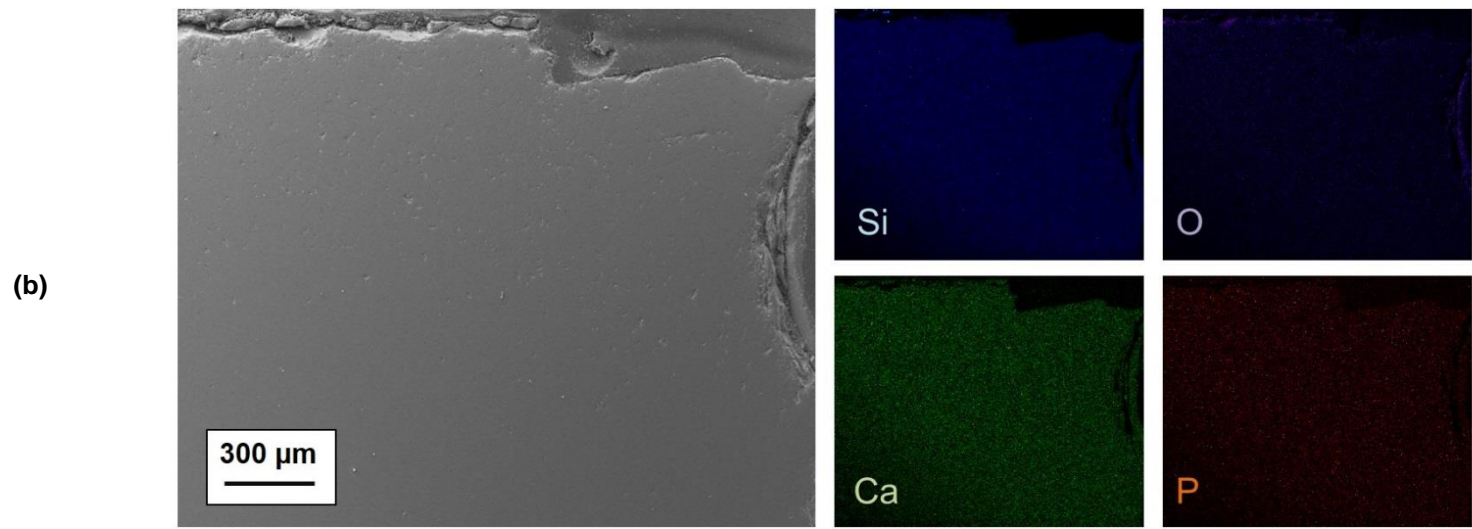
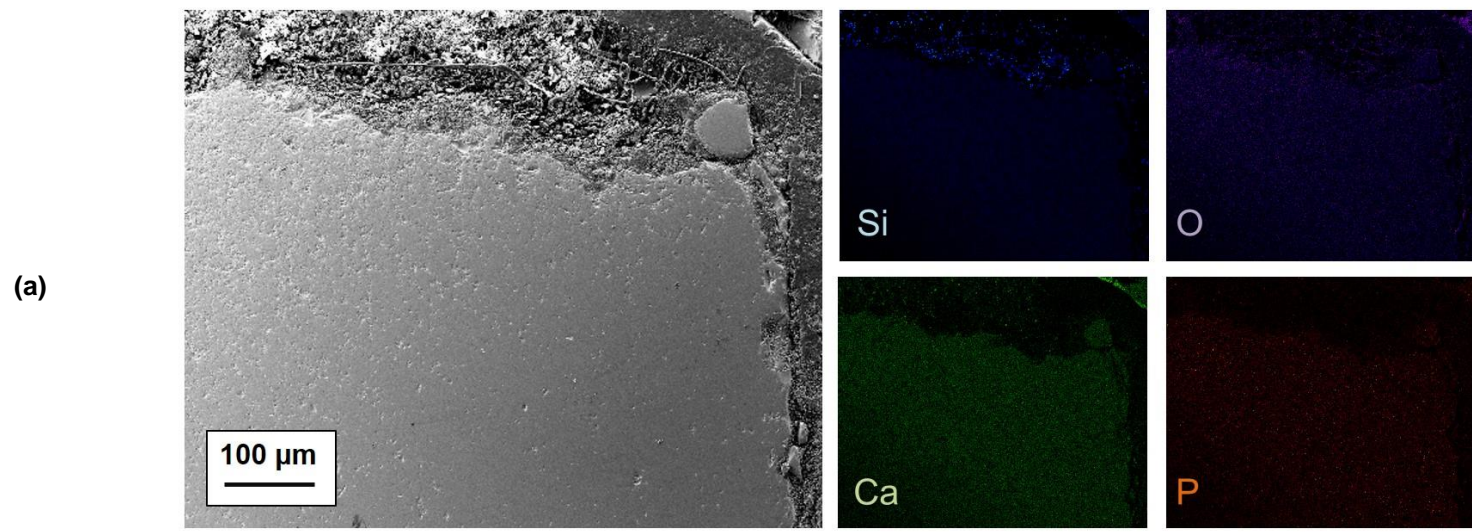
Cant 003



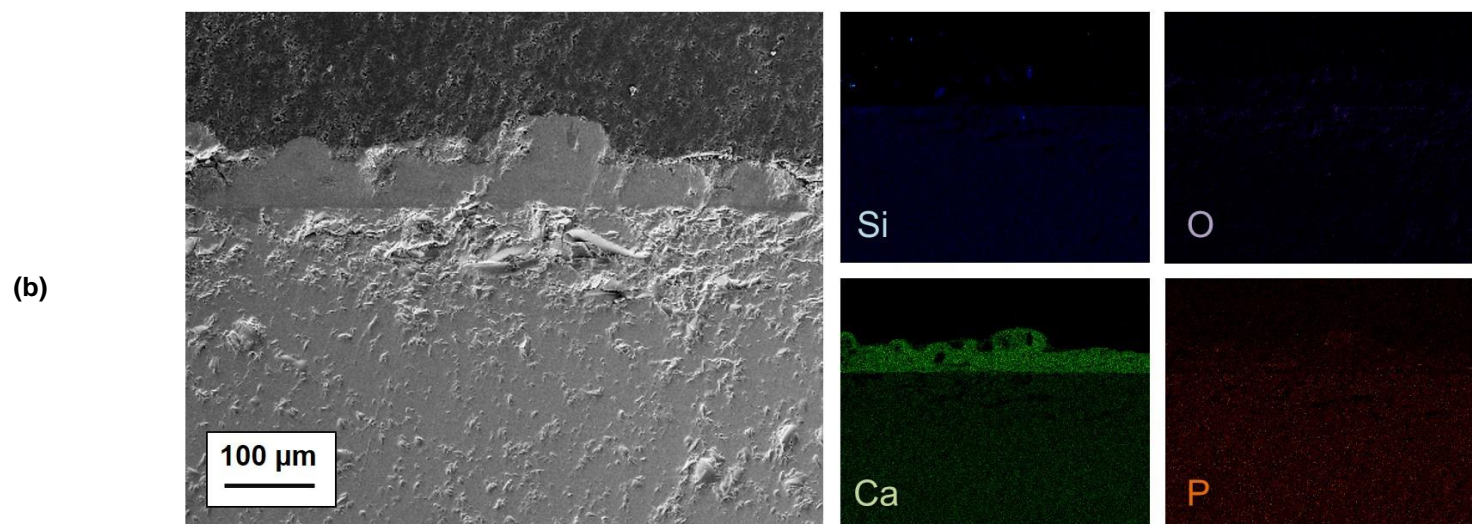
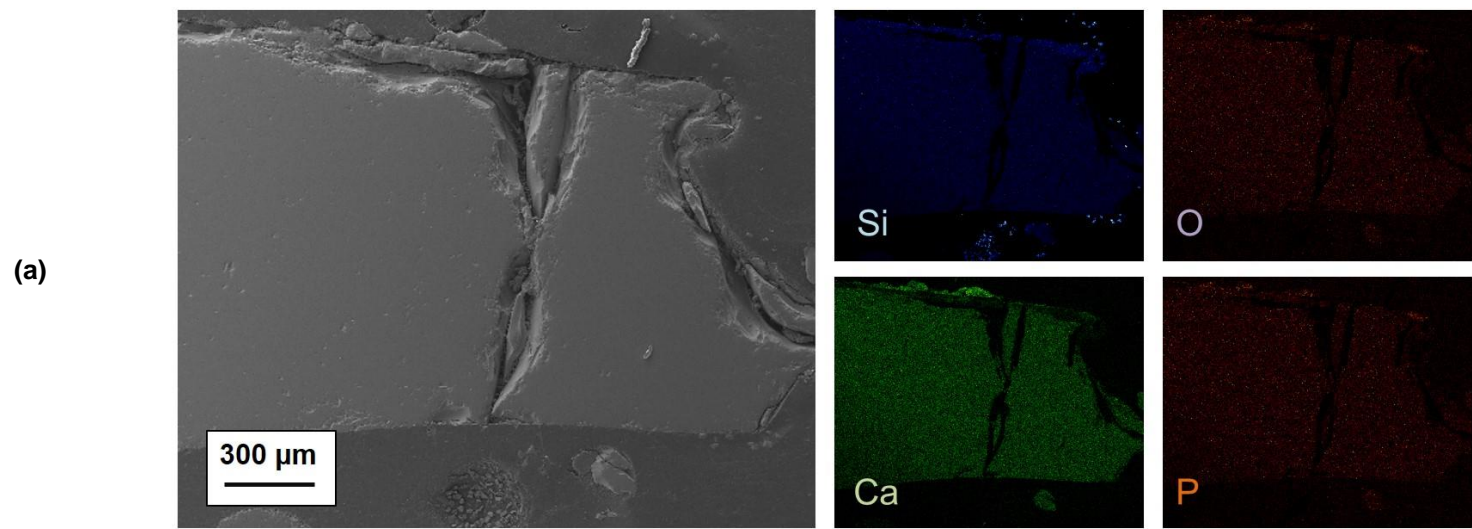
Cant 004



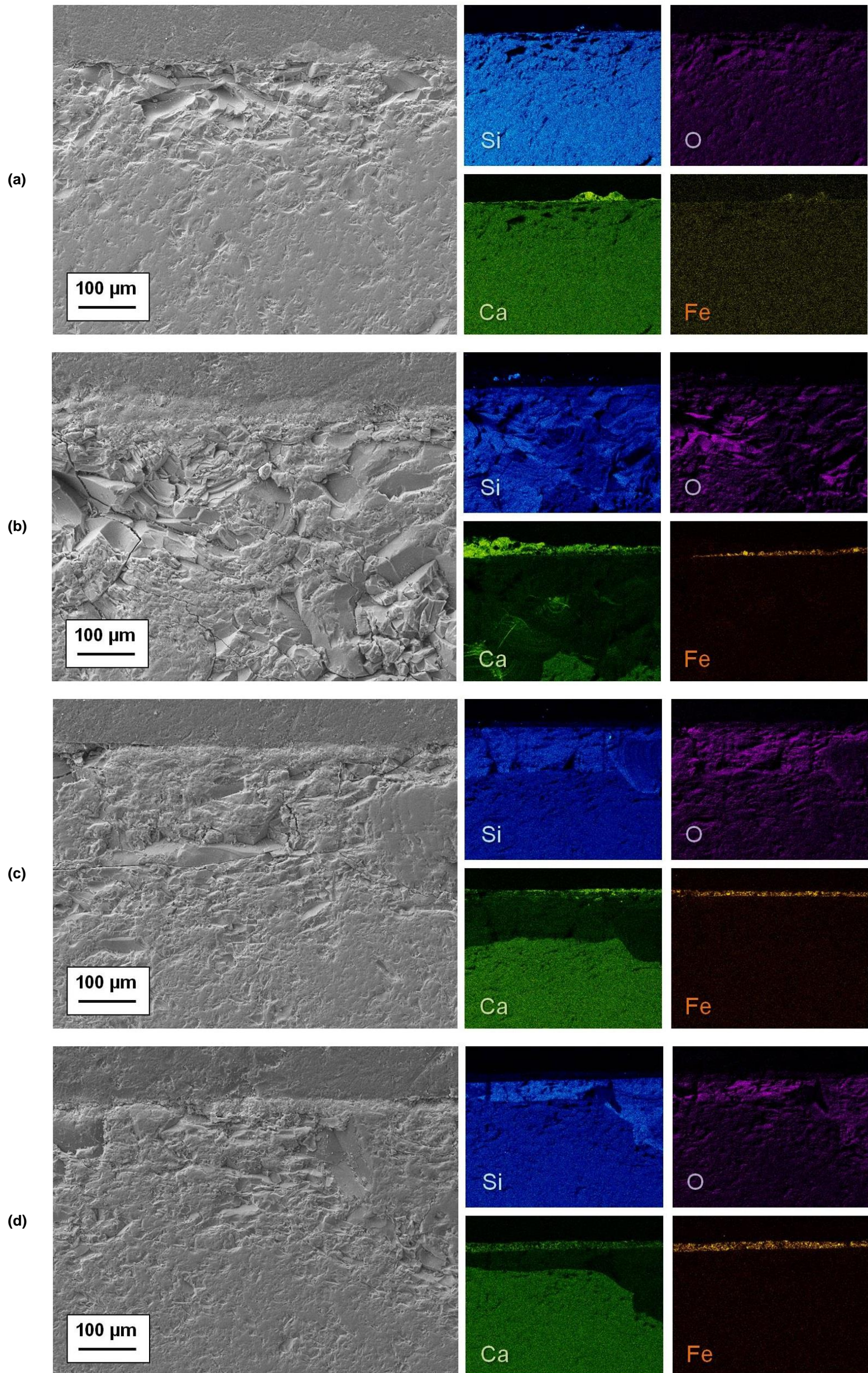
Cant 005



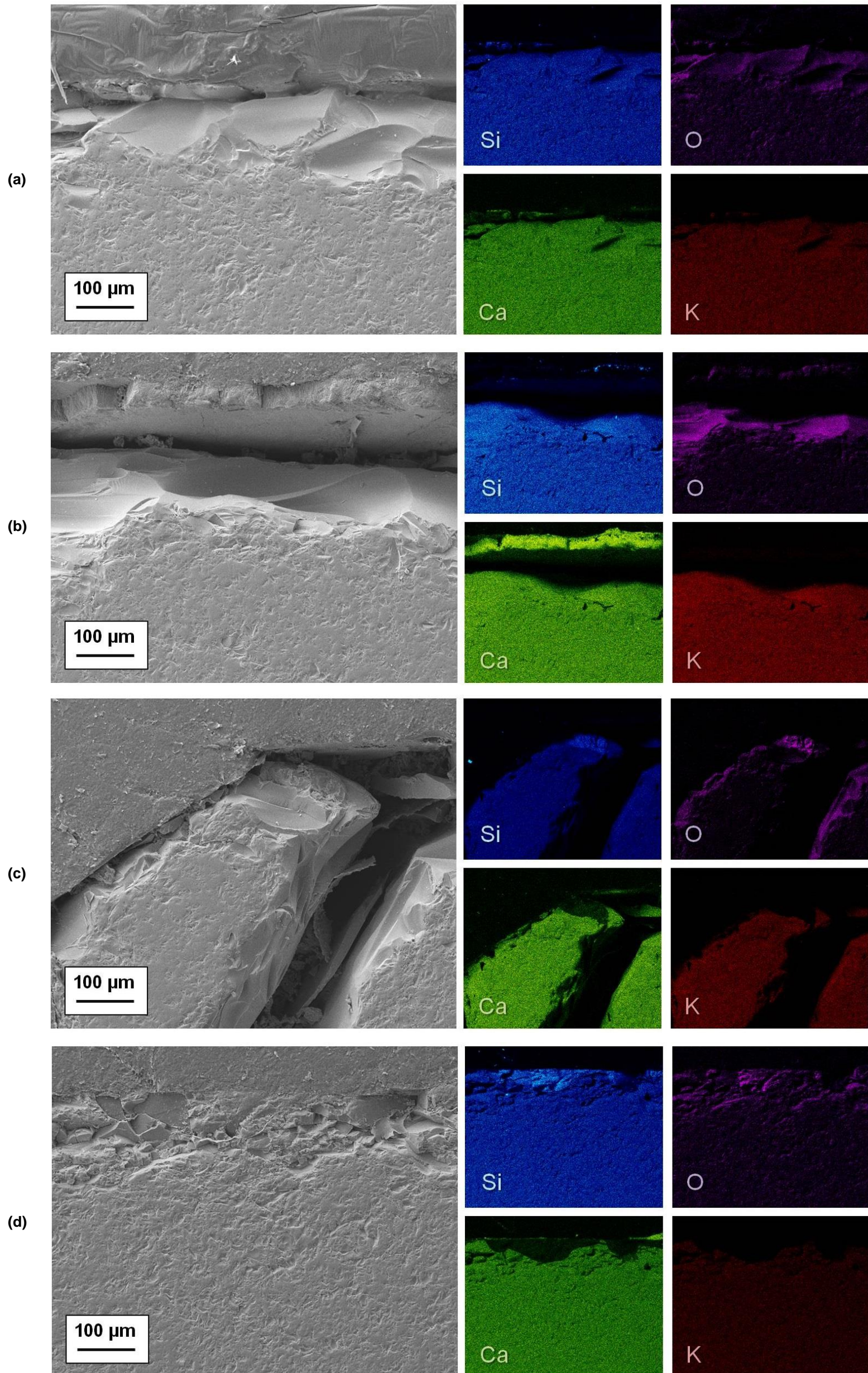
Cant 006



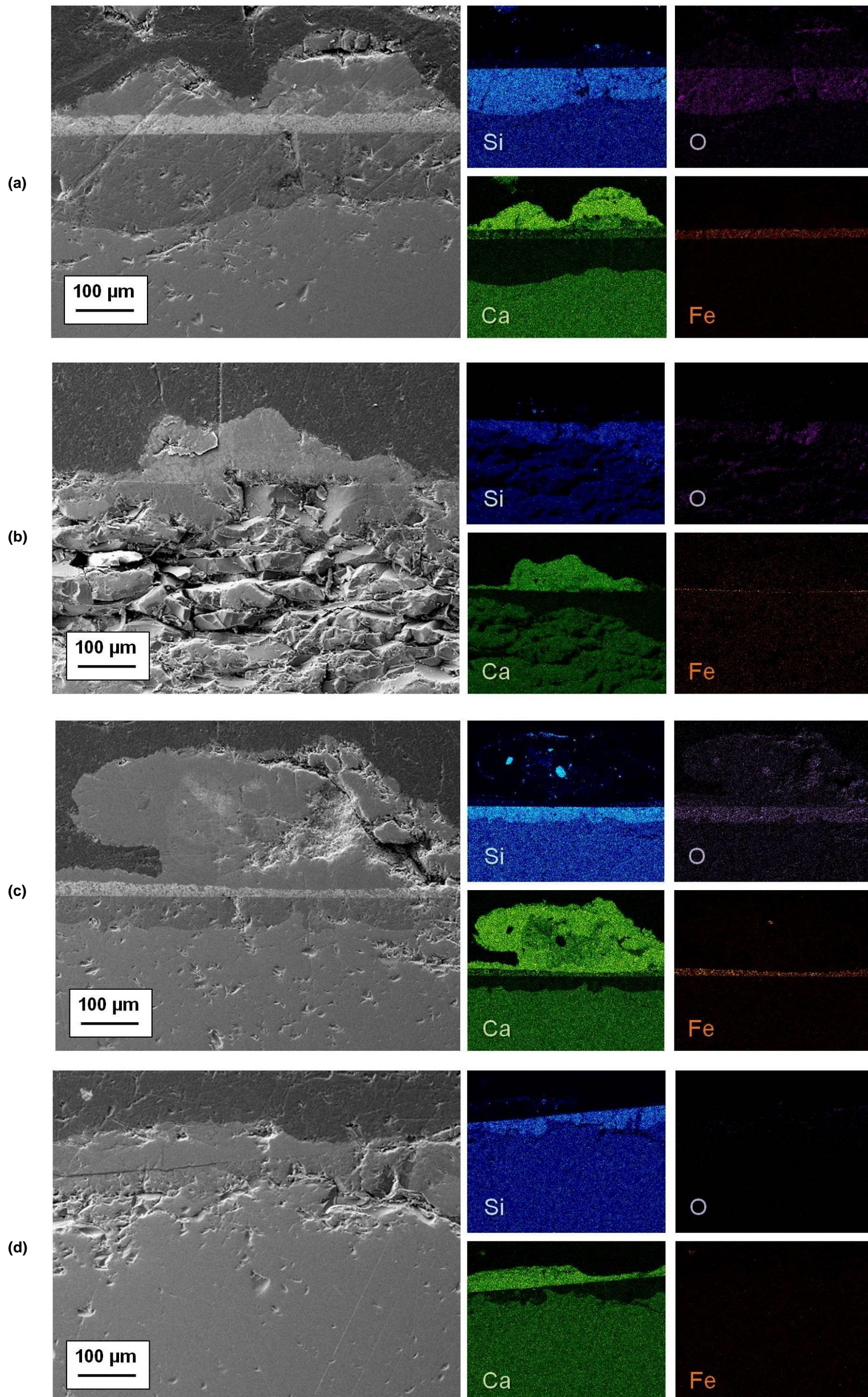
Cant 028



Cant 033



Cant 034



iii) Cant 042 before and after corrosion removal using the [P_{6,6,6,14}][ANS] IL.

Before



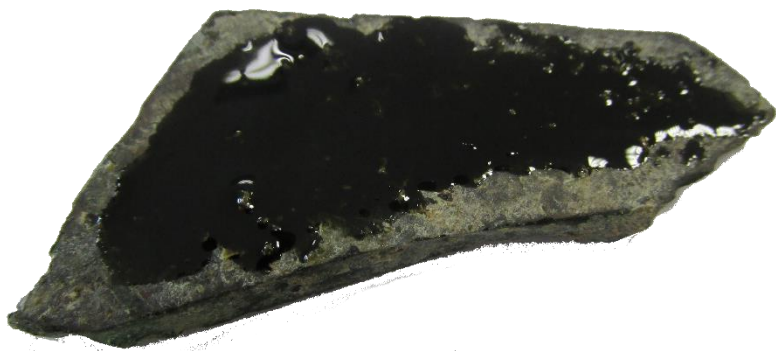
After



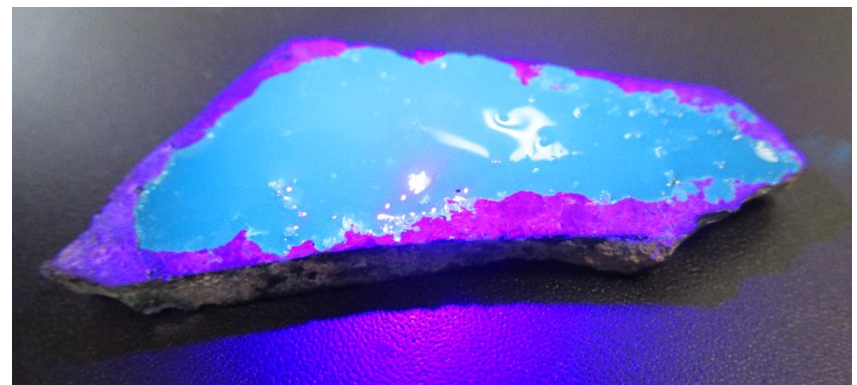
Note: before the application of the IL, the sample was cleaned with a swab impregnated with a water:ethanol (1:1, v:v) solution.

During

Under natural light



Under UV-light



Note: IL left on the surface of the fragment for 10 minutes, then removed using a swab impregnated with a water:ethanol (1:1, v:v) solution.

After

Under UV-light



With transmitted and reflected light

